

**NMR STUDIES OF THE CONFORMATION OF A TRIAZINE DENDRIMER
AND THE SYNTHESIS OF A PLATINATED TRIAZINE DENDRIMER**

A Dissertation

by

KARLOS XAVIER MORENO

Submitted to the Office of Graduate Studies of
Texas A&M University
in partial fulfillment of the requirements for the degree of

DOCTOR OF PHILOSOPHY

December 2007

Major Subject: Chemistry

**NMR STUDIES OF THE CONFORMATION OF A TRIAZINE DENDRIMER
AND THE SYNTHESIS OF A PLATINATED TRIAZINE DENDRIMER**

A Dissertation

by

KARLOS XAVIER MORENO

Submitted to the Office of Graduate Studies of
Texas A&M University
in partial fulfillment of the requirements for the degree of

DOCTOR OF PHILOSOPHY

Approved by:

Chair of Committee,	Eric E. Simanek
Committee Members,	David E. Bergbreiter
	François P. Gabbai
	Andy C. LiWang
Head of Department,	David H. Russell

December 2007

Major Subject: Chemistry

ABSTRACT

NMR Studies of the Conformation of a Triazine Dendrimer and the Synthesis of a
Platinated Triazine Dendrimer. (December 2007)

Karlos Xavier Moreno, B.S., The University of Texas at San Antonio

Chair of Advisory Committee: Dr. Eric E. Simanek

A general picture of dendrimer conformation has appeared through studies of various dendrimer systems. Though the studies define some conformational abilities of a dendrimer, the studies are only able to examine one portion of the general picture. NMR studies of a generation three melamine dendrimer with unique NMR signatures from core to periphery describes most, if not all, of the general concepts of dendrimers in one system.

A generation three melamine dendrimer was synthesized by a convergent route using diamines identified from competition reactions towards a monochlorotriazine. The cyclic monoamines surveyed displayed a relative reactivity range of 40x, expanding the previously identified series to a range of 320x. Azetidine is 40x more reactive than the cyclic, nine-membered ring ($C_8H_{17}N$), and 320x more reactive than benzyl amine. Sterics and pKa values explain the differences in reactivity of the cyclic monoamines. Differences in the nucleophilicity of the amine groups consisting of 2-aminoazetidine, 2-aminopyrrolidine, and 4-aminopiperidine are 180x, 70x and 20x, respectively.

One-dimensional NMR spectra of the exchangeable NH region show that the dendrimer supports a rich rotamer population. Observations of the data show that the rotamer populations change from a preferred extended conformation to a more closed conformation, indicative of sterics being a driving force of conformational architecture. Variable temperature NOESY studies show that the peripheral groups backfold into the interior of the dendrimer in DMSO- d_6 . The backfolding can be removed by changing the solvent to either CDCl₃ or CD₃OD. Variable temperature (VT) coefficients measured for the exchangeable NH protons implies that solvent may be excluded from the interior of the dendrimer. Proton relaxation studies provide evidence that the dendrimer tumbles slowly in solution, and the periphery moves more freely than the interior.

Synthesis towards the attachment of carboplatin-like peripheral groups on a generation three dendrimer was unsuccessful. A diethyl malonate unit was attached to the periphery of the dendrimer followed by capping with 4-aminomethylpiperidine. Hydrolysis of the esters and treatment with activated platinum led to a black precipitate product. Two alternate routes of achieving the desired platinated dendrimer are described.

DEDICATION

To my loving wife, Lilly, for her support throughout my time in graduate school

TABLE OF CONTENTS

	Page
ABSTRACT	iii
DEDICATION	v
TABLE OF CONTENTS	vi
LIST OF FIGURES	viii
LIST OF TABLES	x
 CHAPTER	
I INTRODUCTION: CONFORMATIONAL ANALYSIS OF NON-TRIAZINE DENDRIMERS	1
Computational Studies	3
Poly(amidoamine) (PAMAM) Dendrimers	5
Poly(aryl ether) or Fréchet-type Dendrimers	8
Poly(propyleneimine) (PPI) Dendrimers	10
Secondary Interactions	12
Conclusions	15
II IDENTIFICATION OF DIAMINE LINKERS AND THEIR APPLICATION IN THE SYNTHESIS AND CHARACTERIZATION OF A MELAMINE DENDRIMER BEARING UNIQUE NMR SIGNALS	16
Introduction	16
Results and Discussion	19
Synthesis	22
NMR Characterization	22
Conclusions	31
Experimental Section	32
III USING NMR SPECTROSCOPY TO PROBE THE CHOREOGRAPHY OF A DENDRIMER DANCE	43

TABLE OF CONTENTS cont'd

CHAPTER	Page
Introduction	43
Results and Discussion.....	47
Lesson One: nOe Complexity Emerges with Globular Structure ..	49
Lesson Two: Solvent Is Largely Excluded from Interior of the Dendrimer	52
Lesson Three: Each 'Layer' of the Dendrimer Has Different Mobility	55
Conclusions	57
Experimental Section	58
IV SYNTHESIS OF AND CHARACTERIZATION OF A PLATINATED TRIAZINE DENDRIMER.....	69
Introduction	69
Synthesis.....	74
Characterization	76
Conclusions	80
Experimental Section	83
V SUMMARY	87
REFERENCES	90
APPENDIX A	101
APPENDIX B	139
APPENDIX C	163
VITA	172

LIST OF FIGURES

FIGURE	Page
1.1 Examples of a PAMAM, a Poly(Aryl Ether) and a PPI dendrimer	1
1.2 Illustration of divergent and convergent pathways of dendrimer synthesis	2
1.3 G1 examples of PAMAM dendrimers studied by Tomalia and Meltzer	6
1.4 Density of packing between ‘early’ generation PAMAM dendrimers and ‘late’ generation PAMAM dendrimers	7
1.5 Polyarylether dendrimers studied by Wooley and De Backer.	9
1.6 G2 examples of paramagnetic and diamagnetic core Fréchet-type dendrimers studied by Gorman	10
1.7 Examples of PPI dendrimers	11
1.8 a) β -Alanine dendrimer studied by Mong et. al. ³⁷ b) Glutamic acid dendrimer studied by Appoh et. al. ³⁸	13
1.9 a) Poly(glycerol succinic acid) dendrimer studied by Grinstaff. ³⁹ b) Adamantyl terminated PPI dendrimer studied by Meijer. ^{40,41}	15
2.1 Relative reactivity map for the substitution of monochlorotriazines	18
2.2 Diamine linkers chosen for dendrimer synthesis	20
2.3 Synthesis of G3 dendrimer, 2.8	21
2.4 (¹ H– ¹ H) TOCSY spectrum of 2.8 in DMSO- <i>d</i> ₆ at 75 °C	23
2.5 Model compounds used for assignment of NMR spectra of dendrimer intermediates	23
2.6 ¹ H NMR spectra (0.5 – 5.0 ppm) of intermediates 2.1-2.6 and dendrimer 2.8	25

LIST OF FIGURES cont'd

FIGURE	Page
2.7 ¹ H NMR spectra (6.0 – 9.0 ppm, NH region) of intermediates 2.1-2.6 and dendrimer 2.8	29
2.8 Rotamers of the pyrrolidine, piperidine and azetidine groups	29
3.1 Cartoon and molecular representation of dendrimer and models.....	48
3.2 Observed nOes of models and full dendrimer.....	49
3.3 NOESY spectrum of 2.8 in DMSO- <i>d</i> ₆ (2 % w/v) at 40 °C	52
3.4 <i>T</i> ₁ / <i>T</i> ₂ vs temperature plot of the various linkers within 2.8	57
4.1 Currently approved platinum antitumor drugs around the world.....	69
4.2 Possible hydrolysis products of <i>cis</i> -platin	70
4.3 Possible cross-links formed by <i>cis</i> -platin.....	71
4.4 Polymer-platinum conjugates studied for chemotherapy.....	72
4.5 Synthesis of a triazine dendrimer	76
4.6 ¹ H spectra (0.5 – 5.5 ppm) of compounds 4.1-4.4	77
4.7 ¹⁹⁵ Pt NMR spectrum of 4.7 in acetone with a D ₂ O external reference	78
4.8 First alternate approach to a platinated dendrimer	81
4.9 Second alternate approach to a platinated dendrimer.....	82

LIST OF TABLES

TABLE		Page
1	VT Coefficients ($\Delta\delta/\Delta T$) of Dendrimer and Model Compound NHs	54
2	Observed Frequencies of $\text{PtI}_2(\text{NH}_3)_2$	80
3	Rotamer Populations – 1	130
4	Rotamer Populations – 2	131
5	Rotamer Populations – 3	132
6	Rotamer Populations – 4	133
7	Rotamer Populations – 5	134
8	Rotamer Populations – 6	135
9	Rotamer Populations – 7	137

CHAPTER I
INTRODUCTION: CONFORMATIONAL ANALYSIS OF NON-TRIAZINE
DENDRIMERS

Introduction

Ideally, dendrimers are perfect monodisperse macromolecules with a regular and highly branched three-dimensional architecture.¹ Synthesis of dendrimers proceeds through an iterative process, in which each additional iteration leads to a higher generation material. The first reported iterative synthesis was by Vögtle, who named this procedure a ‘cascade synthesis’.² Some of the most frequently studied dendrimers are Tomalia’s poly(amidoamine) (PAMAM) dendrimers,³ Fréchet’s poly(aryl ether) dendrimers⁴ and Meijer’s poly(propylene imine) (PPI) dendrimers⁵ (Figure 1.1).

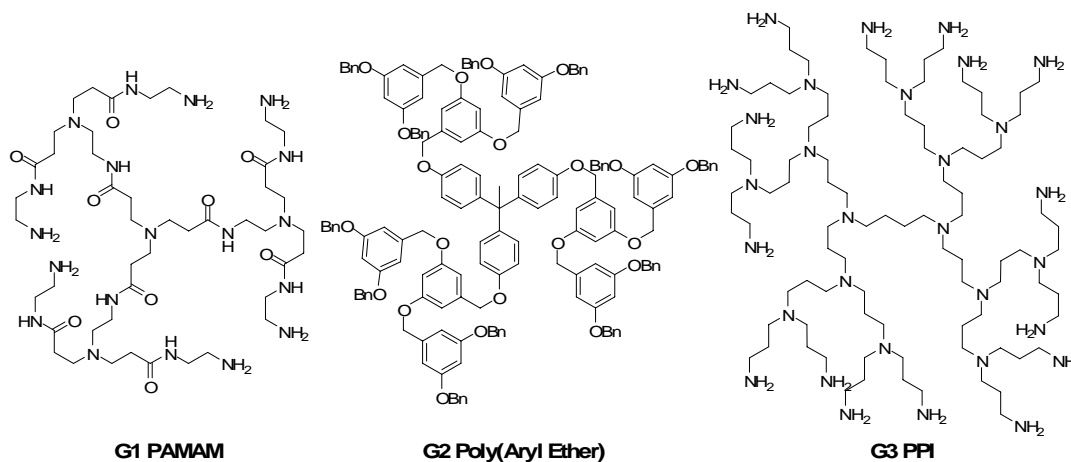


Figure 1.1. Examples of a PAMAM, a Poly(Aryl Ether) and a PPI dendrimer.

Dendrimers may be synthesized in two ways: divergently³ or convergently⁴ (Figure 1.2). Each synthetic route has advantages and disadvantages. In the divergent synthesis, the dendrimer is grown stepwise from the core. The number of reactions required to complete in each step increases exponentially. As the dendrimer grows, completion of each step becomes more difficult leaving incomplete reactions. Achieving large quantities quickly and high generation dendrimers is possible through the divergent method. In the convergent synthesis, the dendrimer is grown from the periphery towards the core. The number of reactions required to complete each step is kept low and constant providing higher purity material. Sterics prohibits high generation dendrimer synthesis.

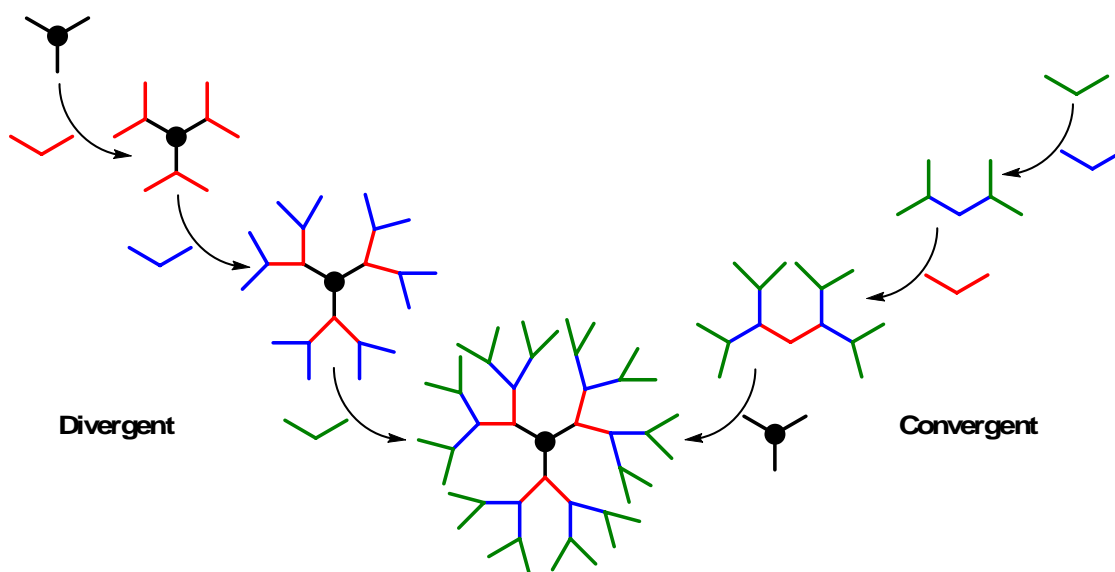


Figure 1.2. Illustration of divergent and convergent pathways of dendrimer synthesis.

One of the fundamental questions to ask about macromolecules is, “What conformation does the molecule adopt in solution?” or “How does it interact with its local environment?” Since the first reported synthesis of dendrimers,¹⁻³ there have been many efforts to determine the conformation of the macromolecules in solution using both experiment and theory.⁶⁻⁴¹

Computational Studies

Using a self consistent-field model, de Gennes and Hervet proposed that the dendrimer extends outwardly from the core having all of the end groups on or near the periphery of the molecule (*i.e.*, dense shell).⁶ Starburst growth was determined to exist within only a finite number of generations. Their concluding thoughts were that the molecule is very flexible for small generations but very rigid in higher generations. Naylor et al. used computer-assisted molecular modeling to conclude that generations 1-3 are highly asymmetric and generations 5-7 are nearly symmetrical.⁷ Generation 4 was believed to be the transition between the asymmetric and symmetrical forms. The average structures for the early generations were very open, domed shapes, while the latter generations were more dense and spheroid-like.

In contrast, Lescanec and Muthukumar's simplified kinetic model using a computer simulation of dendritic growth found that the chain ends may reside within the molecule for a given generation.⁸ A maximum density between the core and the periphery derives from a backfolding of the chain ends. A more recent self consistent-field model by Boris and Rubinstein supports the dense core model: density decreased monotonically from the center of the molecule.⁹ Monte Carlo calculations performed by Mansfield and

Klushin found the chain ends to be distributed throughout the structure.¹⁰ The calculations revealed some hollowness may be present through a range of dendrimer generations. This occurs with the core maximally extended, creating cavities within the architecture and the end groups backfold inadequately filling these voids. Also using Monte Carlo calculations, Welch and Muthukumar observed that under low electrostatic conditions, the end groups are located near the surface of the molecule.¹¹ By increasing the salt concentration, the molecule rearranges to a more dense core architecture.

Molecular dynamics (MD) simulations of dendrimers that incorporate solvent effects have been performed.¹²⁻¹⁴ Murat and Grest provided a model which predicted backfolding of the chain ends for various solvent qualities.¹² Their conditions provided a high density core and an increase in dendrimer density with a decrease in solvent quality. More recently, MD simulations performed in explicit solvent have suggested that dendrimers can backfold in solution.^{13,14} Karatasos et al. found that as the generation of the dendrimer increases the extent of backfolding also increases.¹³ ‘Dynamic layering’ was observed in the simulation. The authors find that the internal layer of the dendrimer has slow dynamics, while the peripheral layer has fast dynamics: ‘slow layer’ and ‘fast layer’, respectively. Suek and Lamm studied both solvophobic and solvophilic dendrimers and found that in solvophobic dendrimers the maximum density is located near the core.¹⁴ The density decreased as the dendrimer exterior is approached. In solvophilic dendrimers of less than generation six, the peripheral groups were found to be extended away from the core. For G6 or greater, the peripheral groups were found throughout the molecule possibly forced back due to steric crowding. In

summary, most of the theoretical studies suggest that backfolding is a common process of dendrimers.

Poly(amidoamine) (PAMAM) Dendrimers

Using hydrodynamic radius values, Tomalia et al observed a change in conformation as the generation of poly(amidoamine) PAMAM dendrimers increased (Figure 1.3).¹⁵ Plotting the hydrodynamic radii values vs generation number gave a linear relationship for generations 1.0-3.5. However, the authors noticed a slight deviation for higher generations towards values displayed by extended CPK values. The deviation was thought to be the dendrimer being engorged (extended) solvent or a sterically induced hollowness (extension) was observed. Meltzer et al. demonstrated that the chain dynamics did not change dramatically up to the tenth generation using NMR spectroscopy.^{16,17} The relaxation of the interior carbons was faster than the exterior carbons. Relaxation of the terminal carbons decreased as the molecular weight of the dendrimer increased. They conclude that the branches backfold to some extent to relieve steric crowding based on ²H NMR. Small-angle X-ray scattering (SAXS) measurements showed that the density of the dendrimer with a molecular weight greater than 50 kDa appears to be independent of the generation.¹⁸ The terminal groups were able to reside on the surface of the molecule but backfolded arrangements were possible.

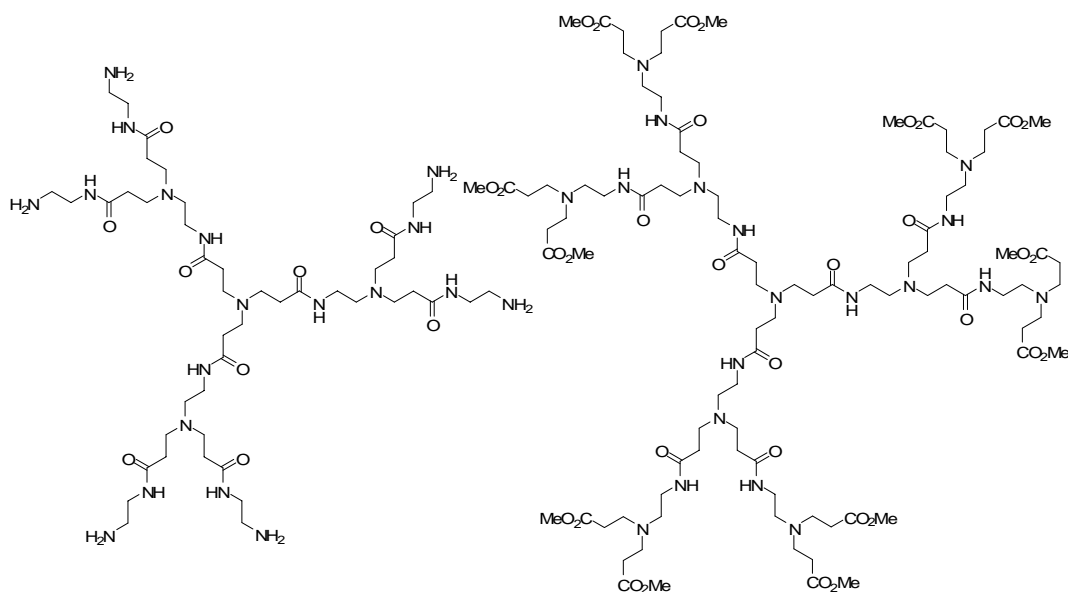


Figure 1.3. G1 examples of PAMAM dendrimers studied by Tomalia¹⁵ and Meltzer.^{16,17}

A pyrene fluorescence probe revealed that structural differences between early ($G \leq 3.5$) generations and late ($G \geq 4.5$) generation of PAMAM dendrimers exist.¹⁹ The early generations tend to be more hydrophilic in nature with a large separate between the surface groups (Figure 1.4). The later generations are more hydrophobic and are more densely packed (Figure 1.4). Electron paramagnetic resonance (EPR) studies using Cu (II) or nitroxide complexes with PAMAM dendrimers support evidence found from fluorescence studies.^{20,21} In these studies, the probe was able to move freely in early generation PAMAM dendrimers. This free moving behavior was indicative of an extended structure. The probe's motion was slower because of the dendrimer's more compact structure.

Poly(aryl ether) or Fréchet-type Dendrimers

In addition to PAMAM dendrimers, polyarylether dendrimers have also been examined. Mourey et al. studied polyaryl ether dendrimers using size exclusion chromatography and differential viscometry (Figure 1.5).²⁴ The polyarylether dendrimers had hydrodynamic radii that increased linearly as a function of molecular weight and a maximum in the intrinsic viscosity as a function of molecular weight was found. According to the authors, the data suggested the structures expanded to approximately two-thirds their theoretical extended length. De Backer and co-workers observed through fluorescence depolarization measurements that the dendrimer conformation can change by varying the solvent (Figure 1.5).²⁵ A more extended structure was observed for the dendrimer in medium to good solubilizing solvents (acetone and toluene, respectively). In a poor solubilizing solvent such as acetonitrile, the hydrodynamic volume of the dendrimer decreased significantly, suggesting a more compact structure. The studies of Mourey and De Backer are in qualitative agreement with the theoretical study of Lescanec and Muthukumar⁸ in which the end groups can be found throughout the dendrimer volume, *i.e.* backfolding occurs. De Backer's study also correlated well with of Murat and Grest¹² in which solvent can change the conformational behavior of the molecule.

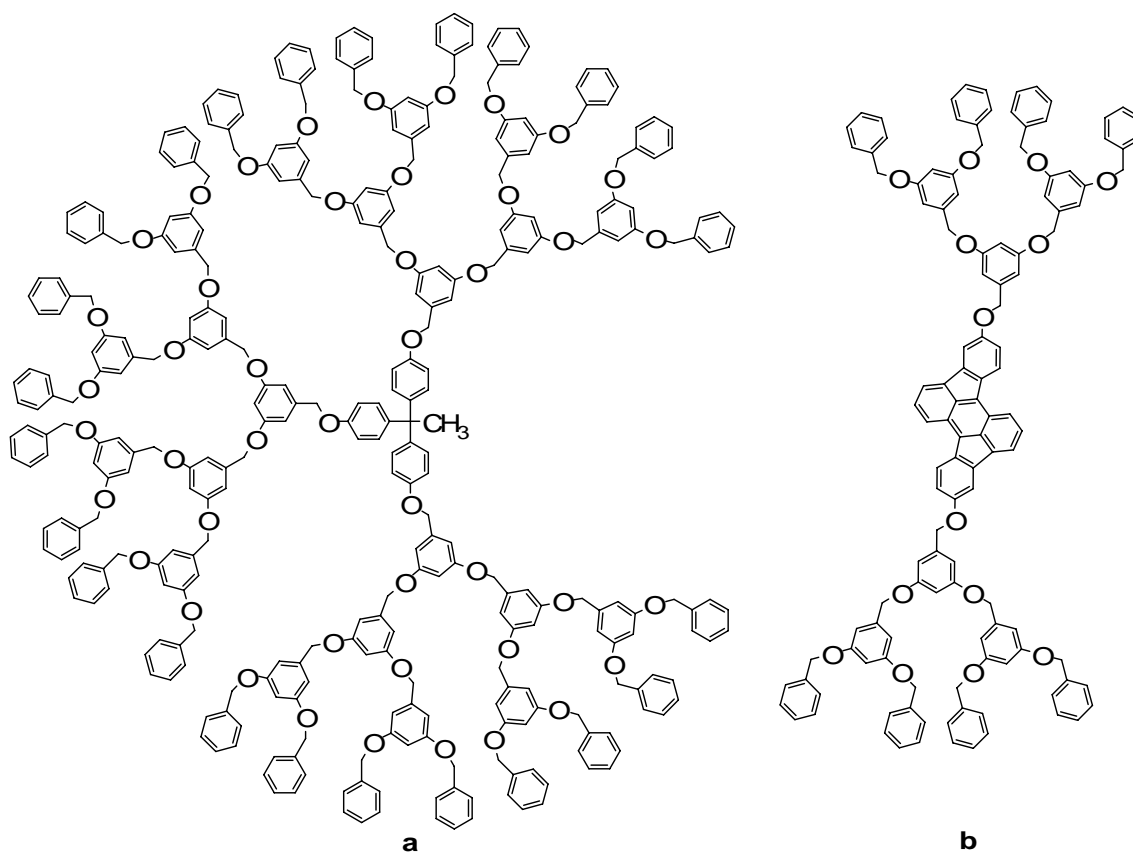


Figure 1.5. Polyarylether dendrimers studied by Wooley^{24,26} (a) and De Backer²⁵ (b).

Backfolding in the solid-state was observed by Wooley et al using rotational-echo double-resonance (REDOR) NMR.²⁶ The core of the polyarylether dendrimer was ¹⁹F labeled and the periphery was ¹³C labeled. Dipolar coupling between ¹³C-¹⁹F was used to determine that the periphery groups were backfolding. Increasing the generation number decreased the dipolar coupling, suggesting a decrease in interpenetration of the peripheral groups to the core. Additionally, Gorman and co-workers were able to establish that the end groups of Fréchet-type dendrimers come in close proximity to the core.²⁷ Two sets of Fréchet-type dendrimers, G1-G3, were used: one with a

diamagnetic core and the other with a paramagnetic FeS core (Figure 1.6). A noticeable shortening of the spin-lattice relaxation (T_1) times of various protons of the paramagnetic core dendrimer was observed when compared to the diamagnetic core dendrimer. The shortening of T_1 was attributed to each layer of the molecule coming in close contact with the paramagnetic core, *i.e.* backfolding was occurring. Backfolding was attributed to be the major cause of the very rapid electronic energy transfer in polyaryl ether dendrimers.²⁸

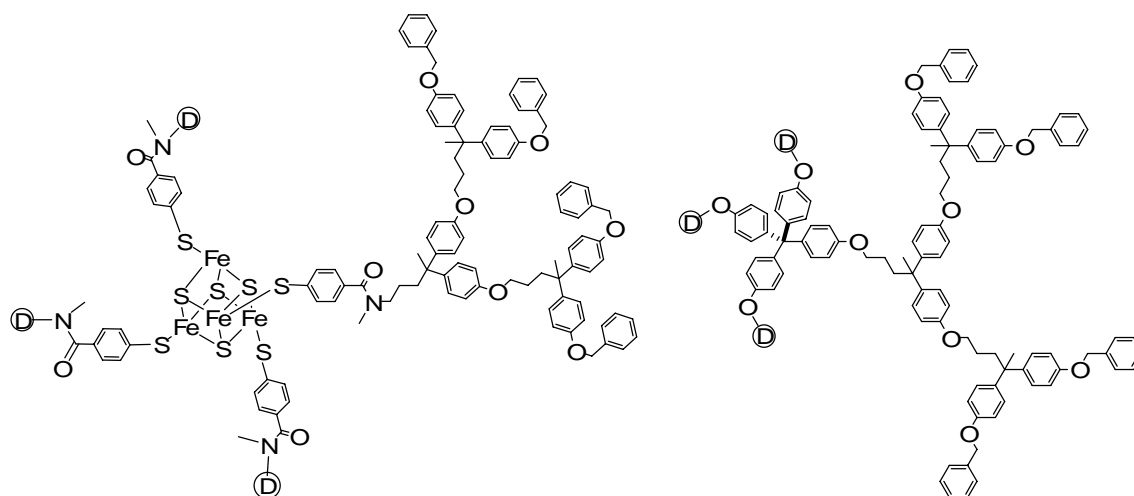


Figure 1.6. G2 examples of paramagnetic and diamagnetic core Fréchet-type dendrimers studied by Gorman.²⁷

Poly(propyleneimine) Dendrimers

Small-angle neutron-scattering (SANS) and viscometry measurements of both nitrile and amine terminated poly(propylene imine) (PPI) dendrimers by Scherrenberg and co-workers found a linear relationship between the radius of the dendrimer and its

generation number.²⁹ This linear relationship was independent of the type of end group or solvent used. These results correlate well with the theoretical results of Murat and Grest¹² indicating that PPI dendrimers are flexible with a relatively uniform density distribution resulting from some degree of backfolding. An extensive SANS study by Vögtle and co-workers demonstrated that the peripheral groups of the dendrimer are dispersed throughout the dendrimer (Figure 1.7).³⁰ A maximum density was located in the center of the molecule, suggesting the end groups are backfolded. This supports the dense-core model of Boris and Rubinstein.⁹

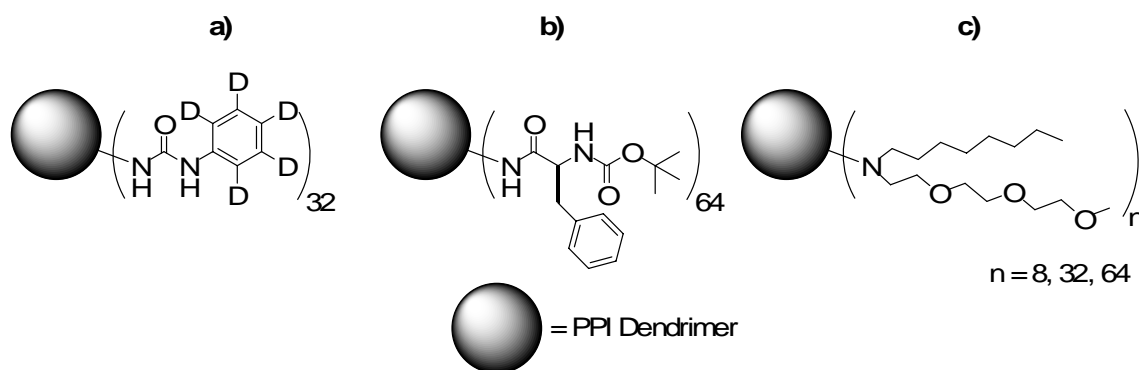


Figure 1.7. Examples of PPI dendrimers. a) G4 PPI dendrimer studied by Vögtle.³⁰ b) G5 PPI dendrimer ('Dendritic Box') studied by Meijer.^{31,32} c) Amphiphilic PPI dendrimer studied by Ford.³⁶

The 'dendritic box', Figure 1.7, synthesized by Jansen et al. takes advantage of the end group backfolding to encapsulate guest molecules.^{31,32} Spin-lattice (T_1) and spin-spin (T_2) relaxation experiments showed that the higher generation dendrimers were tumbling more slowly than the lower generation derivatives. Crystal data later provided direct evidence of the end groups backfolding via hydrogen-bond interactions.³³

Secondary interactions such as hydrogen-bonding were attributed to the backfolding of the peripheral groups.

Through the use of a high field spectrometer, Chai and co-workers were able to perform an extensive NMR study of PPI dendrimers finding evidence for backfolding using 2D NOESY.^{34,35} Two-dimensional NOESY studies of PPI dendrimer and solvent were performed to study the interpenetration of solvent with the dendritic volume. Benzene was found to be excluded from the dendrimer interior, while chloroform was found to interpenetrate the dendritic volume, thus creating a solvent poor and solvent rich environment, respectively. Studying the interactions of the dendritic arms in the two solvents showed a difference in conformation. In benzene solution, the arms tended to backfold, while in chloroform solution nOes were not observed between the dendritic arms suggesting an extended structure was induced. Similar conclusions were observed by Pan and Ford studying the ^{13}C T_1 times of a PPI dendrimer with both hydrophilic and hydrophobic end groups.³⁶ In polar solvent, such as methanol, the hydrophilic arms moved more freely, while the hydrophobic arms moved more slowly. The reverse was true in a more nonpolar solvent such as chloroform.

Secondary Interactions

To study the secondary interactions of the peripheral groups, VT coefficients and hydrogen/deuterium (H/D) exchange studies have been performed.^{33,37,38} Variable temperature coefficients of a G1 PPI dendrimer provided evidence that the terminal groups were backfolding.³³ Higher-order secondary interactions did not exist in β -alanine dendrimers studied by Mong et al (Figure 1.8).³⁷ They came to this conclusion

by observing that the coefficients were more negative than -4 ppb/K, the threshold for observing secondary interactions. The VT studies were able to show that the inner most NHs were less exposed to solvent than the peripheral NHs of the molecule. Hydrogen/deuterium exchange supports this conclusion. The rate of exchange was enhanced when the NHs were 'dendronized'. Comparison of model compounds and the dendrimer showed a large decrease in the exchange rate. The glutamic acid dendrimers studied by Appoh and co-workers showed strong H-bond interactions based on temperature coefficients (Figure 1.8).³⁸ The coefficients were similar at both high and low concentrations suggesting intramolecular hydrogen-bonding. Their NMR results were supported by IR investigations with the glutamic acid dendrimers.

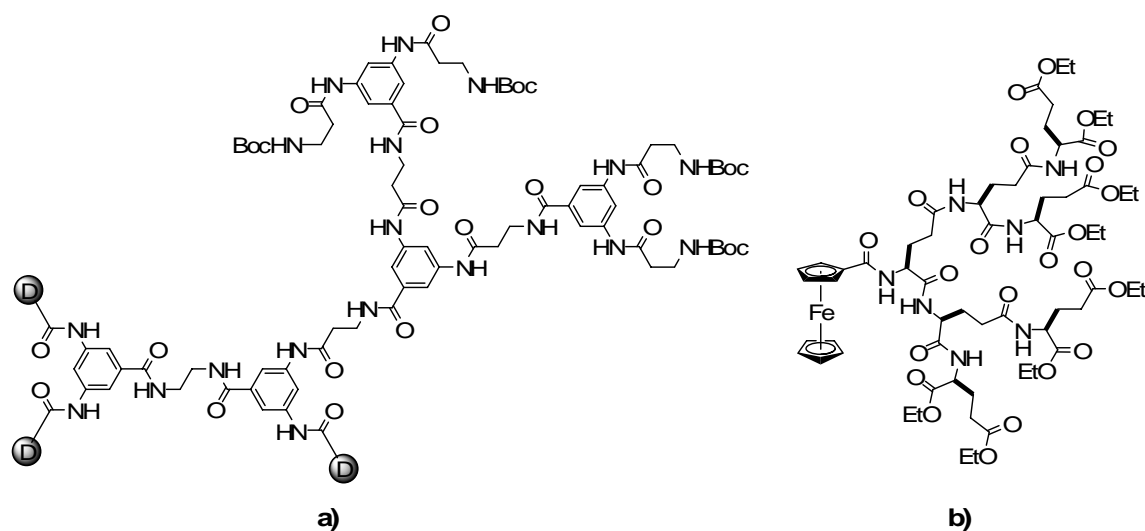


Figure 1.8. a) β -Alanine dendrimer studied by Mong et. al.³⁷ b) Glutamic acid dendrimer studied by Appoh et. al.³⁸

Multi-dimensional NMR techniques have been used to characterize dendrimers, determine their conformation and to observe host-guest interactions within them. To evaluate host-guest interactions, Morgan et al.,³⁹ Banerjee et al.⁴⁰ and Broeren et al.⁴¹ (Figure 1.9) used 2D NOESY to confirm that the guest molecule was interacting with the dendrimer. Meijer's dendritic box was one of the first examples of the physical encapsulation of guest molecules by a dendrimer.^{31,32} An NMR study by Morgan et al. showed that a G4 poly(glycerol succinic acid) dendrimer could encapsulate Reichardt's dye (Figure 1.9).³⁹ Comparison of the proton spectra of the free dye in solution to that of the encapsulated dye showed distinct broadening of the NMR resonances. The T_1 and T_2 relaxation of the dye also decreased significantly, suggesting encapsulation by the dendrimer. A 2D NOESY spectrum provided nOes between the dye and dendritic arms. Multi-dimensional NMR experiments showed that a guest molecule could bind to targeted binding sites on a PPI dendrimer.⁴⁰ More recently, heteronuclear NMR techniques were used to prove that the guest binds not only to the targeted binding sites but many other sites within the PPI dendrimer.⁴¹

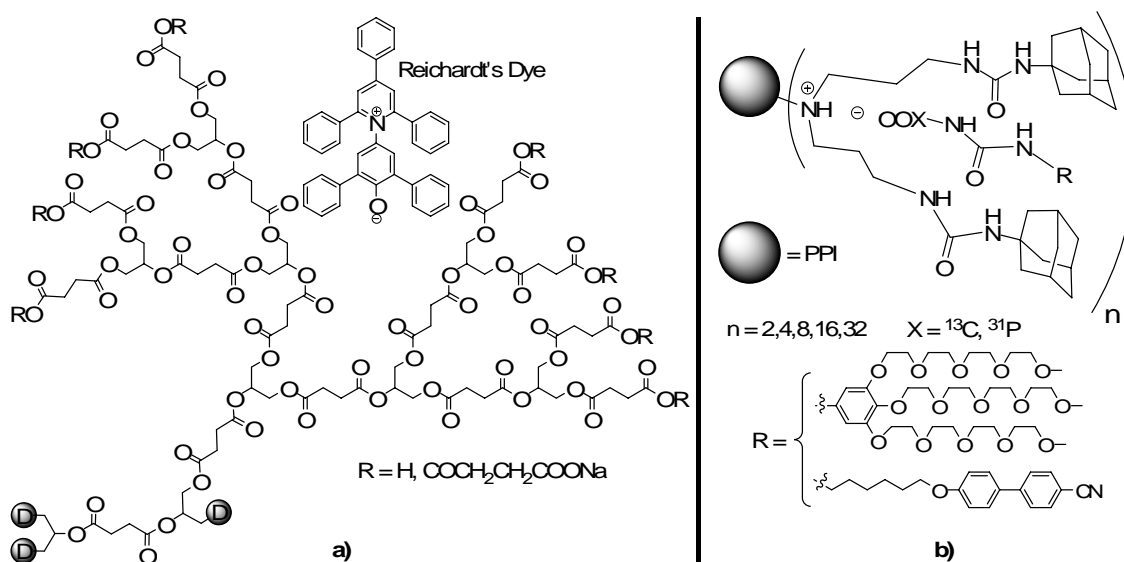


Figure 1.9. a) Poly(glycerol succinic acid) dendrimer studied by Grinstaff.³⁹ b) Adamantyl terminated PPI dendrimer studied by Meijer.^{40,41}

Conclusions

Conformational analysis of various dendrimer systems has been well studied through the use of many techniques. Many of these studies suggest that the dendritic arms backfold to some extent when high generations are achieved.^{7-10,13-15,19-21} Several experimental studies, including simulations, have suggested that the conformation of the dendrimer can be changed either through a change in solvent, pH or ionic concentration.^{8,11-14,22,23,25,35,36} This dissertation attempts to describe the conformational analysis of a triazine-based dendrimer using various NMR techniques. The goals of these studies are to confirm many of these observations in a single dendrimer system and elaborate on more subtle issues of conformation.

CHAPTER II

**IDENTIFICATION OF DIAMINE LINKERS AND THEIR APPLICATION IN
THE SYNTHESIS AND CHARACTERIZATION OF A MELAMINE
DENDRIMER BEARING UNIQUE NMR SIGNALS***

Introduction

Our group has invested significant energies in the synthesis of dendrimers based on triazines, also referred to as dendrimers based on melamine deriving from our use of diamine linkers.^{42,43} Our early targets commonly incorporated *p*-aminobenzylamine because of the significant differences in the reactivity of the amines of this group. That is, during a convergent synthesis, protecting group manipulations and functional group interconversions could be avoided because the benzylic amine would react preferentially (essentially exclusively) with the monochlorotriazine dendron being elaborated.^{42,44-48} The low stability of these aniline derivatives required reasonable, but additional, care on handling. While dry distilled solvents, inert atmospheres and refrigerated storage are commonplace, we recognized that these liabilities could impact the broader acceptance of these materials. The low cost and high reactivity of piperazine soon made it a linking diamine of choice for our investigations. However, when using piperazine, dimerization of monochlorotriazines was observed under non-ideal reaction conditions that were usually attributed to concentration, rate of addition, ineffective stirring or lack thereof,

*Reproduced with permission from Moreno, K.X., Simanek, E.E. *Macromolecules*, submitted for publication. Unpublished work copyright 2007 American Chemical Society.

temperature of addition and the magnitude of stoichiometric excess.^{45,49-59} Reactions with either *p*-aminobenzylamine or piperazine could be readily followed by NMR. The shift of the benzylic protons on reaction with the monochlorotriazine dendron or the desymmetrization of the piperazine group was diagnostic, although in the latter case, dimerization was often impossible to detect by NMR unless it occurred to the extent that the methylene groups of the desymmetrized product showed markedly different integrations.

The wealth of commercially available diamines led us to conduct a rational survey of reactivity with the expectation that linkers possessing reactivity differences displayed in *p*-aminobenzylamine without the disadvantages previously described. Asymmetric diamines that unambiguously revealed undesired dimerization events were also desired. Our original study examined a range of primary and secondary amines including the cyclic amines piperidine and two piperazine derivatives (**A-F**, Figure 1). From these studies, aminomethylpiperidine emerged as a diamine linker of choice and was used extensively.^{42,43,48,50,56-58,60,61} The relative reactivity difference measured for the cyclic secondary amine and primary amine is ~ 20 based on competition experiments. Theoretically, 5% of the product formed might derive from reaction of the monochlorotriazine dendron with the primary amine instead of the desired secondary amine. As this population difference approaches the limit of detection by NMR spectroscopy, the efforts described here were undertaken to identify other suitable diamine linkers. These amines are identified as **G-K** in Figure 2.1.

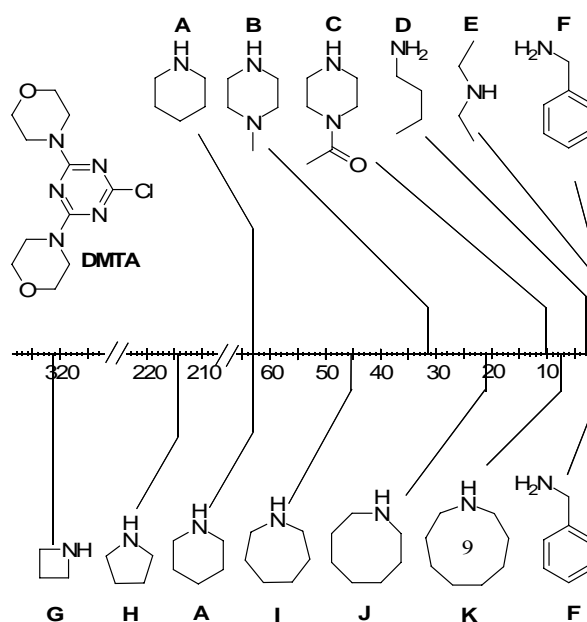


Figure 2.1. Relative reactivity map for the substitution of monochlorotriazines. The reactivity difference between consecutive amines is shown on the scale.

The diamine linkers identified from the relative reactivity data were incorporated into a dendrimer as a proof-of-concept. However, during the course of the synthesis, it became clear that these linkers displayed unique signatures in the ^1H NMR spectra. This observation suggested that in addition to routine analyses that are especially useful during the step by step synthesis of dendrimers, the incorporation of these diamines allowed the core, the middle ‘layer’, and the periphery to be uniquely identified throughout the dendrimer. There is limited precedent for this level of characterization. Using aliphatic polyesters, Ihre estimated the hydrodynamic radii utilizing molecular self-diffusion studies by pulsed field spin echo ^1H NMR.⁶² Gorman used paramagnetic and diamagnetic polyaryl ether dendrimers to illustrate backfolding of the end groups utilizing spin-lattice relaxation measurements.²⁷ Lellek and Stibor used binap

derivatized dendrimers to probe how chiral groups affect the conformation of the dendrimer and their feasibility for use in catalysis.⁶³ Seebach reported on the synthesis and properties of multiple diastereomeric polyaryl ether dendrimers.⁶⁴ Rinaldi was able to observe unique NMR signals for poly(propylene imine) (PPI) dendrimers from core to periphery using a high-field spectrometer.³⁵ Meijer and co-workers were able to observe the resonances of different nitrogens, by ¹⁵N NMR, of PPI dendrimers from core to periphery at natural abundance.⁶⁵ Given the power of multidimensional NMR, we hypothesized that additional structural information might result if the dendrimer could be adequately characterized. This chapter concludes with the characterization of the generation three dendrimer that results from the utilization of these diamines and the assignment of its NMR spectrum. The following chapter addresses the conformational analysis of the molecule.

Results and Discussion

Previously, the relative reactivity data of various amines (**A** – **F**) towards a monochlorotriazine **DMTA** (Figure 2.1) was determined and used to identify diamine linkers for dendrimer synthesis.⁴² Here, expansion of this data included the relative reactivity of various cyclic amines (**G** – **K**) towards **DMTA**. The competition studies were carried out in a manner identical to our original protocol: three equivalents of each amine competed for reaction with **DMTA**.⁴² To facilitate comparison of **G-K** to **A-F** (published previously), we used both **A** and **F** in these reactivity studies. The reactivity map was obtained by determining the product ratios using ¹H NMR after disappearance

of **DMTA**. These values for individual competition studies are consistent multiplicatively across the range of amines within experimental error.

The data show that as ring size decreases, the reactivity of the amine increases.⁶⁶ The most reactive amines (**G**, **H**, and **A**) have pK_a s of 11.3, while the less reactive amines (**I-K**) have pK_a s of 10.8.^{67,68} Sterics can be used to rationalize the difference in reactivity within these subgroups.

From this data, diamine linkers can be identified. These linkers were chosen based on three criteria: 1) a minimum reactivity difference of ~ 20 between the amines is desired in order to keep the number of side products to a minimum, 2) one or more unique ^1H NMR signals for characterization during synthesis, and 3) commercial availability or accessibility in a minimal number of steps. Diamine linkers **L1-3** (Figure 2.2) were chosen because they meet the criteria and are commercially available. A single enantiomer of 2-aminopyrrolidine was used.

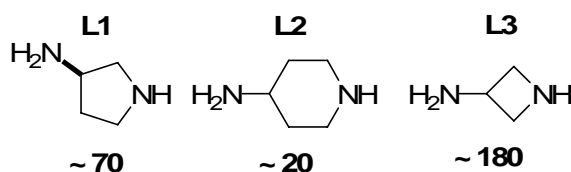


Figure 2.2. Diamine linkers chosen for dendrimer synthesis. Reactivity difference between amines shown below each linker.

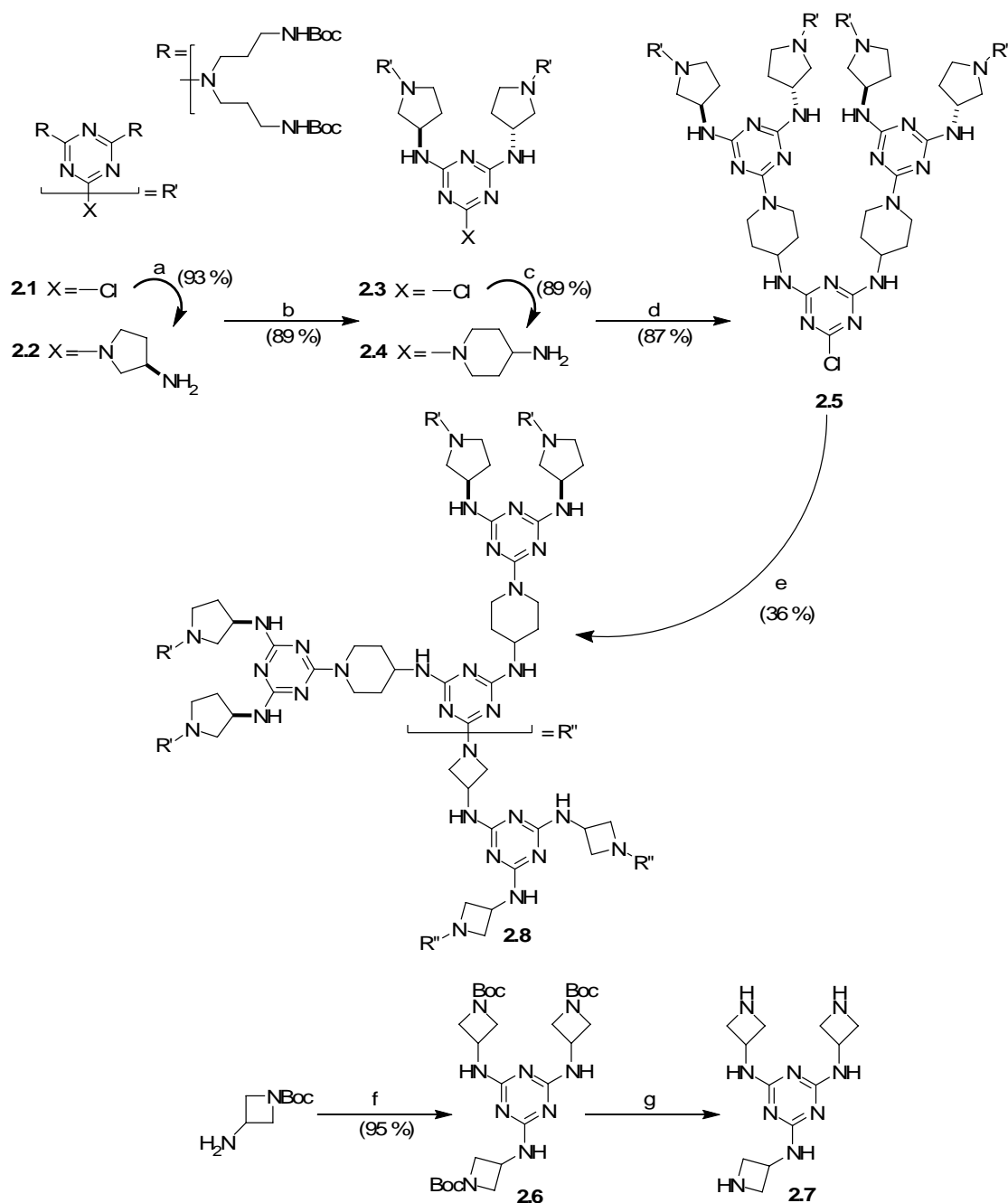


Figure 2.3. Synthesis of G3 dendrimer, **2.8**. a) THF, rt, 14h. b) THF, cyanuric chloride, Hunig's Base (DIPEA), 40 °C, 14h. c) THF, rt, 14h. d) THF, cyanuric chloride, Hunig's Base (DIPEA), 40 °C, 2d. e) THF, **2.7**, BEMP resin, 70 °C, 7d. f) THF, cyanuric chloride, Hunig's Base (DIPEA), 70 °C, 7d. g) (1:1) TFA:DCM, rt, 14h.

Synthesis

Figure 2.3 shows the convergent strategy used to synthesize dendrimer **2.8**. Following selective protection of the primary amines of 3,3'-diaminodipropylamine with BOC-ON, treatment with cyanuric chloride affords monochlorotriazine **2.1**. Intermediate **2.1** is treated with an excess of **L1** to produce **1.2**. In an iterative fashion, the synthesis continues with reaction of cyanuric chloride to form **2.3**, then **L2** to generate **2.4**. Cyanuric chloride treated with a slight excess of **2.4** gives **2.5**. While iteration with 2-aminoazetidine progresses the sequence, sterics precludes trimerization with a cyanuric chloride core. Instead, a less sterically encumbered core, **2.7**, is synthesized by treating cyanuric chloride with **L3** followed by deprotection. This strategy affords a highly reactive core possessing three azetidine groups which yield dendrimer, **2.8**, after reaction with a large excess of **2.5**. The reported yield represents the amount of material obtained in pure form after extensive chromatography, and is not a reflection of an unsuccessful reaction. Indeed, we estimate conversion to product occurred in >80%.

NMR Characterization

Dendrimer **2.8** contains nineteen unique protons in DMSO- d_6 at room temperature. The magnitude of the NMR signal reflects the location of the group; groups on the periphery are present in larger number than those on the core as a result of the exponential growth of the dendrimer. Complete assignment of the resonances is difficult based on simple inspection of a spectrum. Complete and unambiguous assignment

required both model compounds, and HMQC⁶⁹ and COSY⁷⁰ correlations. The data of Figure 2.4 is representative.

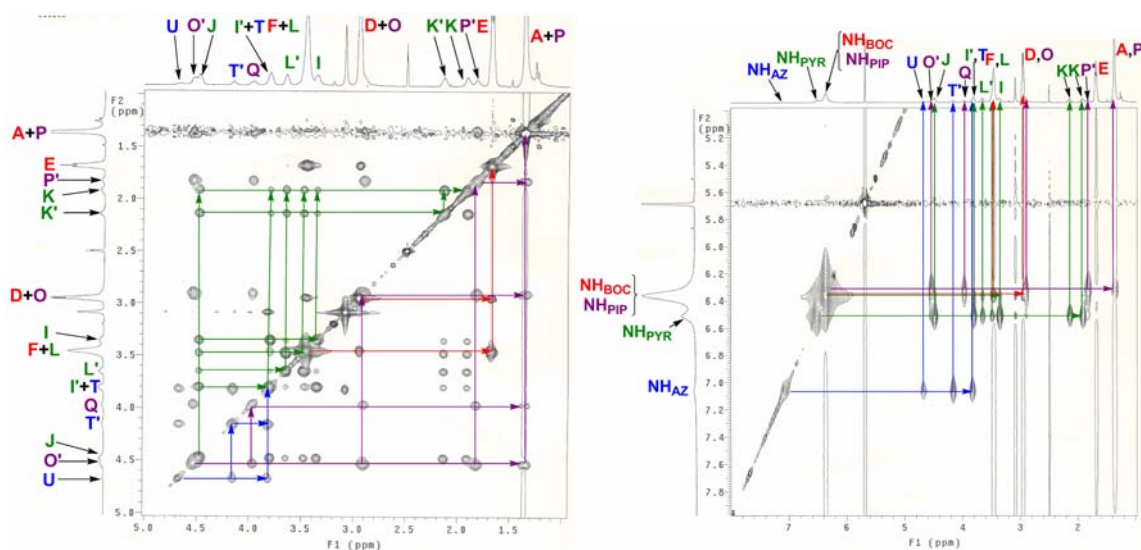


Figure 2.4. (^1H - ^1H) TOCSY spectrum of **2.8** in $\text{DMSO-}d_6$ at $75\text{ }^\circ\text{C}$.

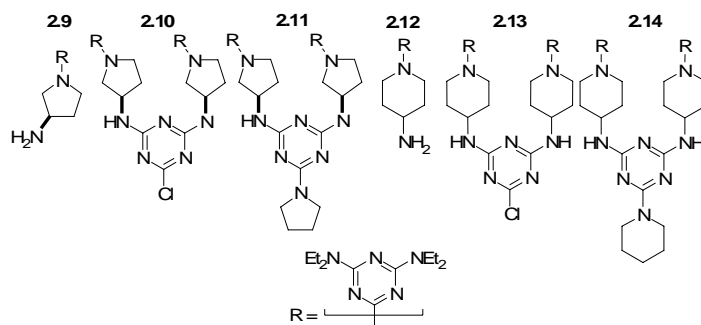


Figure 2.5 Model compounds used for assignment of NMR spectra of dendrimer intermediates.

The model compounds used to corroborate assignment are shown in Figure 2.5. These particular compounds, **2.9-2.14**, were chosen to provide insight into the position of the chemical shift for various protons of each linker. The diethylamino substituent was chosen due to its beneficial impact on solubility, NMR signatures, and symmetry which precludes the existence of rotamers that would have resulted had ethylamino groups been used. Proton spectra for each linker and comparison with the appropriate intermediate are found in Appendix A. All NMR spectra were taken in DMSO- d_6 for three reasons: 1) to observe the NH signals downfield from the rest of the resonances, 2) to sharpen the spectrum of the dendrimer in chloroform was very broad and complex with the NH signals upfield, and 3) the dendrimer did not show structural biases in deuterated methanol or chloroform. The discussion of the NMR spectra is divided into two parts. The first part addresses the upfield region of the spectra between 0.5 ppm and 5 ppm. The second part describes the exchangeable NH region of the spectra between 6.0 ppm and 8.5 ppm.

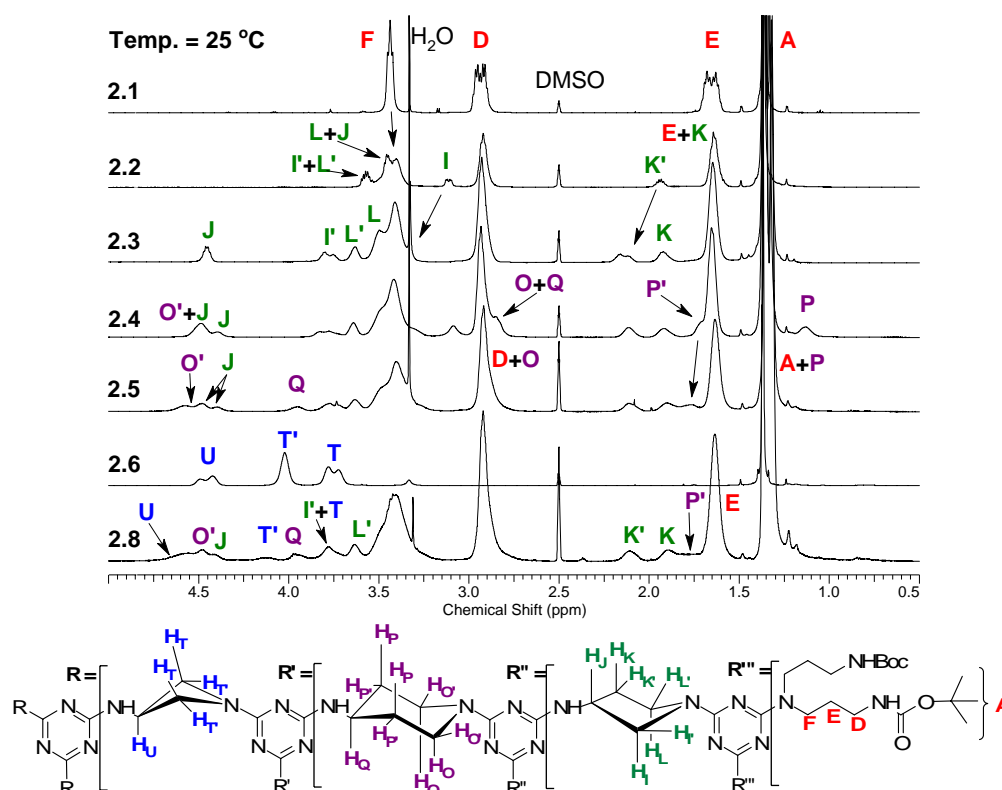


Figure 2.6. ^1H NMR spectra (0.5 – 5.0 ppm) of intermediates **2.1-2.6** and dendrimer **2.8**. Lines that shift as a result of the synthesis are reassigned in subsequent spectra. All spectra taken in $\text{DMSO-}d_6$ at 25 $^\circ\text{C}$. Omitted letters correspond to carbon atoms that do not bear hydrogen atoms.

The Upfield Region of the Spectra. Assigning the upfield region of the spectra is challenging due to broad lines and similar chemical shifts. However, the systematic appearances of lines, shifts of certain lines downfield upon reaction, and disparity in chemical shifts between axial and equatorial ring protons allows us to step through these spectra with an assignment that is ultimately corroborated by 2D NMR techniques and model compounds. These trends are shown in Figure 2.6. The discussion of these spectra is divided by linking diamine or group.

The Surface BOC group. Resonances corresponding to the BOC-protected triamine surface groups, $\mathbf{H}_{A,D-F}$, are a dominating feature of all the spectra. These resonances show little change in chemical shift over the course of the synthesis. While rotamers do not exist based on symmetry, slow rotation around the triazine-N bond make both environments of the surface group unique in the expected 1:1 ratio. These two environments are most discernable in the spectrum of monochlorotriazines, a feature that we attribute to the inductive effects of the chlorine atom giving rise to greater double bond character in the triazine-N bond. On replacement of chlorine with an amine linker, the lines no longer appear distinct (instead, a broad peak) except for the protons most sensitive to the two environments, \mathbf{H}_F .

The Aminopyrrolidine Linker. Intermediate **2.2** introduces pseudo-axial and pseudo-equatorial resonances, the latter of which more downfield than the former by ~ 0.5 ppm. Protons adjacent to a nitrogen atom appear between 3.2 and 3.6 ppm (\mathbf{H}_I and \mathbf{H}_L overlap at 3.6 ppm, \mathbf{H}_L and \mathbf{H}_J overlap at 3.45 ppm, \mathbf{H}_I appears at 3.2 ppm), while the aliphatic methylene resonances, $\mathbf{H}_{K,K'}$, have chemical shifts of 1.6, and 1.9 ppm, respectively. For **2.3**, most of the pyrrolidine protons are shifted downfield. Protons $\mathbf{H}_{J,L,I',K',K}$ can be unambiguously assigned separately from the rest of the resonances; the remaining resonances of the pyrrolidine ring, $\mathbf{H}_{L,I}$, overlap at 3.4 ppm with the \mathbf{H}_F resonance of the peripheral group. The existence of rotamers is seen for \mathbf{H}_I first in **2.3**, and then \mathbf{H}_J protons in **2.4**, but increasing broadness of lines precludes any discussion of changing rotamer populations based on these peaks alone. As expected the chemical

shift of \mathbf{H}_J shifts downfield by almost 1 ppm on substitution of the chlorine atom for a linking diamine.

The Aminopiperidine Group. The trends observed in the linker are more pronounced in the aminopiperidine group. Axial and equatorial protons of a methylene show greater differences in chemical shift. Protons adjacent to an amine ($\mathbf{H}_{O,O'Q}$) appear more downfield than more aliphatic methylenes $\mathbf{H}_{P,P'}$. Upon substitution of the chlorotriazine, \mathbf{H}_Q shifts ~ 1 ppm downfield. Broad lines are suggestive of rotamer populations, but these cannot be unambiguously identified from this region of the spectrum.

The Core. The spectrum of the protected core, **2.6**, reveals rotamers that become less evident in this region of the spectrum for the final dendrimer. Both the pseudo-axial and pseudo-equatorial protons of the azetidine ring can be distinguished and the protons proximate to the nitrogen see a more pronounced change in chemical shift on reaction that results from the attachment of a triazine ring.

Total correlated spectroscopy (TOCSY) correlations of **2.8** confirms the assignment (Figure 2.4). The cross-peaks between the 1-5 ppm (CH) region and 5-8 ppm (NH) region of the spectrum indicate protons common to a correlated spin system, or linking diamine. The only protons not correlated to any spin system are those of the tert-butyl protons of the surface group, \mathbf{H}_A . The spectrum shows the three methylene resonances and one carbamate resonance for the surface group (red), the seven CH resonances and one NH resonance for the pyrrolidine ring (green), the five CH resonances and one NH resonance of the piperidine ring (maroon), and the three CH resonances and one NH resonance of the azetidine ring (blue).

The Exchangeable NH Region of the Spectra. The region of the ^1H NMR spectra between 6 and 8.5 ppm displays a significant amount of structural complexity commencing with the NH protons of the carbamate group of intermediate **2.1** which appear as two discernable sets of peaks labeled in red as NH_{BOC} (Figure 2.7). We attribute this complexity to the *anti* and *syn* conformation of the carbamate group.⁷¹ The complexity of NH region increases with the incorporation of the pyrrolidine group of **2.2** as the set of NH peaks increases from two to at least three in a ratio of 8:7:1 (downfield to upfield). The complexity may arise from issues surrounding slow rotation around C-N bonds of both the carbamate group and the triazine-amine group. An exact assignment of these lines has not been made. This complexity is unaffected upon subsequent iteration to **2.3**. The NH_2 group of **2.2** is not observed in these spectra; it is expected upfield. The pyrrolidine region of **2.3** displays at least three peaks in a ratio of 13:6:1. These peaks are attributed to the existence of rotamers as shown in Figure 2.8. We have applied a *local stereochemistry* approach to describe the triazine rotamers using the *E,Z* nomenclature of amides (Figure 2.8).^{72,73}

Studies of atrazine reveal the barrier for interconversion is 16.5 kcal/mol in aprotic solvent with relative populations of the rotamers as $5(E_{\text{Et}}, E_{\text{iPr}}): 3(Z_{\text{Et}}, E_{\text{iPr}}): 3(E_{\text{Et}}, Z_{\text{iPr}}): 1(Z_{\text{Et}}, Z_{\text{iPr}})$ (Figure 2.8).^{74,75} According to the atrazine studies, the *E,E* rotamer is the most downfield and the *Z,Z* rotamer is the most upfield. By extrapolation, we assign the *E,E* rotamer as the major isomer in **2.3**. The carbamate moiety in **2.3** displays an NH ratio of 9:8:1, an insignificant change in populations from **2.2**.

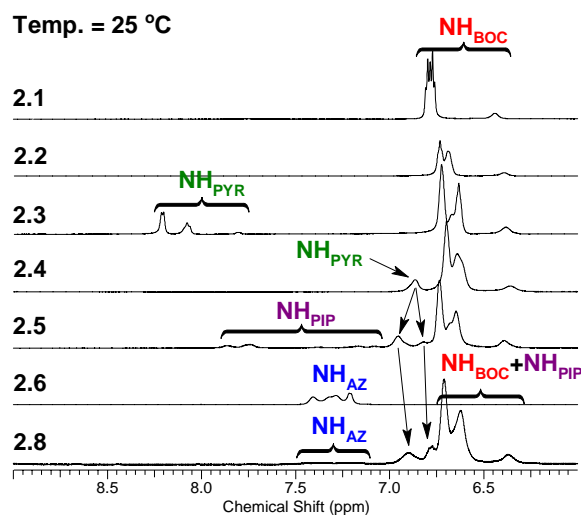


Figure 2.7. ^1H NMR spectra (6.0 – 9.0 ppm, NH region) of intermediates **2.1-2.6** and dendrimer **2.8**. Lines that shift as a result of the synthesis are reassigned in subsequent spectra. All spectra taken in $\text{DMSO-}d_6$ at 25 °C.

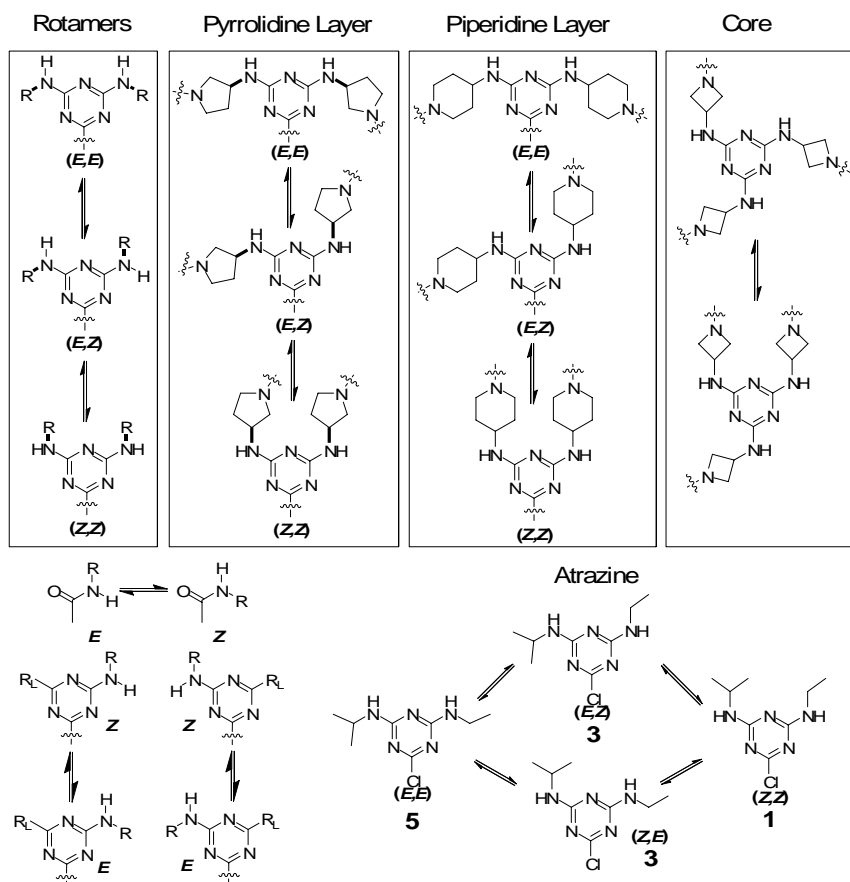


Figure 2.8. Rotamers of the pyrrolidine, piperidine and azetidine groups. Rotamers of atrazine shown with rotameric ratio below each rotamer.

Iteration of **2.3** to **2.4** reveals the pyrrolidine NHs shift upfield. Substitution of the chlorine atom by 4-aminopiperidine removes the deshielding effects the chlorine had on the pyrrolidine NH. The NH₂ of **2.4** is not observed in these spectra, it is expected upfield. The three major resonances of the carbamate moiety remain but with a slight increase in the two main populations, 12:10:1. Spectra show that only one pyrrolidine NH is observed. A COSY spectrum identifies one pyrrolidine NH resonance buried under the most downfield carbamate NH resonance at 6.70 ppm. This could explain the slight increase in the carbamate NH populations.

Intermediate **2.5** provides another layer of complexity to the rotamer populations. The carbamate NH populations remain largely unchanged. The ratio of 7:6:1 falls within the percentage previously seen in **2.2** and **2.3** but not **2.4**, supporting our belief that the slight increase in the population from **2.4** was the result of overlap of the pyrrolidine NH. Two pyrrolidine NH resonances attributed to the (*E,E*) and (*E,Z*) conformations can be identified in a ratio of 2.5:1. We presume that the (*Z,Z*) rotamer exists below the limits of detection for the spectrometer: it was not observed in the COSY spectrum. The appearance of the five isomers of piperidine in **2.5**, adds the most complexity to this discussion. Although we were unable to assign rotamers to these resonances, COSY crosspeaks verify the resonances as piperidine NHs. The five sets of peaks suggest that the isomerism and conformational preferences are being communicated through the dendrimer as is seen with Parquette's systems, or that additional sources of isomerism (i.e. ring conformations) are emerging.

Analysis of the spectrum of **2.6** shows four sets of resonances for the azetidine NH (Figure 2.7) in a 1:1:1:1 ratio. Figure 2.8 displays two primary rotamers for this molecule. Subsequent reaction of the core with **2.5** forms **2.8**. In **2.8**, the broadness of the azetidine NHs precludes us from obtaining a reliable population ratio. Through the use of a TOCSY⁷⁶ spectrum, we were able to confirm that indeed the azetidine NHs were present. The ratio for the pyrrolidine NHs in **2.8** changes significantly from those observed for **2.3-2.5**. The rotamer population shifts to favor the (*E,Z*) rotamer, 6.77 ppm, over the (*E,E*) rotamer, 6.90 ppm, in ratio of 1.3(*E,Z*):1(*E,E*). The (*Z,Z*) rotamer was not observed in the TOCSY spectrum of **2.8**. The remaining NHs resonances have a ratio of 9:9:1. Though the majority of the population belongs to the carbamate NH, the piperidine NH is also overlapped within these resonances. This precludes us from identifying how the dendrimer affects the piperidine NH populations. Regardless, this final observation is significant as it supports the emergence of peripheral crowding of surface groups and emergence of a “globular” or “hard sphere” architecture.

Conclusions

With the use of competition studies, we have been able to quantify the relative nucleophilicity of amines towards a model monochlorotriazine effectively expanding our range to 320x. From these data, three new diamine linkers were designed and used to synthesize a melamine dendrimer. Each linker offers interesting features that can be exploited in future work. Aminoazetidine (**L1**) offers a highly reactive and sterically unencumbered amine that might find use in situations where piperidine-type amines are unreactive or sluggish. Aminopyrrolidine (**L2**) offers opportunities to explore chiral

environments in these dendrimers. Aminopiperidine (**L3**) offers an inexpensive linker that aligns with our current reliance on aminomethylpiperidine groups. In addition, these linkers convey spectroscopically unique signatures to different regions of the dendrimer architecture; an effect only rarely observed in related architectures.^{27,35,62-65}

While a more rigorous discussion of conformational analysis of this dendrimer is presented in the following paper, clues from these 1D spectra provide preliminary insight into structure. The complexity of the NH-region of the spectra and broad features observed in upfield lines suggests that a rich population of rotamers exists. Through the iteration of the dendrimer synthesis, the carbamate NH populations do not change. The most significant changes were observed from the pyrrolidine NH populations. An initial 2:1 ratio of (*E,E*):(*E,Z*) expected for a conformationally unhindered molecule shifted a 1:1.3 ratio indicative of a sterically congested architecture.

Experimental Section

Chemicals were purchased from Aldrich and Acros and used without further purification. All solvents were ACS grade and used without further purification. NMR spectra were recorded on an Inova 500 MHz spectrometer in CDCl₃ or DMSO-*d*₆. All mass spectral analyses were carried out by the Laboratory for Biological Mass Spectrometry at Texas A&M University.

2D TOCSY NMR. The ¹H-¹H TOCSY⁷⁶ spectra were performed using the same 500 MHz spectrometer. The data was collected using a $\pi/2$ pulse width of 7.3 μ s, a relaxation delay of 10 s, 4.5 kHz spectral window and 0.228 s acquisition time; a spin-

lock pulse was applied for a period of 0.046 s with a spin-lock field of 5.4 kHz with MLEV-17 modulation; 16 transients were averaged for each of the 2 x 256 increments using the States method⁷⁷ of phase sensitive detection. The data were zero-filled to a 1024 x 1024 data matrix before Fourier transformation.

Typical competition reaction. Pyrrolidine (107 mg, 1.5 mmol) and piperidine (128 mg, 1.5 mmol) were added to a vial with THF (10 mL).⁷⁸ To this solution dimorpholino-monochlorotriazine (DMTA, 143 mg, 0.5 mmol) was added and the reaction was left to stir for 18 hr. TLC confirmed the absence of DMTA for all reactions. The solvent was then removed and the residue was passed through a silica gel column containing DCM:Methanol (9:1) to remove excess amines. Fractions containing UV-active material that were not positive to ninhydrin staining (those excluding benzylic amines) were combined and analyzed using ¹H NMR.

Dimorpholino-monochlorotriazine (DMTA). To a solution of cyanuric chloride (10.3 g, 55.8 mmol) in THF (250 mL) at 0 °C, morpholine (9.70 mL, 111 mmol) and Hunig's base (20.0 mL, 115 mmol) were added. After six hours, the solution was filtered and the solvent removed. The crude product was dissolved in hot methanol and precipitated by cooling. The product was reprecipitated from methanol again yielding a white solid (12.6 g, 79 %). ¹H NMR (300 MHz, CDCl₃, δ): 3.78 (br m, 8H), 3.70 (t, *J* = 4.95 Hz, 8H). ¹³C NMR (75 MHz, CDCl₃, δ): 171.4, 164.7, 66.9, 44.1; MS (ESI) mass calc'd for C₁₆H₃₃N₃O₄ = 285.73; found 286.3 [M+H]⁺.

Bis(3-BOC-3-aminopropyl)amine. A solution of BOC-ON (2-(*tert*-butoxycarbonyloxyimino)-2-phenylacetonitrile) (40.11 g, 162.9 mmol) in THF (320 mL)

was added drop wise over a period of 2 h to an ice – bath cooled solution of bis(3-aminopropyl)amine (11.62 mL, 81.47 mmol) and Hunig’s base (43.0 mL, 247 mmol) in THF (65 mL). The reaction warmed to room temperature over a period of 4 h. The solvent was subsequently removed by reduced – pressure evaporation. The yellow – green liquid residue was dissolved in DCM and washed with three portions of 5% (w/v) NaOH. The organic layer was dried over MgSO₄, filtered, and the solvent removed by reduced – pressure evaporation to give thick clear oil. The product was precipitated from petroleum ether to give a white solid (22.85 g, 84.6 %). ¹H NMR (300 MHz, CDCl₃, δ): 5.3 (brs, NH), 3.16 (br m, 4H), 2.61 (t, *J* = 6.6 Hz, 4H), 1.61 (m, 4H), 1.4 (s, 18H); ¹³C NMR (75 MHz, CDCl₃, δ): 156.4, 79.2, 47.6, 39.0, 29.9, 28.6. MS (ESI) mass calc’d for C₁₆H₃₃N₃O₄ = 331.45; found 332.26 [M+H]⁺.

Intermediate 2.1. A solution of bis(3-Boc-3-aminopropyl)amine (12.3 g, 37.1 mmol) and Hunig’s Base (20 mL, 115 mmol) in THF (100 mL) was added to a solution of cyanuric chloride (3403 mg, 18.45 mmol) in THF (30 mL) at room temperature. After stirring overnight, the solvent was removed by reduced pressure evaporation to give an oil. The oil was dissolved in 70 mL DCM and washed with three 70 mL portions (5 %) HCl solution, four 70 mL portions (5 %) NaOH solution, and three 70 mL portions of brine solution. The organic layer was dried over MgSO₄ and filtered. The solvent was removed from the filtrate to give off-white colored foam. The foam was dissolved in DCM and a silica gel column was performed using a DCM:Methanol (50:1) solvent system. Fractions containing product, as determined by TLC, were combined and had their solvent removed by reduced pressure evaporation to give white foam

(10083.6 mg, 70.6 %). ^1H NMR (500 MHz, DMSO- d_6 , δ): 6.8 (m, NH), 3.42 (t, $J = 7.0$ Hz, 8H), 2.92 (m, 4H), 1.64 (m, 4H), 1.4 (s, 36H). ^{13}C NMR (125 MHz, DMSO- d_6 , δ): 169.1, 164.7, 156.5, 156.4, 78.4, 78.4, 55.8, 45.9, 45.3, 38.8, 38.4, 29.2, 28.9, 28.6; MS (ESI) mass calc'd for $\text{C}_{35}\text{H}_{64}\text{ClN}_9\text{O}_8 = 774.39$; found 774.48 $[\text{M}+\text{H}]^+$.

Intermediate 2.2. A solution of **2.1** (10.262 g, 13.251 mmol) in THF (50 mL) was added dropwise to a solution of *R*-3-aminopyrrolidine (2.60 mL, 29.7 mmol) in THF (10 mL) at room temperature. After stirring overnight, the solvent was removed by reduced pressure evaporation to give red foam. The foam was dissolved in DCM and passed through a silica gel column using DCM:Methanol (19:1). Fractions containing product, as determined by TLC, were combined and solvent removed yielding pale yellow foam (10.32 g, 94.5 %). ^1H NMR (500 MHz, DMSO- d_6 , δ): 6.7 (br m, NH), 6.4 (br s, NH), 3.32-3.59 (br m, 12H), 3.15 (m, 1H), 2.92 (m, 8H), 1.96 (m, 1H), 1.64 (m, 9H), 1.4 (s, 36H). ^{13}C NMR (125 MHz, DMSO- d_6 , δ): 165.2, 164.1, 156.5, 78.4, 54.2, 51.3, 44.9, 44.7, 44.6, 38.9, 38.7, 38.4, 34.3, 29.3; MS (ESI) mass calc'd for $\text{C}_{35}\text{H}_{64}\text{ClN}_9\text{O}_8 = 823.56$; found 824.59 $[\text{M}+\text{H}]^+$, 312.74 $[\text{M}+2\text{H}]^{+2}$, 262.71 $[\text{M}+2\text{H}]^{+2}$, 212.68 $[\text{M}+2\text{H}]^{+2}$.

Intermediate 2.3. A solution of **2.2** (5.95 g, 7.22 mmol) and Hunig's base (4.0 mL, 23 mmol) in THF (30 mL) was added to a solution of cyanuric chloride (634 mg, 3.44 mmol) in THF (5 mL) at room temperature. The reaction was heated to 40 °C overnight. The solvent was removed by reduced pressure evaporation to give a pale yellow foam. The foam was dissolved in DCM and passed through a silica gel column using DCM:Methanol (30:1). Fractions containing product, as determined by TLC, were combined and solvent removed yielding a pale yellow foam (5.373 g, 88.8 %). ^1H NMR

(500 MHz, DMSO- d_6 , δ): 6.78 (br s, NH), 6.73 (br s, NH), 6.7 (br s, NH), 4.48 (br m, 2H), 3.80 (br m, 2H), 3.66 (br m, 2H), 3.4-3.6 (br m, 24H), 2.96 (br m, 16H), 2.17 (br m, 2H), 1.94 (br m, 2H), 1.68 (br m, 16H), 1.4 (s, 36H), 1.36 (s, 36H). ^{13}C NMR (125 MHz, DMSO- d_6 , δ): 169.2, 168.7, 166.0, 165.2, 164.1, 156.5, 156.3, 78.4, 78.3, 51.2, 50.9, 50.6, 50.5, 45.0, 44.6, 38.9, 38.6, 38.4, 31.5, 31.3, 29.2, 29.1; MS (MALDI) mass calcd for $\text{C}_{81}\text{H}_{144}\text{ClN}_{25}\text{O}_{16}$ = 1759.62; found 1760.21 $[\text{M}+\text{H}]^+$, 1783.18 $[\text{M}+\text{Na}]^+$, 1799.15 $[\text{M}+\text{K}]^+$, 1659.12 $[\text{M}+\text{H}-\text{Boc}]^+$, 1560.04 $[\text{M}+\text{H}-2 \text{ Boc}]^+$, 1359.00 $[\text{M}+\text{H}-4 \text{ Boc}]^+$.

Intermediate 2.4. A solution of **2.3** (7.00 g, 3.98 mmol) in THF (15 mL) was added dropwise to a solution of 4-aminopiperidine (1.26 mL, 12.0 mmol) in THF (5 mL) at room temperature. After reacting overnight, the solvent was removed by reduced pressure evaporation and the residue passed through a silica gel column using DCM:Methanol (19:1). Fractions containing product, as determined by TLC, were combined and solvent removed yielding white foam (6474.4 mg, 89.3 %). ^1H NMR (500 MHz, DMSO- d_6 , δ): 8.20 (br s, NH), 8.08, (br s, NH), 7.80 (br s, NH), 6.72 (br s, NH), 6.63 (br s, NH), 6.38 (br s, NH), 4.45 (br m, 2H), 3.80 (br m, 1H), 3.75 (br m, 1H), 3.63 (br m, 2H), 3.50 (br m, 2H), 3.41, (br m, 16H), 3.36 (br m, 2H), 2.93 (br m, 16H), 2.16 (br m, 1H), 2.11 (br m, 1H), 1.65 (br m, 16H), 1.36 (s, 44H), 1.32 (s, 28H). ^{13}C NMR (125 MHz, DMSO- d_6 , δ): 168.2, 167.8, 165.2, 165.0, 164.7, 164.2, 163.2, 155.5, 155.4, 155.3, 155.1, 77.4, 77.3, 50.2, 49.9, 49.7, 49.5, 44.0, 43.6, 37.9, 37.6, 37.4, 30.6, 30.3, 28.2, 28.1; MS (MALDI) mass calcd for $\text{C}_{86}\text{H}_{155}\text{N}_{27}\text{O}_{16}$ = 1823.32; found 1824.00 $[\text{M}+\text{H}]^+$, 1845.97 $[\text{M}+\text{Na}]^+$, 1861.94 $[\text{M}+\text{K}]^+$, 1723.96 $[\text{M}+\text{H}-\text{Boc}]^+$.

Intermediate 2.5. A solution of **2.4** (5.28 g, 2.89 mmol) and Hunig's base (1.5 mL, 8.6 mmol) in THF (5 mL) was added to a solution of cyanuric chloride (243 mg, 1.31 mmol) in THF (5 mL) at room temperature. The reaction was heated to 40 °C and allowed to react for 2 days. The solvent was removed by reduced – pressure evaporation and the residue was passed through a silica gel column using DCM:MeOH (25:1). Fractions containing product, as determined by TLC, were combined and solvent removed yielding a pale yellow foam (4.31 mg, 87 %). ¹H NMR (500 MHz, DMSO-d₆, δ): 7.86 (br s, NH), 7.75 (br s, NH), 6.95 (br s, NH), 6.82 (br s, NH), 6.73 (br s, NH), 6.67 (br s, NH), 6.64 (br s, NH), 6.38 (br s, NH), 4.56 (br m, 2H), 4.47 (br m, 2H), 4.39 (br m, 2H), 3.94 (brs, 1 H), 3.77 (br m, 2 H), 3.71 (br s, 1 H), 3.62 (br m, 4H), 3.4 -3.6 (br m, 40H), 2.91 (br m, 32H), 2.11 (br m, 4H), 1.89 (br m, 2H), 1.76 (br m, 2H), 1.62 (br m, 33H), 1.35 (s, 92H), 1.31 (s, 52H). ¹³C NMR (125 MHz, DMSO-d₆, δ): 165.6, 164.2, 163.2, 155.6, 155.4, 155.1, 77.4, 50.7, 49.6, 49.1, 48.1, 47.7, 47.4, 44.0, 43.8, 43.6, 41.4, 38.0, 37.6, 37.4, 31.0, 30.7, 28.2; MS (MALDI) mass calcd for C₁₇₅H₃₀₈ClN₅₇O₃₂ = 3758.13; found 3759.02 [M+H]⁺, 3780.95 [M+Na]⁺, 3795.93 [M+K]⁺, 3657.97 [M+H-Boc]⁺, 3557.89 [M+H-2 Boc]⁺.

Intermediate 2.6. 1-Boc-3-amino-azetidine (172 mg, 0.999 mmol) and Hunig's base (DIPEA, diisopropylethylamine) (0.690 mL, 1.33 mmol) was added to a stirred solution of cyanuric chloride (61.4 mg, 0.333 mmol) in THF (2 mL) at room temperature. The reaction was then heated to 70 °C for seven days. The solvent was removed by reduced pressure evaporation and the residue passed through a silica gel column using (20:1:3) DCM:MeOH:Ethyl Acetate to give a white solid (186.4 mg, 94.6

%). ^1H NMR (500 MHz, DMSO- d_6 , δ): 7.3 (br m, NH), 4.45 (br m, 3H), 4.02 (s, 6H), 3.74 (br m, 6H), 1.4 (s, 27H); ^{13}C NMR (125 MHz, DMSO- d_6 , δ): 166.1, 165.9, 156.5, 156.3, 79.4, 57.4, 56.6, 41.0, 29.0; MS (ESI) mass calc'd for $\text{C}_{27}\text{H}_{45}\text{N}_9\text{O}_6 = 591.7$; found 592.37 $[\text{M}+\text{H}]^+$, 614.33 $[\text{M}+\text{Na}]^+$.

Dendrimer (2.8). One milliliter of a 1:1 mixture of DCM:TFA was added to a solution of **2.6** (54.0 mg, 0.0912 mmol) in DCM (1 mL). After an hour, the solvent was removed by reduced pressure evaporation. The residue was redissolved several times in a MeOH/triethylamine (TEA) solution and evaporated under reduced – pressure. The residue was dissolved in THF (1.5 mL) followed by the addition of BEMP resin (0.508 g, ~ 1.118 mmol). A solution of **5** (3.67 g, 0.976 mmol) in THF (8.5 mL) was added. The slurry was heated to 70 °C and allowed to react for 7 days. After 7 days, the reaction was allowed to cool and then filtered. The filter cake was washed several times with THF to recover as much material as possible. The solvent from the filtrate was removed by reduced – pressure evaporation and residue passed through a silica gel column using (25:1:10) CHCl_3 :MeOH:Ethyl Acetate (EtOAc). Once the spot for compound **5** passed through, the solvent system was switched to (20:1:1) CHCl_3 :MeOH:EtOAc to collect product. Fractions containing pure product, as determined by TLC, were combined and solvent removed to give white foam (378 mg, 36.2 %). ^1H NMR (500 MHz, DMSO- d_6 , δ): 7.37 (br s, NH), 7.18, (br s, NH), 6.89 (br s, NH), 6.71, (br s, NH), 6.62 (br s, NH), 6.37 (br s, NH), 4.56 (br m, 15H), 4.47 (br m, 6H), 4.40 (br m, 6H), 4.11, (br m, 6H), 3.93 (br m, 6H), 3.77 (br m, 18H), 3.63 (br m, 12H), 3.55 – 3.25 (br m, 120H), 2.91 (br m, 108H), 2.10 (br m, 12H), 1.88 (br m, 12H),

1.75 (br m, 12H), 1.63 (br m, 96H), 1.35 (s, 271H), 1.31 (s, 173H). ^{13}C NMR (125 MHz, CDCl_3 , δ): 165.9 (br), 165.3, 165.1, 164.8, 164.1, 156.2, 156.0, 79.3, 79.1, 78.9, 52.0 (br), 50.1 (br), 48.3, 47.9, 44.1, 43.1 (br), 42.1 (br), 41.9 (br), 39.3, 38.2, 37.0 (br), 36.6 (br), 32.4 (br), 31.9 (br), 28.6, 28.3, 27.9, 27.8; MS (MALDI) mass calcd for $\text{C}_{537}\text{H}_{942}\text{N}_{180}\text{O}_{96} = 11449.44$; found 11479.26.

Bis(Diethylamino)-monochlorotriazine (BDMC). To a solution of cyanuric chloride (4.04 g, 21.9 mmol) in THF (90 mL) at 0 °C, diethylamine (4.70 mL, 45.4 mmol) and Hunig's base (17 mL, 98 mmol) were added. After an hour, the solution was allowed to warm to room temperature. After 1 day, the solvent was removed by reduced – pressure evaporation leaving a yellow oil. This oil was passed through a silica gel column using (10:1) Hexanes (Hx): EtOAc. Fractions containing pure product were combined to give a clear, colorless thick oil (5.54 g, 98 %). ^1H NMR (500 MHz, CDCl_3 , δ): 3.55 (q, $J = 7.1$ Hz, 4H), 3.51 (q, $J = 7.1$ Hz, 4H), 1.15 (t, $J = 7.1$ Hz, 12H). ^{13}C NMR (125 MHz, CDCl_3 , δ): 169.1, 164.1, 41.8, 41.5, 13.5, 12.9; MS (ESI) mass calc'd for $\text{C}_{11}\text{H}_{20}\text{ClN}_5 = 257.14$; found 258.13 $[\text{M}+\text{H}]^+$.

Model 2.9. A solution of **BDMC** (868 mg, 3.37 mmol) in THF (8 mL) was added to a solution of *R*-3-aminopyrrolidine (650.0 μL , 7.42 mmol) in THF (5 mL). After one day, the solvent was removed by reduced – pressure evaporation and the residue passed through a silica gel column using (10:1) Hx:EtOAc until the first two spots passed through. The solvent was then switched to (8:2:1 %) DCM:MeOH: NH_4OH to collect the product. Fractions containing pure product were combined and solvent removed to give a yellow oil. Colorless crystals began to form after allowing the oil to stand in open

air. After some time, the crystals were filtered (965 mg, 93.2 %). ^1H NMR (500 MHz, DMSO- d_6 , δ): 3.36 – 3.57 (m, 12H), 3.06 (dd, 1H), 1.94 (m, 1H), 1.59 (m, 1H), 1.08 (t, $J = 6.9$ Hz, 12H). ^{13}C NMR (125 MHz, CDCl_3 , δ): 164.6, 164.3, 54.1, 51.2, 44.1, 41.0, 34.5, 13.6; MS (ESI) mass calc'd for $\text{C}_{15}\text{H}_{29}\text{N}_7 = 307.25$; found 308.24 $[\text{M}+\text{H}]^+$.

Model 2.10. A solution of **model 2.9** (707 mg, 2.30 mmol) and Hunig's base (0.500 mL, 2.87 mmol) in THF (2 mL) was added to a solution of cyanuric chloride (128.6 mg, 0.6973 mmol) in THF (1 mL) at room temperature. The reaction was subsequently heated to 50 °C where it was allowed to react for several days. The solvent was removed by reduced – pressure evaporation and the residue passed through a silica gel column using (5:1) Hx:EtOAc. Fractions containing pure product were combined and had their solvent removed to give a colorless foam (479.6 mg, 94.7 %). ^1H NMR (500 MHz, DMSO- d_6 , δ): 8.14 (d, NH), 8.04 (d, NH), 8.00 (d, NH), 7.72 (br m, NH), 4.39 (m, 2H), 3.80 (m, 1H), 3.70 (m, 1H), 3.60 (br m, 2H), 3.48 (m, 16H), 3.43 (m, 2H), 3.37 (m, 2H), 2.16 (m, 2H), 1.92 (m, 2H), 1.08 (t, 24H). ^{13}C NMR (125 MHz, CDCl_3 , δ): 168.9, 165.5, 164.5, 164.3, 51.6, 51.3, 50.8, 50.6, 43.7, 41.0, 31.8, 31.5, 13.5; MS (ESI) mass calc'd for $\text{C}_{33}\text{H}_{56}\text{ClN}_{17} = 725.46$; found 726.53 $[\text{M}+\text{H}]^+$.

Model 2.11. A solution of **model 2.10** (154.8 mg, 0.2131 mmol) in THF (1 mL) was added to a solution of pyrrolidine (100 μL , 1.2 mmol) in THF (1 mL) at room temperature. After allowing to react overnight, the solvent was removed by reduced – pressure evaporation and the residue passed through a silica gel column using (9:1) DCM:MeOH. Fractions containing pure product were combined and had their solvent removed to give a colorless foam (160.1 mg, 98.7 %). ^1H NMR (500 MHz, DMSO-

d_6 , δ): 6.92 (NH), 6.78 (NH), 6.67 (NH), 4.39 (m, 2H), 3.87 (m, 1H), 3.78 (m, 1H), 3.60 (m, 2H), 3.47 (m, 16H), 3.38 (m, 6H), 3.25 (m, 2H), 2.10 (m, 2H), 1.91 (m, 2H), 1.82 (m, 4H), 1.07 (m, 24H). ^{13}C NMR (125 MHz, CDCl_3 , δ): 164.6, 164.4, 51.8, 50.3, 46.1, 43.9, 41.0, 31.9, 25.4, 13.6; MS (MALDI) mass calc'd for $\text{C}_{37}\text{H}_{64}\text{N}_{18}$ = 760.56; found 761.46 $[\text{M}+\text{H}]^+$.

Model 2.12. A solution of **BDMC** (814 mg, 3.16 mmol) in THF (8 mL) was added to a solution of 4-aminopiperidine (1.00 mL, 9.52 mmol) in THF (5 mL). After one day, the solvent was removed by reduced – pressure evaporation and the residue passed through a silica gel column using (19:1) DCM:MeOH until the first spot passed through. The solvent system was then switched to (8:2:1 %) DCM:MeOH: NH_4OH . Fractions containing pure product were combined and had their solvent removed to give a pale yellow solid (739 mg, 72.8 %). ^1H NMR (500 MHz, CDCl_3 , δ): 4.46 (m, 2H), 3.47 (q, J = 7.0 Hz, 8H), 2.82 (m, 2H), 2.76 (m, 1H), 1.69 (m, 2H), 1.08 (m, 14H). ^{13}C NMR (125 MHz, CDCl_3 , δ): 165.4, 164.9, 49.7, 42.1, 41.1, 35.4, 13.6; MS (ESI) mass calc'd for $\text{C}_{16}\text{H}_{31}\text{N}_7$ = 321.26; found 322.28 $[\text{M}+\text{H}]^+$.

Model 2.13. A solution of **model 2.12** (700 mg, 2.2 mmol) and Hunig's base (0.600 mL, 3.44 mmol) in (1:1) THF:DCM (2 mL) was added to a solution of cyanuric chloride (132.5 mg, 0.7186 mmol) in (1:1) THF:DCM (1 mL) at room temperature. The reaction was subsequently heated to 50 °C where it was allowed to react for several days. The solvent was removed by reduced – pressure evaporation and the residue passed through a silica gel column using (10:1) Hx:EtOAc. Fractions containing pure product were combined and had their solvent removed to give a colorless foam (526 mg, 97.1 %). ^1H

NMR (500 MHz, DMSO- d_6 , δ): 7.87 (d, NH), 7.78 (d, NH), 7.71 (d, NH), 7.38 (d, NH), 4.55 (m, 4H), 3.92 (m, 2H), 3.47 (m, 16H), 2.86 (m, 4H), 1.79 (m, 4H), 1.36 (m, 4H), 1.08 (m, 24H). ^{13}C NMR (125 MHz, CDCl_3 , δ): 169.6, 168.8, 165.4, 165.2, 164.9, 49.1, 48.6, 42.0, 41.9, 41.7, 41.2, 32.2, 31.9, 31.8, 13.6; MS (ESI) mass calc'd for $\text{C}_{35}\text{H}_{60}\text{ClN}_{17}$ = 753.49; found 754.59 $[\text{M}+\text{H}]^+$.

Model 2.14. A solution of **model 2.13** (155.7 mg, 0.2063 mmol) in THF (1 mL) was added to a solution of piperidine (110 μL , 1.1 mmol) in THF (1 mL) at room temperature. After allowing to react overnight, the solvent was removed by reduced – pressure evaporation and the residue passed through a silica gel column using (9:1) DCM:MeOH. Fractions containing pure product were combined and had their solvent removed to give a colorless foam (153.3 mg, 92.5 %). ^1H NMR (500 MHz, DMSO- d_6 , δ): . ^{13}C NMR (125 MHz, CDCl_3 , δ): 165.5, 164.9, 48.2, 44.2, 42.1, 41.1, 32.4, 26.0, 25.1, 13.6; MS (ESI) mass calc'd for $\text{C}_{40}\text{H}_{70}\text{N}_{18}$ = 802.6; found 803.51 $[\text{M}+\text{H}]^+$.

CHAPTER III

USING NMR SPECTROSCOPY TO PROBE THE CHOREOGRAPHY OF A DENDRIMER DANCE*

Introduction

Since the first reported synthesis of dendrimers,^{3,4} there have been many efforts to determine the conformation of the macromolecules in solution using both experiment and theory.^{1,6-41,79,80} One of the most straightforward questions to ask is, “Where are the groups on the periphery (the so-called surface or end groups)?” Using a self consistent-field model, de Gennes and Hervet proposed that the dendrimer extends outwardly from the core having all of the end groups on or near the periphery of the molecule (*i.e.*, dense shell).⁶ In contrast, Lescanec and Muthukumar’s simplified kinetic model using a computer simulation of dendritic growth suggested the maximum density is between the assumed dense core and the periphery of the dendrimer as a result of the backfolding of the chain ends.⁸ A more recent self consistent-field model by Boris and Rubinstein supports the dense core model: density decreased monotonically from the center of the molecule.⁹ Naylor et al. used computer-assisted molecular modeling to infer that as the size increases, the dendrimer’s shape progresses from an open structure to a closed spheroid with well-developed cavities and a dense surface.⁷ Monte Carlo calculations performed by Mansfield and Klushin found the chain ends to be distributed throughout

*Reproduced with permission from Moreno, K.X., Simanek, E.E. *Macromolecules*, submitted for publication. Unpublished work copyright 2007 American Chemical Society.

the structure and revealed a density maximum midway between the center of mass and the periphery.¹⁰ Also using Monte Carlo calculations, Welch and Muthukumar reported that by varying the ionic strength of the solvent, a reversible transition between a dense core and dense shell structure could be achieved.¹¹ Molecular dynamics (MD) simulations of dendrimers that incorporate solvent effects have been performed by Murat and Grest.¹² Their model predicts significant backfolding of the chain ends and a high density area located near the core for all independent of the solvent quality. Their model predicts an overall increase in dendrimer density with decreasing solvent quality. More recently, MD simulations performed in explicit solvent have suggested that dendrimer can backfold in solution.^{13,14} In summary, most of the theoretical studies suggest that backfolding is a common process of dendrimers.

Experimental evidence for backfolding has been achieved using various techniques.^{1,15-36,79,80} In poly(amidoamine) (PAMAM) dendrimers, Meltzer et al. demonstrated that the chain dynamics did not change dramatically up to the tenth generation using NMR spectroscopy.¹⁶ They conclude that the branches backfold to some extent to relieve steric crowding based on ²H NMR.¹⁷ More recently, Chen and co-workers demonstrated that upon changing the pH of the solution, a conformational change can be induced.²² Unfortunately, the authors could not determine what degree of backfolding, if any, was occurring in their system. In addition to PAMAM dendrimers, polyarylether dendrimers have also been examined. Mourey et al. studied polyaryl ether dendrimers using size exclusion chromatography and differential viscometry.²⁴ They found that the hydrodynamic radii increased nearly linearly with dendrimer generation

and a maximum in the intrinsic viscosity as a function of molecular weight was found. More recently, De Backer and co-workers came to similar results using fluorescence depolarization measurements.²⁵ Both of these studies are in qualitative agreement with the theoretical study of Lescanec and Muthukumar⁸ in which the end groups can be found throughout the dendrimer volume, *i.e.* backfolding occurs. Using rotational-echo double-resonance (REDOR) NMR, Wooley et al. was able to show that backfolding occurs in the solid state.²⁶ Additionally, Gorman and co-workers were able to establish that the end groups of polyaryl ether dendrimers come in close proximity to the core.²⁷ Their studies were performed using a paramagnetic core and measuring the spin-lattice relaxation (T_1) times of the molecule. Backfolding was attributed to be the major cause of the very rapid electronic energy transfer in polyaryl ether dendrimers.²⁸

Using viscometry and small-angle neutron-scattering (SANS) measurements of both nitrile and amine terminated poly(propylene imine) (PPI) dendrimers, Scherrenberg et al. found a linear relationship between the radius of the dendrimer and its generation number.²⁹ This linear relationship was independent of the type of end group or solvent used. These results correlate well with the theoretical results of Murat and Grest¹² indicating that PPI dendrimers are flexible with a relatively uniform density distribution resulting from some degree of backfolding. More recently, an extensive SANS study demonstrated that the maximum density is located in the center of the molecule and that the end groups are backfolded.³⁰ The ‘dendritic box’ synthesized by Jansen et al. takes advantage of the end group backfolding to encapsulate guest molecules.³¹ Crystal data later provided direct evidence of the end groups backfolding via hydrogen-bond

interactions.³³ Chai and co-workers performed an extensive NMR study of PPI dendrimers finding evidence for backfolding using 2D NOESY³⁴ and interactions between chloroform and dendrimer.³⁵ Their results provide further evidence of the flexibility of PPI dendrimers: they observed either a collapsed (backfolded) or extended conformation depending on the solvent used.

The use of NMR to study biomolecules, such as proteins, is a well-established and powerful tool. However, it is difficult to apply these strategies to dendrimers due to the degeneracies of signals resulting from the repetitive nature of the macromolecule. The ability to incorporate unique spectral signatures on the end groups greatly facilitates inquiry into a fundamental question, backfolding. Still, size, morphology and dynamics of dendrimers have been probed in a limited number of systems. Studying T_1 and spin-spin relaxation (T_2) times of PAMAM dendrimers allowed Meltzer et al. determine that there is a gradual increase in segment density and that the terminal groups are not densely packed.^{16,17} By studying the ^{13}C T_1 times of a PPI dendrimer with both hydrophilic and hydrophobic end groups, Pan and Ford were able to determine that the conformation may change by varying the solvent.³⁶ Multi-dimensional NMR techniques have been used to characterize dendrimers, determine their conformation and to observe host-guest interactions within them. Chai et al. used 2D and 3D NMR techniques to both characterize and determine the conformation of PPI dendrimers.³⁵ To evaluate host-guest interactions, Morgan et al., Banerjee et al. and Broeren et al. used 2D NOESY to confirm that the guest molecule was interacting with the dendrimer.³⁹⁻⁴¹ To study the

secondary interactions of the end groups, VT coefficients and hydrogen/deuterium (H/D) exchange studies have been performed.^{33,37,38}

The goals of these studies are to confirm many of these observations in a single dendrimer system and elaborate on more subtle issues of conformation. In the previous chapter, the synthesis of a melamine dendrimer with unique NMR signals from periphery to core to aid the investigations of the conformations of triazine dendrimers was detailed. Figure 3.1 reveals the cartoon and chemical structures of the dendrimer and a series of models studied in this report.

Results and Discussion

The results and discussion are organized around major lessons learned from these studies. In the preceding chapter, the analysis of the 1D NMR led to the conclusion that the dendrimer is rich in rotamer populations. These isomers, resulting from hindered rotation about the triazine-N bond, give rise to spectral complexity in the context of signal number, degeneracy, and broadness of lines. Here, three additional lessons emerge. The first lesson learned is that nOe complexity arises with globular structure. The implication of this observation as it pertains to backfolding and inter-branch communication is described. The second lesson learned is that solvent is largely excluded from the interior of the dendrimer. The third lesson learned is that each ‘layer’ of the dendrimer has different mobility and in a distinct order as evaluated by relaxation studies.

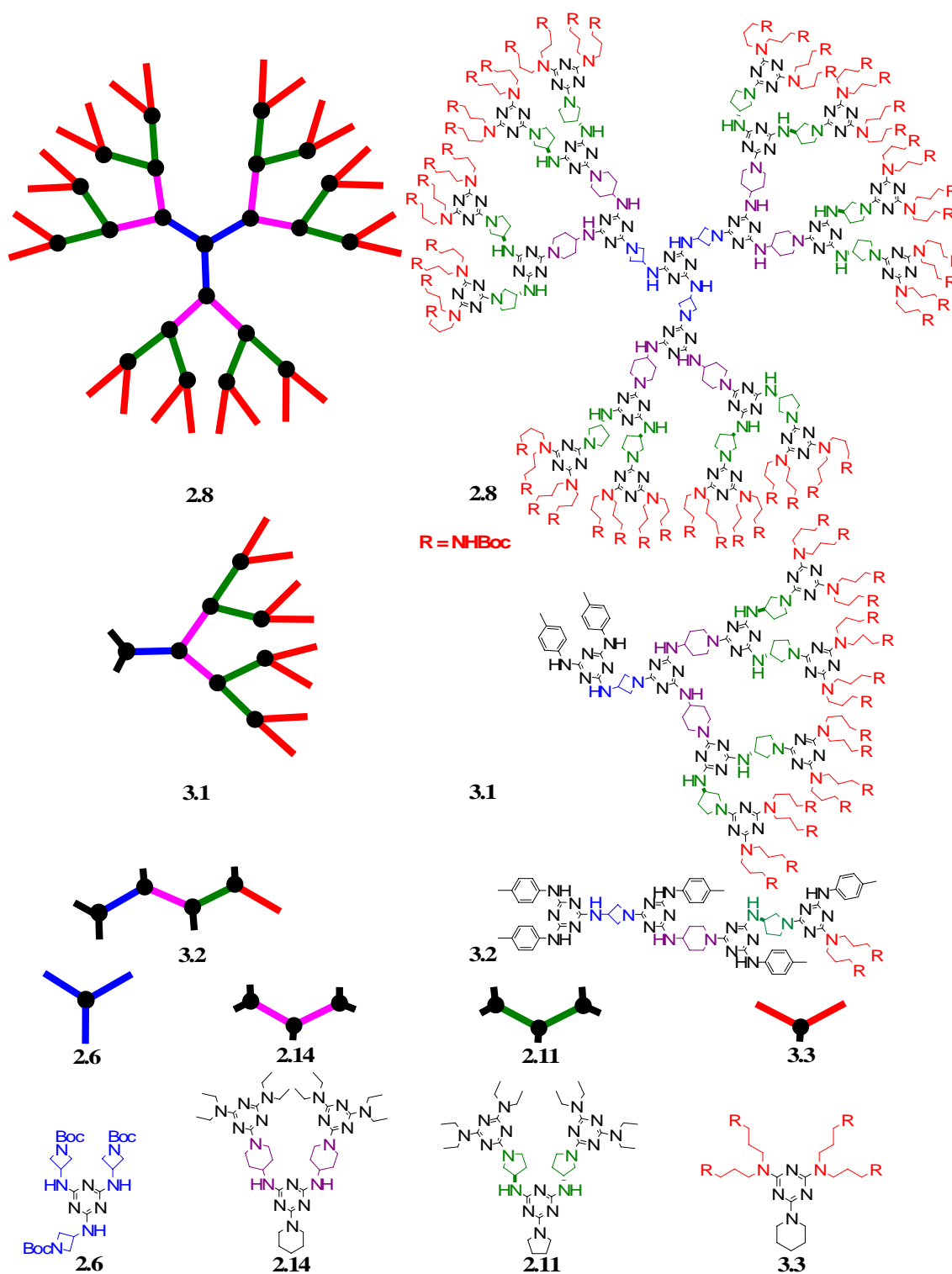


Figure 3.1. Cartoon and molecular representation of dendrimer and models.

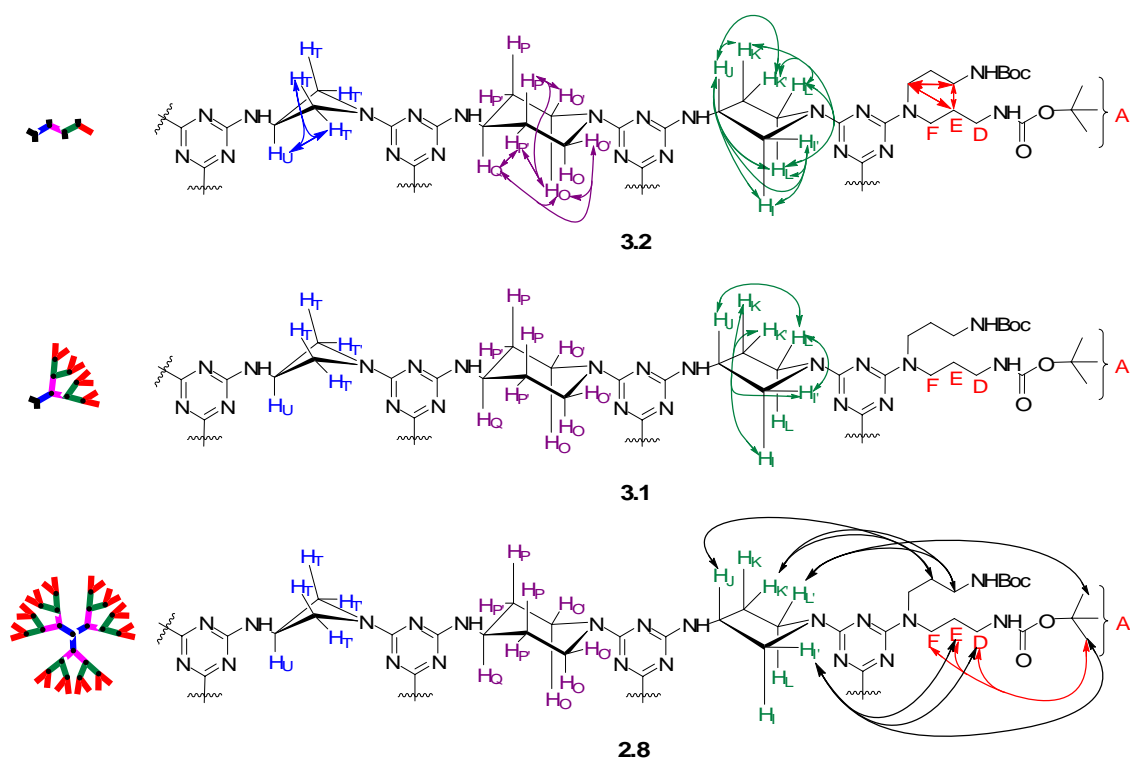


Figure 3.2. Observed nOes of models and full dendrimer. Linear model, **3.2**, shows intra – residue nOes. Arm model, **3.1**, identifies additional nOes not observed in **3.2**. Dendrimer, **2.8**, identifies additional nOes not observed in **3.2** or **3.1**.

Lesson One: nOe Complexity Emerges with Globular Structure

Figure 3.2 shows the onset of nOe complexity when comparing the linear model **3.2** to macromolecule **3.1**, representing 1/3 of the dendrimer, to the entire dendrimer **2.8**. For clarity, only new nOes are shown for **3.1** and **2.8** respectively. The intra-residue nOes are observed in all architectures, but *only* intraresidue nOes are seen in model **3.2**. These nOes in the azetidine and piperidine rings suggest that ring interconversion may be occurring. If so, these motions are either conserved in the more complex architectures or are supplanted by inter-residue nOes of similar magnitude. The

pyrrolidine ring and peripheral groups separately display nOe between neighboring protons.

Model 3.1 shows evidence for inter-branch communication. In addition to the nOes observed in **3.2**, **3.1** has nOes that can only be explained by the two pyrrolidine rings interacting with each other (Figure 3.2); specifically, an nOe observed between protons \mathbf{H}_K — \mathbf{H}_I and \mathbf{H}_L — \mathbf{H}_P . We do not expect an nOe between these resonances unless there is inter-branch communication or spin diffusion occurring. Spin diffusion may occur in macromolecular systems when $\tau_c \gg \omega_0^{-1}$.⁸¹ While this affect can lead to additional cross-peaks observed between all protons within the same spin system, adjusting the mixing time of the NOESY experiment to very short times precludes cross relaxation steps from occurring, thus eliminating the cross-peak. Decreasing the mixing time of the NOESY experiment from 300 ms to 50 ms resulted in no noticeable differences in the cross-peaks, thus ruling out spin diffusion as a possible cause.

Dendrimer (2.8) provides evidence for both inter-branch communication and backfolding of peripheral groups. NOESY experiments were performed at various temperatures (30–75 °C) and concentrations (0.1–10 %, w/v) in DMSO-*d*₆. Figure 3.3 shows a typical NOESY spectrum of **2.8** in the range of 1.0 to 5.0 ppm at 40 °C. Multiple cross-peaks are observed in the spectrum both between different spin systems and the same spin systems. Interactions between the peripheral groups and the pyrrolidine groups are the only interactions between different spin systems, suggesting that the dendrimer end groups are backfolding. Backfolding of the peripheral groups was even observed up to 75 °C. Upon changing the solvent to CDCl₃ or CD₃OD,

backfolding was no longer observed. A possible explanation for this result might be that DMSO- d_6 does not permeate within the dendrimer and only resides outside of the dendrimer molecule, while $CDCl_3$ or CD_3OD may be able to permeate within the dendrimer. While DMSO- d_6 would ordinarily be considered a “good solvent” based on similarity in dielectric constants (DMSO = 47.2, MeOH = 33, $CHCl_3$ = 5.5), the most readily identifiable difference to us is the inability of DMSO- d_6 to donate a hydrogen bond. When the concentration of the dendrimer was increased from 0.001 M to 0.01 M, there was little to no change in chemical shift, potentially supporting that DMSO- d_6 resides outside of the dendrimer molecule. With the solvent molecules residing outside of the molecule, this leaves a void within the interior of the dendrimer and the arms are most likely to fold back into the dendrimer. In $CDCl_3$ or CD_3OD , the arms are most likely in an extended conformation. Rinaldi came to a similar conclusion with PPI dendrimers:³⁵ backfolding occurred in benzene (2.3) but not chloroform (5.5).

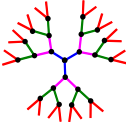
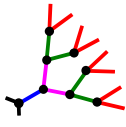
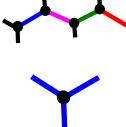
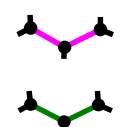
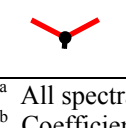


the NH is exposed to solvent and not involved in intramolecular hydrogen-bonding, while a temperature coefficient greater than -4 ppb/K is considered to be involved in intramolecular hydrogen bonding.⁸² Although, dendrimers are considered to be similar in size to proteins, using similar temperature coefficient constraints to evaluate hydrogen bonding of a non-amide NH resonance of our dendrimer in organic solvents may not be accurate. The use of model compounds should be able to give insight into how exposed an NH resonance of the dendrimer is to solvent, assuming the NH resonance of the model compound is completely exposed to solvent. These experiments are inherently challenging in that multiple NH lines are observed and the addition of a hydrogen bond donating solvent like MeOD affects the structure of this dendrimer.

Table 1 shows the tabulated temperature coefficients of the various NH resonances of the dendrimer and model compounds, **2.6**, **2.11**, **2.14** and **3.1-3.3**. Most useful for us is the comparison of the NH resonances of the dendrimer, **2.8**, with the respective model (**2.6**, **2.11**, **2.14** and **3.3**). Differences between these values are evident, and support a conformation wherein the azetidine, pyrrolidine and carbamate NH's become less exposed to solvent. Under the current architecture of the dendrimer, the piperidine NH can not be observed.

Coefficients for the arm (**3.1**) and linear (**3.2**) models when compared with model compounds **2.6**, **2.11**, **2.14** and **3.3** echo similar trends, but direct comparisons between these two architectures and the dendrimer are less instructive. For **3.1**, the NH resonances for the carbamate and pyrrolidine seem to be less exposed to solvent than **2.8**, while the azetidine NH is even more shielded from solvent. As with the dendrimer,

the piperidine NH could not be observed. For **3.2**, we expected the NH resonances to have similar coefficients as **2.6**, **2.11**, **2.14** and **3.3**, but for the carbamate and pyrrolidine NHs the coefficients have similar values as the dendrimer. The primary anomaly for both models is with the azetidine NH resonance, it is more shielded from the solvent than even the azetidines groups of **2.8**. This effect may be due to the fact that the *p*-toluidine groups are somehow prohibiting the NH from interacting with the solvent (no nOes were observed between the azetidine and *p*-toluidine groups were observed).

Table 1. VT Coefficients ($\Delta\delta/\Delta T$) of Dendrimer and Model Compound NHs^a

NH Conformer	Boc			Pyr		Pip ^b			Az	
	<i>Anti</i>	<i>Anti</i>	<i>Syn</i>	<i>(E,E)</i>	<i>(E,Z)</i>	<i>(E,E)</i>	<i>(E,Z)</i>	<i>(Z,Z)</i>		
 2.8	-6.88	-5.54	-3.54	-7.61	-5.48				-6.16	-5.25
 3.1	-6.86	-4.27	-3.91	-7.69					-4.46	
 3.2	-7.36	-5.39	-4.90	-6.63			-8.31		-4.41	
 2.6									-6.50	-5.24
 2.14							-8.24	-7.71	-5.10	
 2.11				-8.47	-5.68					
 3.3	-6.23		-4.32							

^a All spectra acquired in DMSO-*d*₆.

^b Coefficient could not be determined for **2.8** and **3.1**.

H/D exchange occurs rapidly for azetidine and pyrrolidine NHs. Hydrogen–deuterium exchange studies complement the variable temperature studies for identifying whether the NH protons are involved in hydrogen-bonding. Hydrogen-bonded NH protons exchange with protic solvents at a much slower rate than NH protons exposed to solvent.⁸³ Preliminary studies with the dendrimer using ¹H NMR suggested that the NH protons of the pyrrolidine and azetidine rings exchange within two minutes, while carbamate NH's did not. Since the piperidine NH protons are buried under the carbamate resonances, no conclusion can be made. Direct comparison between different types of exchangeable protons led us to examine the rate of exchange with model compounds **2.6**, **2.11**, **2.14** and **3.3**. For **2.6**, **2.11**, **2.14** and **3.3**, we observe exchange of the NH protons for **2.11** & **2.14** within two minutes but not for **2.6** or **3.3**. The carbamate protons of **3.3** showed a gradual decrease in signal intensity over a twelve hour period. The NHs of **2.6** decreased more rapidly; equilibrium occurred in about 2-3 hours. The 'slow' exchange of ¹H for ²H of the carbamate NHs of the dendrimer, as compared to **2.14** and **2.11**, led us to conclude that these protons are involved in hydrogen–bonding. A comparison between the VT coefficients and these exchange studies could not be made under the conditions employed. This is due to methanol affecting the dendrimer conformation in solution as evidenced from a 2D NOESY experiment using 5% CD₃OD in DMSO-*d*₆.

Lesson Three: Each 'Layer' of the Dendrimer Has Different Mobility

The mobility of each 'layer' is different as judged from spin–lattice relaxation (T_1) and spin–spin relaxation (T_2) studies. Figure 3.4 displays the results of the proton

relaxation of our dendrimer. The relaxation times depicted here are average values for each linker of the molecule. Evident in both sets of data, we find that each linker exhibits a different relaxation time when compared to the other segments of the dendrimer. The data also show a specific order: for T_1 relaxation, the peripheral groups have the shortest time and the time increasing towards the core of the molecule. For T_2 relaxation, the opposite is true. The peripheral groups have the longest relaxation time, and these times decrease as one moves towards the core of the molecule. This suggests that our dendrimer tumbles slowly or in the 'slow' regime of the T_1/T_2 vs τ_c curve. The conceptual picture that emerges has the peripheral groups are moving more than pyrrolidine segment which moves more than the piperidine and so on. The data also show that while an increase in temperature also increases the movements of the molecule, the changes are greatest near the outer portions of the molecule. In this study, the relaxation is attributed to dipole–dipole relaxation between two nuclei. Meltzer and Gorman previously concluded that other mechanisms for nuclear relaxation are generally insignificant in solution and where chemically identical but topologically different nuclei are considered.^{16,27}

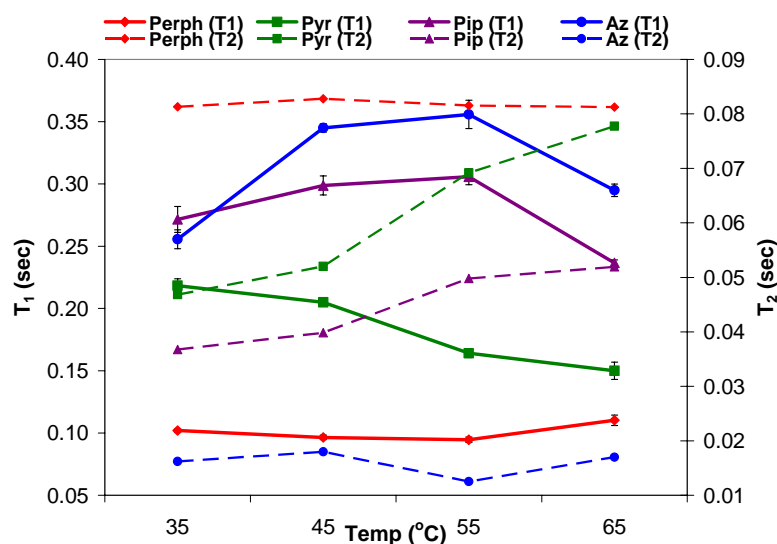


Figure 3.4. T_1/T_2 vs temperature plot of the various linkers within **2.8**. Solid lines refer to T_1 relaxation time and the dashed lines refer to T_2 relaxation time.

Conclusions

The result of these studies is a conceptual image of the conformational musings of a third generation dendrimer based on triazines in DMSO. Evidence from a variety of other, often disparate studies, suggests that this picture may be more general. These results are in agreement with previously published reports by other groups, such as Lescanec⁸, Meltzer^{16,17}, Wooley²⁶, Gorman²⁷, Meijer^{31,33}, and Rinaldi.³⁵ These reports provide evidence for backfolding in different dendrimer systems using different techniques and different dendrimer architectures. Lescanec used computer simulation of dendritic growth to show the chain ends backfold. Meltzer used ²H NMR and relaxation studies to provide evidence for backfolding in PAMAM dendrimers. Both Wooley and Gorman studied polyaryl ether dendrimers and demonstrated that backfolding occurs using REDOR NMR and relaxation studies, respectively. By using 2D NMR, both

Meijer and Rinaldi showed that PPI dendrimers can backfold. Meijer was able to provide crystallographic evidence with a G1 PPI dendrimer. As with our case, Rinaldi was able to show that the backfolding is a function of solvent. Relaxation studies of PAMAM, PPI and polyaryl ether dendrimers show that the exterior of the dendrimer has more mobility and the interior of the dendrimer.^{16,17,27,31,35} This system not only agrees with these studies but also provides evidence that each layer of the dendrimer has different mobilities.

Most useful to us is to draw an analogy. In consideration of any number of classical dances—the waltz, tango, foxtrot, or chicken—we are disposed to pick the Macarena as most representative of the motions of triazine dendrimers in DMSO-*d*₆. The preliminary studies described in the preceding chapter suggest a richness in rotational isomers (hands up/hands down and bending joints). These studies complement this picture with evidence of backfolding of peripheral groups (hands to head/shoulders/hips). Similarly, in accordance with relaxation studies, these peripheral groups move more rapidly than groups closer to the interior. Finally, relaxation appears to be manifested primarily by these movements and less so by tumbling events (jump). The lack of concentration dependence on these events suggests that the molecule dances alone and not in concert with other partners. Finally, when the solvent/music changes, a different dance results.

Experimental Section

Materials. Chemicals were purchased from Aldrich and Acros and used without further purification. All solvents were ACS grade and used without further purification. All mass spectral analyses were carried out by the Laboratory for Biological Mass

Spectrometry at Texas A&M. Synthetic descriptions for **2.5**, **2.6**, **2.8**, **2.11**, **2.14**, and **3.3** can be found in chapter II. Selected spectra of the compounds can be found in Appendix B.

Preparation of NMR samples. All compounds were pumped before use. Deuterated solvents were purchased from Acros, used without further purification, and kept under moisture free conditions. DMSO-*d*₆ was purchased in 1.0 mL N₂ flushed ampules. Preparation of the DMSO-*d*₆ samples was performed in a glovebox under nitrogen. Dendrimer samples were prepared in concentrations of 0.001 M (12 mg/mL) solutions. The remaining compounds were prepared in 30 mg/mL solutions in the appropriate solvent.

NMR measurements. (a) 1D NMR experiments. NMR spectra were recorded on a Varian Inova 500 MHz spectrometer in CDCl₃, CD₃OD or DMSO-*d*₆. Unless otherwise noted, all 1D ¹H and ¹³C spectra were recorded at 25.0 ± 0.1 °C and 2D spectra at 35.0 ± 0.1 °C. In CDCl₃, ¹H spectra were referenced to 7.26 ppm and ¹³C to 77.16 ppm. In CD₃OD, ¹H spectra were referenced to 3.31 ppm. In DMSO-*d*₆, ¹H spectra were referenced to 2.50 ppm and ¹³C spectra to 39.52 ppm. The ¹H spectra of the dendrimer were acquired at 500 MHz by using a 3.5 s acquisition time, 4.5 kHz spectral window, and a 7.3 μs pulse width. The ¹H spectra of the model compounds were acquired at 500 MHz by using a 3.5 s acquisition time, 5.25 kHz spectral window, and a 2.3 μs pulse width. All ¹³C spectra were acquired at 125 MHz by using a 2.0 s acquisition time, 22.6 kHz spectral window, 1.0 s relaxation delay and a 5.6 μs pulse width with WALTZ-16 modulated ¹H decoupling.

(b) 2D NMR experiments. Various NOESY experiments were carried out for the dendrimer and two different ones for **2** and **3**. All NOESY experiments for the dendrimer were carried out with a 4.5 kHz spectral window in f_1 and f_2 , 0.227 s acquisition time, 7.3 μ s (90°) pulse width, 10.0 s relaxation delay, and 16 transients were averaged for each of the 2 x 256 increments. One set of experiments varied the temperature from 35 to 75 $^\circ$ C with a mixing time of 0.300 s. A final experiment used a mixing time of 0.050 s and a temperature of 35 $^\circ$ C. NOESY experiments for the model compounds, **3.1** and **3.2**, differed from the dendrimer parameters by using a 5.25 kHz spectral window in f_1 and f_2 and using a temperature of 35 $^\circ$ C for all experiments. Two experiments were performed for each compound, one with a mixing time of 0.300 s and another with a mixing time of 0.050 s. All spectra were zero-filled to a 1024 x 1024 data matrix before Fourier transformation.

Relaxation studies. Spin-lattice (T_1) relaxation was determined using a typical inversion recovery experiment ($180-\tau-90$). Spin-spin (T_2) relaxation was determined using a Carr-Purcell-Meiboom-Gill spin-echo experiment.⁸⁴⁻⁸⁶ For each experiment, variable delays (τ) were selected to span a range sufficient to probe relaxation up to five times the values of all of the protons under consideration. A minimum of 7 τ values were employed. Data were fit using Varian's integrated software. Samples were prepared as described above.

Proton-deuterium exchange experiment. Samples were prepared by making a 10 mg/mL solution using dry DMSO- d_6 (0.750 mL) and CD₃OD (0.050 mL) in a dry NMR tube. A series of 1 H NMR spectra were taken at increasing intervals over a period of 6

hrs (minimum interval = 1 min, maximum interval = 30 min). Parameters used were those stated above for ^1H spectra of dendrimer.

Variable-temperature NMR experiments. A dendrimer sample was prepared as stated in the sample preparation section. A dry screw-cap NMR tube was used. The VT-NMR experiment was performed using a Varian Inova 500 MHz spectrometer. The spectra were recorded at 298, 308, 318, 328, 338, 348 K, as set by a temperature programmer. The temperature coefficient ($\Delta\delta/\Delta T$) was obtained by measuring the slope of a graph of chemical shift (δ) versus temperature (K).

2,4-Bis(*p*-toluidine)-6-(1-Boc-3-amino-azetidine)-1,3,5-triazine. Bis(*p*-toluidine)-monochloro-triazine (721.8 mg, 2.22 mmol) and BEMP resin (2.32 g, ~ 5.1 mmol) was added to a solution of 1-boc-3-amino-azetidine (400.4 mg, 2.32 mmol) in THF (7 mL) at room temperature. The reaction was heated to 70 °C and left to react for several days. The BEMP resin was filtered out and solvent removed by reduced pressure evaporation. The residue was passed through a silica gel column using (50:1) DCM:MeOH. Fractions containing pure product were combined and solvent removed to give a colorless foam (1.00 g, 98.1 %). ^1H NMR (500 MHz, CDCl_3 , δ): 7.40 (d, $J = 8.4$ Hz, 4H), 7.11 (d, $J = 8.4$ Hz, 4H), 5.52 (br s, NH), 4.63 (m, 1H), 4.22 (t, $J = 8.46$ Hz, 2H), 3.72 (dd, 2H), 2.32 (s, 6H), 1.82 (br s, NH), 1.45 (s, 9H). ^{13}C NMR (125 MHz, CDCl_3 , δ): 165.64, 164.48, 156.25, 136.11, 129.43, 121.20, 120.65, 79.80, 56.83, 40.81, 28.52, 20.94; MS (ESI) mass calc'd for $\text{C}_{25}\text{H}_{31}\text{N}_7\text{O}_2 = 461.25$; found 462.25 $[\text{M}+\text{H}]^+$.

Arm model (3.1). 2,4-Bis(*p*-toluidine)-6-(1-Boc-3-amino-azetidine)-1,3,5-triazine (61.0 mg, 0.1322 mmol) was treated with a (1:1) mixture of DCM/TFA (4 mL)

overnight at room temperature. The solvent was removed by reduced pressure evaporation. The residue was redissolved in a MeOH/TEA solution and then removed by reduced pressure evaporation. This was accomplished 3 times or until acid was neutralized. The residue was dissolved in THF (2 mL) followed by the addition of BEMP resin (500 mg, ~ 1.1 mmol) and solid **1.5** (1504.8 mg, 0.4004 mmol). The slurry was then heated to 70 °C and left to react for several days. The solution was then allowed to cool and filtered to remove the BEMP resin. The solvent was removed by reduced – pressure evaporation and the residue passed through a silica gel column using (50:1) DCM:MeOH. Fractions containing pure product were combined to give a colorless foam (327.96 mg, 60.8 %). ¹H NMR (500 MHz, DMSO-d₆, δ): 8.99 (br s, NH), 8.87 (br s, NH), 7.63 (m, 4H), 7.58 (br s, NH), 7.05 (m, 4H), 6.90 (br s, NH), 6.79 (br s, NH), 6.72 (br s, NH), 6.66 (br s, NH), 6.63 (br s, NH), 6.37 (br s, NH), 4.68 (m, 1H), 4.56 (m, 4H), 4.47 (m, 4H), 4.40 (m, 2H), 4.19 (m, 2H), 3.94 (m, 2H), 3.87 (m, 2H), 3.77 (m, 4H), 3.63 (m, 4H), 3.40 (m, 36H), 3.26 (m, 4H), 2.91 (m, 36H), 2.24 (s, 6H), 2.11 (m, 4H), 1.89 (m, 4H), 1.77 (m, 4H), 1.63 (m, 32H), 1.41–1.25 (m, 148H). ¹³C NMR (125 MHz, DMSO-d₆, δ): 166.47, 165.48, 165.09, 164.79, 164.19, 163.90, 163.11, 155.49, 155.36, 137.55, 130.39, 128.61, 120.11, 119.93, 77.38, 56.37, 50.64, 49.53, 49.07, 47.78, 47.38, 46.77, 43.97, 43.74, 43.55, 41.54, 41.06, 37.94, 37.63, 37.46, 31.63, 30.66, 28.21, 20.35. MS (MALDI) mass calc'd for C₁₉₅H₃₃₀N₆₄O₃₂ = 4080.62; found 4081.96 [M+H]⁺.

Mono(*p*-toluidine)-dichlorotriazine (pTolCl₂). A solution of *p*-toluidine (4.39 g, 41 mmol) and Hunig's base (DIPEA, 15.0 mL, 86 mmol) in THF (100 mL) was added

dropwise to an ice-cold solution of cyanuric chloride (7.56 g, 41 mmol) in THF (100 mL). The reaction was allowed to stir for 2 hours at 0 °C. The solvent was removed by reduced–pressure evaporation and the residue passed through a silica gel column using (50:1) CHCl₃:MeOH. Fractions containing pure product were combined and solvent removed to give an orange solid (8.3 g, 79.5 %). ¹H NMR (500 MHz, CDCl₃, δ): 7.64 (brs, 1H), 7.39 (d, *J* = 8.48 Hz, 2H), 7.20 (d, *J* = 8.45 Hz, 2H), 2.36 (s, 3H). ¹³C NMR (125 MHz, CDCl₃, δ): 171.43, 170.21, 164.23, 136.02, 133.11, 129.93, 121.69, 21.10. MS (ESI) mass calc'd for C₁₀H₈Cl₂N₄ = 254.01; found 255.02 [M+H]⁺.

Mono(*p*-toluidine)-mono(Bis(3-Boc-3-aminopropyl)amine)-monochlorotriazine (pTol-BBT-Cl). Hunig's base (DIPEA, 12.0 mL, 69 mmol) was added to a slurry of pTolCl₂ (8.0 g, 31.4 mmol) in THF:DCM (1:1, 150 mL), which allowed the starting material to dissolve. Solid bis(3-BOC-3-aminopropyl)amine (10.42g, 31.4 mmol) was then added to the solution at room temperature. The reaction was allowed to stir for overnight at room temperature. The solvent was removed by reduced–pressure evaporation and the residue passed through a silica gel column using (50:1) CHCl₃:MeOH. Fractions containing pure product were combined and solvent removed to give an orange solid (12.73 g, 73.8 %). ¹H NMR (500 MHz, DMSO-d₆, δ): 9.98 (br s, NH), 7.58 (m, 2H), 7.13 (d, 2H), 6.84 (br m, NH), 6.79 (br m, NH), 6.47 (br m, NH), 3.50 (m, 4H), 2.99 (m, 2H), 2.94 (m, 2H), 2.25 (s, 3H), 1.73 (m, 2H), 1.67 (m, 2H), 1.37 (m, 18H). ¹³C NMR (125 MHz, DMSO-d₆, δ): 167.88, 164.21, 162.94, 155.58, 155.48, 136.28, 131.68, 128.96, 119.76, 77.50, 77.45, 45.34, 44.62, 37.88, 37.50, 28.22, 28.20,

27.78, 27.44, 20.38. MS (ESI) mass calc'd for $C_{26}H_{40}ClN_7O_4 = 549.28$; found 550.31 $[M+H]^+$.

Mono(*p*-toluidine)-mono(Bis(3-BOC-3-aminopropyl)amine)-monopyrrolidino-triazine (pTol-BBT-Pyr). A solution of **pTol-BBT-Cl** (7.0 g, 12.8 mmol) in THF (55 mL) was added dropwise to a solution of *R*-3-amino-pyrrolidine (2.5 mL, 28.6 mmol) in THF (5 mL) at room temperature. After 1 day, the solvent was removed by reduce–pressure evaporation and the residue passed through a silica gel column using (9:1) $CHCl_3:MeOH$. Fractions containing pure product were combined and solvent removed to give an orange foam (7.48 g, 97.4 %). 1H NMR (500 MHz, $DMSO-d_6$, δ): 8.78 (m, NH), 7.65 (d, 2H), 7.04 (d, 2H), 6.79 (br s, NH), 6.70 (br s, NH), 6.51 (br s, NH), 6.41 (br s, NH), 3.60 (m, 2H), 3.49 (m, 6H), 3.30 (m, 1H), 3.15 (m, 1H), 2.95 (m, 4H), 2.22 (s, 3H), 1.97 (m, 1H), 1.68 (m, 5H), 1.37 (s, 18H). ^{13}C NMR (125 MHz, $DMSO-d_6$, δ): 164.29, 163.53, 163.16, 155.54, 155.43, 138.24, 129.54, 128.61, 119.11, 77.41, 54.21, 54.06, 50.54, 50.39, 44.19, 44.08, 43.97, 43.73, 37.97, 37.76, 37.61, 33.92, 33.82, 28.22, 28.11, 20.30. MS (ESI) mass calc'd for $C_{30}H_{49}N_9O_4 = 599.39$; found 600.41 $[M+H]^+$.

Bis(*p*-toluidine)-mono(Bis(3-BOC-3-aminopropyl)amine)-monopyrrolidine-mono-chlorotriazine (pTol₂-BBT-Pyr-Cl). A solution of Hunig's base (DIPEA, 4.1 mL, 23.5 mmol) and **pTol-BBT-Pyr** (6.93 g, 11.56 mmol) in THF (25 mL) was added to a solution **pTolCl₂** (2.95 g, 11.56 mmol) in THF (25 mL) at room temperature. After allowing to react overnight, the solvent was removed by reduced–pressure evaporation and the residue passed through a silica gel column using (50:1) $CHCl_3:MeOH$. Fraction containing pure product were combined and solvent removed to give a foam (9.11 g,

96.3 %). ^1H NMR (500 MHz, DMSO- d_6 , δ): 10.08 (br s, NH), 10.03 (br s, NH), 9.89 (br s, NH), 8.85 (br s, NH), 8.80 (br s, NH), 8.50 (br s, NH), 8.46 (br s, NH), 8.35 (br s, NH), 7.70-7.56 (br m, 4H), 7.15-7.02 (br m, 4H), 6.80 (br s, NH), 6.72 (br s, NH), 6.62 (br s, NH), 4.55 (20 %) & 4.45 (80 %) (m, 1H), 3.89-3.75 (br m, 1H), 3.74-3.65 (br m, 1H), 3.64-3.55 (br m, 2H), 3.49 (m, 4H), 2.97 (m, 4H), 2.24 (s, 3H), 2.23(s, 3H), 2.18 (m, 1H), 2.01 (m, 1H), 1.69 (m, 4H), 1.37 (s, 15H), 1.33 (s, 3H). ^{13}C NMR (125 MHz, DMSO- d_6 , δ): 168.18, 167.72, 165.20, 164.28, 163.45, 163.22, 155.55, 155.44, 138.10, 136.31, 136.16, 131.85, 129.66, 128.98, 128.87, 128.64, 128.58, 120.14, 119.85, 119.19, 119.13, 77.41, 51.10, 50.65, 50.15, 49.75, 43.99, 43.87, 37.98, 37.70, 30.26, 29.80, 28.22, 20.40, 20.35, 20.31, 20.24. MS (MALDI) mass calc'd for $\text{C}_{40}\text{H}_{56}\text{ClN}_{13}\text{O}_4 = 817.43$; found 818.13 $[\text{M}+\text{H}]^+$.

Bis(*p*-toluidine)-mono(Bis(3-BOC-3-aminopropyl)amine)-monopyrrolidine-mono-piperidinotriazine (pTol₂-BBT-Pyr-Pip). A solution of **pTol₂-BBT-Pyr-Cl** (8.52 g, 10.42 mmol) in THF (45 mL) was added dropwise to a solution of 4-aminopiperidine (3.50 mL, 33.34 mmol) in THF (5 mL) at room temperature. After allowing to stir overnight the solvent was removed by reduced-pressure evaporation and the residue passed through a silica gel column using (19:1) CHCl_3 :MeOH. After all impurities were purified away, the solvent system was switched to (9:1) CHCl_3 :MeOH to collect the product. Fractions containing pure product were combined and solvent removed to give a colorless foam (8.1 g, 88.1 %). ^1H NMR (500 MHz, DMSO- d_6 , δ): 8.94 (br s, NH), 8.91 (br s, NH), 8.84 (br s, NH), 8.81 (br s, NH), 8.72 (br s, NH), 7.69–7.58 (br m, 4H), 7.15 (br s, NH), 7.12, (br s, NH), 7.04 (m, 4H), 6.96 (br s, NH), 6.80 (br

s, NH), 6.72 (br s, NH), 6.65 (br s, NH), 6.51 (br s, NH), 6.42 (br s, NH), 4.57–4.42 (br m, 3H), 3.81 (m, 1H), 3.70 (m, 1H), 3.53 (br m, 2H), 3.50–3.39 (br m, 4H), 3.01 – 2.86 (br m, 6H), 2.81 (m, 1H), 2.22 (s, 5H), 2.17 (m, 2H), 1.99 (m, 1H), 1.77–1.62 (br m, 6H), 1.37 (75 %) & 1.34 (25 %) (m, 18H), 1.13 (m, 2H). ^{13}C NMR (125 MHz, DMSO- d_6 , δ): 165.56, 165.44, 164.30, 164.23, 164.02, 163.51, 163.23, 155.54, 155.41, 138.19, 138.15, 138.01, 129.88, 129.60, 128.61, 119.50, 119.30, 119.14, 77.40, 51.65, 51.21, 51.04, 49.84, 49.60, 48.41, 44.12, 44.00, 43.76, 41.42, 37.97, 37.70, 34.83, 30.71, 30.48, 30.17, 28.22, 20.20. MS (ESI) mass calc'd for $\text{C}_{45}\text{H}_{67}\text{N}_{15}\text{O}_4 = 881.55$; found 882.22 $[\text{M}+\text{H}]^+$.

Tris(*p*-toluidine)-mono(Bis(3-BOC-3-aminopropyl)amine)-monopyrrolidine-monopiperidine-monochlorotriazine (pTol₃-BBT-Pyr-Pip-Cl). A solution of **pTol₂-BBT-Pyr-Pip** (5.35 g, 6.06 mmol) in THF (20 mL) was added to a solution of **pTolCl₂** (1.54 g, 6.05 mmol) and Hunig's base (2.2 mL, 12.6 mmol) in THF (5 mL) at room temperature. The solution was heated for 8 hr and then solvent was removed by reduced – pressure evaporation. The residue was passed through a silica gel column using (50:1) CHCl_3 :MeOH. Fractions containing product were combined and solvent removed to give a yellow foam (6558.26 mg, 98.5 %). ^1H NMR (500 MHz, DMSO- d_6 , δ): 10.01 (br s, NH), 9.84 (br s, NH), 9.00 (br s, NH), 8.97 (br s, NH), 8.84 (br s, NH), 8.81 (br s, NH), 8.78 (br s, NH), 8.22 (br s, NH), 7.99 (br s, NH), 7.71–7.58 (br m, 6H), 7.23 (br s, NH), 7.19 (br s, NH), 7.12 (d, 2H), 7.09–7.00 (br m, 4H), 6.97 (br s, NH), 6.80 (br s, NH), 6.72 (br s, NH), 6.65 (br s, NH), 6.51 (br s, NH), 6.42 (br s, NH), 4.71–4.58 (br m, 2H), 4.56–4.45 (br m, 1H), 4.10–3.95 (br m, 1H), 3.84 (m, 1H), 3.80–3.67 (br m, 1H),

3.55 (m, 2H), 3.48 (m, 4H), 2.98 (m, 6H), 2.25 (s, 3H), 2.22 (s, 6H), 2.19 (m, 1H), 2.00 (m, 1H), 1.96–1.82 (br m, 2H), 1.70 (m, 4H), 1.44 (m, 2H), 1.37 (80 %) & 1.34 (20 %) (m, 18H). ^{13}C NMR (125 MHz, DMSO- d_6 , δ): 168.39, 167.76, 165.61, 165.48, 164.70, 164.34, 164.29, 164.08, 163.53, 163.27, 155.55, 155.43, 138.19, 137.96, 136.32, 131.85, 129.99, 129.09, 128.90, 128.87, 128.72, 128.63, 120.28, 119.92, 119.58, 119.36, 119.16, 77.41, 51.72, 51.12, 49.91, 49.63, 48.72, 47.87, 44.14, 44.01, 43.78, 41.60, 38.00, 37.70, 31.22, 30.82, 30.20, 28.22, 20.40, 20.35, 20.31. MS (ESI) mass calc'd for $\text{C}_{55}\text{H}_{74}\text{ClN}_{19}\text{O}_4 = 1099.59$; found 1100.10 $[\text{M}+\text{H}]^+$.

Linear model (3.2). **2,4-Bis(*p*-toluidine)-6-(1-Boc-3-amino-azetidine)-1,3,5-triazine** (450 mg, 0.977 mmol) was deprotected using a solution of (1:1) TFA:DCM (2 mL). After a couple of hours, the solvent was removed by reduced-pressure evaporation to give a yellow oil. The oil was dissolved in MeOH and the solvent removed again. This procedure of dissolving in MeOH was performed multiple times until the scent of TFA was no longer detected. The residue was dissolved in THF (10 mL) followed by the addition of BEMP resin (1.72 g, ~ 3.78 mmol) and **pTol₃-BBT-Pyr-Pip-Cl** (3.23 g, 2.93 mmol). The reaction was then heated to 70 °C and allowed to stir for several days. Upon completion of the reaction, the BEMP resin was filtered and washed. The filtrate was subsequently concentrated and passed through a silica gel column using (50:1) CHCl_3 :MeOH: . Fractions containing product were combined and solvent removed to give a colorless foam (198.7 mg, 14.3 %). ^1H NMR (500 MHz, DMSO- d_6 , δ): 9.04 (br s, NH), 9.03 (br s, NH), 8.98 (br s, NH), 8.95 (br s, NH), 8.89 (br s, NH), 8.84 (br s, NH), 8.81 (br s, NH), 8.76 (br s, NH), 7.70–7.60 (br m, 10H), 7.24–7.13 (br m, NH),

7.10–7.00 (br m, 10H), 6.96 (br s, NH), 6.80 (br s, NH), 6.72 (br s, NH), 6.66 (br s, NH), 6.50 (br s, NH), 6.42 (br s, NH), 4.75 (m, 1H), 4.71–4.57 (br m, 2H), 4.56–4.45 (br m, 1H), 4.35–4.21 (br m, 2H), 4.09–4.02 (br m, 1H), 4.02–3.91 (br m, 2H), 3.83 (m, 1H), 3.79–3.65 (br m, 1H), 3.54 (m, 2H), 3.48 (m, 4H), 2.96 (m, 6H), 2.25 (s, 6H), 2.22 (s, 9H), 2.18 (m, 1H), 1.99 (m, 1H), 1.95–1.84 (br m, 2H), 1.69 (m, 4H), 1.44 (m, 2H), 1.37 (80 %) & 1.33 (20 %) (m, 18H). ^{13}C NMR (125 MHz, DMSO- d_6 , δ): 166.15, 165.59, 165.45, 165.09, 164.81, 164.30, 164.20, 164.03, 163.90, 163.81, 163.51, 163.23, 155.54, 155.41, 138.15, 138.06, 137.97, 137.55, 130.45, 129.88, 129.60, 128.64, 120.13, 119.96, 119.49, 119.28, 119.15, 77.40, 56.52, 51.67, 51.01, 49.85, 49.56, 47.78, 47.38, 44.12, 44.00, 43.77, 41.81, 41.11, 41.00, 37.98, 37.68, 31.51, 30.73, 30.15, 28.22, 20.36, 20.29. MS (ESI) mass calc'd for $\text{C}_{75}\text{H}_{96}\text{N}_{26}\text{O}_4 = 1424.81$; found 1425.16 $[\text{M}+\text{H}]^+$.

CHAPTER IV
SYNTHESIS OF AND CHARACTERIZATION OF A PLATINATED TRIAZINE
DENDRIMER

Introduction

First synthesized in 1845,⁸⁷ *cis*-diamminedichloroplatinum(II)'s (*cis*-platin) antitumor activity was discovered by Rosenberg in 1965 by demonstrating the inhibition of cell division in *E. coli* cells.^{88,89} Since the first patient received *cis*-platin as an antitumor agent in 1971, *cis*-platin received worldwide approval for general oncology treatment 1978.⁹⁰ Worldwide, only four platinum complexes are approved for the treatment of cancer (Figure 4.1): *cis*-platin (worldwide), carboplatin (worldwide), nedaplatin (Japan), and oxaliplatin (Europe).⁹¹ More recently, other antitumor drugs, such as paclitaxel, 5-fluorouracil, methotrexate, bleomycin, and cytarabine, have been used in combination with these platinum complexes to fight drug resistance.⁹²⁻⁹⁷

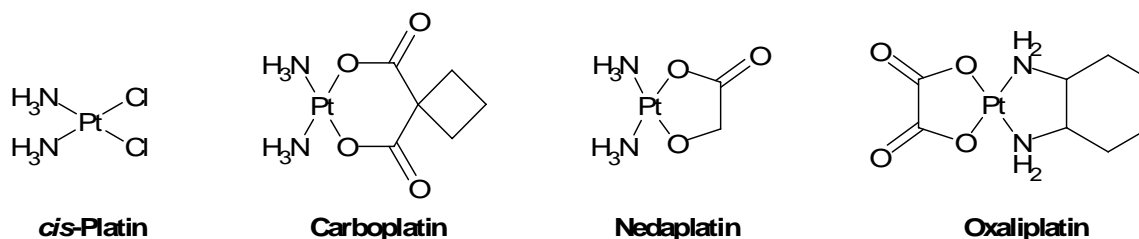


Figure 4.1. Currently approved platinum antitumor drugs around the world.

Hydrolysis of *cis*-Platin is dependent on the pH, temperature, time and concentration of associated reactants: chloride and ammonia.^{94,98-101} Due to the high concentration of

chloride in the blood, hydrolysis of *cis*-platin is minimized (circled in Figure 4.2). *cis*-Platin enters the cell through diffusion. Low chloride concentration in the cell hydrolyzes *cis*-platin to the mono aqua or diaqua species (boxed in Figure 4.2). It is believed that the active intracellular form is the mono aqua species.

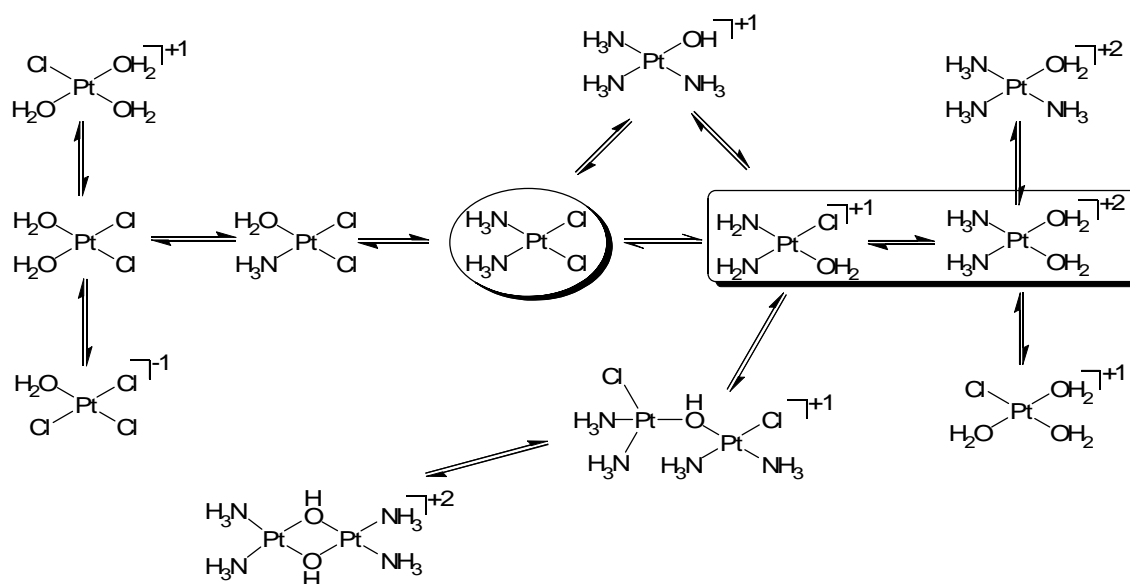


Figure 4.2. Possible hydrolysis products of *cis*-platin.¹⁰⁴

Binding of the mono aqua species with DNA nucleotides appears to correlate with the antineoplastic activity of *cis*-platin.¹⁰² Formation of inter/intrastrand cross-links between the DNA bases causes perturbations of the secondary structure of DNA, which inhibits DNA replication and transcription leading to cell death.^{93,103} Guanine binding is the preferred site of complexation through the N⁷ atom of the purine ring. Though guanine is preferred binding may also occur with the purine ring of adenine and the N³ of the pyrimidine ring in cytosine and uracil. Figure 4.3 shows the three general cross-links

that exist: interstrand, DNA-protein, and intrastrand. Some of the cross-links are too small to be repaired by damage recognition proteins.¹⁰⁴

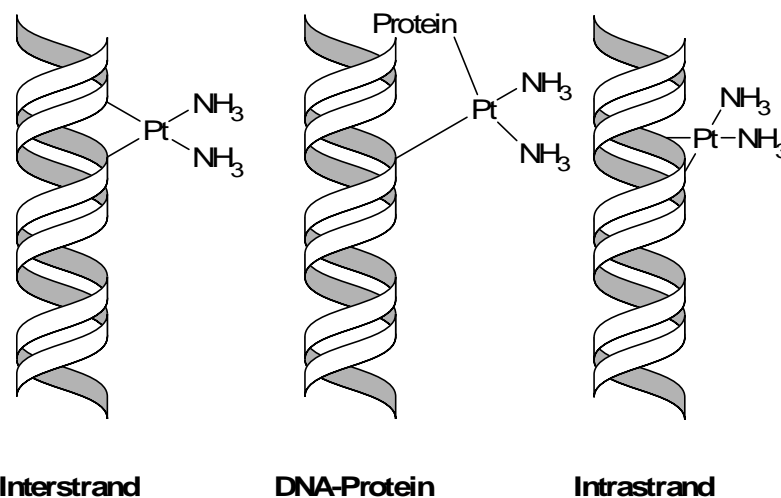


Figure 4.3. Possible cross-links formed by *cis*-platin.

As with most chemotherapeutic drugs, toxicity is an issue. Some side effects include gastrointestinal problems such as acute nausea, vomiting, diarrhea; occasional liver dysfunction; myelosuppression involving anemia, leukopenia, and thrombocytopenia; nephrotoxicity, immunosuppression, hypomagnesia, hypocalcemia, and cardiotoxicity.^{90,91,104} Kidney damage is believed to be the most serious side effect due to the rapid excretion of the platinum within hours of administration, exposing them to bursts of high concentrations of platinum.^{98,105,106}

Polymer-bound platinum(II) conjugates, such as platinum(II)-polyamines (Figure 4.4), have shown promise in being antitumor agents by displaying lower toxicity towards normal cells, thus increasing the dosage.¹⁰⁴ The activity of the *cis*-platin derivative was

not affected by the polymer and solution stability of the platinum is increased when bound to a polymer as compared to *cis*-platin in solution.^{107,108} High polydispersity and higher toxicity of some polyamine polymers are problems for the polymers to be used as chemotherapeutic drugs.¹⁰⁹

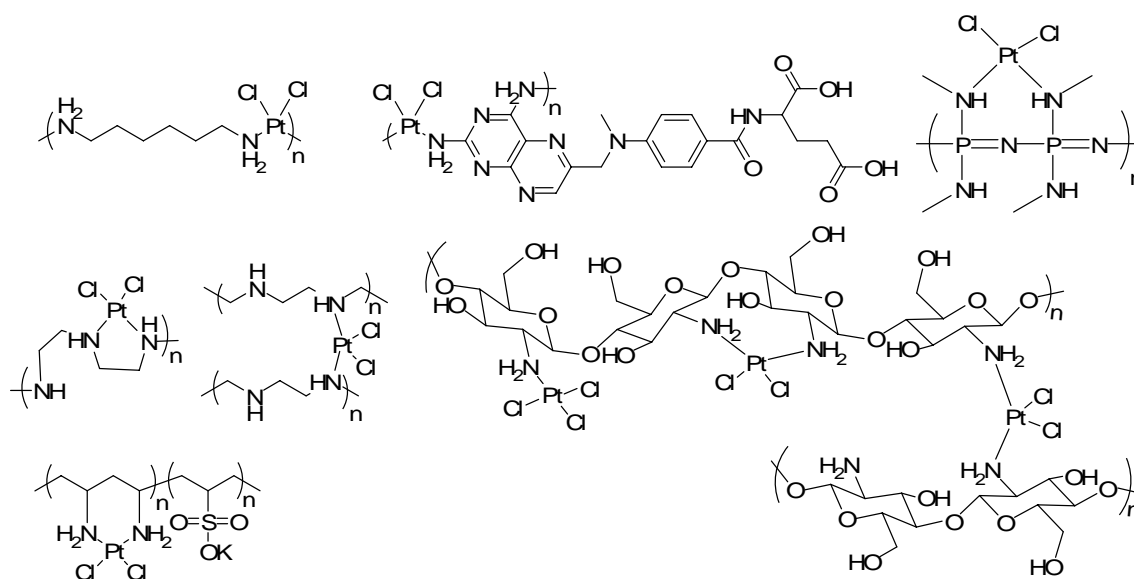


Figure 4.4. Polymer-platinum conjugates studied for chemotherapy.

Though the polydispersity of polymers was an issue, studies did continue to investigate the possibility of using polymer-platinum conjugates as chemotherapeutic agents.^{108,110-117} Allcock and coworkers prepared polyphosphazene based platinum complexes and found an inhibition of 86% in the Ehrlich ascites tumor regression test and a 5/7 survival after the eighth day for the P388 lymphocytic leukemia survival mouse test.^{110,111} Conjugation of polyetheleneimine (PEI) with tetrachloroplatinum (II) formed 5-membered rings within the polymer structure (Figure 4.4).^{112,113} Though the

ring systems were favored, cross-linking was possible. Insoluble portions in DMSO were assumed to be cross-linker polymers. Tests against L929 cells and HeLa cells, the polymers showed equivalent activity as *cis*-platin but at lower concentrations than *cis*-platin. Platinum was bound to the polysaccharide, chitosan (Figure 4.4), to introduce not only water solubility but also biodegradability. Three binding architectures of tetrachloroplatinum (II) with chitosan are possible and lack of complete solubility was consistent with some cross-linking between the polymer chains.^{114,115} Duncan studied various copolymers of *N*-(2-hydroxypropyl)methacrylamide (HPMA) and peptidyl spacers that contained either carboxylate or amino-end groups for platinum attachment.¹¹⁶ Platinum release rates showed that the carboxylated polymers were more than 15X faster than the amine polymer. The cytotoxicity of the carboxylated polymer was similar to that of *cis*-platin in vitro but the amine polymer showed no signs of cytotoxicity. When studied intraperitoneally (IP), neither *cis*-platin nor the HPMA polymers showed signs of activity; but intravenously (IV), *cis*-platin was still inactive but the HPMA polymers showed significant antitumor activity.

Few studies exist for dendrimer-platinum systems for cancer therapeutics.¹¹⁷⁻¹²⁰ Jansen and co-workers used a generation one PPI dendrimer to complex four *cis*-platin molecules forming a tetra[(tri-amino)monochloroplatinum] complex.¹¹⁷ Jansen was able to show that the tetranuclear complex could bind four molecules of guanosinemonophosphate (GMP) at their N⁷ position. The dendrimer-platinum complex showed lowered cytotoxicity compared to *cis*-platin against L1210 cells and seven human cell lines. Also studying a G1 PPI dendrimer complexed to platinum, Kapp et. al.

found that the dendrimer showed higher transport of platinum to the cell (20X) and DNA binding (700X) than free *cis*-platin.¹¹⁸ Interestingly, this dendrimer-platinum complex was not as cytotoxic as free *cis*-platin, though more cytotoxic than other small molecule platinum complexes studied. Duncan et. al. were able to demonstrate that G3.5 PAMAM dendrimers treated with *cis*-platin showed similar activity IP as free *cis*-platin against L1210 cells and showed antitumor activity IV against subcutaneous B16F10 tumors, while free *cis*-platin was not active.¹¹⁹ The platinum loading of the dendrimers was about 23 wt %. The dendrimer was 8 fold less toxic than free *cis*-platin and showed selective accumulation in the solid tumor tissue by the enhanced permeability and retention (EPR) effect.

This chapter describes the efforts to synthesize a G3 triazine-based dendrimer with malonic acid end-groups to bind a dihalogen-diamineplatinum (II) complex, thus mimicking carboplatin. Characterization of the intermediates includes ¹H and ¹⁹⁵Pt NMR, mass analysis and IR. The use of these techniques helps identify the existence of the appropriate intermediates. The chapter ends with a discussion about future directions for this project and efforts to modify the synthesis to more soluble products.

Synthesis

The platinated dendrimer was synthesized by modification of an amine-terminated generation two triazine dendrimer, **4.2** (Figure 4.5).^{56,121} The ester peripheral group, **4.1**, was synthesized by treating 2-amino malonate diethyl ester with cyanuric chloride. Treatment of **4.2** with a slight excess of **4.1** gives **4.3**. Triazine dendrimers are inherently water insoluble. To make the dendrimer more water soluble, a reactive group

must be installed to attach water solubilizing groups such as polyethylene glycol (PEG). 4-Aminomethylpiperidine was chosen to provide enough reactivity to react with the twelve monochloro groups of the dendrimer and have a free amine for attachment of PEG. Substitution of the chlorides with 4-aminomethylpiperidine gives **4.4**. Attempts were made to attach the PEG groups and purify the pegylated dendrimer. It became apparent that with the PEG groups attached, characterization or the synthesis of the final product was going to be difficult. Once the PEG groups were attached, the crowding the PEG groups would cause around the malonic acid groups may not allow for the platinum to bind. The proton NMR signal would be saturated with the PEG signal impeding any noticeable shifts of the protons α to the carboxylates upon platinum binding. The synthesis of the final dendrimer, **4.9**, was continued without the PEG attached to be certain the platinum could be installed. Compound **4.4** was hydrolyzed in basic solution and neutralized with acid to form **4.5**. The barium salt of the carboxylates, **4.6**, was formed and left in solution.

Synthesis of the reactive platinum (II) species proceeded using known literature procedures.^{122,123} Tetrachloroplatinum (II) was treated with potassium iodide in aqueous solution followed by aqueous ammonium hydroxide to form **4.7**. The diaqua species, **4.8**, was formed by reaction of **4.7** with silver sulfate. The aqueous solution of **4.8** was added to an aqueous solution of **4.6** to form dendrimer **4.9**. The precipitation of BaSO₄ drives the reaction. After workup of the reaction, a white precipitate was collected. Several days passed and the material turned black consistent with Pt⁰ being formed suggesting the intended product was not formed.

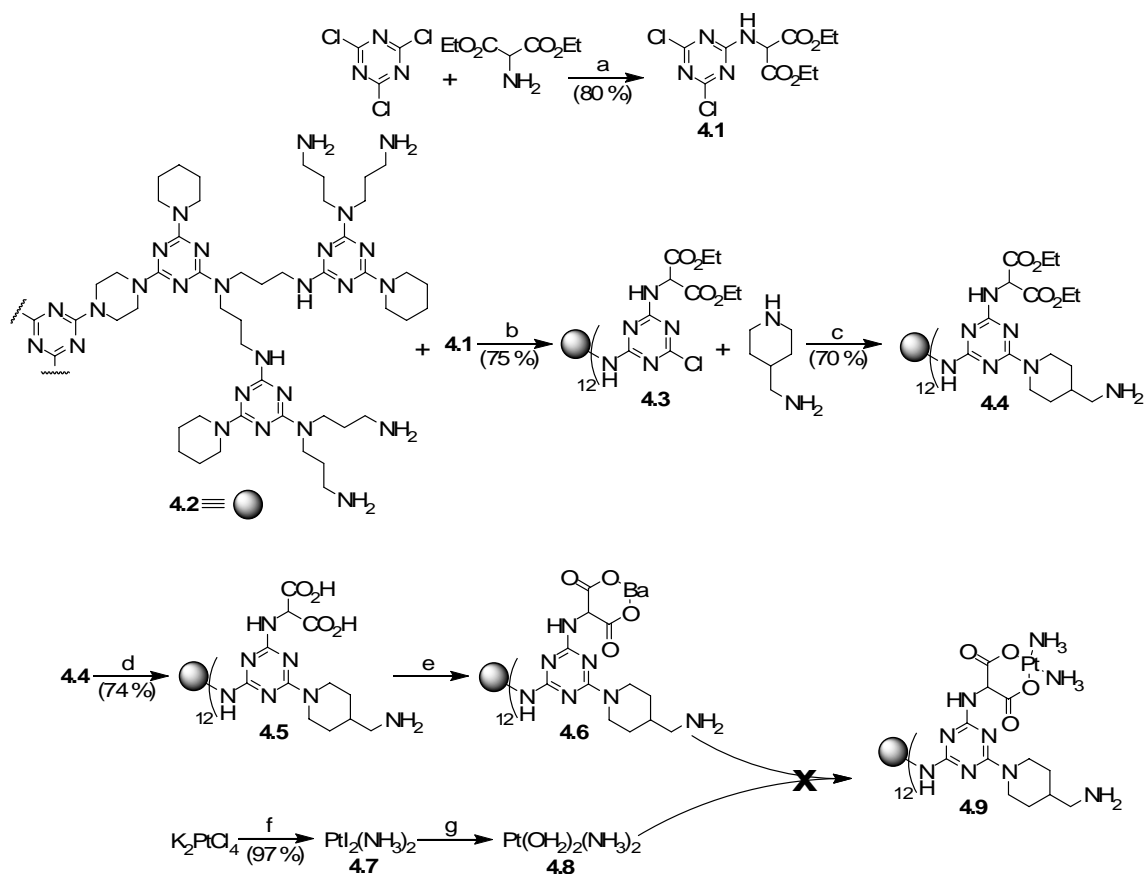


Figure 4.5. Synthesis of a Triazine Dendrimer. a) NaHCO₃, acetone/H₂O, 0 °C, 3h. b) **4.1** (15 eq), DIPEA, CHCl₃, RT, overnight. c) AMP (36 eq), DCM, RT, overnight. d) 1 M NaOH (0.41 mL), MeOH, 0 °C, overnight. e) Ba(OH)₂·8H₂O (12 eq), H₂O, RT. f) i. KI, H₂O. ii. NH₄OH, H₂O. g) Ag₂SO₄, H₂O, RT, 4h.

Characterization

The synthesis of **4.1-4.5** can be followed by 1D NMR or mass spectrometry. Figure 4.6 displays the proton NMR spectra of **4.1-4.4**. All spectra were taken in CDCl₃ at room temperature. Unlike **2.8**, the assignment of the NMR resonances for **4.4** is much simpler. Comparison of the spectra for **4.1** and **4.2** reveals which resonances correlate to the ethyl ester and the α proton of the malonate in **4.3** at 1.25, 4.25 and 5.1 ppm. Compound **4.4** provides the resonances for 4-aminomethylpiperidine at 1.05 (β), 2.6 (δ),

2.7 (α) and 4.7 ppm (α'). The remaining resonances, β' and γ , for 4-aminomethylpiperidine are buried under the resonance at 1.6 ppm. The proton spectrum for the hydrolysis product, **4.5**, was not obtained due to poor solubility. Only mass spectral data was obtained to provide evidence that hydrolysis had occurred. Mass spectra for **4.1-4.5** can be found in Appendix C.

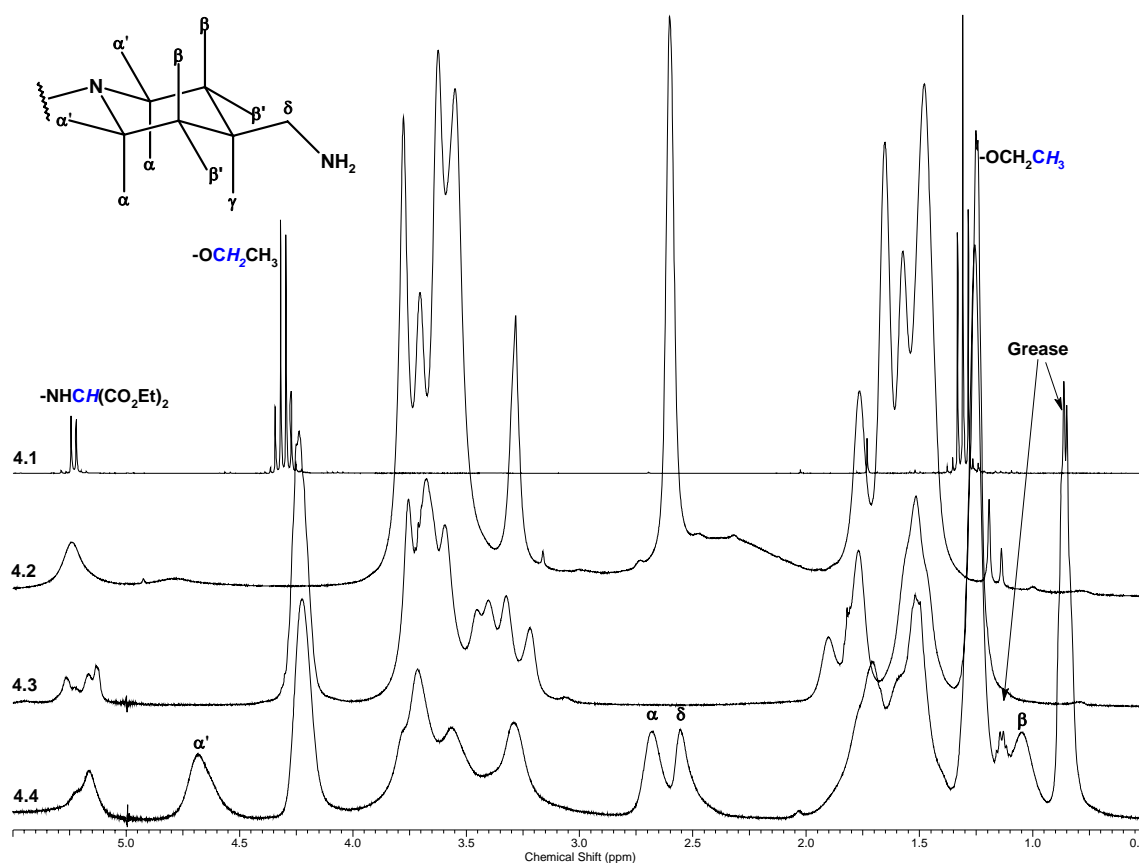


Figure 4.6. ^1H spectra (0.5 – 5.5 ppm) of Compounds **4.1-4.4**.

The platinum compounds were characterized by two methods: ATR-IR and ^{195}Pt NMR. Figure 4.7 displays the ^{195}Pt NMR spectra of **4.7** and potassium

tetrachloroplatinum (II). Comparison of the two spectra shows the shift of platinum nucleus upfield when the tetrachloro complex, -1624 ppm, is converted to **4.7**, -3280 ppm. The chemical shift of **4.7** is similar to those obtained to literature chemical shifts of *cis*-PtI₂(NH₃)₂.^{124,125} In DMF-*d*₇, Appleton et al. obtained a chemical shift of -3198 ppm, while Lippard et al. obtained a chemical shift of -3264 ppm in CDCl₃. Chemical shifts of the *trans* isomer have not been reported in the literature. Obtaining a better signal to noise ratio was difficult because of poor solubility and amount of time available to acquire the spectrum.

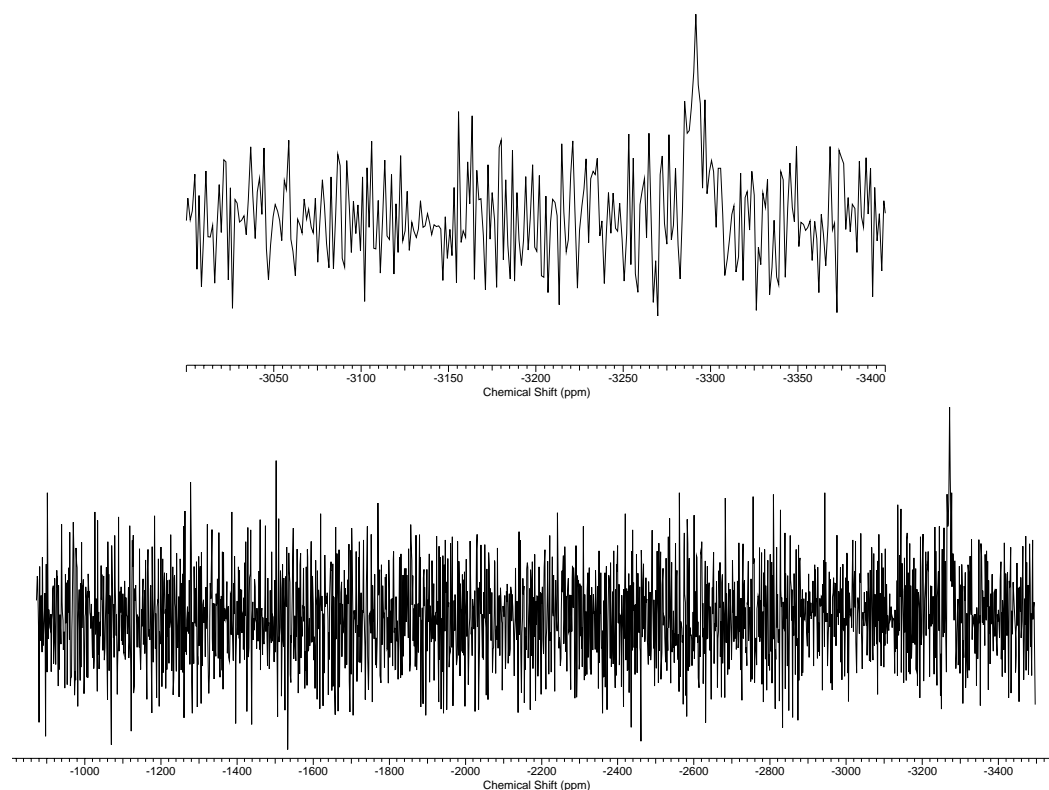


Figure 4.7. ¹⁹⁵Pt NMR spectrum of **4.7** in acetone with a D₂O external reference. Top: -3000 to -3400 ppm. Bottom: -800 to -3500 ppm.

A second characterization technique for **4.7** was employed to verify composition. An ATR-IR spectrum was obtained and compared to literature IR spectra of known *cis*-PtI₂(NH₃)₂. Table 2 displays the stretching frequencies of **4.7** and literature values of the *cis* and *trans* complexes.¹²⁶ Analysis of the data affords diagnostic signals indicative of a *cis* conformation for **4.7**. Analysis of the data for the known complexes shows distinct differences between the two. Each complex has similar frequencies at 1530 and 1290 cm⁻¹. The *cis* complex has one frequency lower in energy than 1290 cm⁻¹ and one in higher energy than 1530 cm⁻¹. The *trans* complex has two frequencies higher in energy than 1530 cm⁻¹ and none lower in energy than 1290 cm⁻¹. In the low energy end of the spectrum, the *cis* has two frequencies and the *trans* has one. Comparing the frequencies of **4.7** with those of the known compounds finds additional stretching frequencies in the 3200 cm⁻¹ region. Although the additional frequencies around 3200 cm⁻¹ in **4.7** are not reported in Nakamoto's data, they can be attributed to the newer spectrometers having better resolution than the ones available to Nakamoto in the 1960s. Unfortunately, none of the frequencies in this region help determine whether **4.7** is *cis* or *trans*. Only one frequency of **4.7** in the 1500-1700 cm⁻¹ region matches the *cis* isomer and none match the *trans* isomer. In the 1300 cm⁻¹ region, **4.7** displays two signals similarly to the *cis* isomer, *trans* only has one in this region. In the final region, 800 cm⁻¹, **4.7** again displays two signals like the *cis* isomer. This data combined with the ¹⁹⁵Pt data suggest that **4.7** is *cis*-Pt I₂(NH₃)₂.

Table 2. Observed Frequencies of PtI₂(NH₃)₂

4.7	<i>cis</i>	<i>trans</i>	Band Assignment
3348	---	---	
3274	3294	3268	ν(NH)
3213	3230	3200	
3165	---	---	
1668	---	1620	
1597	1604	1579	δ(NH ₃)
1520	1532	1534	
1288	1293	1290	
1273	1278	---	
810	806	806	ρ _r (NH ₃)
756	752	---	

Conclusions

Though platinum complexes have been used for the treatment of cancer since the 1970s, the use of dendrimers for platinum conjugation has been recent and limited. Dendrimer conjugation of the platinum complexes has shown to be more active than the free metal complexes. The synthetic approach described in this chapter do provide steps towards achieving a triazine-based dendrimer-platinum complex, it is not the most practical route.

The biggest issue with this dendrimer is water solubility. After hydrolysis of the esters, neutralization causes the dendrimer to be insoluble in water and organic solvents, thus precluding sufficient characterization. The insolubility of the dendrimer in water is probably due to extensive hydrogen-bonding between the carboxylate and the free amine of aminomethylpiperidine. Circumventing this problem could be accomplished in two ways (Figure 4.8). The first approach would be to use the current dendrimer

architecture. Hydrolysis of the esters would occur in the presence of 1 M potassium hydroxide. Removal of the alcohol under reduced-pressure evaporation would leave an aqueous solution of the hydrolyzed dendrimer. Formation of the barium salt, **4.6**, is accomplished by heating the dendrimer solution and addition of $\text{Ba}(\text{OH})_2 \cdot 8\text{H}_2\text{O}$.¹²⁷ Purification of the compound, followed by dissolution in water and finally addition of an aqueous solution of **4.8** should produce dendrimer **4.9**.

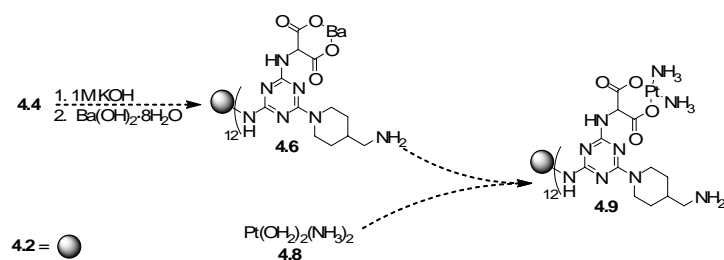


Figure 4.8. First alternate approach to platinate dendrimer.

The second approach involves the addition of water-solubilization groups at an earlier stage of the synthesis (Figure 4.9). In addition to synthesizing dichloride **4.1**, monochloro **4.10** would be synthesized as well. Treating **4.10** with 1-Bocpiperazine forms **4.11**. Attachment of amine terminated tetraethyleneglycol is accomplished through direct amidation of the esters to form **4.12**. Deprotection of the Boc group produces **4.13**. Treatment of **4.3** with **4.13** generates **4.14**. The remaining synthetic pathway would proceed through the steps outlined in Figure 4.8 to produce **4.16**.

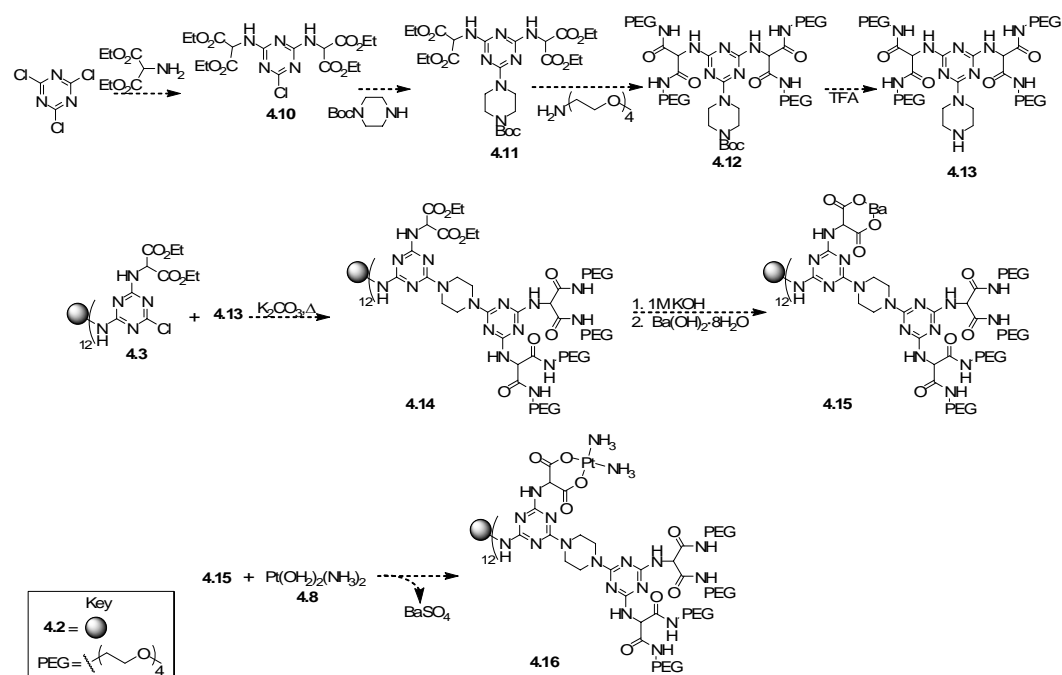


Figure 4.9. Second alternate approach to a platinumated dendrimer.

Each approach should provide platinumated dendrimer. Characterizing the final product will be accomplished through ^{195}Pt NMR. Pellechia and co-workers studied the binding sites of tetrachloroplatinum (II) with a G2 or G4 PAMAM dendrimer.¹²⁸ They were able to observe multiple platinum species bound to the dendrimer. In this study, three general platinum species existed: PtCl_3N , PtCl_2N_2 , PtClN_3 . Two types of N-bonds were available for the platinum to bind, a tertiary nitrogen (NA) and an amide nitrogen (NH). With these two types of nitrogens available, the authors were able to deduce that seven distinct platinum complexes existed: $\text{PtCl}_3(\text{NA})$, $\text{PtCl}_3(\text{NH})$, $\text{PtCl}_2(\text{NA})_2$, $\text{PtCl}_2(\text{NH})(\text{NA})$, $\text{PtCl}(\text{NA})_3$, $\text{PtCl}(\text{NA})_2(\text{NH})$, $\text{PtCl}(\text{NH})_3$. Their studies showed a preference for the tertiary nitrogen over the amide nitrogen. Observation of **4.9** and **4.16** shows many tertiary, secondary and amide nitrogens available for platinum binding.

Even with these possible binding sites, the key process involved here is the amount of platinum loading able to be determined and can the release be slow enough to reach the target but quick enough to provide therapeutic results.

Experimental Section

Materials. Chemicals were purchased from Aldrich, Acros and Strem Chemicals and used without further purification. All solvents were ACS grade and used without further purification. All mass spectral analyses were carried out by the Laboratory for Biological Mass Spectrometry at Texas A&M. Synthetic descriptions for **4.2** can be found in the literature.^{56,121} Selected spectra of the compounds can be found in Appendix C.

Preparation of NMR samples. All compounds were pumped before use. Deuterated solvents were purchased from Acros, used without further purification, and kept under moisture free conditions. Dendrimer samples were prepared in concentrations of 0.01—0.1 M solutions. Non-dendritic platinum samples were prepared in 0.01 M solutions in the appropriate solvent; D₂O or acetone.

NMR measurements. NMR spectra were recorded on a Varian Inova 500 MHz spectrometer in CDCl₃ or D₂O for ¹H and ¹³C spectra. For ¹⁹⁵Pt spectra, the data collected using a Varian Inova 400 MHz spectrometer in D₂O. Unless otherwise noted, all 1D ¹H, ¹³C and ¹⁹⁵Pt spectra were recorded at 25.0 ± 0.1 °C. In CDCl₃, ¹H spectra were referenced to 7.26 ppm and ¹³C to 77.16 ppm. In D₂O, ¹H spectra were referenced to 4.79 ppm. For ¹⁹⁵Pt, the spectra were referenced with K₂PtCl₄ in D₂O to – 1624 ppm. All ¹H spectra were acquired at 500 MHz by using a 1.8 s acquisition time, 5.5 kHz

spectral window, and a 3.5 μ s pulse width. All ^{13}C spectra were acquired at 125 MHz by using a 2.0 s acquisition time, 22.6 kHz spectral window, 1.0 s relaxation delay and a 5.6 μ s pulse width with WALTZ-16 modulated ^1H decoupling. All ^{195}Pt spectra were acquired at 85 MHz by using a 1.0 s acquisition time, 200 kHz spectral window, 1.0 s relaxation delay and a 17.0 μ s pulse width.

Mono(diethyl amino malonate)-dichlorotriazine (4.1). Diethyl-2-aminomalonate \cdot HCl (10.14 g, 47.94 mmol) was suspended in DCM (480 mL) and washed once with saturated Na_2CO_3 (480 mL). The organic layer was dried over MgSO_4 and filtered. The filtrate was concentrated to give a colorless oil (7.48 g, 42.68 mmol, 89 %). The oil was dissolved in cold acetone (70 mL) and NaHCO_3 (3.63 g, 43.16 mmol) was dissolved in cold DI H_2O (70 mL). Cyanuric chloride (7.872 g, 42.68 mmol) was dissolved in cold acetone (170 mL) and added to cold DI H_2O (185 mL) to form a slurry. The malonate solution and the NaHCO_3 solution were subsequently added to the cyanuric chloride slurry and allowed to stir for 3 hrs at 0 $^\circ\text{C}$. The mixture was filtered and the precipitate was washed several times with DI H_2O . The precipitate was dried over P_2O_5 *in vacuo* overnight (11.06 g, 80.2 %). ^1H NMR (500 MHz, CDCl_3 , δ): 6.90 (d, $J = 6.61$ Hz, 1H, NH), 5.23 (d, $J = 6.94$ Hz, 1H), 4.31 (q, $J = 7.27$ Hz, 4H), 1.31 (t, $J = 7.27$ Hz, 6H). ^{13}C NMR (125 MHz, CDCl_3 , δ): 171.09, 170.74, 165.19, 63.32, 57.82, 14.12. MS (ESI) mass calc'd for $\text{C}_{10}\text{H}_{12}\text{Cl}_2\text{N}_4\text{O}_4 = 322.02$; found 323.03 $[\text{M}+\text{H}]^+$.

G3-Pip $_9$ Cl $_{12}$ Mal $_{12}$ (4.3). **4.1** (981.4 mg, 3.04 mmol) was added to a solution of **4.2** (598 mg, 0.202 mmol) and DIPEA (1.40 mL, 8.04 mmol) in CHCl_3 (20 mL) at room

temperature. The reaction was allowed to stir overnight. The following day the solvent was removed by reduced – pressure evaporation. The product was precipitated by addition of ethanol. The precipitation was filtered and washed several times with ethanol and dried under vacuum to give a pale yellow precipitate (974.1 mg, 75.3 %). ^1H NMR (500 MHz, CDCl_3 , δ): 9.63 (brs, NH), 9.45 (brs, NH), 7.0-6.65 (NH), 6.50 (brs, NH), 6.39 (brs, NH), 6.3-6.15 (NH), 6.04 (brs, NH), 5.45 (brs, 1H), 5.26 (s, 3H), 5.23 (s, 2H), 5.17 (s, 3H), 5.13 (s, 3H), 4.24 (m, 48H), 3.76 (m, 24H), 3.68 (m, 36H), 3.59 (m, 24H), 3.45 (m, 12H), 3.40 (m, 12H), 3.32 (m, 12H), 3.22 (m, 12H), 1.90 (m, 12H), 1.77 (m, 24H), 1.52 (m, 64H), 1.25 (m, 72H). ^{13}C NMR (125 MHz, CDCl_3 , δ): 169.86, 168.99, 168.42, 166.49, 166.06, 165.96, 165.57, 165.41, 165.26, 165.05, 164.78, 164.70, 164.64, 62.72, 62.63, 58.28, 57.72, 44.39, 44.15, 43.65, 43.20, 38.95, 38.43, 37.70 (br), 29.00, 28.67, 27.79, 25.93, 25.18, 25.07, 14.16. MS (MALDI) mass calc'd for $\text{C}_{261}\text{H}_{384}\text{Cl}_{12}\text{N}_{120}\text{O}_{48} = 6386.76$; found 6388.77 $[\text{M}+\text{H}]^+$.

G3-Pip₉AMP₁₂Mal₁₂ (4.4). 4-Aminomethylpiperidine (AMP, 200 mL, 1.66 mmol) was added to a solution of **4.3** (264.1 mg, 0.0413 mmol) in DCM (10 mL) at room temperature. The solution was allowed to react overnight. The following day the solution was washed 6X with DI water. The organic layer was dried over MgSO_4 and filtered. The filtrate was concentrated and the product precipitated upon addition of petroleum ether. The precipitate was filtered and washed several times with petroleum ether to give a colorless solid. The solid was dissolved in a minimum of DCM and reprecipitated from petroleum ether. The precipitate was washed several times upon filtration (213 mg, 70.4 %). ^1H NMR (500 MHz, CDCl_3 , δ): 6.0-5.5 (NH), 5.22 (brs,

4H), 5.16 (brs, 8H), 4.69 (m, 24H), 4.22 (m, 48H), 3.72 (m, 60H), 3.56 (m, 36H), 3.29 (m, 36H), 2.68 (m, 24H), 2.56 (m, 24H), 1.71 (m, 54H), 1.65-1.38 (m, 72H), 1.25 (m, 72H), 1.05 (m, 24H). MS (MALDI) mass calc'd for $C_{333}H_{540}N_{144}O_{48} = 7324.42$; found 7333.34 $[M+H]^+$.

G3-Pip₉AMP₁₂MalH₁₂ (4.5). To a solution of **4.4** (211.6 mg, 0.0289 mmol) in MeOH (2.8 mL) was added 1M NaOH (aq) (0.41 mL, 0.41 mmol) at 0 °C. The reaction was allowed to stir for 24 hours at 0 °C. The reaction was allowed to warm to room temperature and neutralized to pH 7. Upon neutralization, a white precipitate formed. The precipitate was filtered and washed with MeOH several times and twice with DI water to remove NaCl salts. The precipitate was dried under vacuum (142.66 mg, 74.2 %). MS (MALDI) mass calc'd for $C_{285}H_{444}N_{144}O_{48} = 6651.67$; found 6369.32 $[M+H]^+$.

PtI₂(NH₃)₂ (4.7). Potassium iodide (3.807 g, 22.93 mmol) was added to a solution of potassium tetrachloroplatinum(II) (2.024 g, 4.876 mmol) in DI water (24 mL) at room temperature. Once all the KI dissolved, a solution of NH₄OH (0.82 mL) in DI water (0.82 mL) was added. After several minutes, a mustard yellow precipitate formed. The mixture was transferred to a 50 mL centrifuge tube and was centrifuged at 5000 rpm for 30 min three times. In between each run, the supernatant was decanted and the precipitate resuspended in DI water. The solid was dried over P₅O₅ *in vacuo* (2.254 g, 95.7 %). ¹⁹⁵Pt NMR (85 MHz, D₂O, δ): - 3280. IR (cm⁻¹): ν(N-H) 3348w, 3274s, 3213s, 3165m, δ(NH₃) 1668w, 1597m, 1520w, 1288s, 1273s, ρ_r(NH₃) 810w, 756m.

CHAPTER V

SUMMARY

Many studies have defined a general picture of the conformation of dendrimers. The analyses have been both experimental and theoretical.^{6-41,79,80} Most studies conclude that dendritic arms backfold to some extent, especially at higher generations. The environment of the dendrimer will affect the extent of backfolding.^{7-15,19-23,25,35,36} The dendrimer system described in this dissertation describes how one system can be used to describe most, if not all, the general concepts described in other dendrimer systems.

The synthesis of the dendrimer started with the selection of diamine linkers. To utilize the diamines under unprotected conditions, they needed to meet certain criteria: 20-fold differential reactivity between the amines, presence of unique NMR signals and commercial availability. Previous competition studies between various diamines provided a relative nucleophilic reactivity of amines towards a model monochlorotriazine.⁴² Expansion of this reactivity chart included several cyclic amines, **G-K** (Figure 2.1), and extended the reactivity to greater than 320X compared to benzylamine. From these studies three linkers were chosen that met the criteria: aminoazetidine (**L1**), aminopyrrolidine (**L2**) and aminopiperidine (**L3**). Aminoazetidine (**L1**) offers a highly reactive and sterically unencumbered amine that might find use in situations where piperidine-type amines are unreactive or sluggish. Aminopyrrolidine (**L2**) offers opportunities to explore chiral environments in these dendrimers.

Aminopiperidine (**L3**) offers an inexpensive linker that aligns with the group's current reliance on aminomethylpiperidine groups.

These linkers convey spectroscopically unique signatures to different regions of the dendrimer architecture; an effect only rarely observed in related architectures.^{27,35,62-65} The presence of the unique signatures allowed one to follow the synthesis of the dendrimer by observing shifts of certain protons on each linker. In all, seven protons, excluding NHs, were identified by TOCSY spectra to be unique signals: **H_{P,K,K',L,Q,T}**.

The NH-region of the spectrum that provides insight into the complexity of the structure of the dendrimer that suggests a rich population of rotamers exists. The carbamate NH populations do not change throughout the synthesis, while significant changes were observed for the pyrrolidine NH populations. An initial 2:1 ratio of (*E,E*):(*E,Z*) expected for a conformationally unhindered molecule shifted a 1:1.3 ratio indicative of a sterically congested architecture.

Conformational analysis in DMSO reveals the presence of general concepts of dendrimer conformation. Previously published reports show that backfolding is a common feature of dendritic structure.^{7-10,13-17,19-21,26,27,31,33,35} Two-dimensional NMR studies showed that the peripheral groups of the triazine dendrimer backfolded and interacted with the pyrrolidine groups. Lowering of the concentration did not remove these interactions nor did an increase in temperature. A change in conformation was observed upon changing the solvent from DMSO to chloroform or methanol. Similarly, Rinaldi and co-workers observed comparable results with PPI dendrimers.³⁵ Several experimental studies, including simulations, have suggested that the conformation of the

dendrimer can be changed either through a change in solvent, pH or ionic concentration.^{8,11-14,22,23,25,35,36} Interbranch communication within the dendritic structure was observed through the use of model compounds and 2D NOESY spectra. In an attempt to identify the many cross-peaks of the dendrimer NOESY spectrum (Figure 3.3), the mixing time of the experiment was decreased to eliminate the possibility of spin diffusion occurring.⁸¹ Analysis of the model compounds, **2.1** and **2.2**, shows evidence that interbranch communication was occurring.

Relaxation studies of PAMAM, PPI and polyaryl ether dendrimers show that the exterior of the dendrimer has more mobility and the interior of the dendrimer.^{16,17,27,31,35} This system not only agrees with these studies but also provides evidence that each layer of the dendrimer has different mobilities.

Finally, attempts to synthesize a pharmacologically active triazine dendrimer were unsuccessful using the synthetic route taken. There are few reports in the literature of conjugating platinum to dendritic systems.^{118-121,129} Changes in the synthetic route would provide water soluble dendrimer. Characterization of the complex would be accomplished by ¹H, ¹³C, and ¹⁹⁵Pt NMR, IR and mass analysis. Future studies of this complex include pharmacokinetic data and biodistribution to evaluate the dendrimer's biological significance.

This dissertation has described the use of triazine dendrimers to provide a general conceptual image of dendrimer conformation and the synthesis of a dendrimer prodrug. These two systems should give insight into the versatility of our triazine dendrimers and provide outlets for biological applications.

REFERENCES

- (1) Bosman, A. W.; Janssen, H. M.; Meijer, E. W. *Chem. Rev.* **1999**, *99*, 1665-1688.
And references therein.
- (2) Buhleier, E. W.; Wehner, W.; Vögtle, F. *Synthesis* **1978**, *2*, 155-158.
- (3) Tomalia, D. A.; Baker, H.; Dewald, J.; Hall, M.; Kallos, G.; Martin, S.; Roeck, J.; Ryder, J.; Smith, P. *Polym. J. (Tokyo)* **1985**, *17*, 117-132.
- (4) Hawker, C. J.; Fréchet, J. M. J. *J. Am. Chem. Soc.* **1990**, *112*, 7638-7647.
- (5) De Brabander-van den Berg, E. M. M.; Meijer, E. W. *Angew. Chem., Int. Ed. Engl.* **1993**, *32*, 1308-1311.
- (6) de Gennes, P. G.; Hervet, H. J. *Phys. Lett. Paris* **1983**, *44*, 351-360.
- (7) Naylor, A. M.; Goddard, W. A., III; Kiefer, G. E.; Tomalia, D. A. *J. Am. Chem. Soc.* **1989**, *111*, 2339-2341.
- (8) Lescanec, R. L.; Muthukumar, M. *Macromolecules* **1990**, *23*, 2280-2288.
- (9) Boris, D.; Rubinstein, M. *Macromolecules* **1996**, *29*, 7251-7260.
- (10) Mansfield, M. L.; Klushin, L. I. *Macromolecules* **1993**, *26*, 4262-4268.
- (11) Welch, P.; Muthukumar, M. *Macromolecules* **1998**, *31*, 5892-5897.
- (12) Murat, M.; Grest, G. S. *Macromolecules* **1996**, *29*, 1278-1285.
- (13) Karatasos, K.; Adolf, D. B.; Davies, G. R. *J. Chem. Phys.* **2001**, *115*, 5310-5318.

- (14) Suek, N. W.; Lamm, M. H. *Macromolecules* **2006**, *39*, 4247-4255.
- (15) Tomalia, D. A.; Hall, V. B.; Hedstrand, D. M. *Macromolecules* **1987**, *20*, 1164-1167.
- (16) Meltzer, A. D.; Tirrell, D. A.; Jones, A. A.; Inglefield, P. T.; Hedstrand, D. M.; Tomalia, D. A. *Macromolecules* **1992**, *25*, 4541-4548.
- (17) Meltzer, A. D.; Tirrell, D. A.; Jones, A. A.; Inglefield, P. T. *Macromolecules* **1992**, *25*, 4549-4552.
- (18) Prosa, T. J.; Bauer, B. J.; Amis, E. J.; Tomalia, D. A.; Scherrenberg, R. *J. Polym. Sci. B* **1997**, *35*, 2913-2924.
- (19) Caminati, G.; Turro, N. J.; Tomalia, D. A. *J. Am. Chem. Soc.* **1990**, *112*, 8515-8522.
- (20) Ottaviani, M. F.; Bossmann, S.; Turro, N. J.; Tomalia, D.A. *J. Am. Chem. Soc.* **1994**, *116*, 661-671.
- (21) Ottaviani, M. F.; Cossu, E.; Turro, N. J.; Tomalia, D. A. *J. Am. Chem. Soc.* **1995**, *117*, 4387-4398.
- (22) Chen, W.; Tomalia, D. A.; Thomas, J. L. *Macromolecules* **2000**, *33*, 9169-9172.
- (23) Maiti, P. K.; Cagin, T.; Lin, S.-T.; Goddard, W. A. *Macromolecules* **2005**, *38*, 979-991.
- (24) Mourey, T. H.; Turner, S. R.; Rubinstein, M.; Fréchet, J. M. J.; Hawker, C. J.; Wooley, K. L. *Macromolecules* **1992**, *25*, 2401-2406.

- (25) De Backer, S.; Prinzie, Y.; Veheijen, W.; Smet, M.; Desmedt, K.; Dehaen, W.; De Schryver, F. C. *J. Phys. Chem. A* **1998**, *102*, 5451-5455.
- (26) Wooley, K. L.; Klug, C. A.; Tasaki, K.; Schaefer, J. *J. Am. Chem. Soc.* **1997**, *119*, 53-58.
- (27) Gorman, C. B.; Hager, M. W.; Parkhurst, B. L.; Smith, J. C. *Macromolecules* **1998**, *31*, 815-828.
- (28) Thomas, K. R. J.; Thompson, A. L.; Sivakumar, A. V.; Bardeen, C. J.; Thayumanavan, S. *J. Am. Chem. Soc.* **2005**, *127*, 373-383.
- (29) Scherrenberg, R.; Coussens, B.; van Vliet, P.; Edouard, G.; Brackman, J.; de Brabander, E.; Mortensen, K. *Macromolecules* **1998**, *31*, 456-461.
- (30) Rosenfeldt, S.; Dingenouts, N.; Ballauff, M.; Werner, N.; Vogtle, F.; Lindner, P. *Macromolecules* **2002**, *35*, 8098-8105.
- (31) Jansen, J. F. G. A.; de Brabander – van den Berg, E. M. M.; Meijer, E. W. *Science* **1994**, *266*, 1226-29.
- (32) Jansen, J. F. G. A.; Meijer, E. W.; de Brabander – van den Berg, E. M. M. *J. Am. Chem. Soc.* **1995**, *117*, 4417-4418.
- (33) Bosman, A. W.; Bruining, M. J.; Kooijman, H.; Spek, A. L.; Janssen, R. A. J.; Meijer, E. W. *J. Am. Chem. Soc.* **1998**, *120*, 8547-8548.
- (34) Jeener, J.; Meier, B. H.; Bachmann, P.; Ernst, R. R. *J. Chem. Phys.* **1979**, *71*, 4546-4553.

- (35) Chai, M.; Niu, Y.; Youngs, W. J.; Rinaldi, P. L. *J. Am. Chem. Soc.* **2001**, *123*, 4670-4678.
- (36) Pan, Y.; Ford, W. T. *Macromolecules* **2000**, *33*, 3731-3738.
- (37) Mong, T. K.-K.; Niu, A.; Chow, H.-F.; Wu, C.; Li, L.; Chen, R. *Chem. Eur. J.* **2001**, *7*, 686-699.
- (38) Appoh, F. E.; Thomas, D. S.; Kraatz, H.-B. *Macromolecules* **2005**, *38*, 7562-7570.
- (39) Morgan, M. T.; Carnahan, M. A.; Immoos, C. E.; Ribiero, A. A.; Finkelstein, S.; Lee, S. J.; Grinstaff, M. W. *J. Am. Chem. Soc.* **2003**, *125*, 15485-15489.
- (40) Banerjee, D.; Broeren, M. A. C.; van Genderen, M. H. P.; Meijer, E. W.; Rinaldi, P. L. *Macromolecules* **2004**, *37*, 8313-8318.
- (41) Broeren, M. A. C.; de Waal, B. F. M.; van Genderen, M. H. P.; Sanders, H. M. H. F.; Fytas, G.; Meijer, E. W. *J. Am. Chem. Soc.* **2005**, *127*, 10334-10343.
- (42) Steffensen, M. B.; Simanek, E. E. *Org. Lett.* **2003**, *5*, 2359-2361.
- (43) Steffensen, M. B.; Simanek, E. E. *Angew. Chem. Int. Ed.* **2004**, *43*, 5177-5180.
- (44) Zhang, W.; Simanek, E. E. *Org. Lett.* **2000**, *2*, 843-845.
- (45) Zhang, W.; Simanek, E. E. *Tet. Lett.* **2001**, *42*, 5355-5357.
- (46) Zhang, W.; Nowlan, D. T.; Thomson, L. M.; Lackowski, W. M.; Simanek, E. E. *J. Am. Chem. Soc.* **2001**, *123*, 8914-8922.

- (47) Zhang, W.; Gonzalez, S. O.; Simanek, E.E. *Macromolecules* **2002**, *35*, 9015-9021.
- (48) Zhang, W.; Tichy, S. E.; Perez, L. M.; Maria, G. C.; Lindahl, P. A.; Simanek, E. *J. Am. Chem. Soc.* **2003**, *125*, 5086-5094.
- (49) Bell, S. A.; McLean, M. E.; Oh, S.-K.; Tichy, S. E.; Zhang, W.; Corn, R. M.; Crooks, R. M.; Simanek, E. E. *Bioconjugate Chem.* **2003**, *14*, 488-493.
- (50) Umali, A. P.; Simanek, E. E. *Org. Lett.* **2003**, *5*, 1245-1247.
- (51) Zhang, W.; Jiang, J.; Qin, C.; Perez, L. M.; Parrish, A. R.; Safe, S. F.; Simanek, E. E. *Supramolecular Chemistry* **2003**, *15*, 607-616.
- (52) Neerman, M. F.; Chen, H.-T.; Parrish, A. R.; Simanek, E. E. *Molecular Pharmaceutics* **2004**, *1*, 390-393.
- (53) Neerman, M. F.; Zhang, W.; Parrish, A. R.; Simanek, E. E. *Int. J. Pharm.* **2004**, *281*, 129-132.
- (54) Chen, H.-T.; Neerman, M. F.; Parrish, A. R.; Simanek, E. E. *J. Am. Chem. Soc.* **2004**, *126*, 10044-10048.
- (55) Acosta, E. J.; Gonzalez, S. O.; Simanek, E. E. *J. Poly. Sci, Part A: Polym. Chem.* **2005**, *43*, 168-177.
- (56) Hollink, E.; Simanek, E. E. *Org. Lett.* **2006**, *8*, 2293-2295.
- (57) Yoo, S.; Lunn, J. D.; Gonzalez, S. O.; Ristich, J. A.; Simanek, E. E.; Shantz, D. F. *Chem. Mater.* **2006**, *18*, 2935-2942.

- (58) Simanek, E. E.; Hollink, E. US Patent 041933.
- (59) Crampton, H. L.; Hollink, E.; Perez, L. M.; Simanek, E. E. *New J. Chem.* **2007**, *7*, 1283-1290
- (60) Acosta, E. J.; Carr, C. S.; Simanek, E. E.; Shantz, D. F. *Adv. Mater.* **2004**, *16*, 985-989.
- (61) Lim, J.; Simanek, E. E. *Molecular Pharmaceutics* **2005**, *2*, 273-277.
- (62) Ihre, H.; Hult, A.; Soderlind, E. *J. Am. Chem. Soc.* **1996**, *118*, 6388-6395.
- (63) Lellek, V.; Stibor, I. *J. Mater. Chem.* **2000**, *10*, 1061-1073.
- (64) [2.24] Murer, P. K.; Lapierre, J.-M.; Greiveldinger, G.; Seebach, D. *Helv. Chim. Acta* **1997**, *80*, 1648-1681.
- (65) van Genderen, M. H. P.; Baars, M. W. P. L.; van Hest, J. C. M.; de Brabander – van den Berg, E. M. M.; Meijer, E. W. *Recl. Trav. Chim. Pays – Bas* **1994**, *113*, 573-574.
- (66) Caswell, L. R.; Goldsmith, M. E. *J. Org. Chem.* **1989**, *54*, 5101-5104.
- (67) Searles, S.; Tamres, M.; Block, F.; Quarterman, L. A. *J. Am. Chem. Soc.* **1956**, *78*, 4917-4920.
- (68) Frenna, V.; Vivona, N.; Consiglio, G.; Spinelli, D. *J. Chem. Soc., Perkin Trans. II: Phys. Org. Chem.* **1985**, *12*, 1865-1868.
- (69) Bax, A.; Griffey, R. H.; Hawkins, B. L. *J. Magn. Reson.* **1983**, *55*, 301-315.
- (70) Freeman, R.; Morris, G. A. *Bull. Magn. Reson.* **1979**, *1*, 5-26.

- (71) Marcovici-Mizrahi, D.; Gottlieb, H. E.; Marks, V.; Nudelman, A. *J. Org. Chem.* **1996**, *61*, 8402-8406.
- (72) Hallam, H. E.; Jones, C. M. *J. Mol. Struct.* **1970**, *5*, 1-19. And references therein.
- (73) Drakenberg, T.; Forsen, S. *Chem. Commun.* **1971**, *21*, 1404-1405.
- (74) Mirvish, S. S.; Gannett, P.; Babcook, D. M.; Williamson, D.; Chen, S. C.; Weisenburger, D. D. *J. Agric. Food Chem.* **1991**, *39*, 1205-1210.
- (75) Welhouse, G. J.; Bleam, W. F. *Environ. Sci. Technol.* **1992**, *26*, 959-964.
- (76) Bax, A.; Davis, D. G. *J. Magn. Reson.* **1985**, *65*, 355-360.
- (77) States, D. J.; Haberkorn, R. A.; Ruben, D. J. *J. Magn. Reson.* **1982**, *48*, 286-292.
- (78) Competition studies between azetidine-HCl and piperidine were allowed to equilibrate for 12 hours before the addition of DMTA.
- (79) Peerlings, H. W. I.; Trimbach, D. C.; Meijer, E. W. *Chem. Commun.* **1998**, *4*, 497-498.
- (80) Rosini, C.; Superchi, S.; Peerlings, H. W. I.; Meijer, E. W. *Eur. J. Org. Chem.* **2000**, *1*, 61-71.
- (81) Wuthrich, K. *NMR of Proteins and Nucleic Acids*; John Wiley & Sons: New York, 1986, pp 97-98.
- (82) Kessler, H. *Angew. Chem. Int. Ed. Engl.* **1982**, *21*, 512-523.
- (83) Lenormant, H.; Blout, E. R. *Nature* **1953**, *172*, 770-771.

- (84) Hahn, E. L. *Phys. Rev.* **1950**, *80*, 580-594.
- (85) Carr, H. Y.; Purcell, E. M. *Phys. Rev.* **1954**, *94*, 630-638.
- (86) Meiboom, S.; Gill, D. *Rec. Sci. Instr.* **1958**, *29*, 688-691.
- (87) Peyrone, M. *Ann. Chem. Pharm.* **1845**, *51*, 1.
- (88) Rosenberg, B.; Van Camp, L.; Krigas, T. *Nature* **1965**, *205*, 698-699.
- (89) Rosenberg, B.; Van Camp, L.; Trosko, J. E.; Mansour, V. H. *Nature* **1969**, *222*, 385-386.
- (90) Lebwohl, D.; Canetta, R. *Eur. J. Cancer* **1998**, *34*, 1522-1534.
- (91) Wong, E.; Giandomenico, C. M. *Chem. Rev.* **1999**, *99*, 2451-2466.
- (92) Caldwell, G.; Neuse, E.; Perlwitz, A. *J. Inorg. and Organomet. Polym.* **1997**, *7*, 111-119.
- (93) Murry, V.; Whittaker, V. J.; Temple, M. D.; McFadyen, W. D. *Biochim. Biophys. Acta* **1997**, *1354*, 261-71.
- (94) Hambley, T. W. *Coord. Chem. Rev.* **1997**, *166*, 181-223.
- (95) Dalla Via, L.; DiNoto, V.; Vidali, M.; Scomazzon, F.; Ni, D.; Deana, R. *Chem. Biol. Interact.* **1998**, *110*, 203-220.
- (96) Neuse, E. *Polym. Adv. Technol.* **1998**, *9*, 786-793.
- (97) Caldwell, G.; Neuse, E.; Perlwitz, A. *J. Appl. Polym. Sci.* **1997**, *66*, 911-919.

- (98) Carraher, C.; Scott, W.; Giron, W. In *Bioactive Polymeric Systems* Gebelein, C.; Carraher, C., Eds; Plenum: NY, 1985; ch. 20.
- (99) Neuse, E. S. *Afr. J. Sci.* **1999**, *95*, 509-516.
- (100) Rosenberg, B. *Cancer Treat. Rep.* **1979**, *63*, 1433-1438.
- (101) Zwelling, L. A.; Kohn, K. W. *Cancer Treat. Rep.* **1979**, *63*, 1439-1444.
- (102) Heudi, O.; Cailleus, A.; Pierre, A. *J. Inorg. Biochem.* **1998**, *71*, 61-69.
- (103) Lippert, B. *Coord. Chem. Rev.* **1999**, *182*, 263-295.
- (104) Siegmann-Louda, D. W.; Carraher, C. E. *Macromolecules containing metal and metal-like elements* **2004**, *3*, 119-191. And references therein.
- (105) Gottlieb, J.; Drewinko, B. *Cancer Chemother. Rep., Pt 1* **1975**, *59*, 621-628.
- (106) Stadnicki, S. W.; Fleischman, R. W.; Schaeppi, U.; Merriman, P. *Cancer Chemother. Rep., Pt 1* **1975**, *59*, 467-480.
- (107) Siegmann, D. W.; Carraher, C. E.; Brenner, D. *Polym. Mater. Sci. Eng.* **1989**, *61*, 209-13.
- (108) Siegmann, D. W.; Brenner, D.; Carraher, C. E.; Strother, R. *Polym. Mater. Sci. Eng.* **1989**, *61*, 214-18.
- (109) Giron, D.; Espy, M.; Carraher, C. E.; Lopez, I.; Turner, C. *Polym. Mater. Sci. Eng.* **1984**, *51*, 312-15.
- (110) Allcock, A. R.; Allen, R.; O'Brien, J. US Patent 4151185.

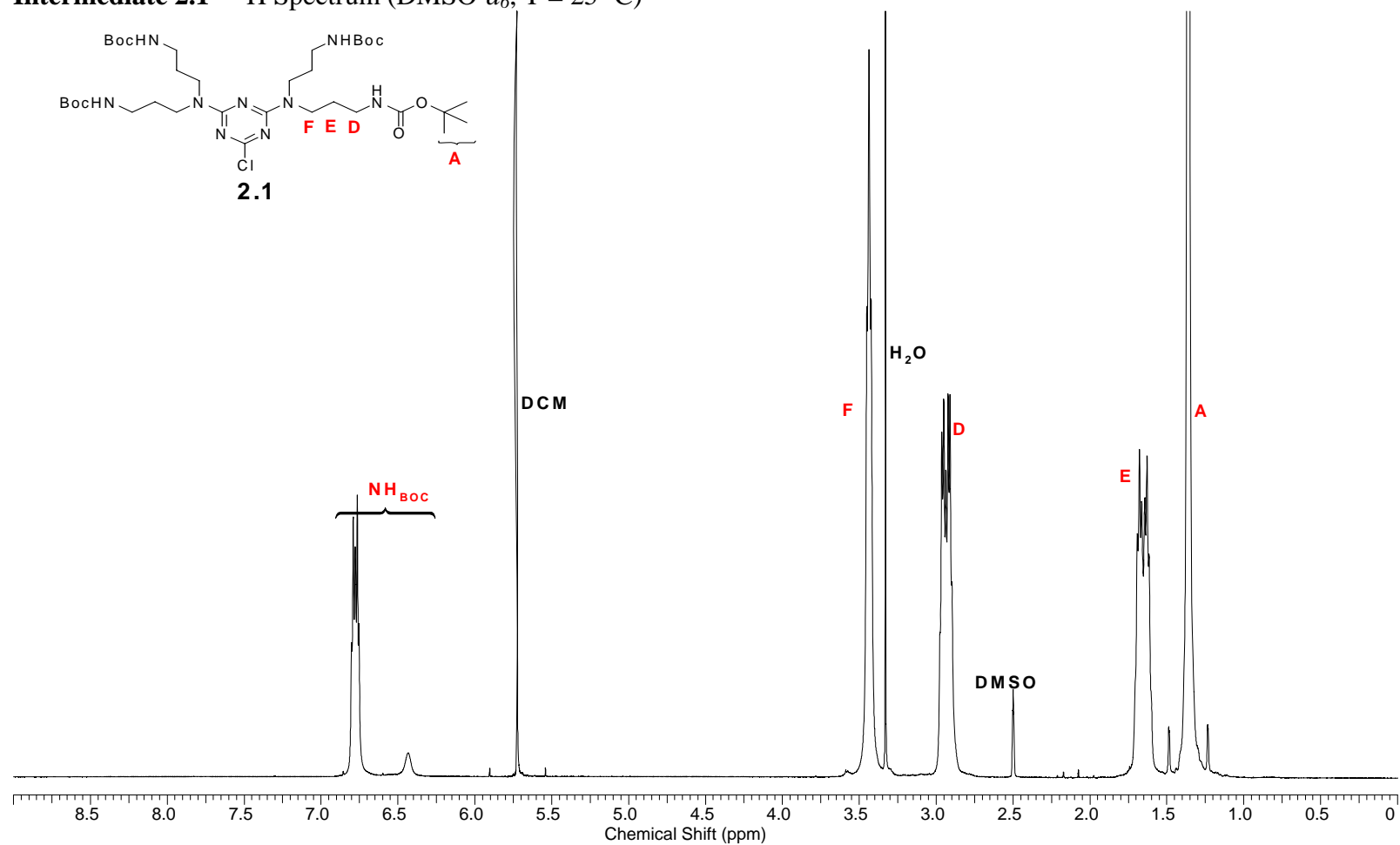
- (111) Allcock, H.; Allen, R.; O'Brien, J. *J. Chem. Soc., Chem Commun.* **1976**, *18*, 717-718.
- (112) Carraher, C. E.; Ademu-John, C.; Fortman, J.; Giron, D.; Linville, R. *Polym. Mater. Sci. Eng.* **1983**, *49*, 210-214.
- (113) Carraher, C. E.; Ademu-John, C.; Fortman, J.; Giron, D.; Turner, C. *J. Polym. Mater.* **1984**, *1*, 116-124.
- (114) Carraher, C. E.; Francis, A.; Siegmann-Louda, D. *Polym. Mater. Sci Eng.* **2001**, *84*, 654-655.
- (115) Carraher, C. E.; Francis, A.; Siegmann-Louda, D. *Polym. Mater. Sci Eng.* **2001**, *84*, 664-665.
- (116) Gianassi, E.; Wasil, M.; Evagorou, E.; Kedde, A.; Wilson, G.; Duncan, R. *Eur. J. Cancer* **1999**, *35*, 994-1002.
- (117) Jansen, B. A. J.; van der Zwan, J.; Reedijk, J.; den Dulk, H.; Brouwer, J. *Eur. J. Inorg. Chem.* **1999**, *1999*, 1429-1433.
- (118) Kapp, T.; Dullin, A.; Gust, R. *J. Med. Chem.* **2006**, *49*, 1182-1190.
- (119) Malik, N.; Evagorou, E. G.; Duncan, R. *Anti-Cancer Drugs* **1999**, *10*, 767-776.
- (120) Bellis, E.; Hajba, L.; Kovacs, B.; Sandor, K.; Kollar, L.; Kokotos, G. *J. Biochem. Biophys. Methods* **2006**, *69*, 151-161.
- (121) Simanek, E. E.; Hollink, E. US Patent 041933.

- (122) Haynes, U. J.; Swigor, J. E.; Pittman, K. A. *J. Labelled Compd. Radiopharm.* **1987**, *24*, 535-539.
- (123) Rochon, F. D.; Gruia, L. M. *Inorg. Chim. Acta* **2000**, *306*, 193-204.
- (124) Appleton, T. G.; Hall, J. R.; Ralph, S. F. *Inorg. Chem.* **1985**, *24*, 4685-4693.
- (125) O'Halloran, T. V.; Lippard, S. J.; Richmond, T. J.; Klug, A. *J. Mol. Biol.* **1987**, *194*, 705-712.
- (126) Nakamoto, K.; McCarthy, P. J.; Fujita, J.; Condrate, R. A.; Behnke, G. *Inorg. Chem.* **1965**, *4*, 36-43.
- (127) Noszticszius, Z.; McCormick, W. D.; Swinney, H. L. *J Phys. Chem.* **1987**, *91*, 5129-5134.
- (128) Pellechia, P. J.; Gao, J.; Gu, Y.; Ploehn, H. J.; Murphy, C. J. *Inorg. Chem.* **2004**, *43*, 1421-1428.

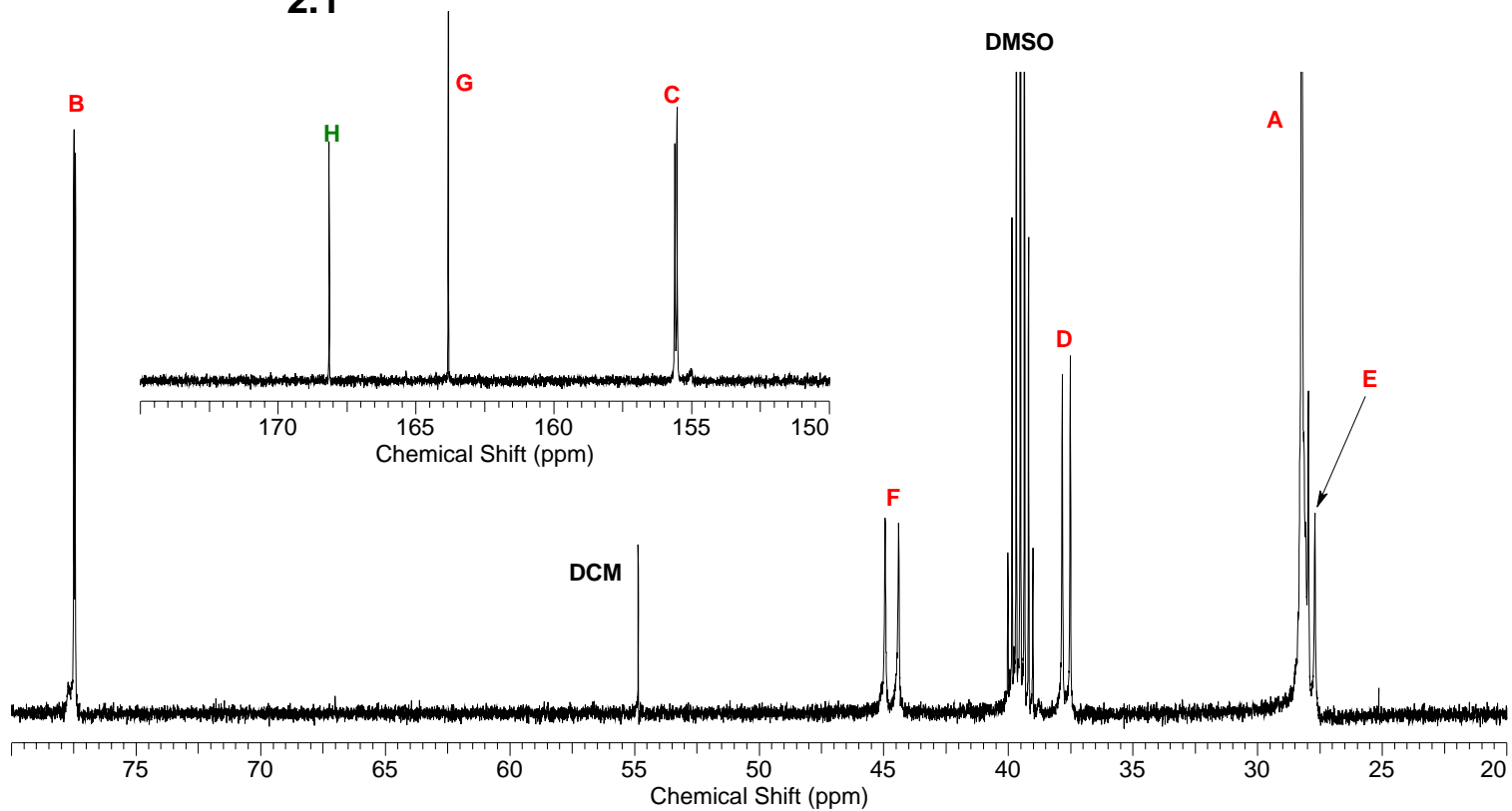
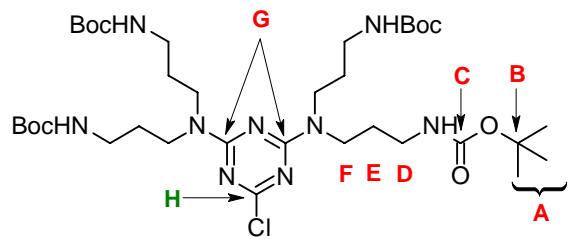
APPENDIX A

SELECTED NMR SPECTRA FOR COMPOUNDS DESCRIBED IN CHAPTER II

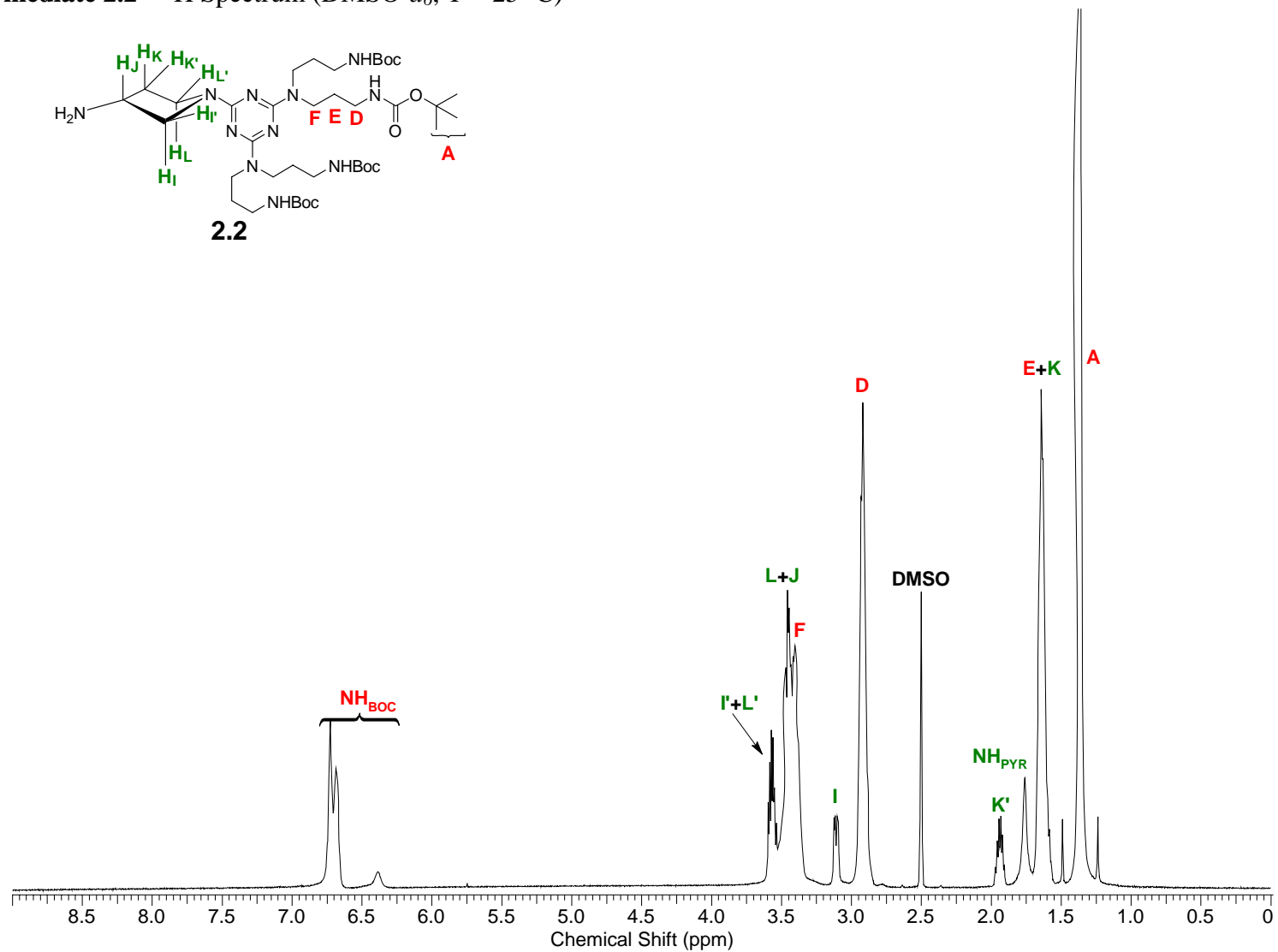
Intermediate 2.1 – ^1H Spectrum (DMSO- d_6 , T = 25 °C)



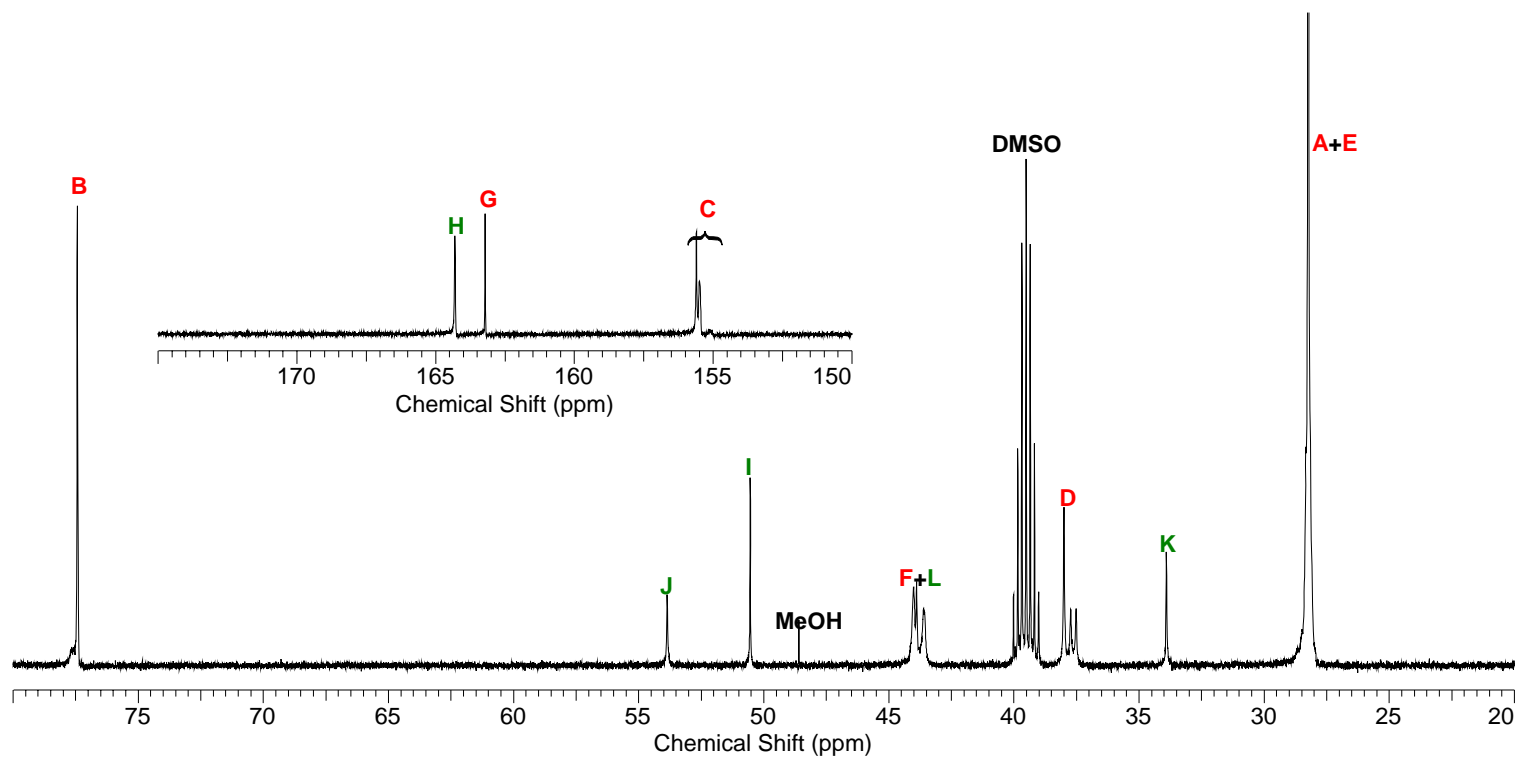
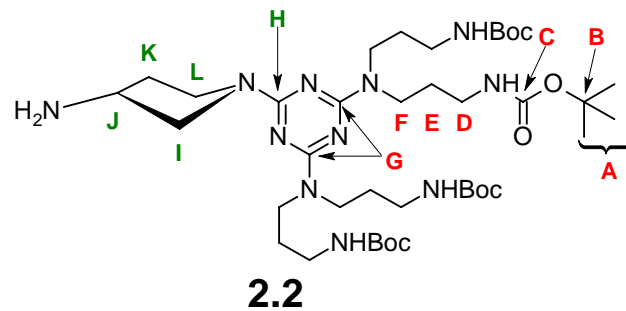
Intermediate 2.1 – ^{13}C Spectrum (DMSO- d_6 , T = 25 °C)



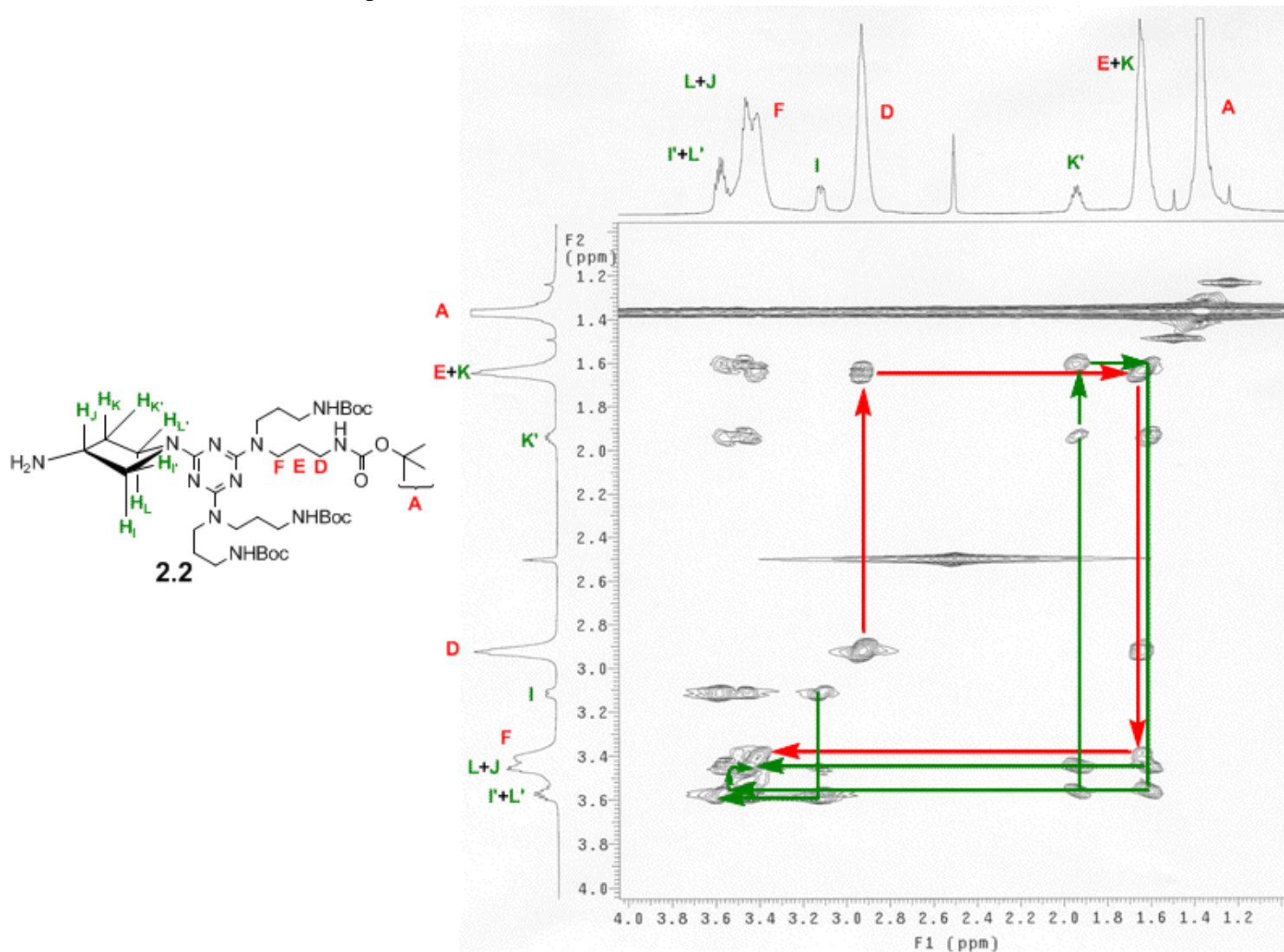
Intermediate 2.2 – ^1H Spectrum (DMSO- d_6 , T = 25 °C)



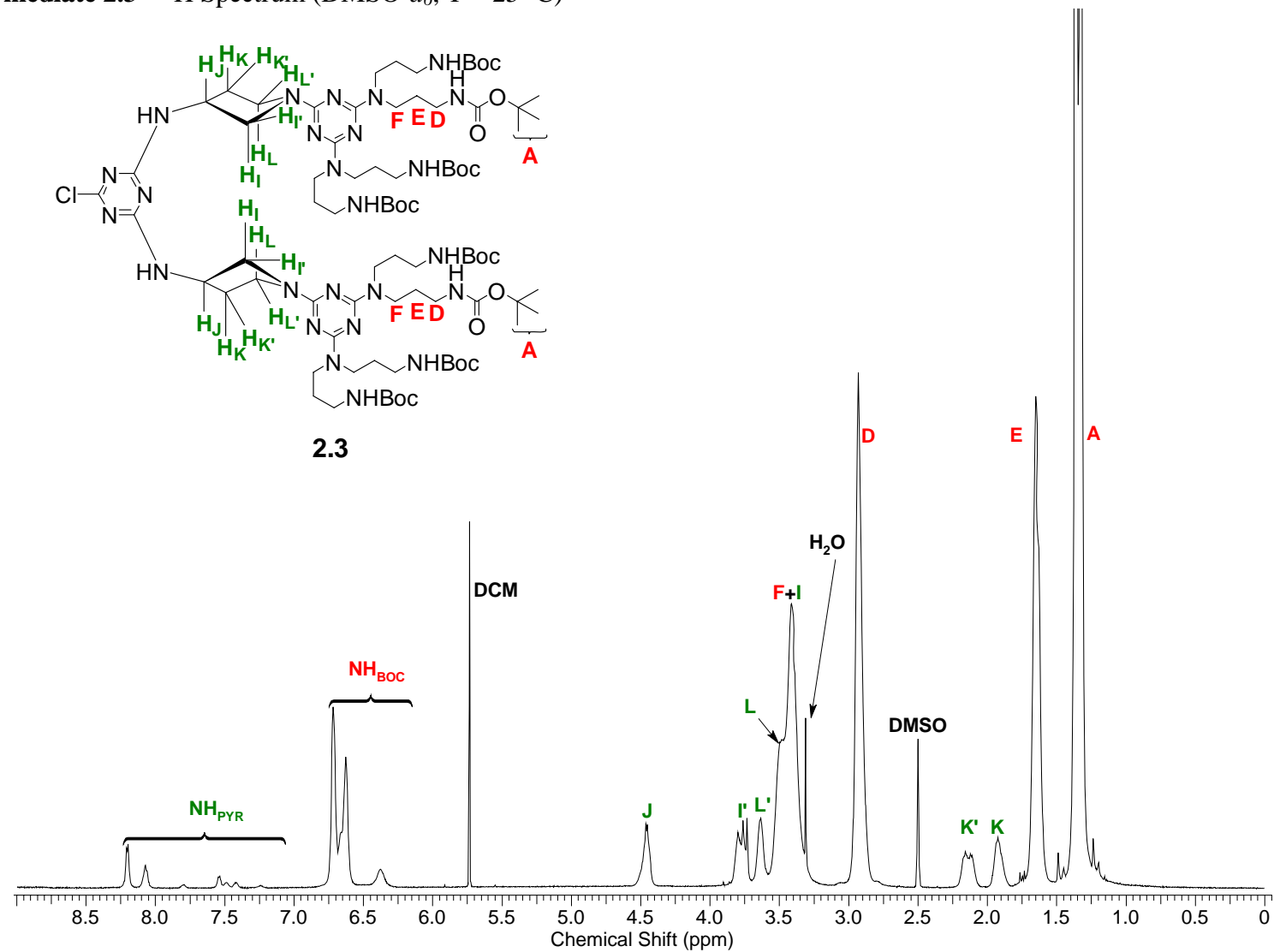
Intermediate 2.2 – ^{13}C Spectrum (DMSO- d_6 , T = 25 °C)



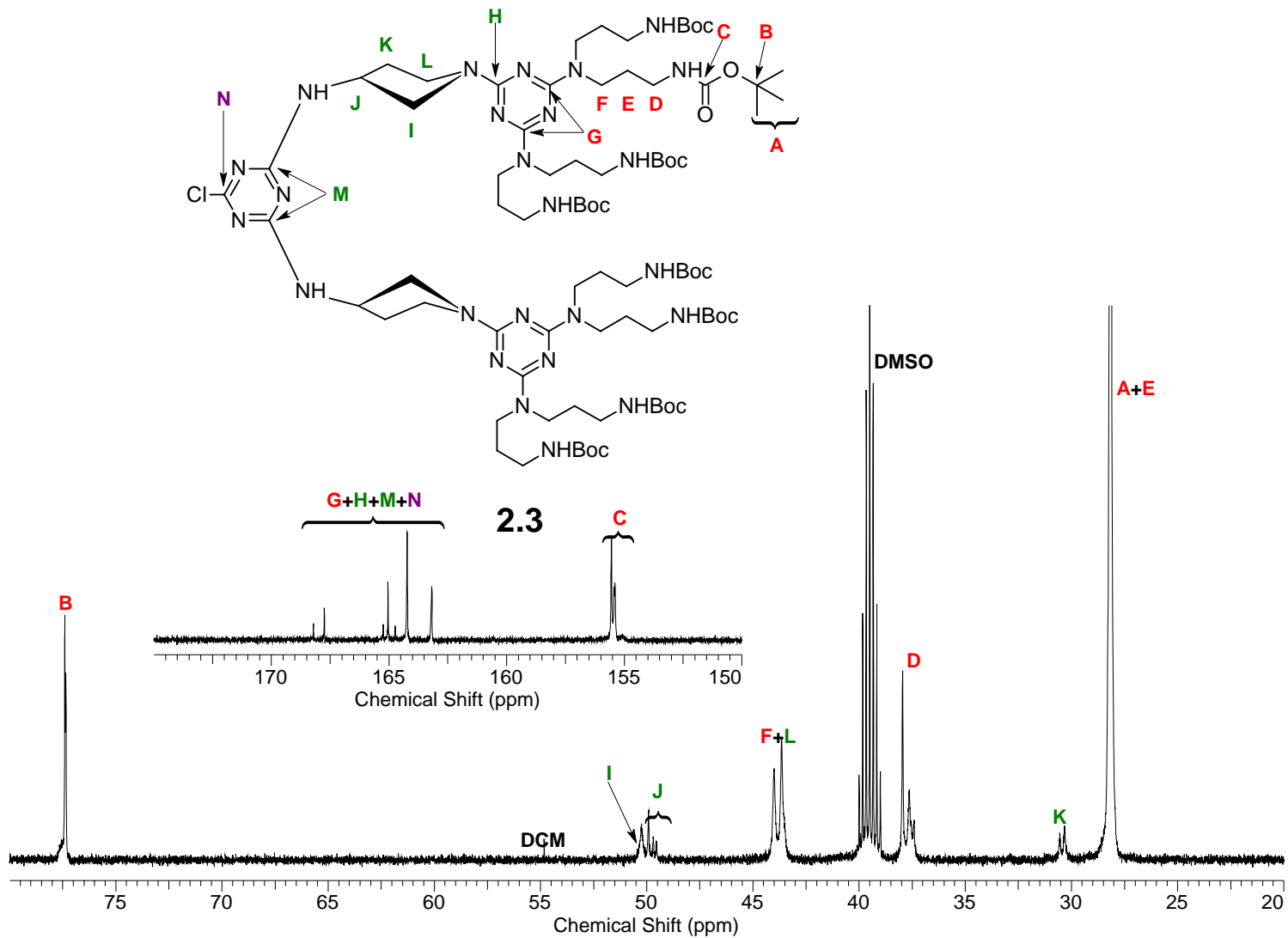
Intermediate 2.2 – (^1H - ^1H) COSY Spectrum (DMSO- d_6 , T = 25 °C)



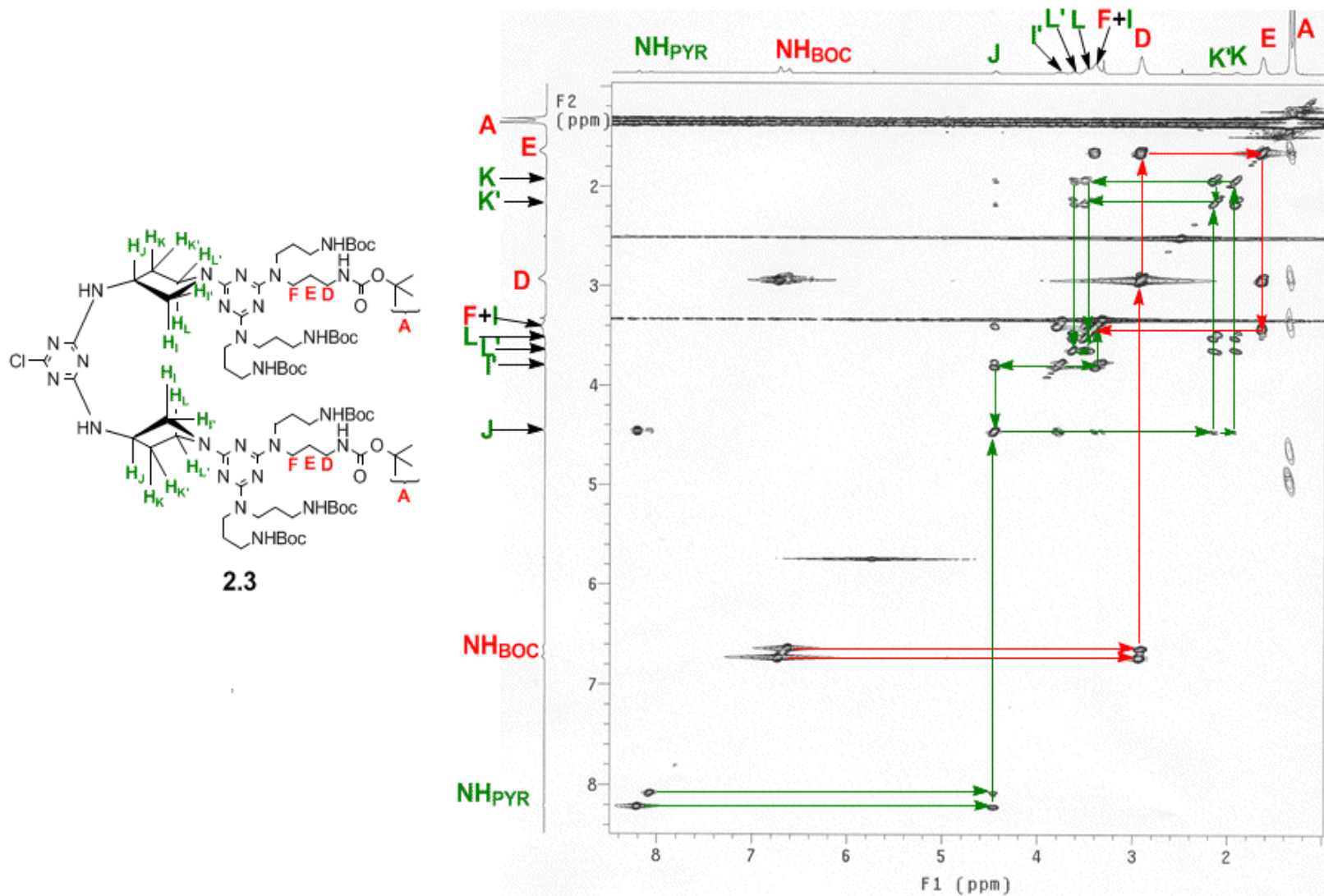
Intermediate 2.3 – ^1H Spectrum (DMSO- d_6 , T = 25 °C)



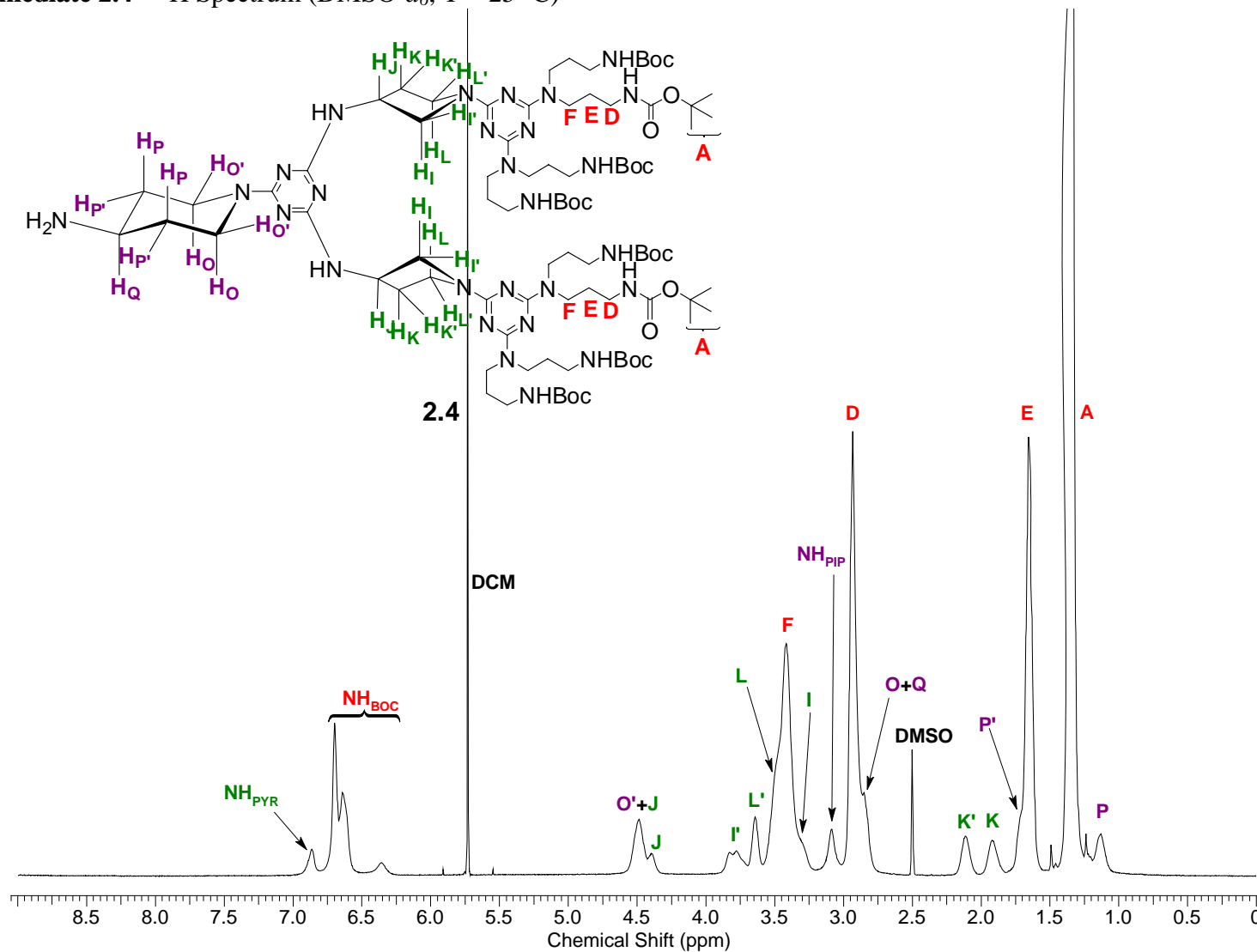
Intermediate 2.3 – ^{13}C Spectrum (DMSO- d_6 , T = 25 °C)



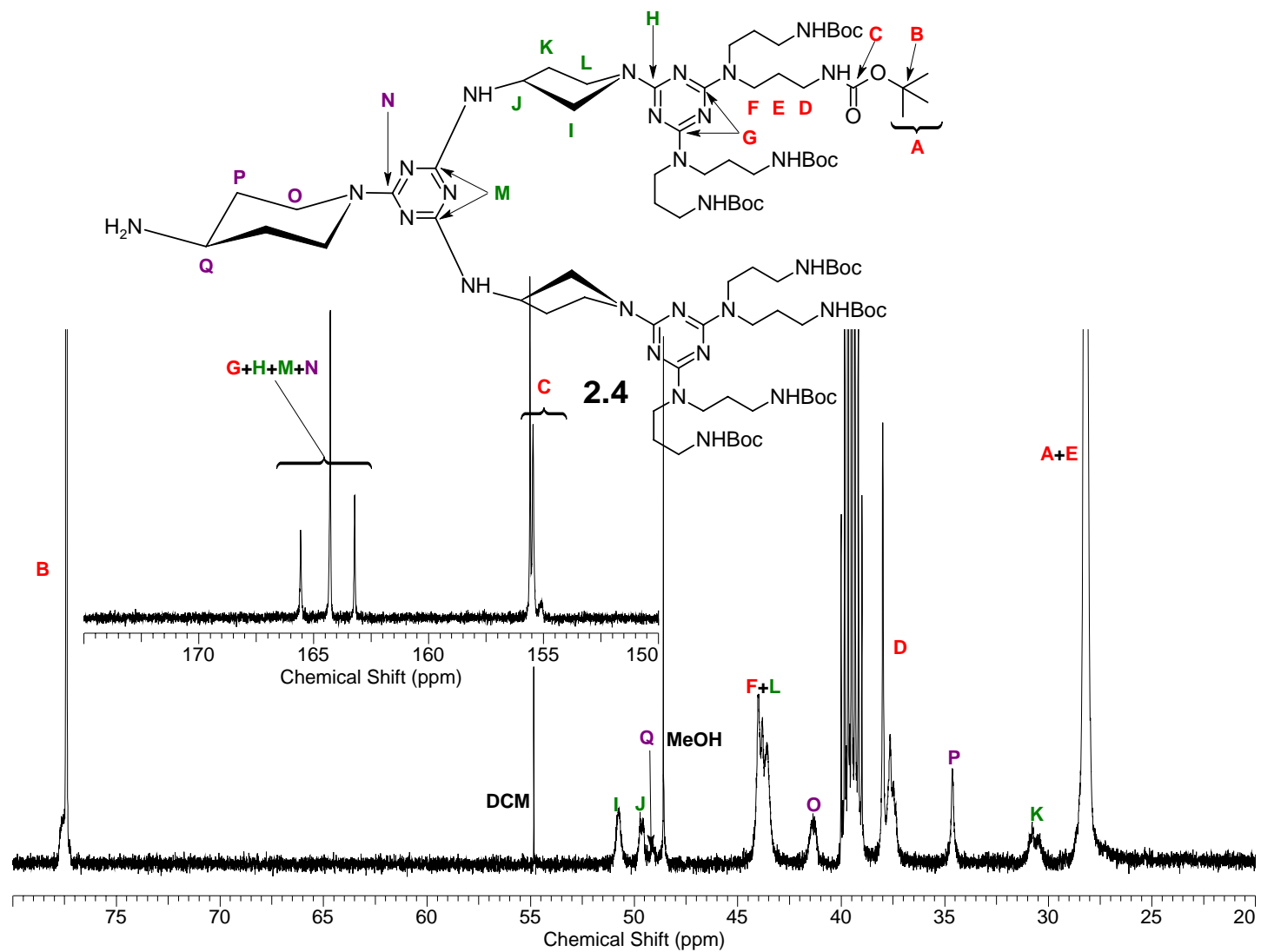
Intermediate 2.3 – (¹H–¹H) COSY Spectrum (DMSO-*d*₆, T = 25 °C)



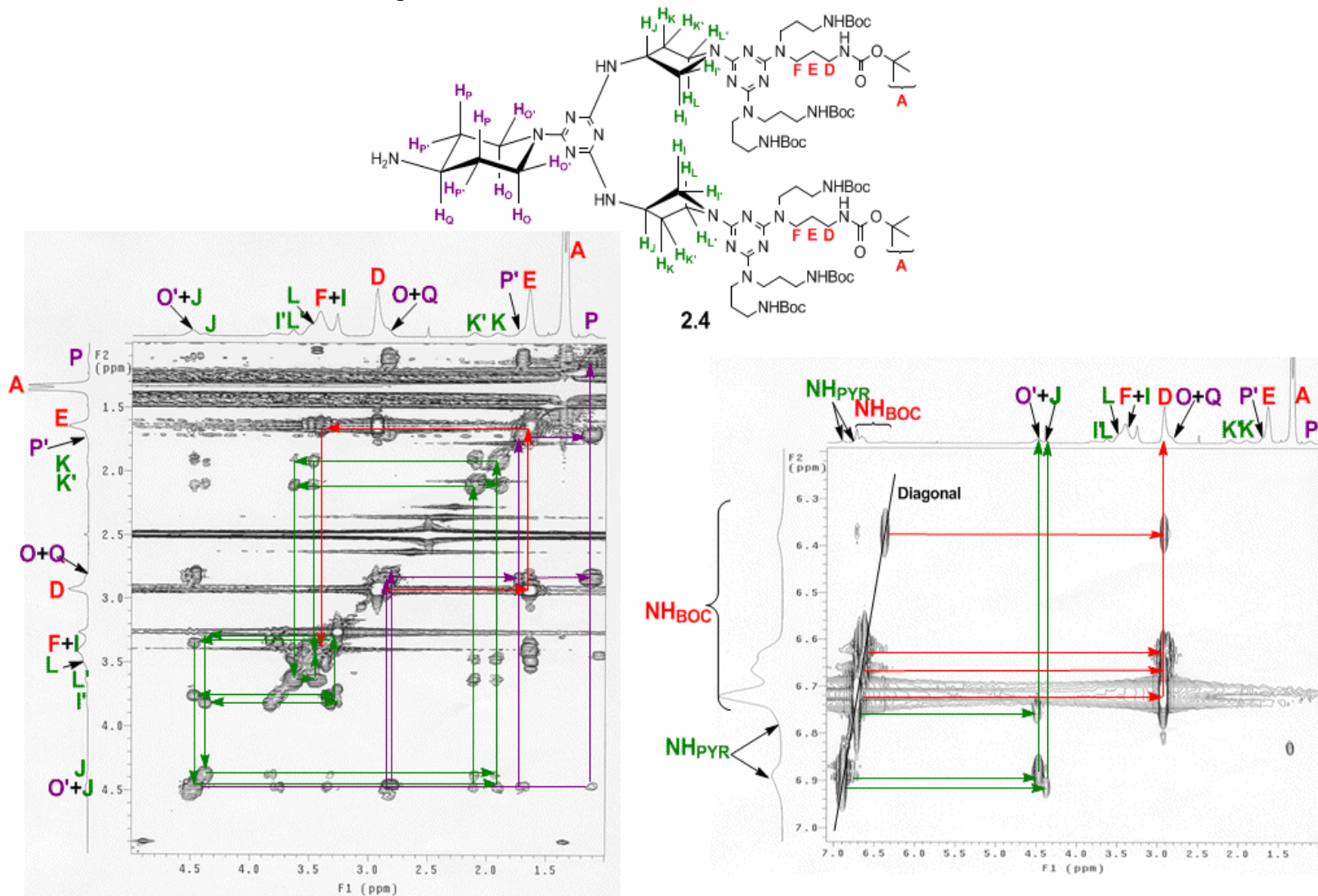
Intermediate 2.4 – ^1H Spectrum (DMSO- d_6 , T = 25 °C)



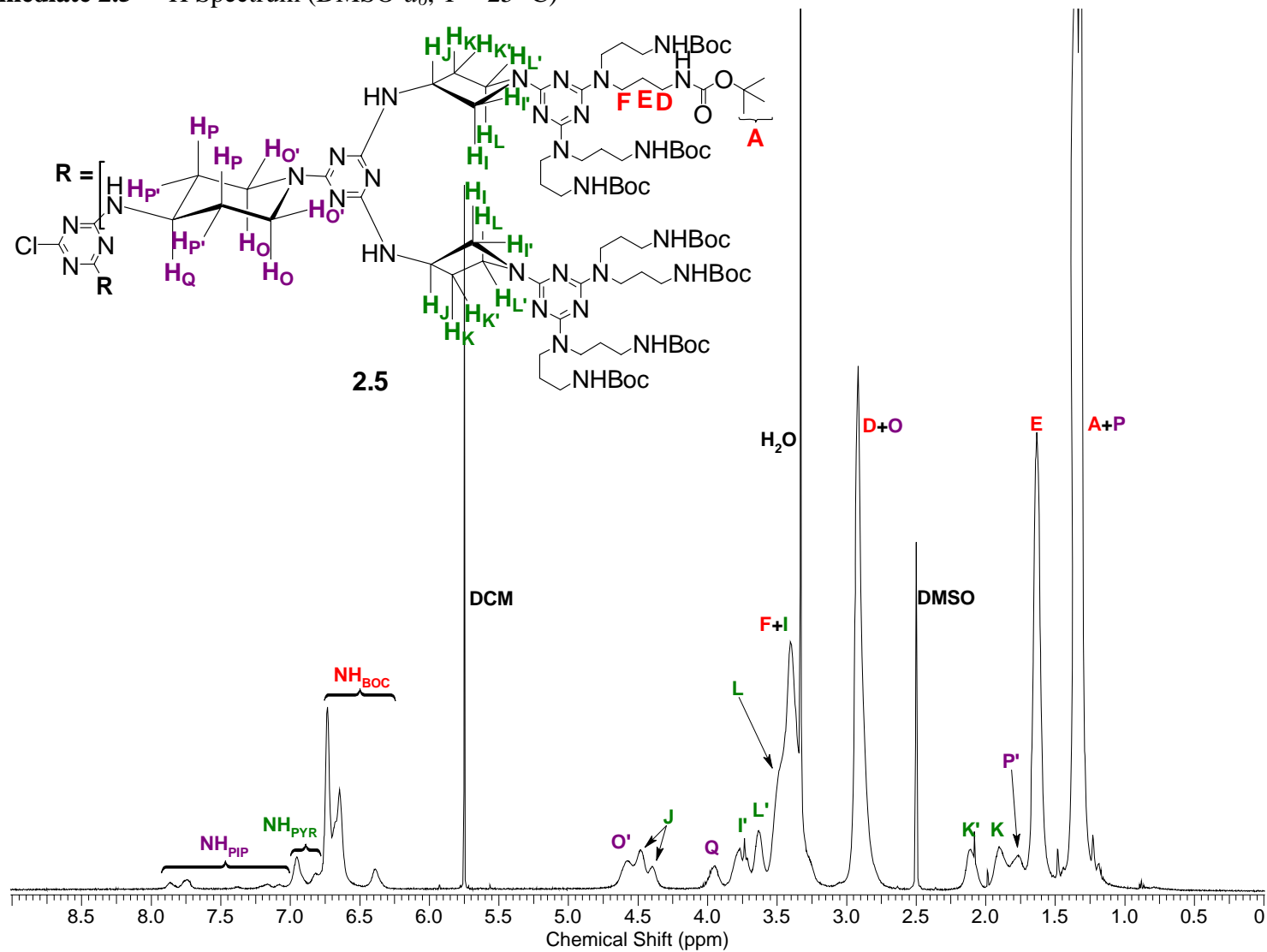
Intermediate 2.4 – ^{13}C Spectrum (DMSO- d_6 , T = 25 °C)



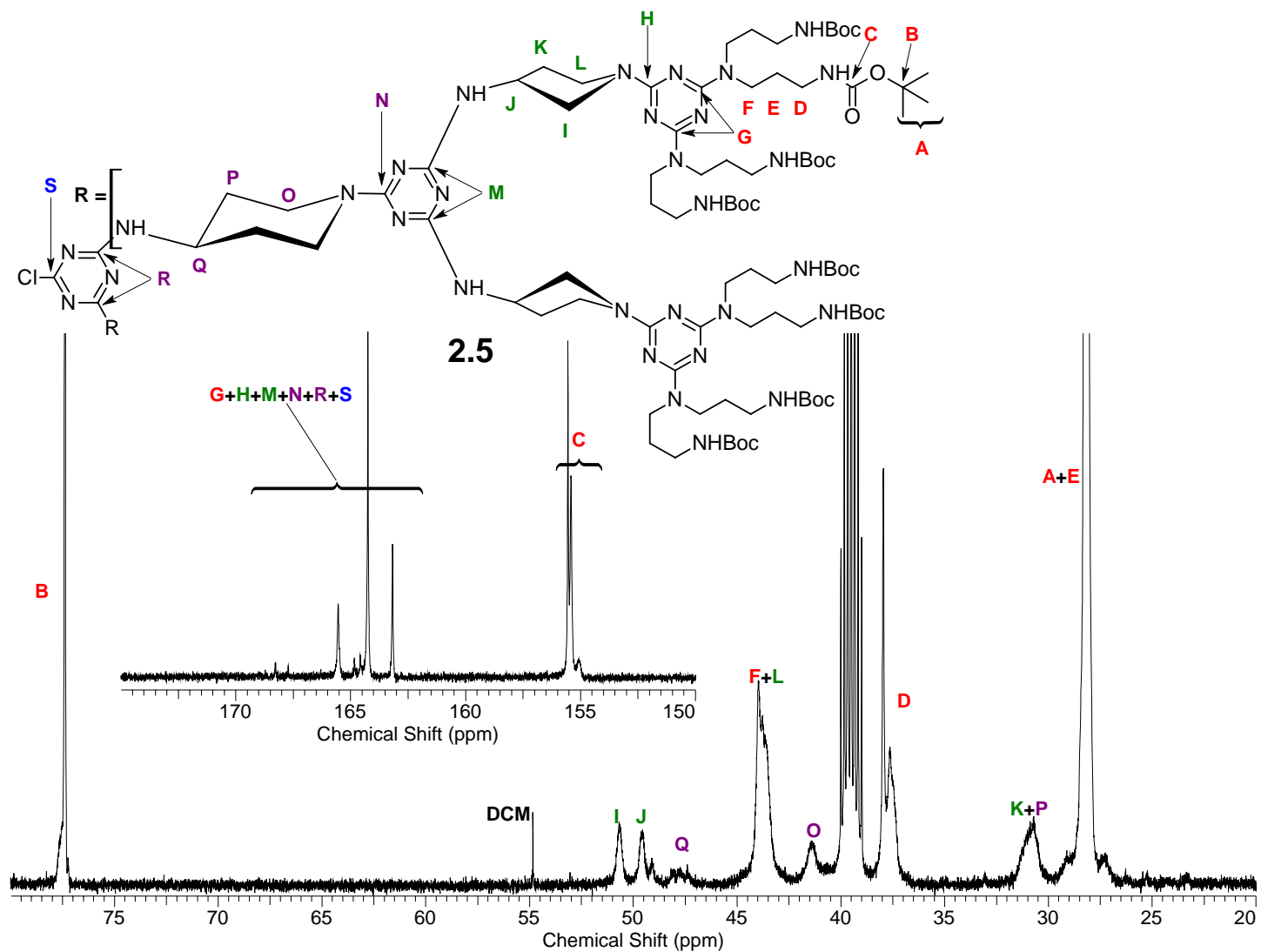
Intermediate 2.4 – (¹H–¹H) COSY Spectrum (DMSO-*d*₆, T = 25 °C)



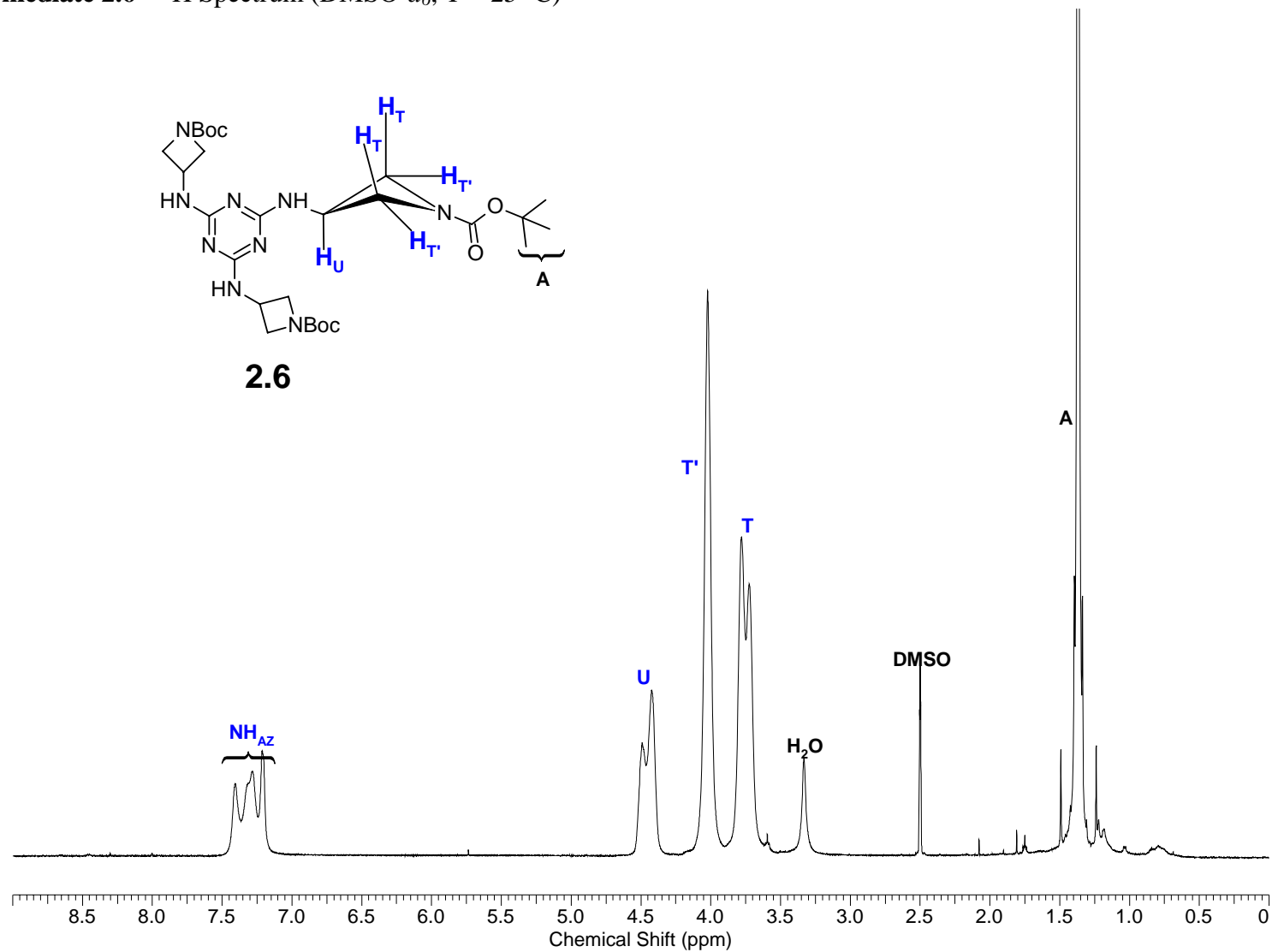
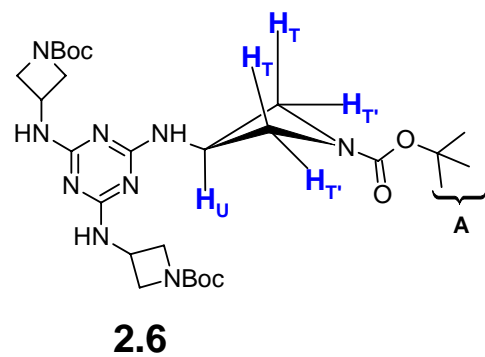
Intermediate 2.5 – ^1H Spectrum (DMSO- d_6 , T = 25 °C)



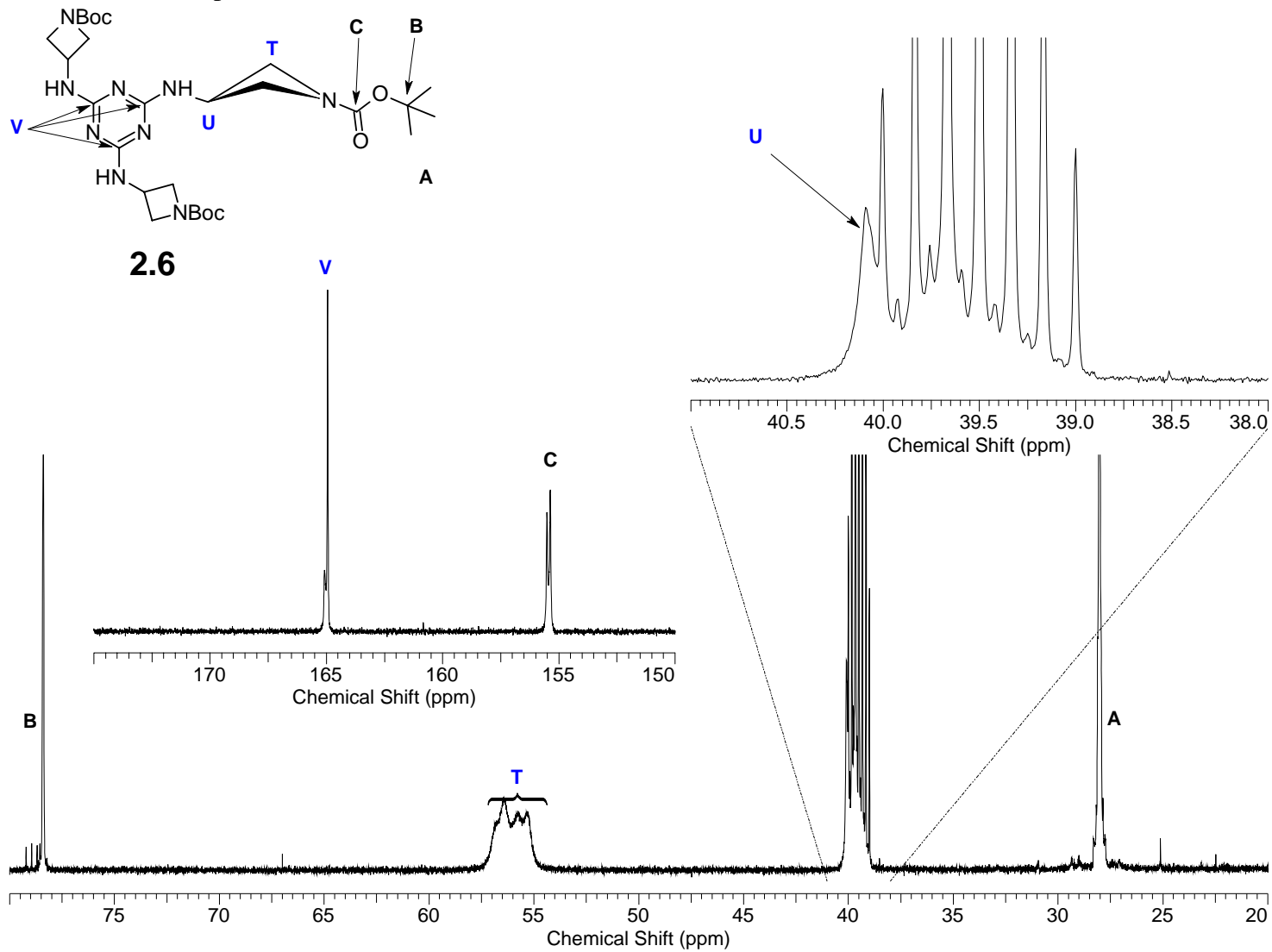
Intermediate 2.5 – ^{13}C Spectrum (DMSO- d_6 , T = 25 °C)



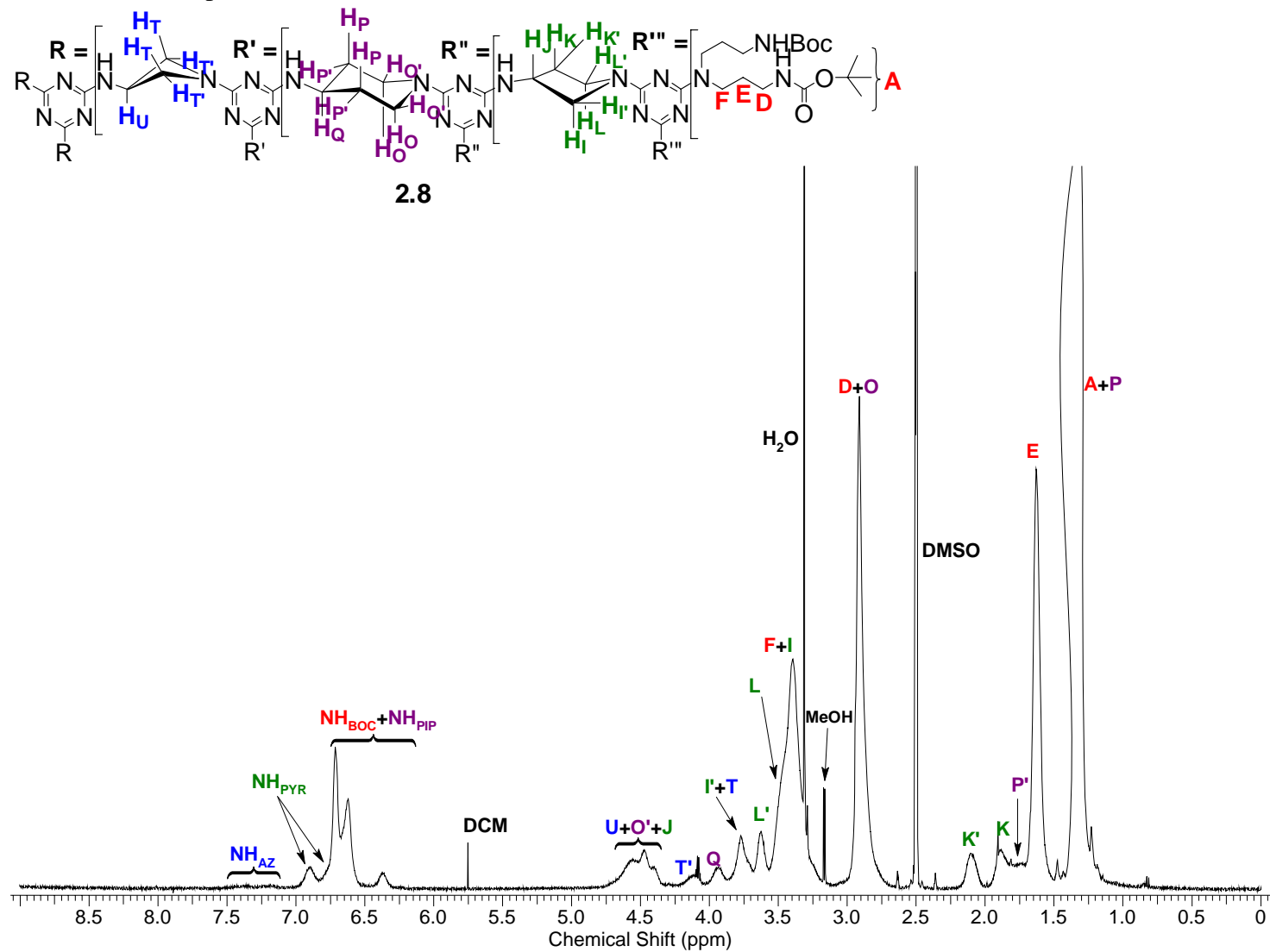
Intermediate 2.6 – ^1H Spectrum (DMSO- d_6 , T = 25 °C)



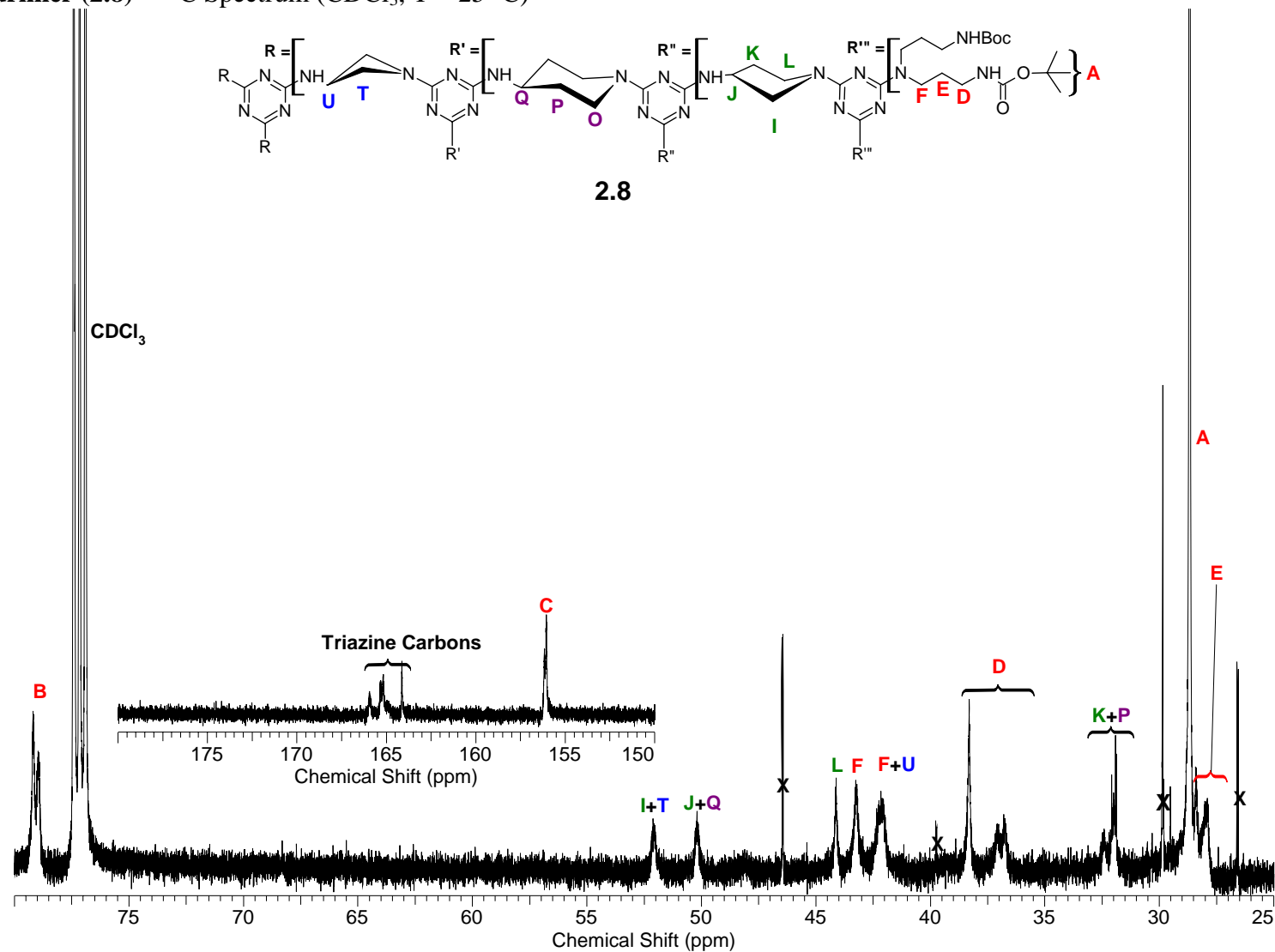
Intermediate 2.6 – ^{13}C Spectrum (DMSO- d_6 , T = 25 °C)



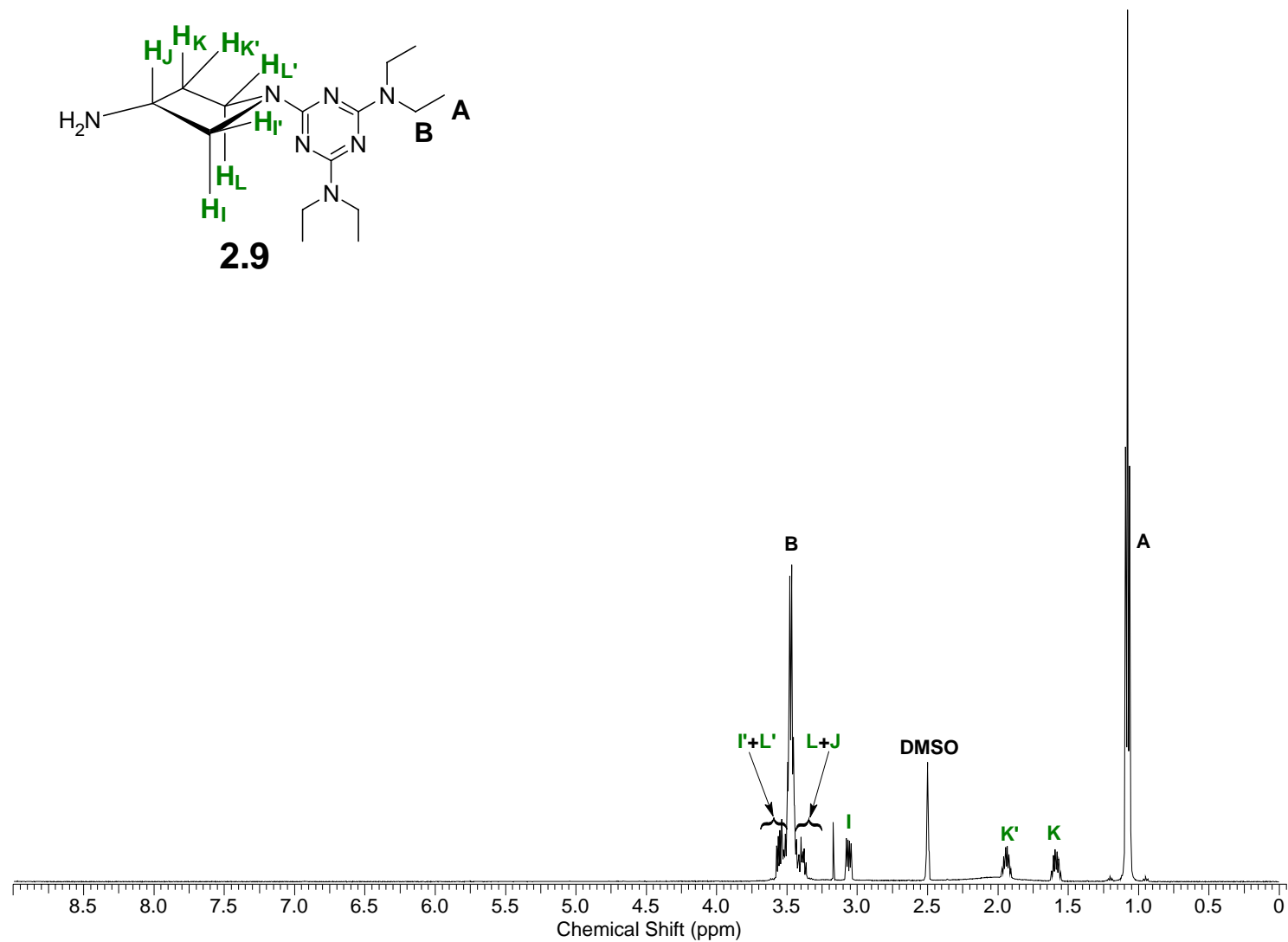
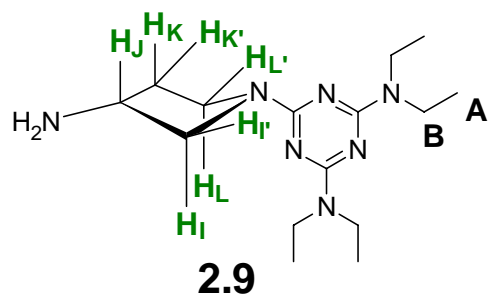
Dendrimer (2.8) – ^1H Spectrum (DMSO- d_6 , T = 25 °C)



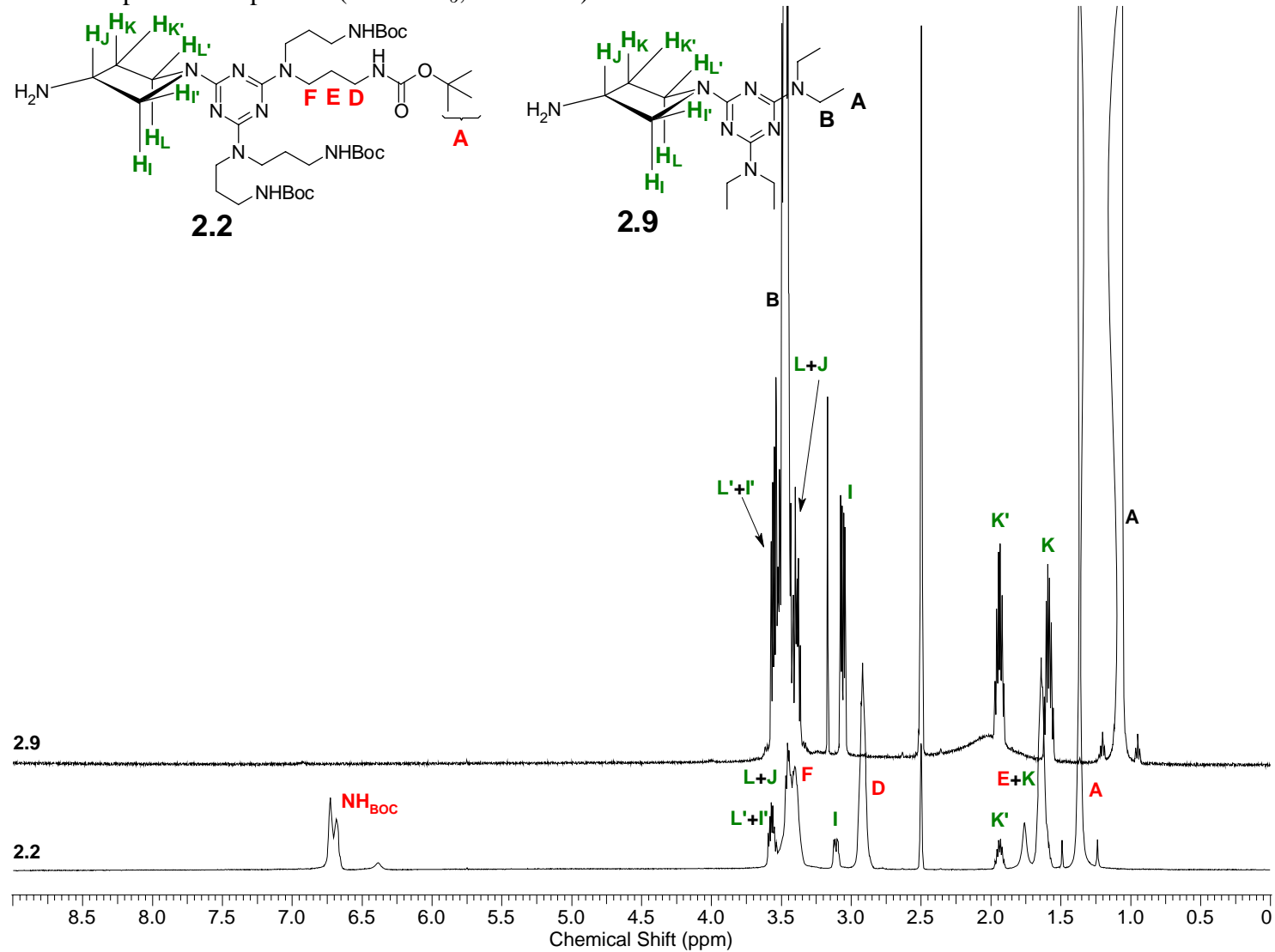
Dendrimer (2.8) – ^{13}C Spectrum (CDCl_3 , $T = 25\text{ }^\circ\text{C}$)



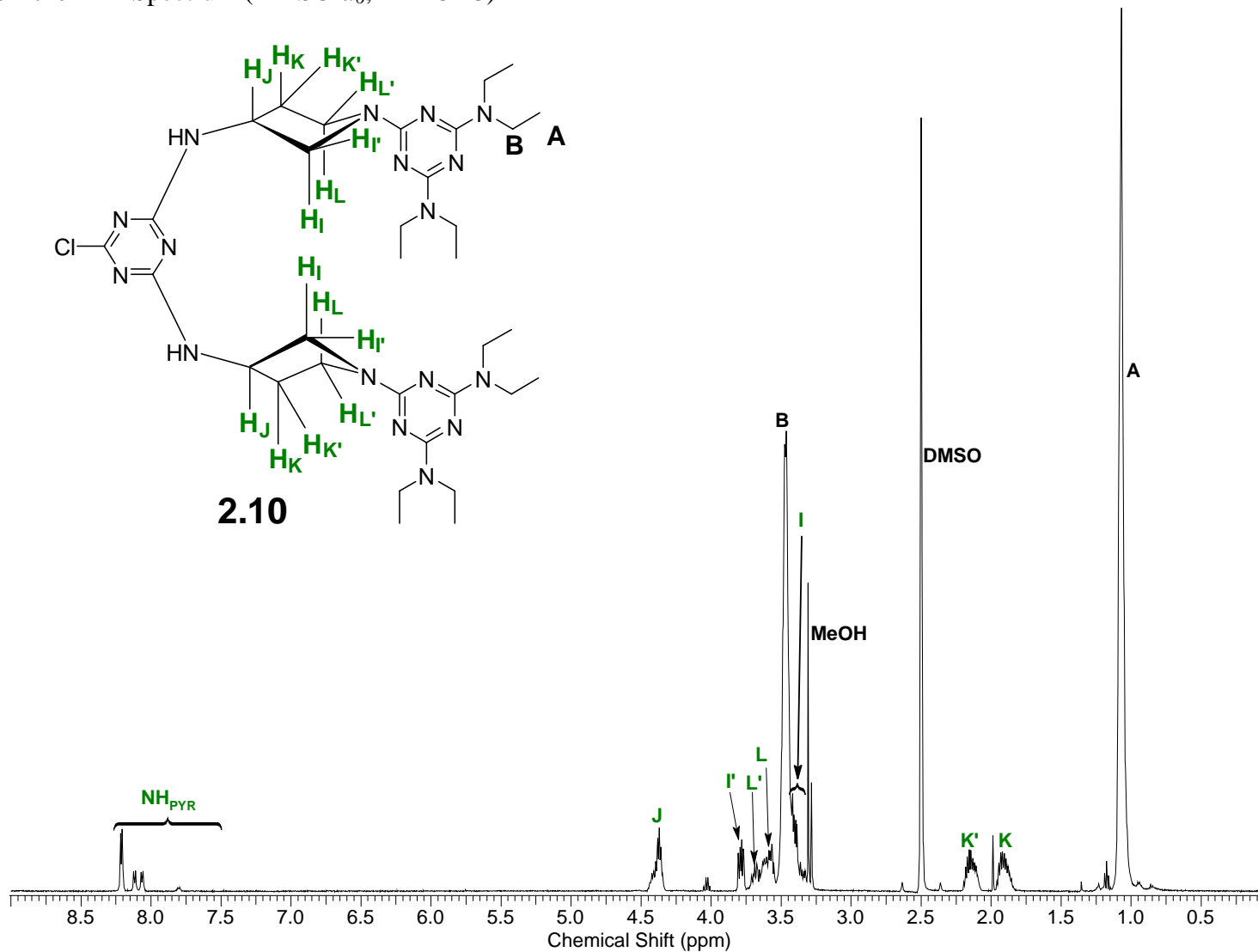
Model 2.9 – ^1H Spectrum (DMSO- d_6 , T = 25 °C)



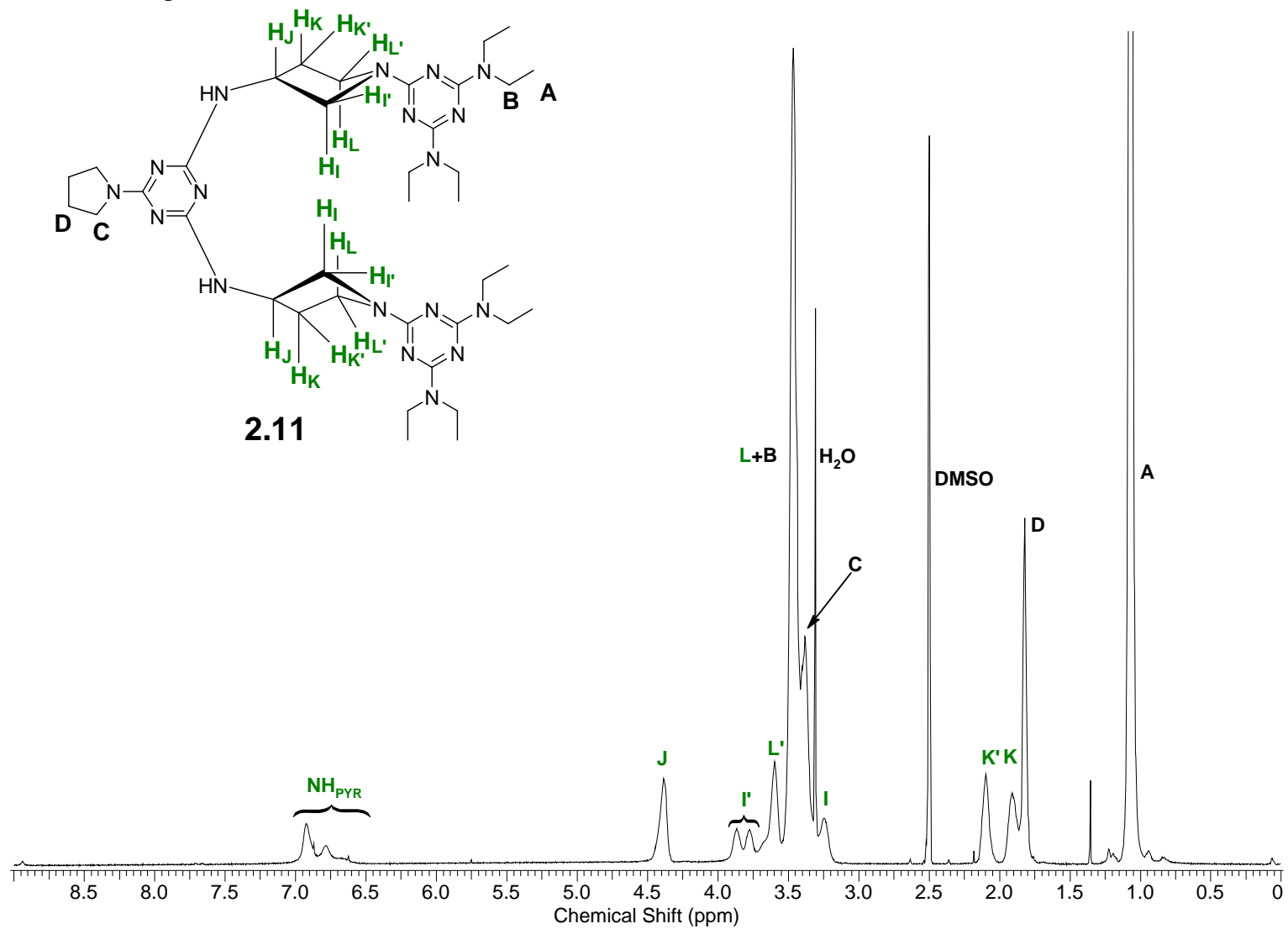
2.2 & 2.9 – ^1H Spectra Comparison (DMSO- d_6 , T = 25 °C)



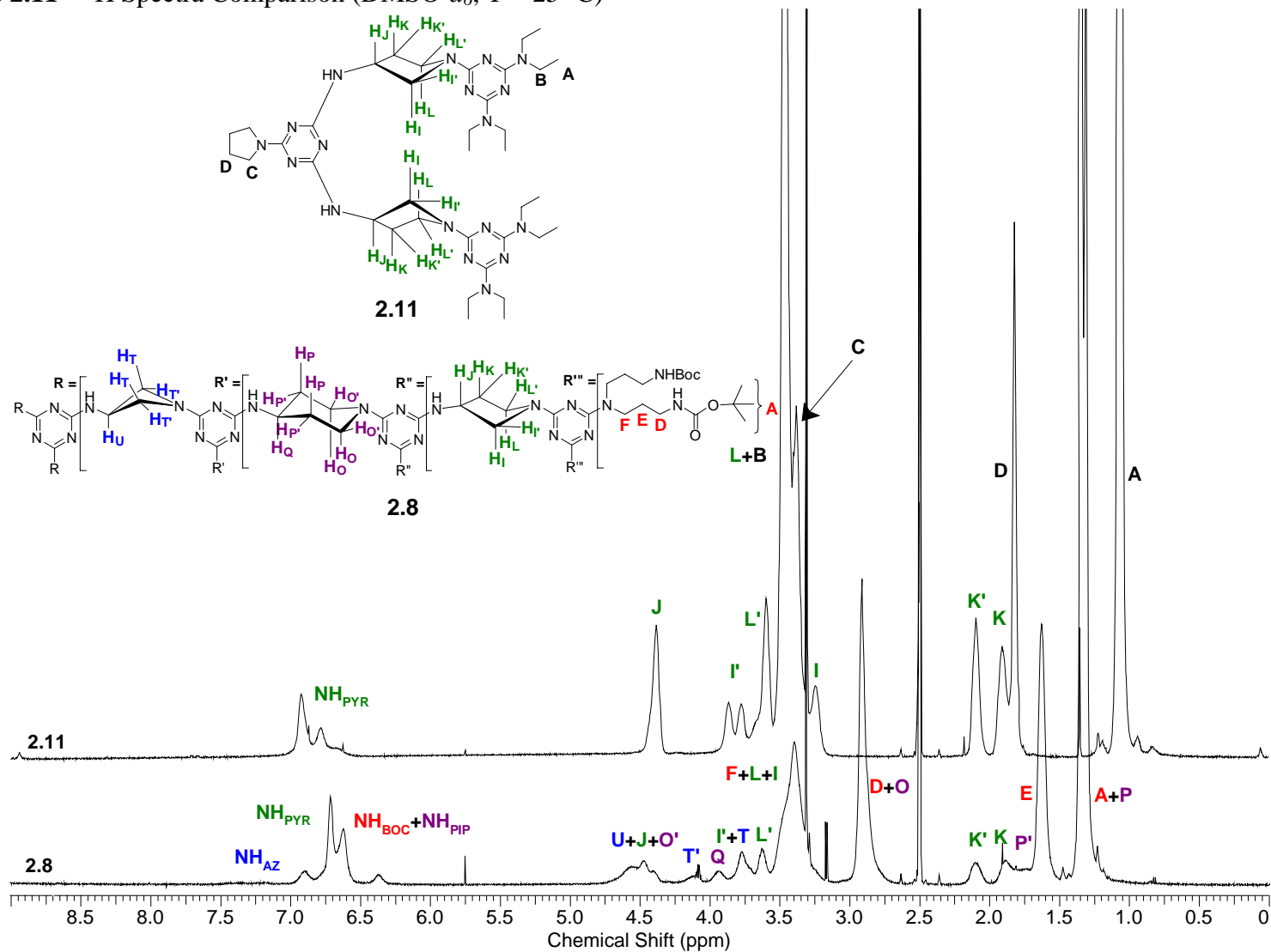
Model 2.10 – ^1H Spectrum (DMSO- d_6 , T = 25 °C)



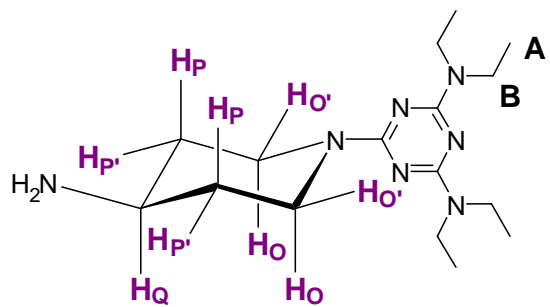
Model 2.11 – ^1H Spectrum (DMSO- d_6 , T = 25 °C)



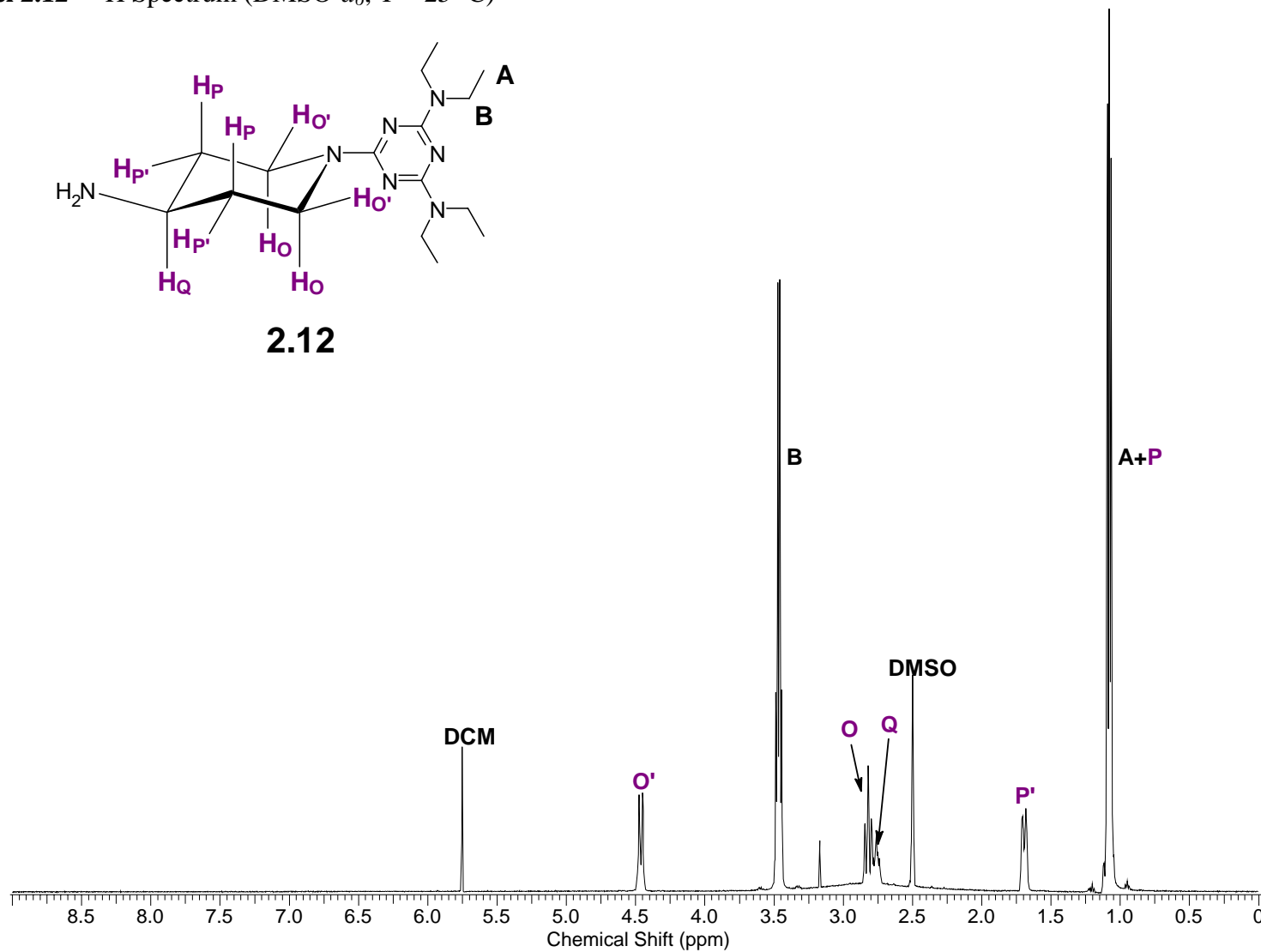
2.8 & 2.11 – ^1H Spectra Comparison (DMSO- d_6 , T = 25 °C)



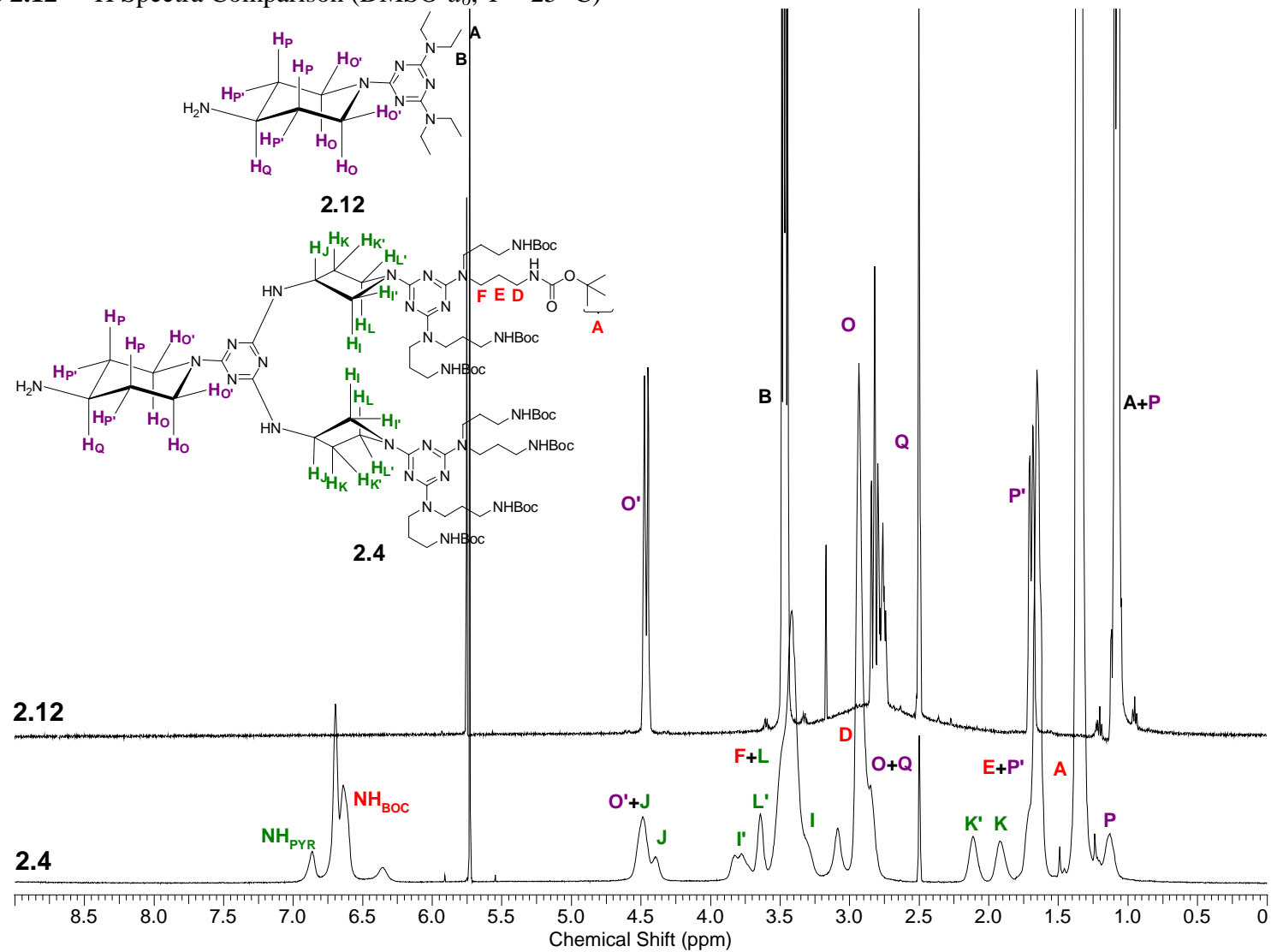
Model 2.12 – ^1H Spectrum (DMSO- d_6 , T = 25 °C)



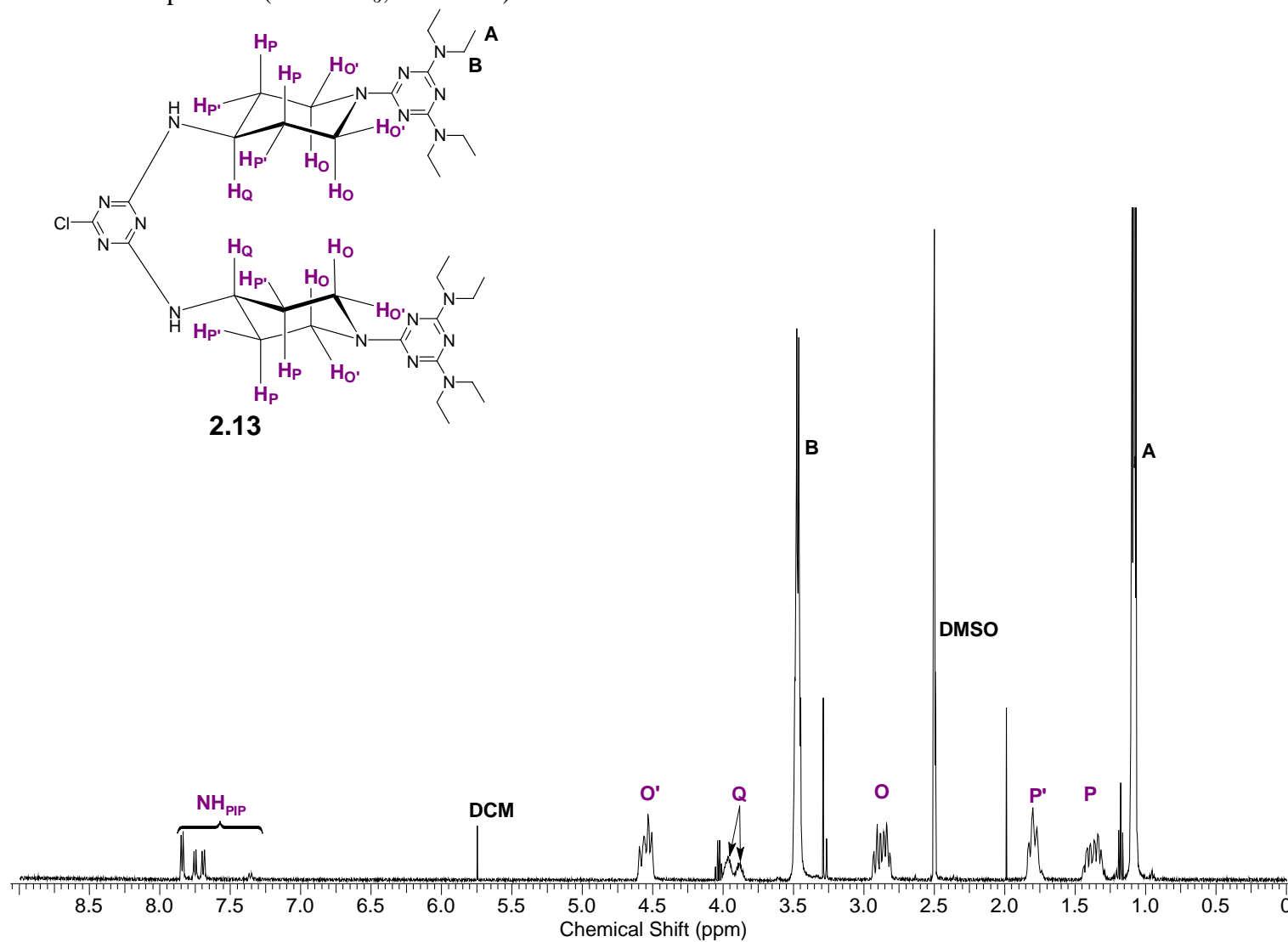
2.12



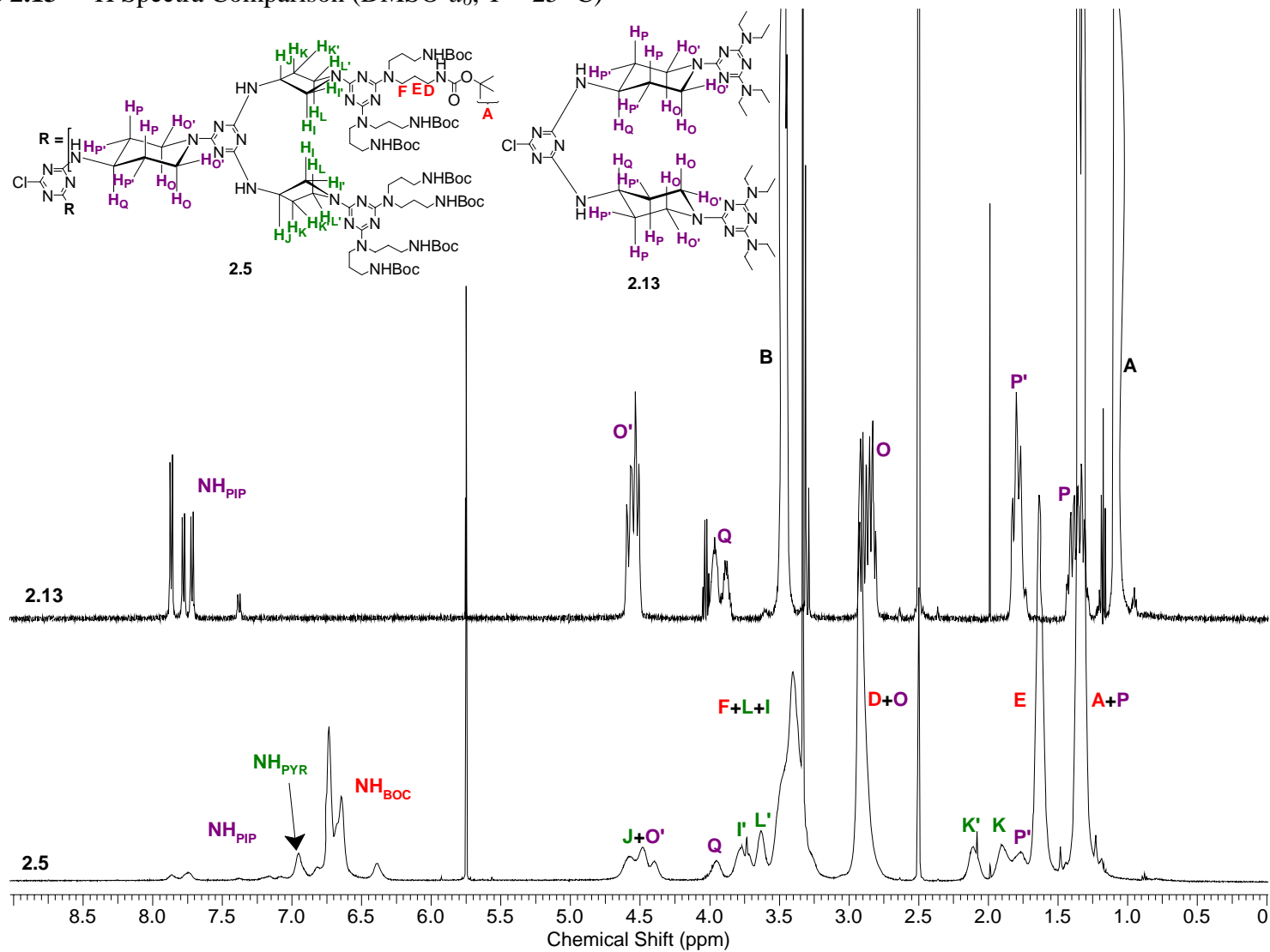
2.4 & 2.12 – ^1H Spectra Comparison (DMSO- d_6 , T = 25 °C)



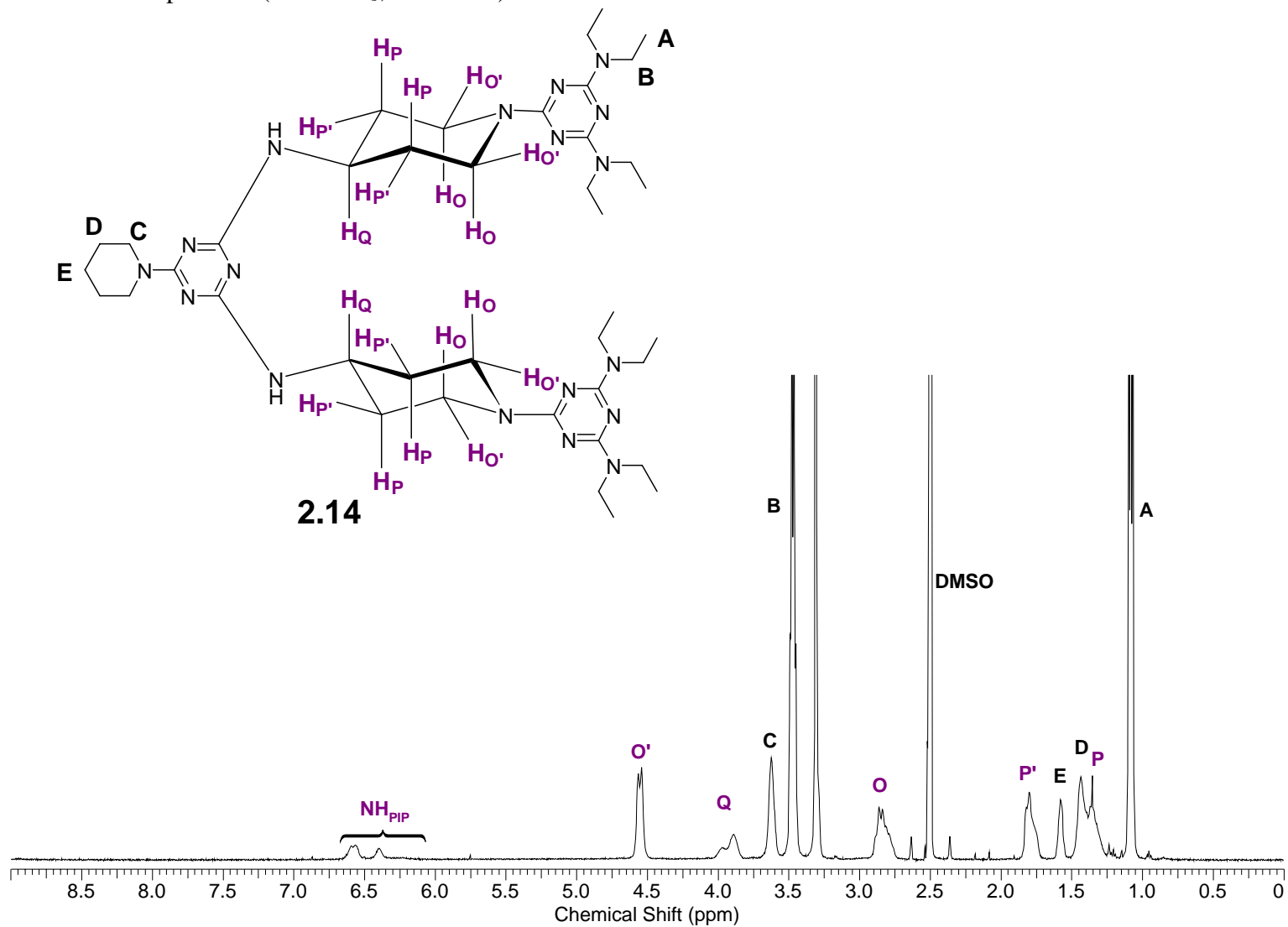
Model 2.13 – ^1H Spectrum (DMSO- d_6 , T = 25 °C)



2.5 & 2.13 – ^1H Spectra Comparison (DMSO- d_6 , T = 25 °C)



Model 2.14 – ^1H Spectrum (DMSO- d_6 , T = 25 °C)



2.8 & 2.14 – ^1H Spectra Comparison (DMSO- d_6 , T = 25 °C)

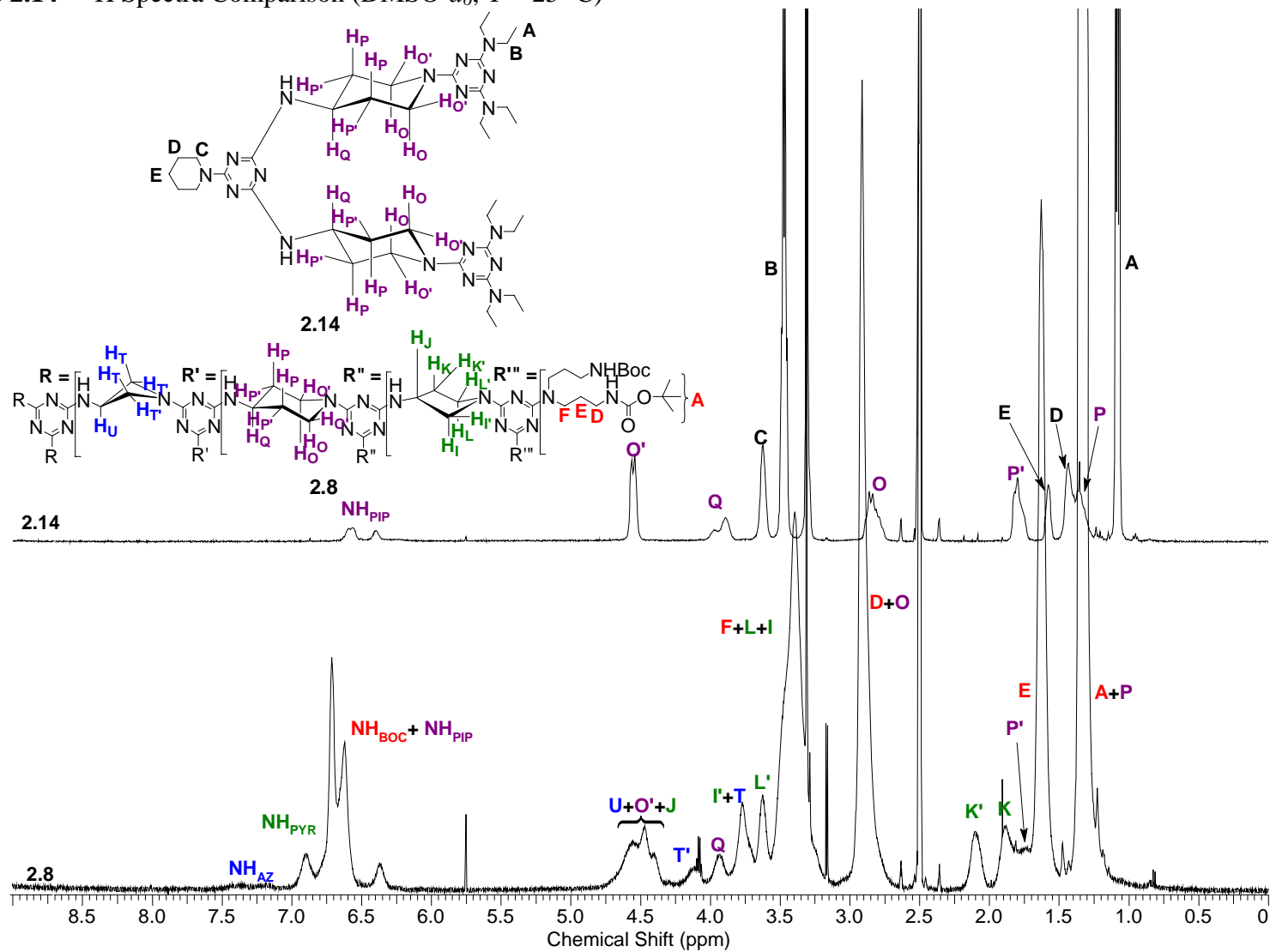


Table 3. Rotamer Populations - 1^a

Compound	Boc	Pyr	Pip	Az
Atrazine ^b	5(<i>E</i> _{Et} , <i>E</i> _{iPr}):3(<i>Z</i> _{Et} , <i>E</i> _{iPr}):3(<i>E</i> _{Et} , <i>Z</i> _{iPr}):1(<i>Z</i> _{Et} , <i>Z</i> _{iPr})			
2.1	12 : 1			
2.2	8 : 7 : 1			
2.3	9 : 8 : 1	13 : 6 : 1		
2.4	12 : 10 : 1 ^c	^d		
2.5	7 : 6 : 1	2.5 : 1	3 : 8 : 1 : 4 : 1	
2.6				1 : 1 : 1 : 1
2.8	9 : 9 : 1 ^e	1 : 1.3	^d	^f
3.3	17 : 1			
2.9				
2.10		14 : 5 : 5 : 1		
2.11		10 : 4 : 1		
2.12				
2.13			5 : 4 : 4 : 1	
2.14			7 : 4 : 1	

^aRatios relate to most downfield NH to most upfield NH for each type. Refer to Figure 4 of manuscript.

^bRefs. 74-75

^cRatio includes Pyr-NH.

^dRatio not determined due to resonances buried under Boc resonances.

^eRatio includes Pip-NH.

^fRatio not determined due to the broadness of the peaks

Table 4. Rotamer Populations - 2

Compound	<i>Anti:Syn</i>
2.1	12:1
3.3	17:1

Highlighted in red are the atoms involved in determining the *syn* or *anti* conformation of the carbamate bond. Comparing the model compound to **2.1**, the *anti* conformation is clearly favored over the *syn* conformation in a 17:1 and 12:1 respectively. This correlates well with literature values of *anti:syn* ratio being 10:1.⁷¹ The spectrum of **2.1** provides potentially more complexity than just the *syn* and *anti* conformations. The resonance for the *anti* conformation is two triplets overlapping one another. This may be due to two of the carbamates being influenced by the deshielding effects of the chlorine atom.

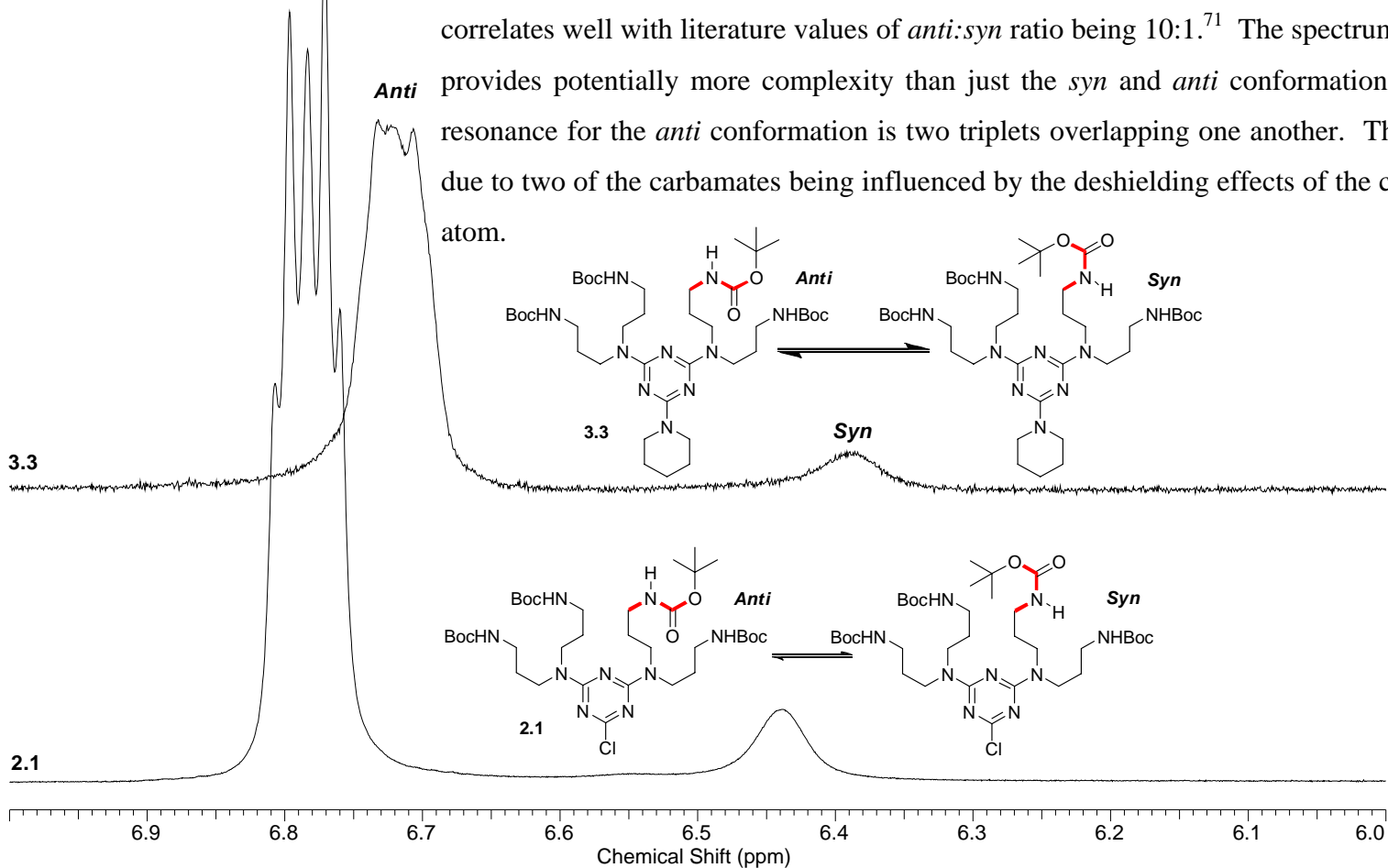


Table 5. Rotamer Populations - 3

Compound	Boc	Pyr
2.1	12:1	
3.3	17:1	
2.2	8:7:1	

Analysis of this spectrum provides evidence that the carbamate resonances are being influenced by the third substituent on the triazine ring, in this case 3-aminopyrrolidine. Here we are able to more distinctly observe the two environments of the *anti* conformation. Comparison of this ratio with **2.1** does not show any significant difference

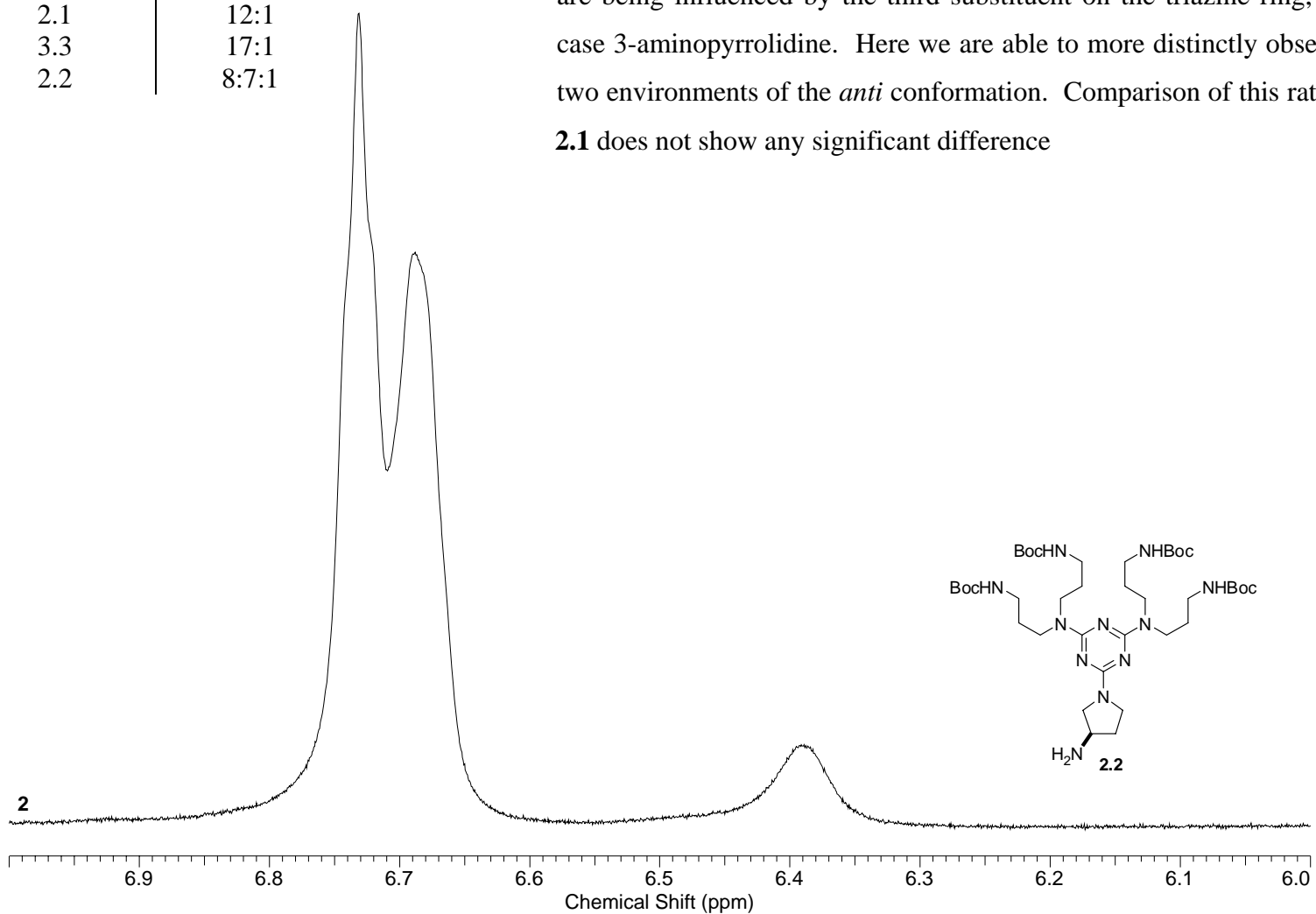


Table 6. Rotamer Populations - 4

Compound	Boc	Pyr
2.1	12:1	
3.3	17:1	
2.2	8:7:1	
2.3	9:8:1	13:6:1
2.10		14:5:5:1

Comparison of **2.3** and **2.10** identifies the rotamers of the pyrrolidine-NH. The deshielding effects of the chlorine atom shift the resonances far downfield. Model **2.10** shows four distinct doublets in a 14:5:5:1 ratio. In **2.3**, this ratio is 13:6:1. The two different chemical shifts for the (*E,Z*) rotamer of M2 has yet to be explained. Observance of the carbamate resonances and a shoulder appears for one of the *anti* resonances.

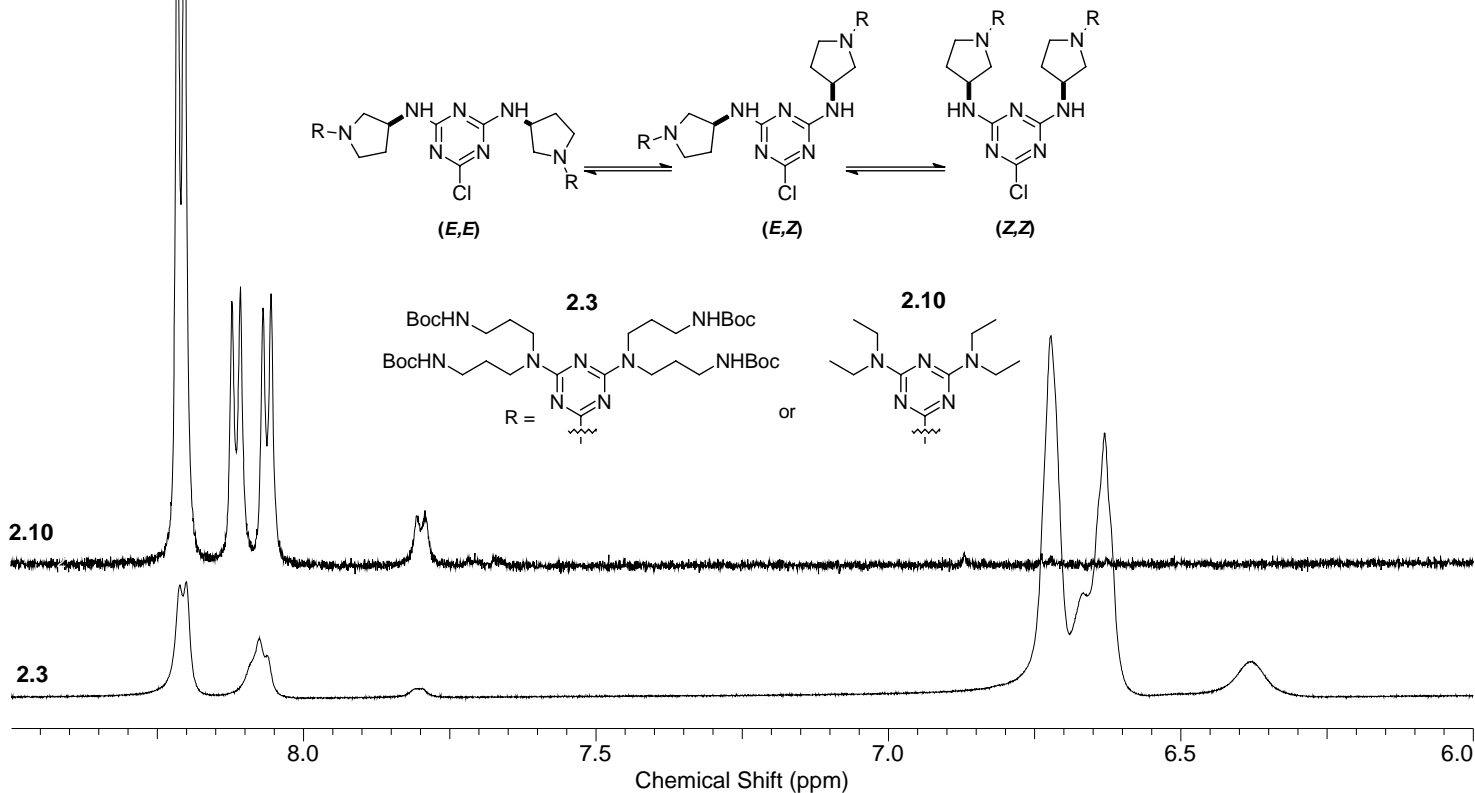
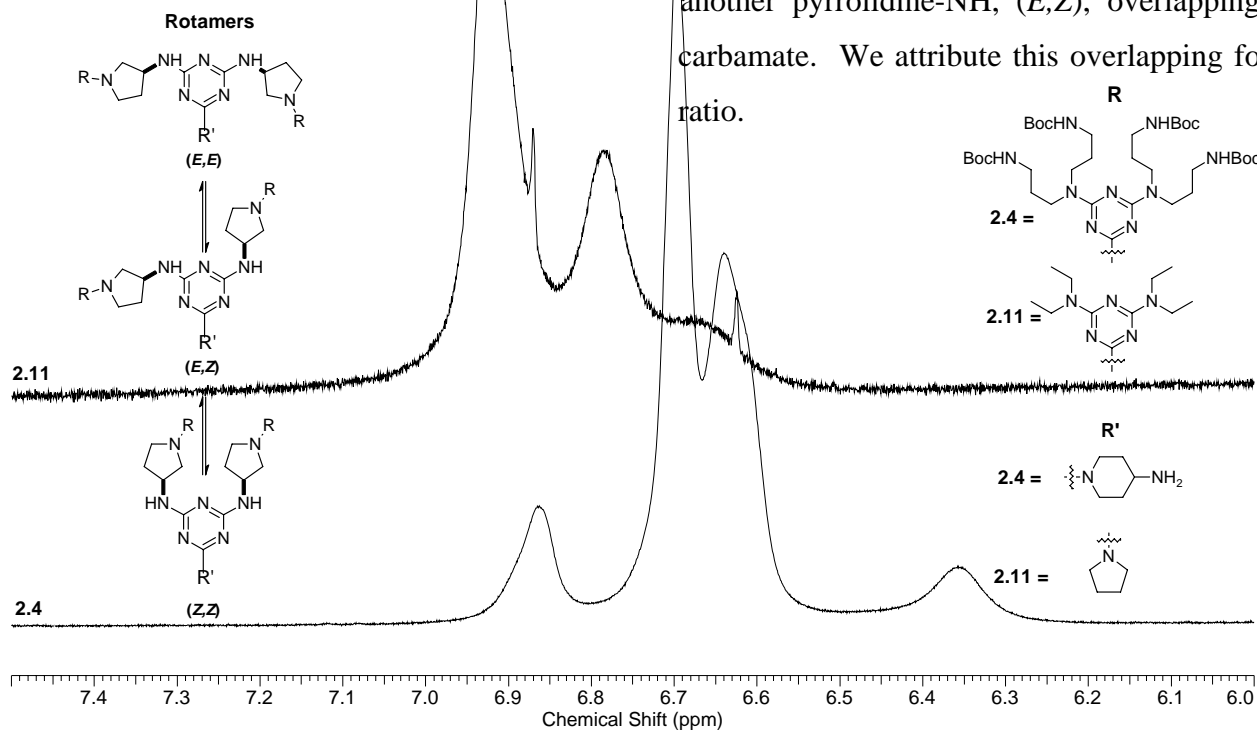


Table 7. Rotamer Populations - 5

Compound	Boc	Pyr
2.1	12:1	
3.3	17:1	
2.2	8:7:1	
2.3	9:8:1	13:6:1
2.10		14:5:5:1
2.4	12:10:1	*
2.11		10:4:1



By displacing the chlorine with either pyrrolidine, for **2.11**, or 4-aminopiperidine, for **2.4**, the deshielding effects of the chlorine atom are removed. We observe a shift upfield of the pyrrolidine resonances. Comparing the model compound with **2.4**, suggests that we should observe three resonances for the pyrrolidine-NH. The only pyrrolidine-NH observed is for the (*E,E*) rotamer. COSY correlations identifies another pyrrolidine-NH, (*E,Z*), overlapping the *anti* resonances of the carbamate. We attribute this overlapping for the increase in the *anti:syn* ratio.

Table 8. Rotamer Populations - 6

Compound	Boc	Pyr	Pip
2.1	12:1		
3.3	17:1		
2.2	8:7:1		
2.3	9:8:1	13:6:1	
2.10		14:5:5:1	
2.4	12:10:1	*	
2.11		10:4:1	
2.5	7:6:1	2.5:1	3:8:other
2.13			5:4:4:1

As with **2.10**, **2.12** displays two sets of resonances for the (*E,Z*) rotamer. As before, we have not been able explain this. Intermediate **2.5** also displays a complex rotamer pattern. Using TOCSY correlations we have been able to determine that five different resonances exist. We have decided to list the ratio as 3:8:other due to the other resonances being much lower. The additional resonances may be due to a protonation event occurring, ring flipping or the globular structure of the molecule. The pyrrolidine-NH resonances are now observed with a 2.5:1 ratio. This is not much different from compound **2.2**. The ratio observed for the carbamate resonances, 7:6:1, helps support our assumption that the pyrrolidine-NH was the cause for the slight increase in **2.4**.

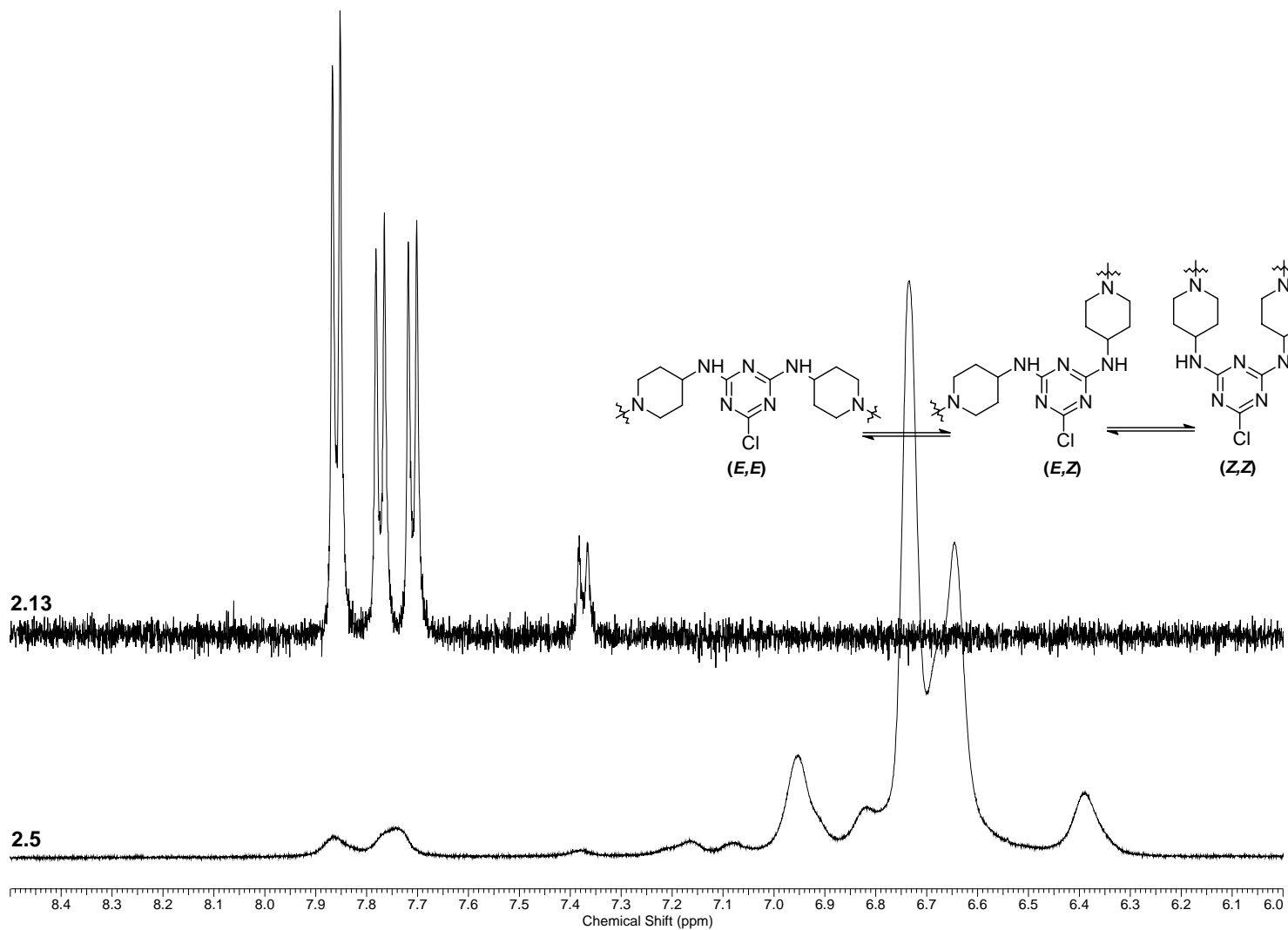
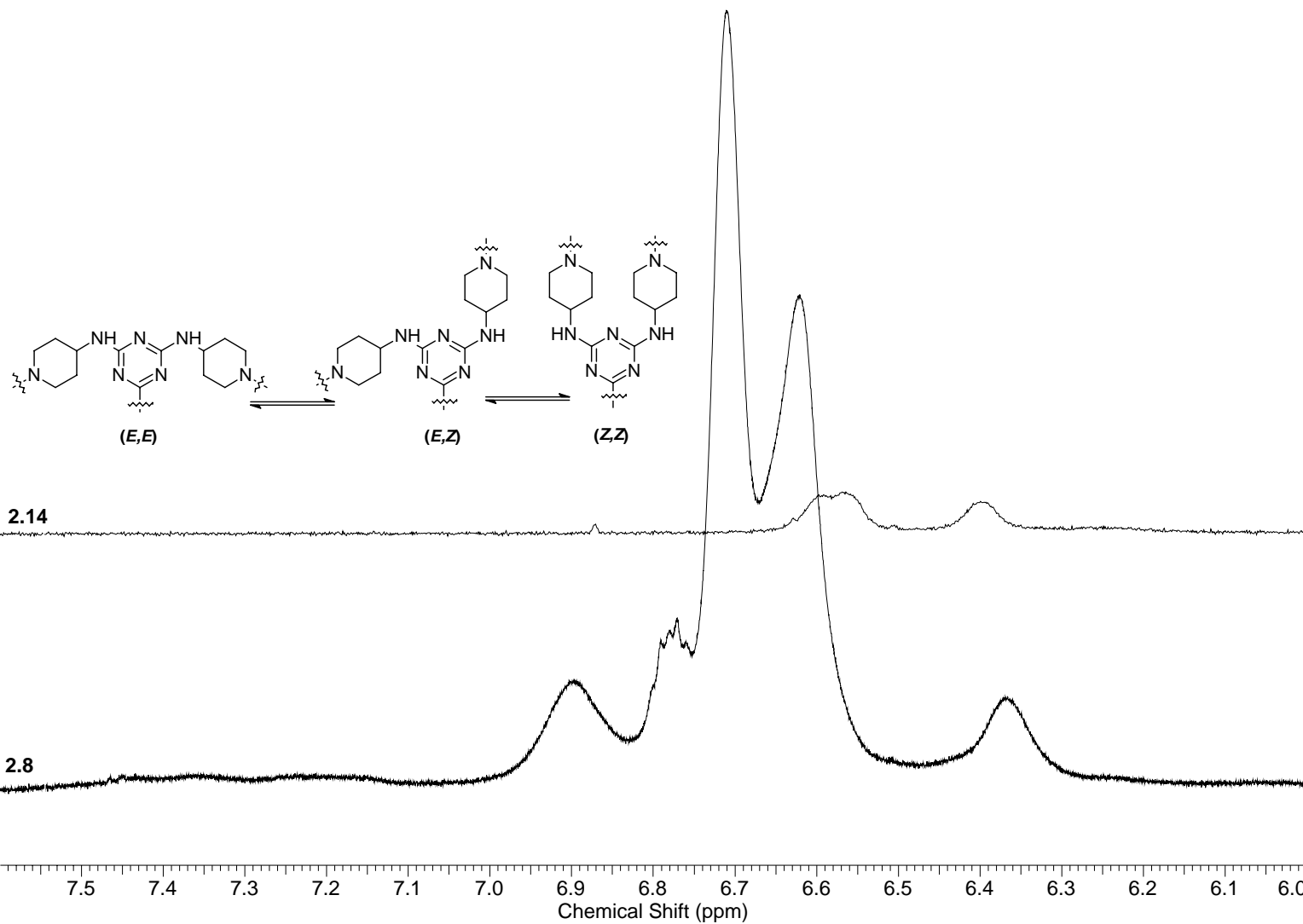


Table 9. Rotamer Populations - 7

Compound	Boc	Pyr	Pip
2.1	12:1		
3.3	17:1		
2.2	8:7:1		
2.3	9:8:1	13:6:1	
2.10		14:5:5:1	
2.4	12:10:1	*	
2.11		10:4:1	
2.5	7:6:1	2.5:1	3:8:other
2.13			5:4:4:1
2.8	9:9:1	1:1.3	**
2.14			7:4:1

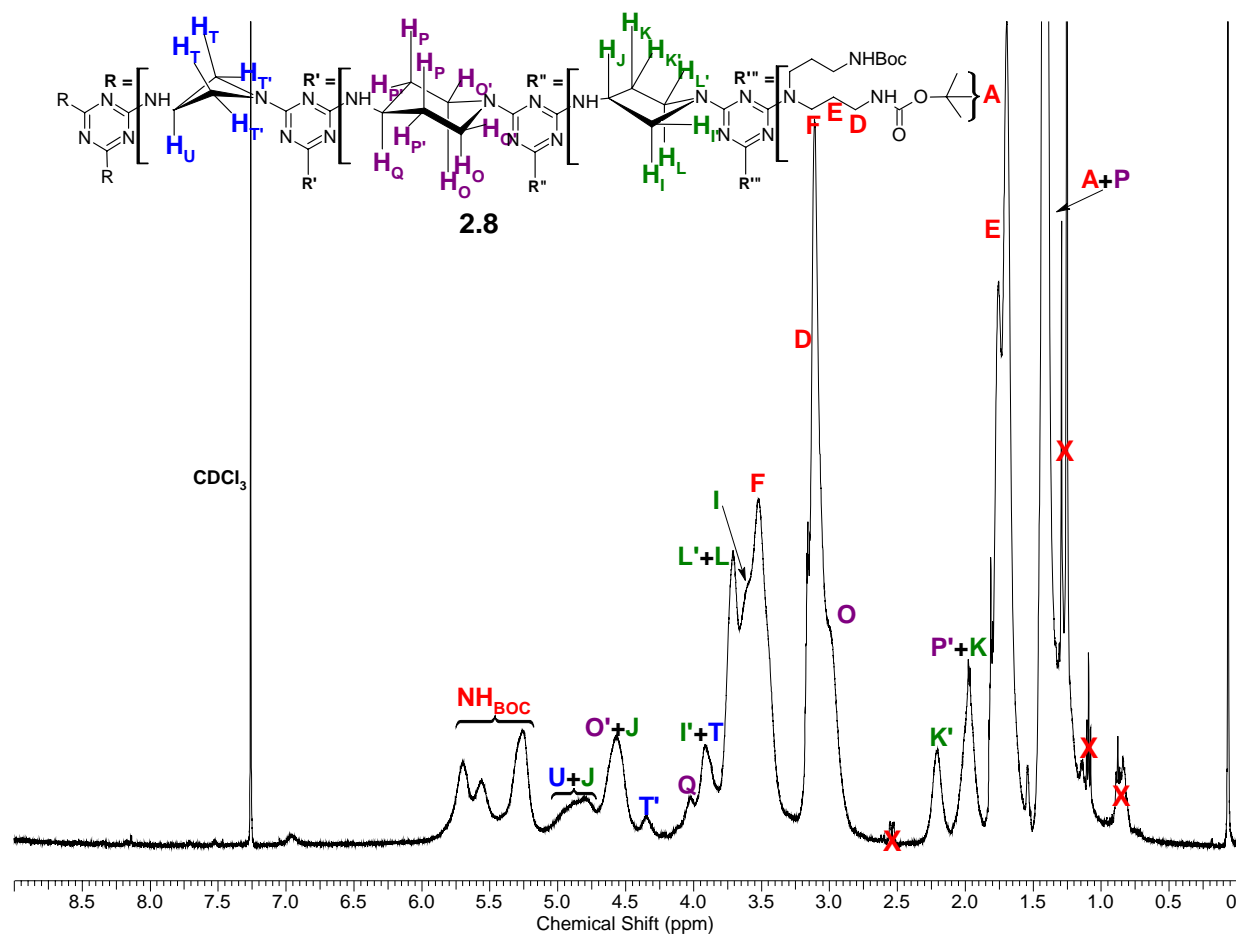
Model **2.14** shows where the resonances for the piperidine-NH rotamers should be in **2.8**. With **2.8**, we are only able to determine the ratios of the pyrrolidine and carbamate resonances. The azetidine-NH was too broad to integrate. The carbamate resonances are increased due to the piperidine-NH resonances being overlapped here as well. The pyrrolidine-NH resonances show a distinct shift towards favoring the (*E,Z*) rotamer with a 1:1.3 ratio. This shows that the globular shape of the dendrimer is influencing the preferred conformation of the rotamers.



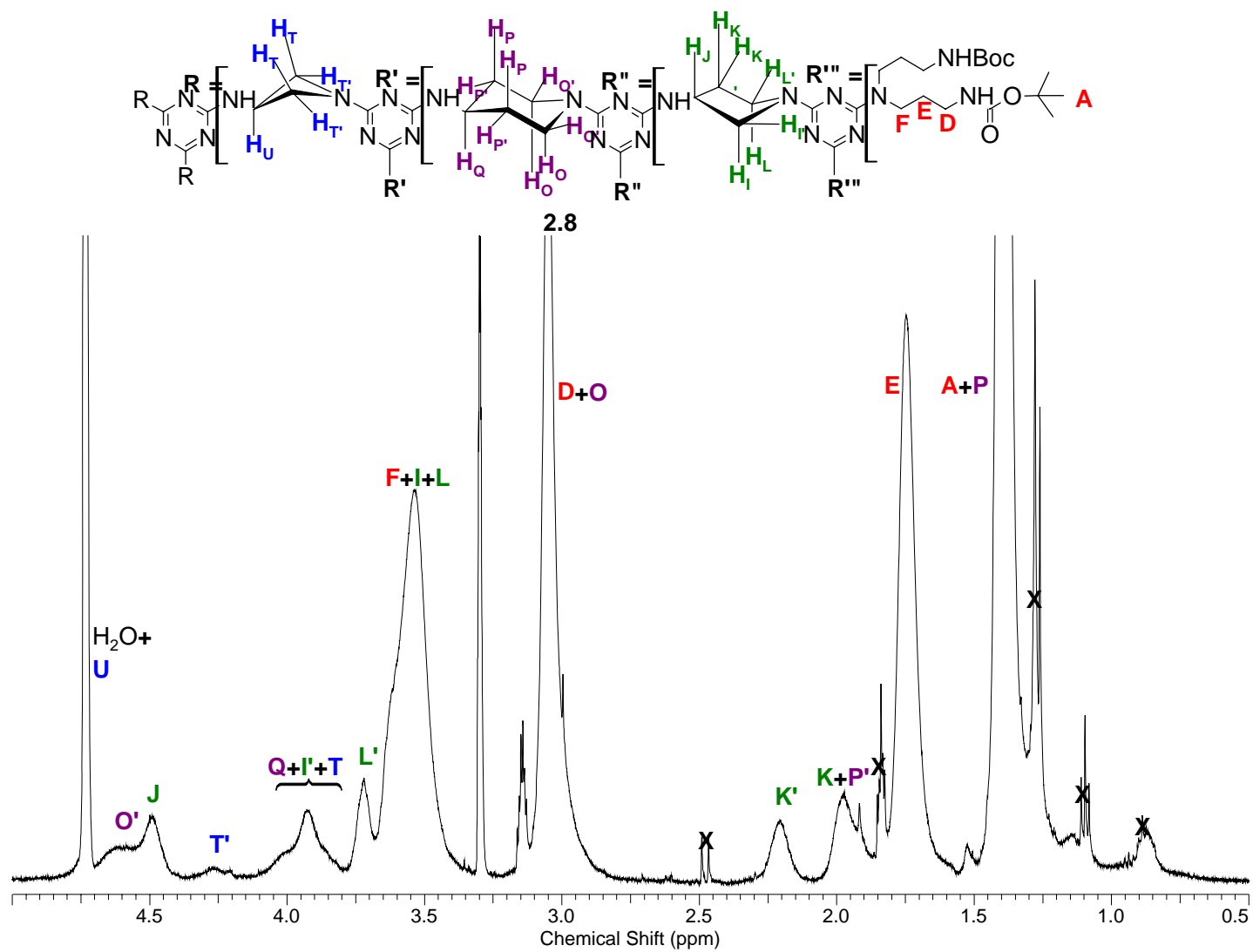
APPENDIX B

SELECTED NMR SPECTRA FOR COMPOUNDS DESCRIBED IN CHAPTER III

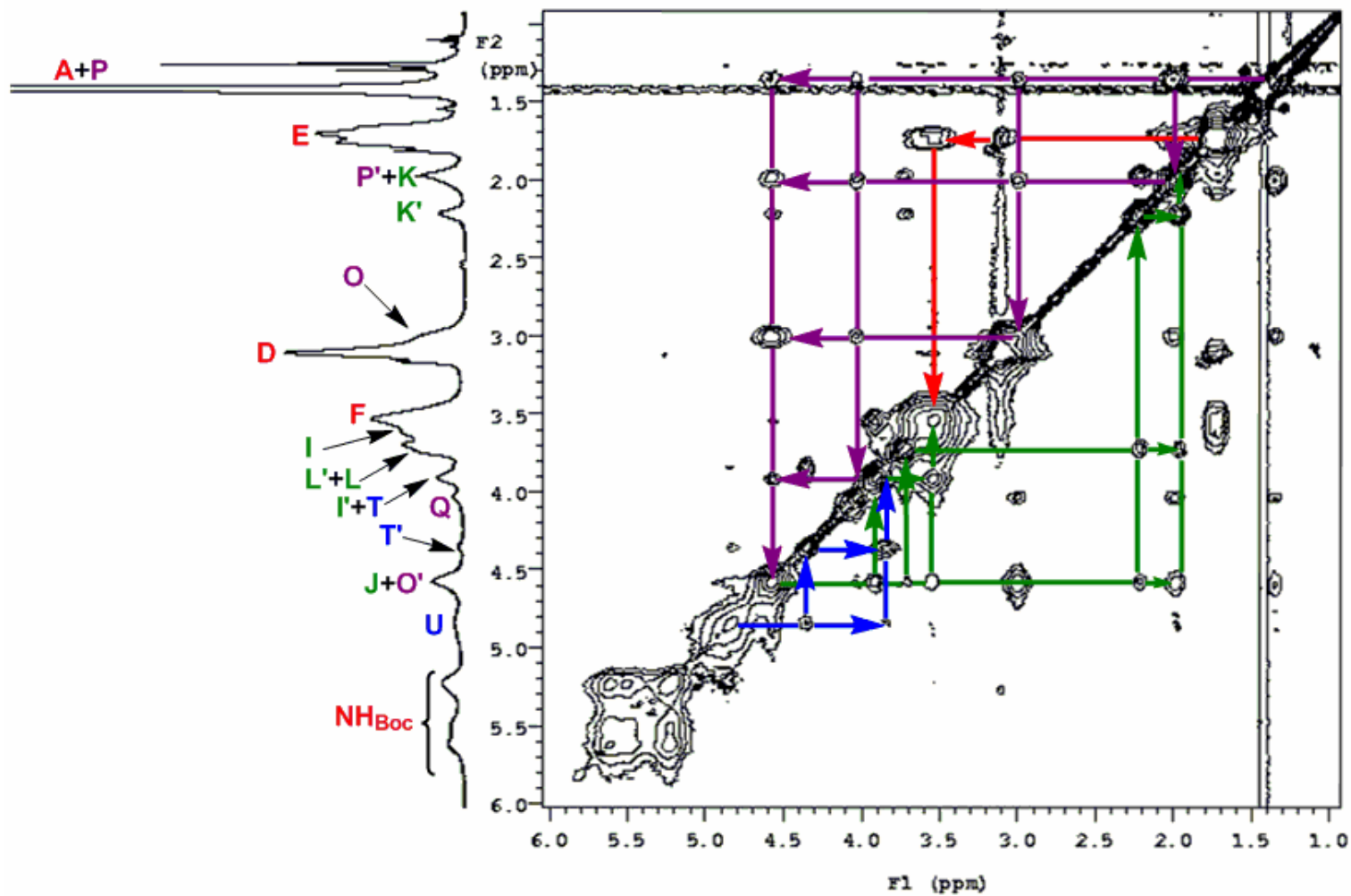
Dendrimer (2.8) – ^1H Spectrum (CDCl_3 , $T = 25^\circ\text{C}$)



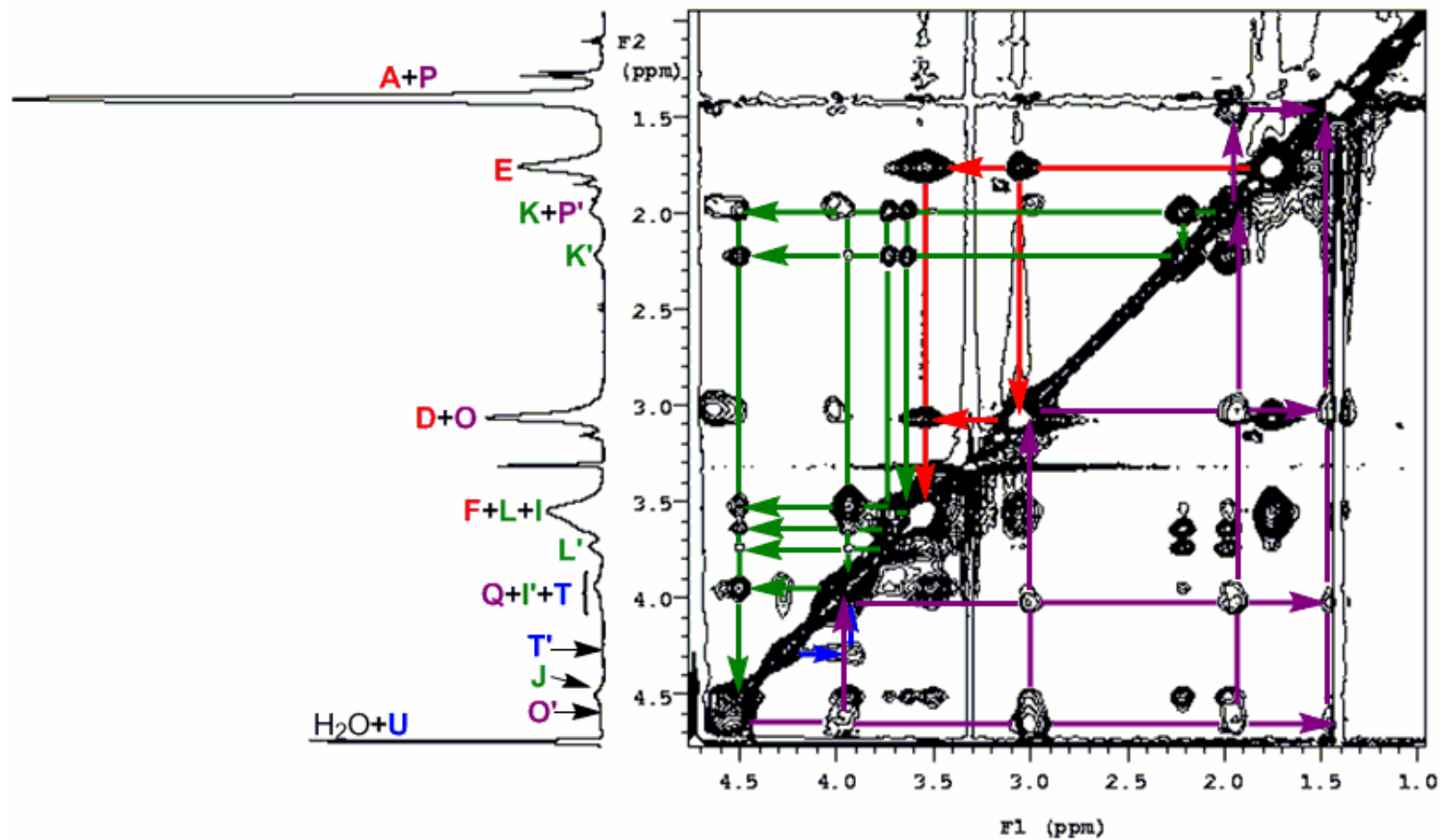
Dendrimer (2.8) – ^1H Spectrum (CD_3OD , $T = 25\text{ }^\circ\text{C}$)



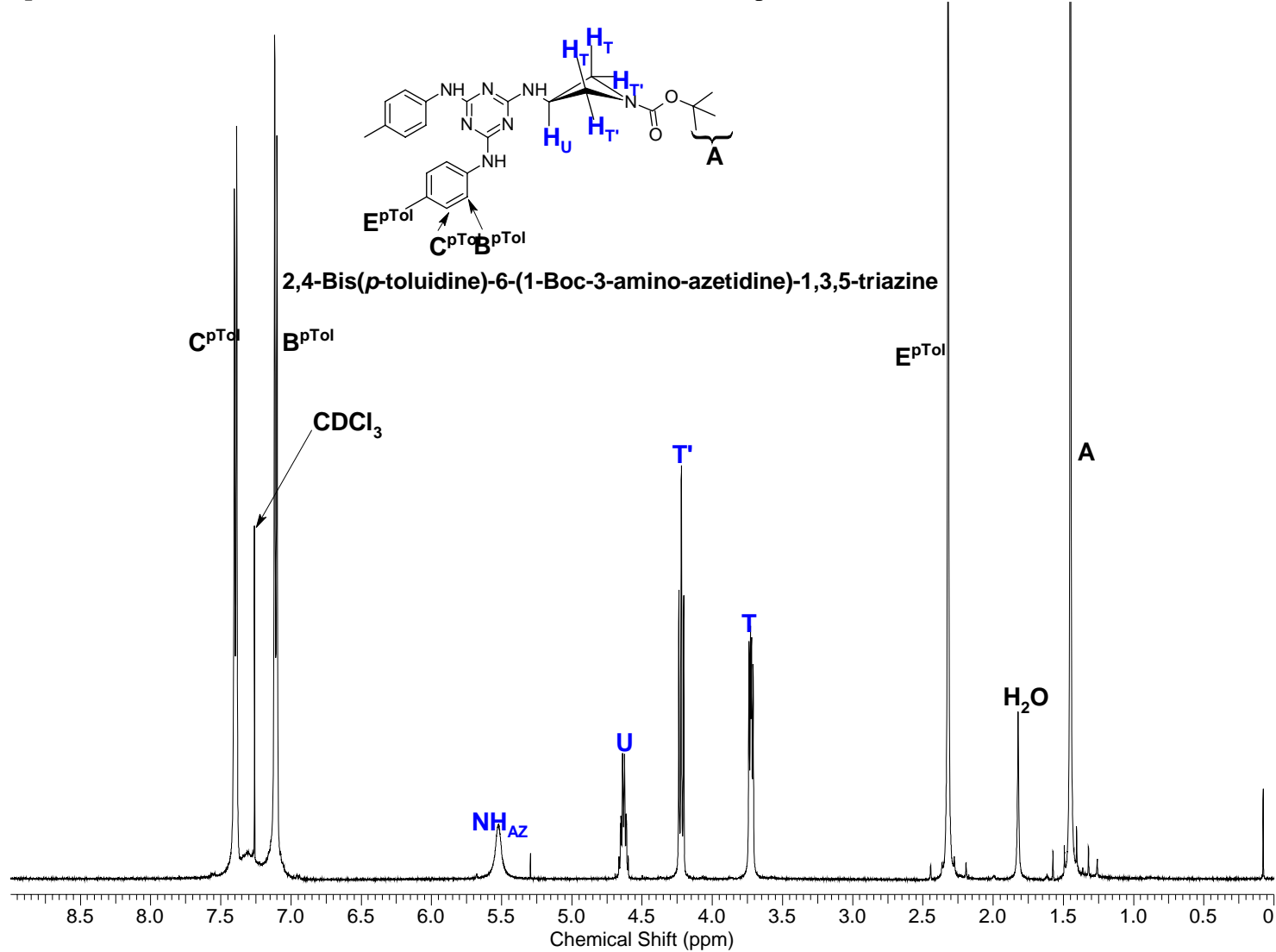
Dendrimer (2.8) – (^1H - ^1H) NOESY Spectrum (CDCl_3 , $T = 35^\circ\text{C}$)



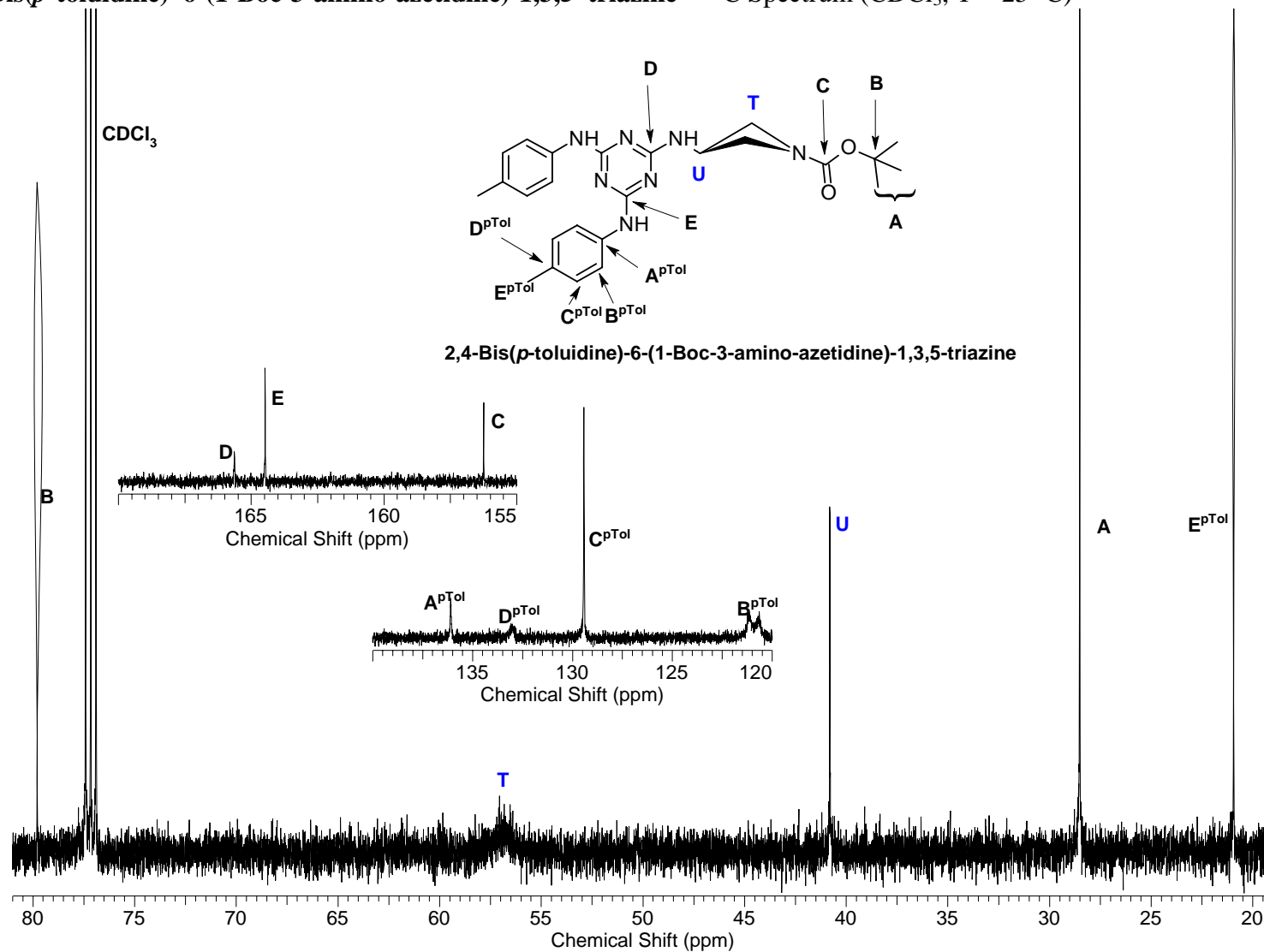
Dendrimer (2.8) – (^1H - ^1H) NOESY Spectrum (CD_3OD , $T = 35^\circ\text{C}$)



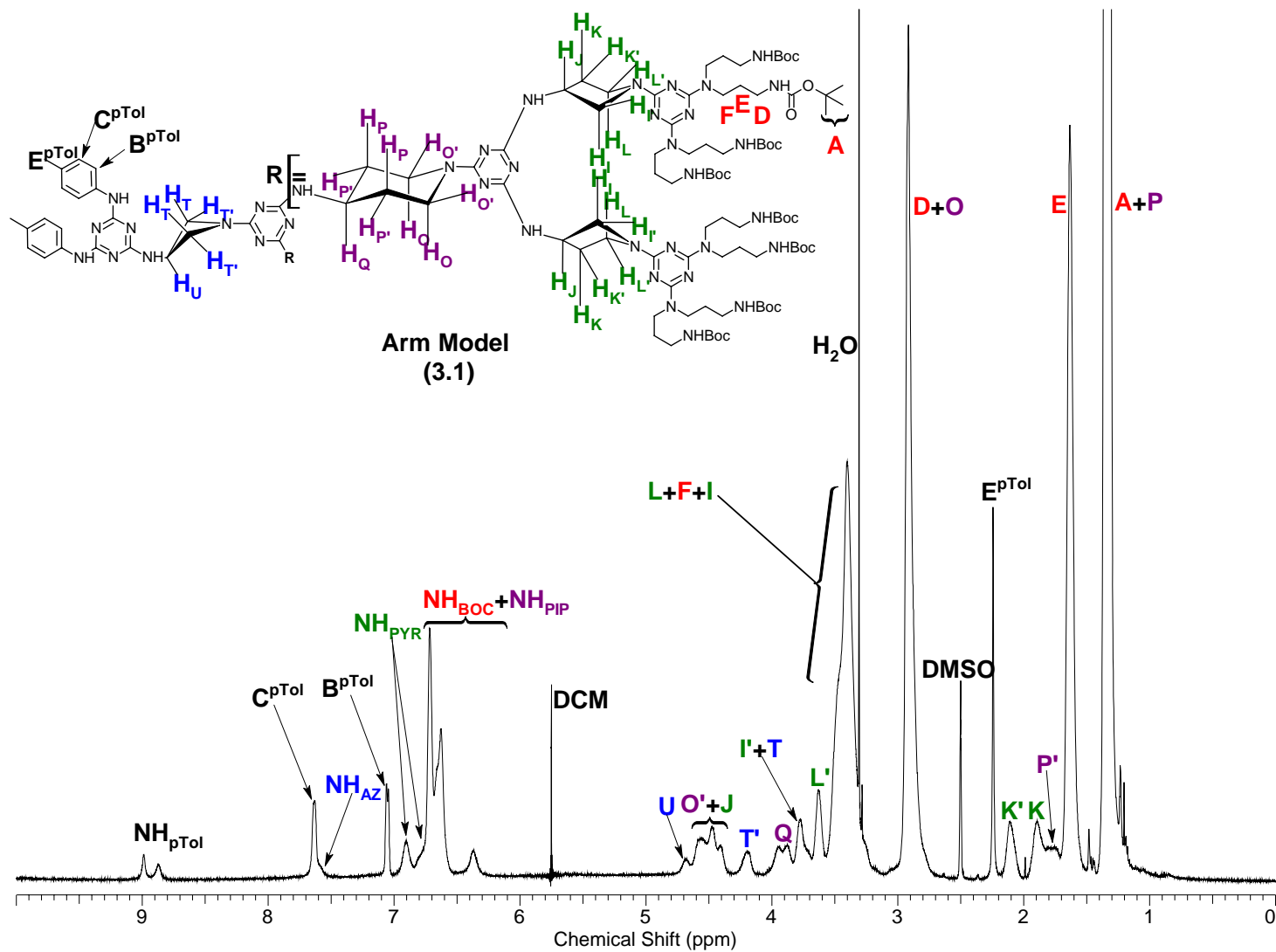
2,4-Bis(*p*-toluidine)-6-(1-Boc-3-amino-azetidine)-1,3,5-triazine – ¹H Spectrum (CDCl₃, T = 25 °C)



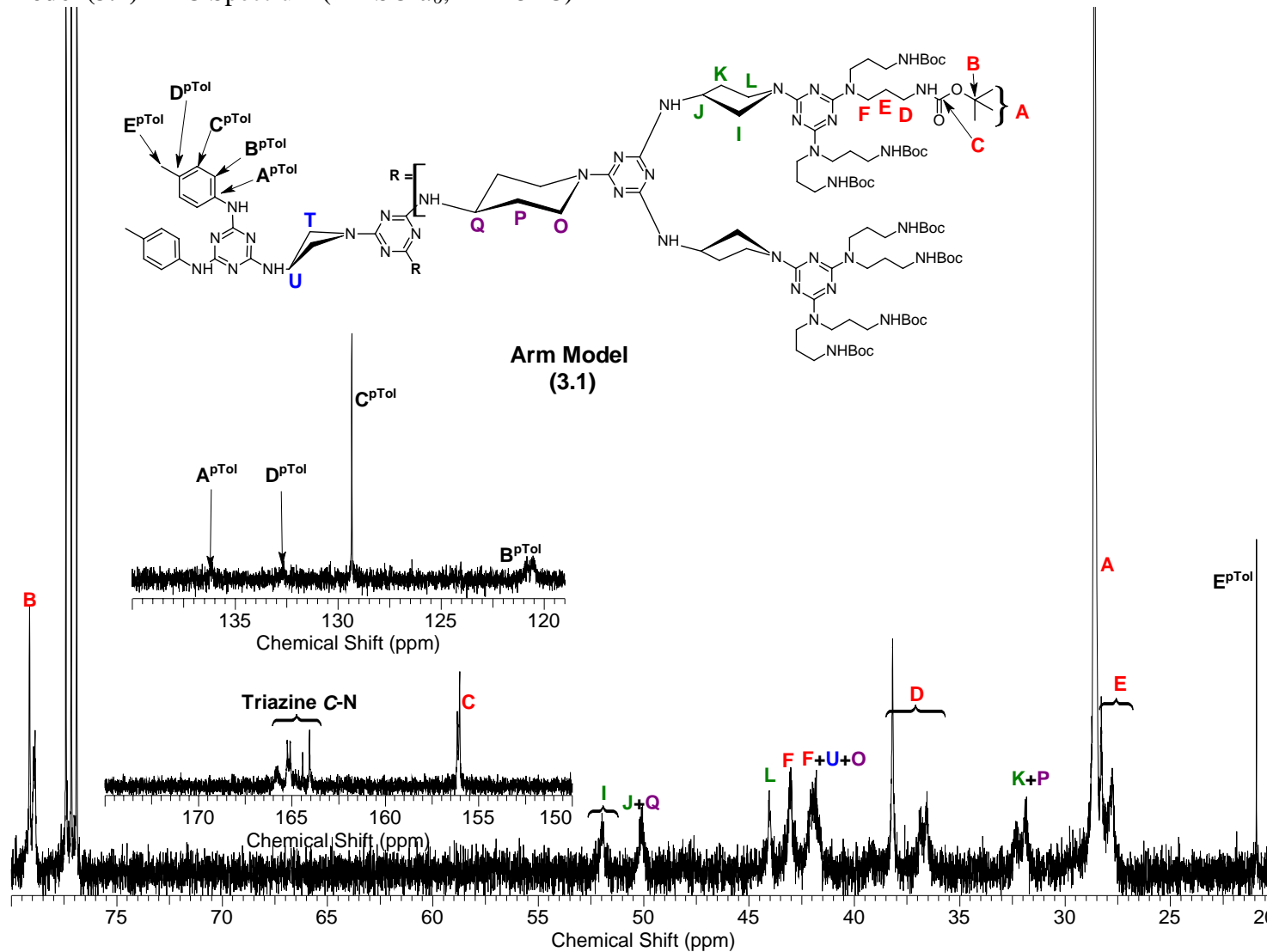
2,4-Bis(*p*-toluidine)-6-(1-Boc-3-amino-azetidine)-1,3,5-triazine – ^{13}C Spectrum (CDCl_3 , $T = 25^\circ\text{C}$)



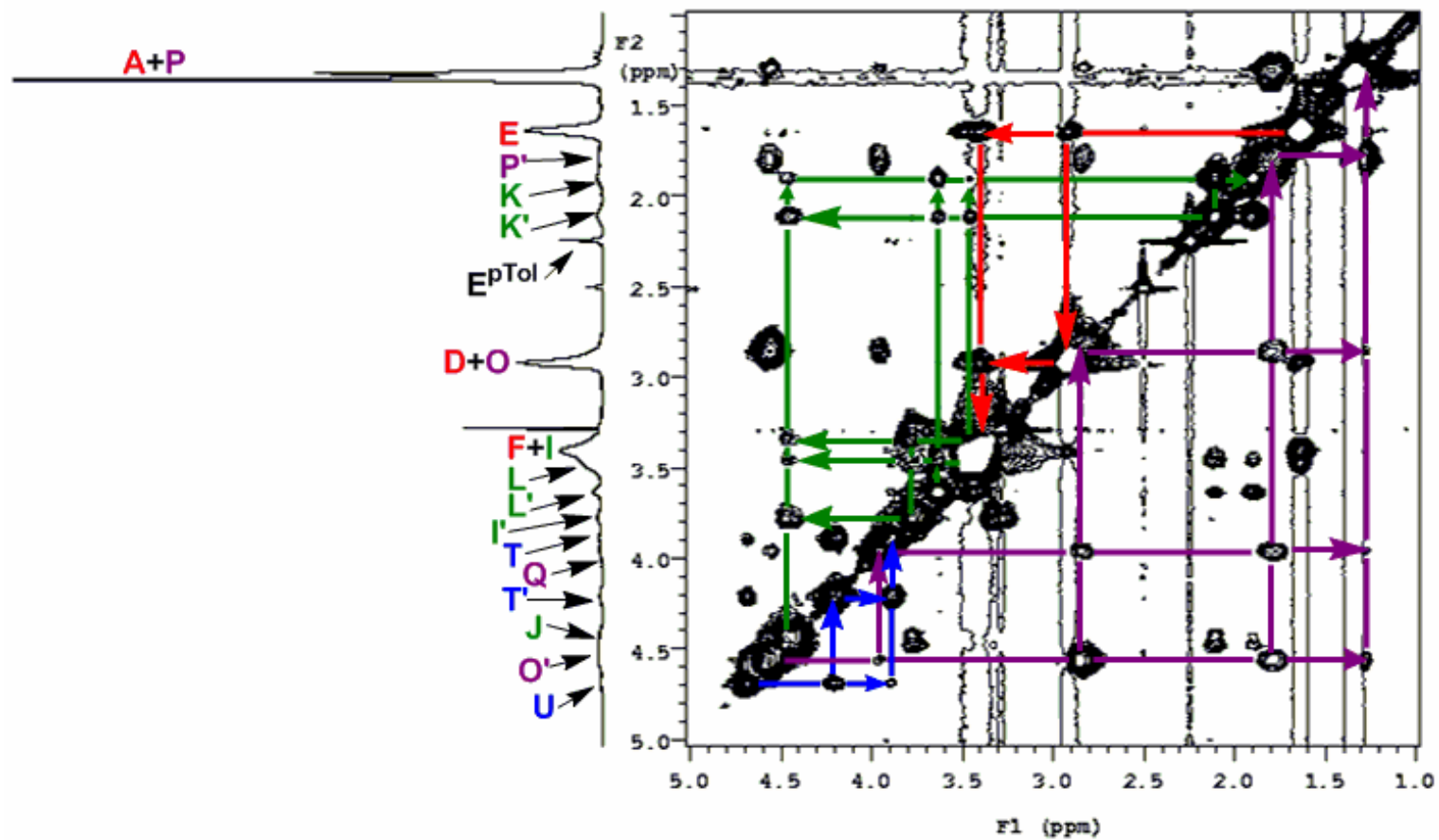
Arm Model (3.1) – ^1H Spectrum (DMSO- d_6 , T = 25 °C)



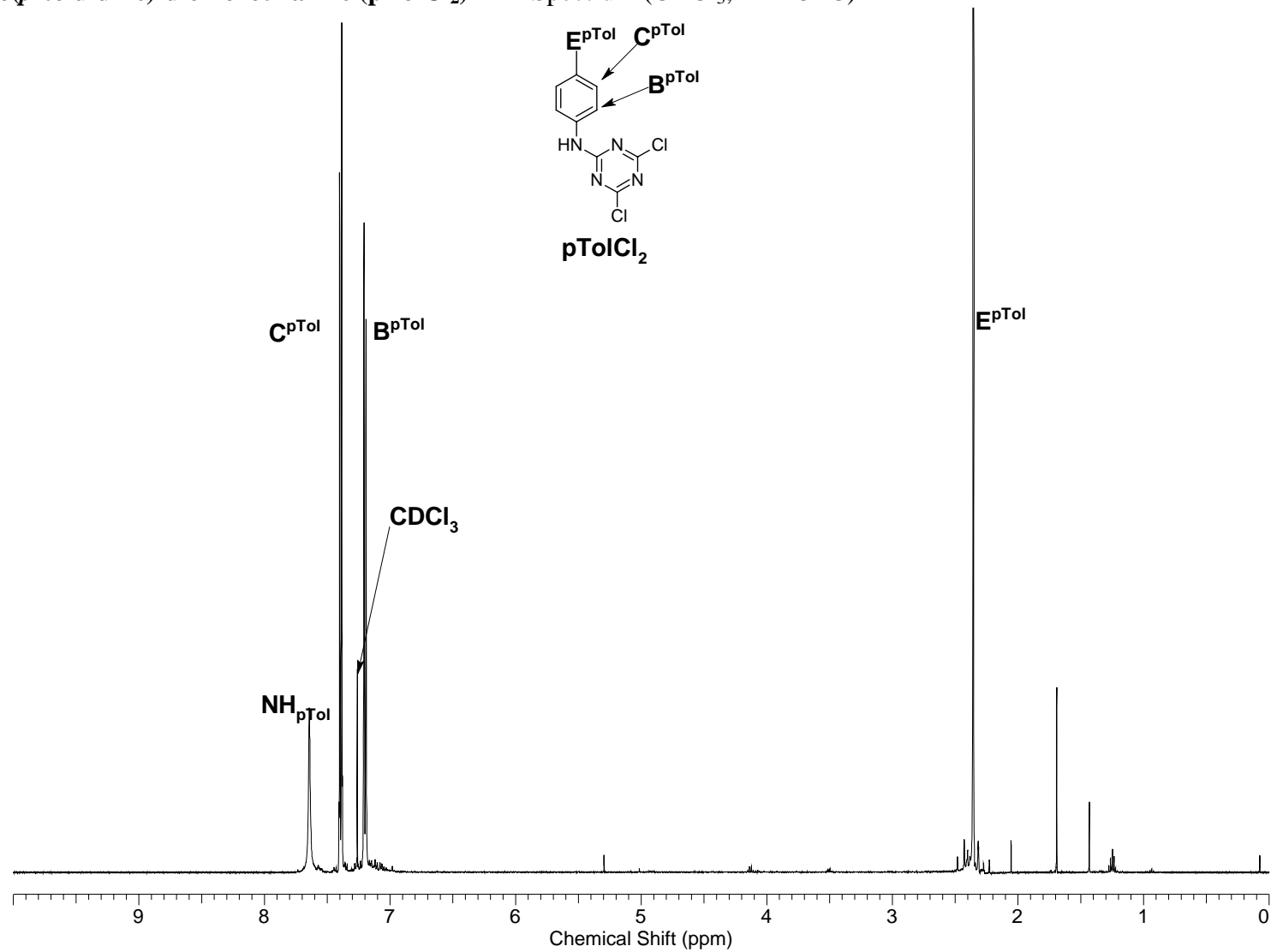
Arm Model (3.1) – ^{13}C Spectrum (DMSO- d_6 , T = 25 °C)



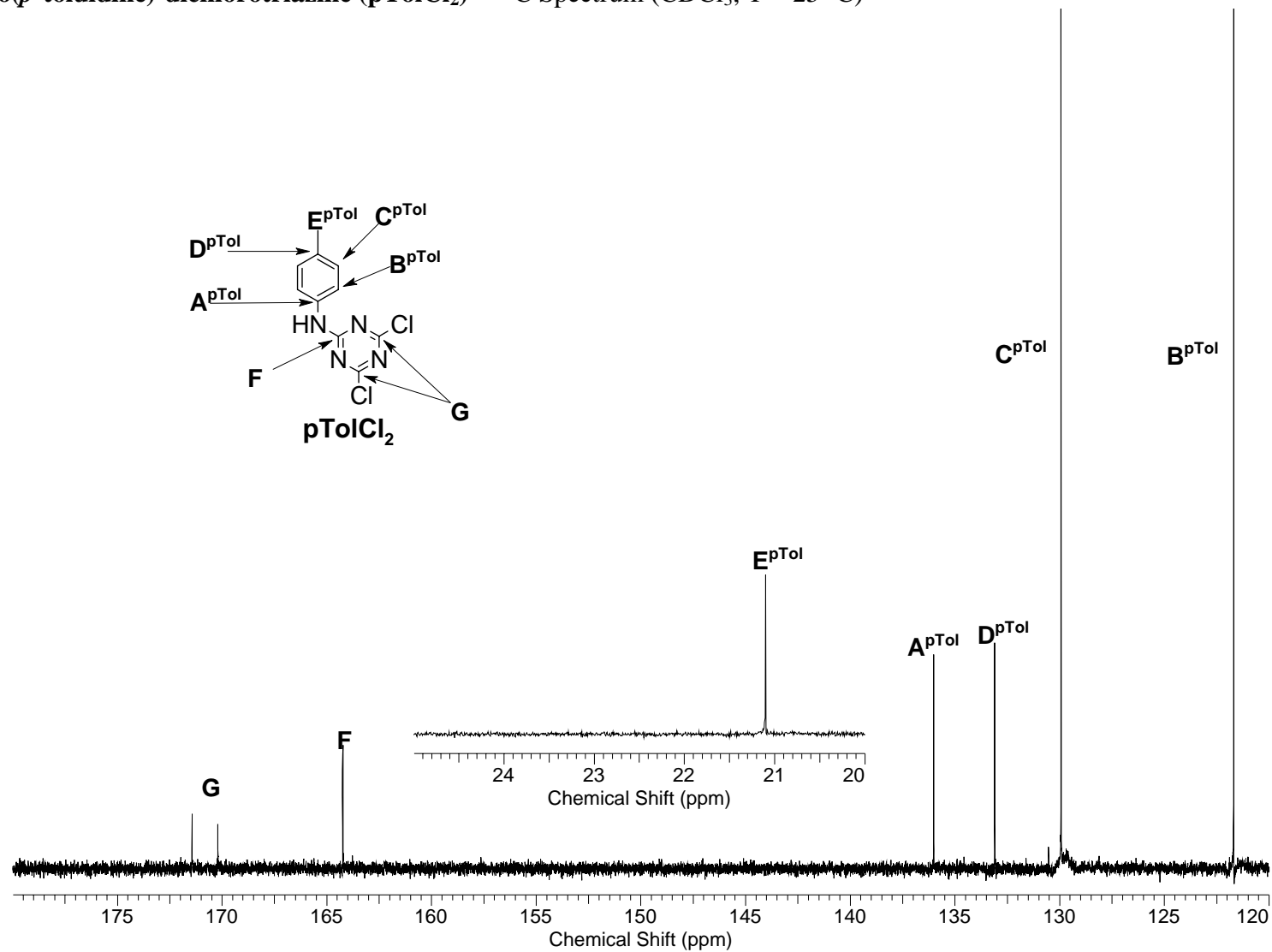
Arm Model (3.1) – (^1H - ^1H) NOESY Spectrum 1–5 ppm (DMSO- d_6 , T = 35 °C)



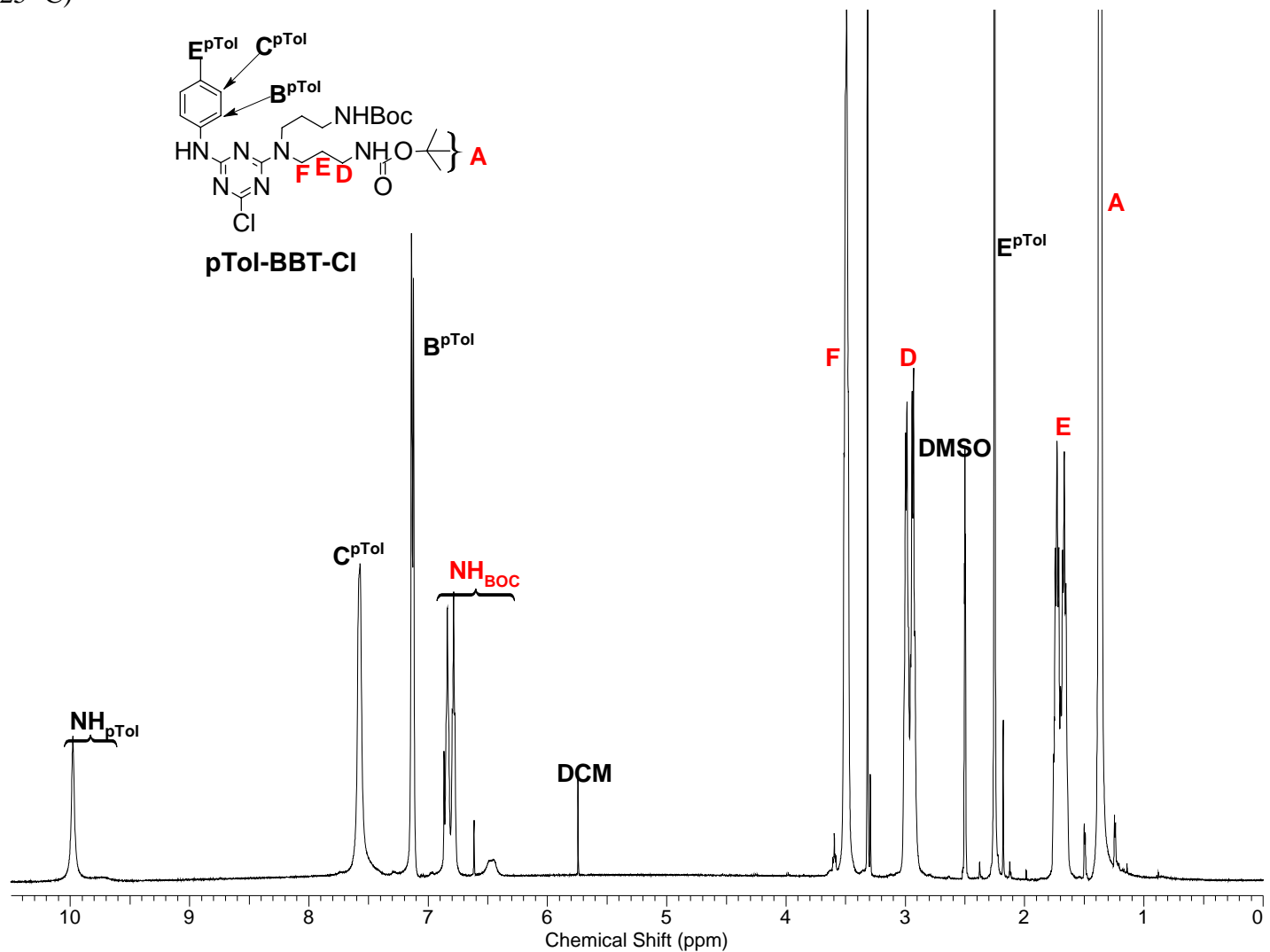
Mono(*p*-toluidine)-dichlorotriazine ($p\text{TolCl}_2$) – ^1H Spectrum (CDCl_3 , $T = 25\text{ }^\circ\text{C}$)



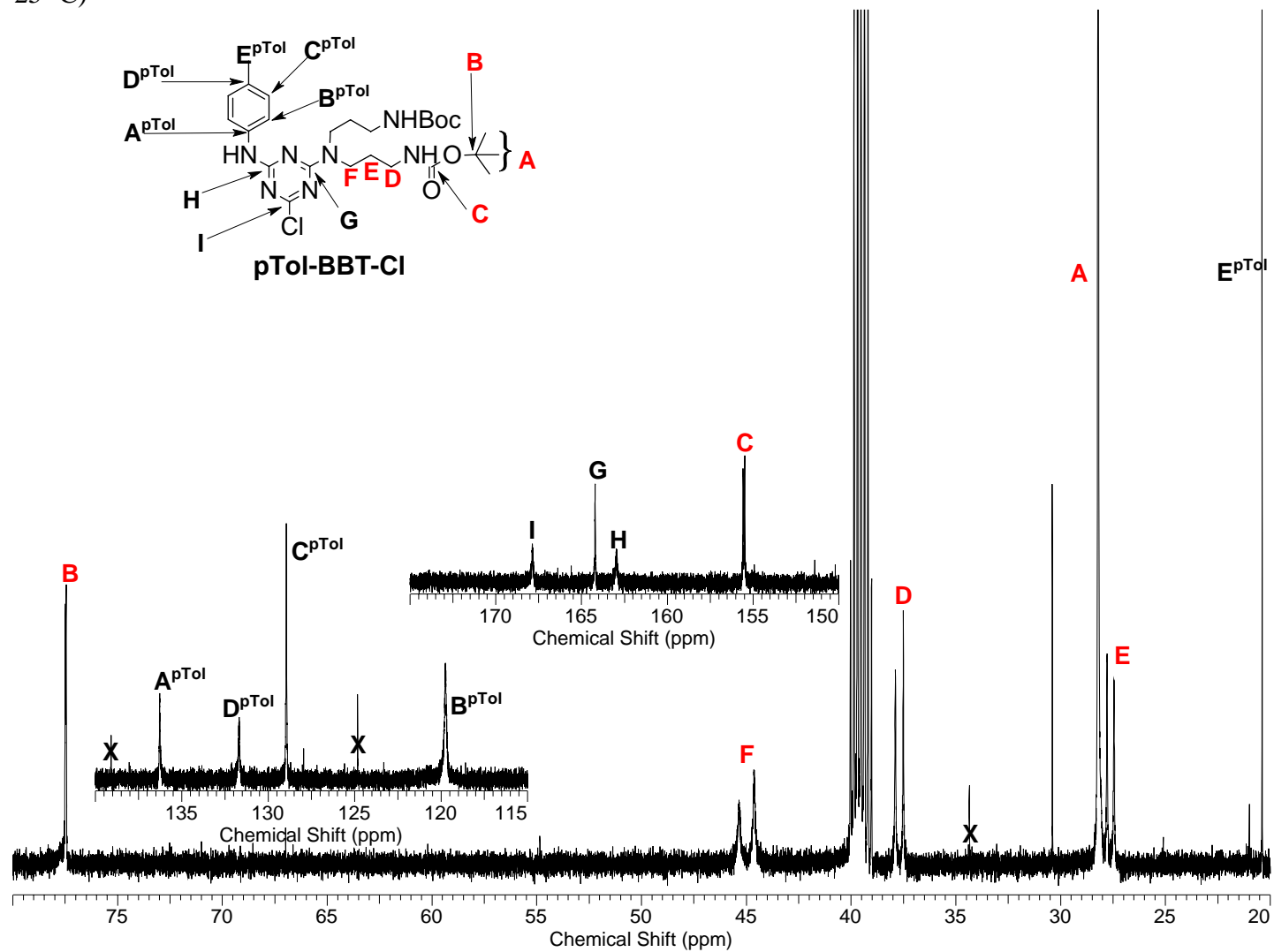
Mono(*p*-toluidine)-dichlorotriazine ($p\text{ToI}Cl_2$) – ^{13}C Spectrum (CDCl_3 , $T = 25\text{ }^\circ\text{C}$)



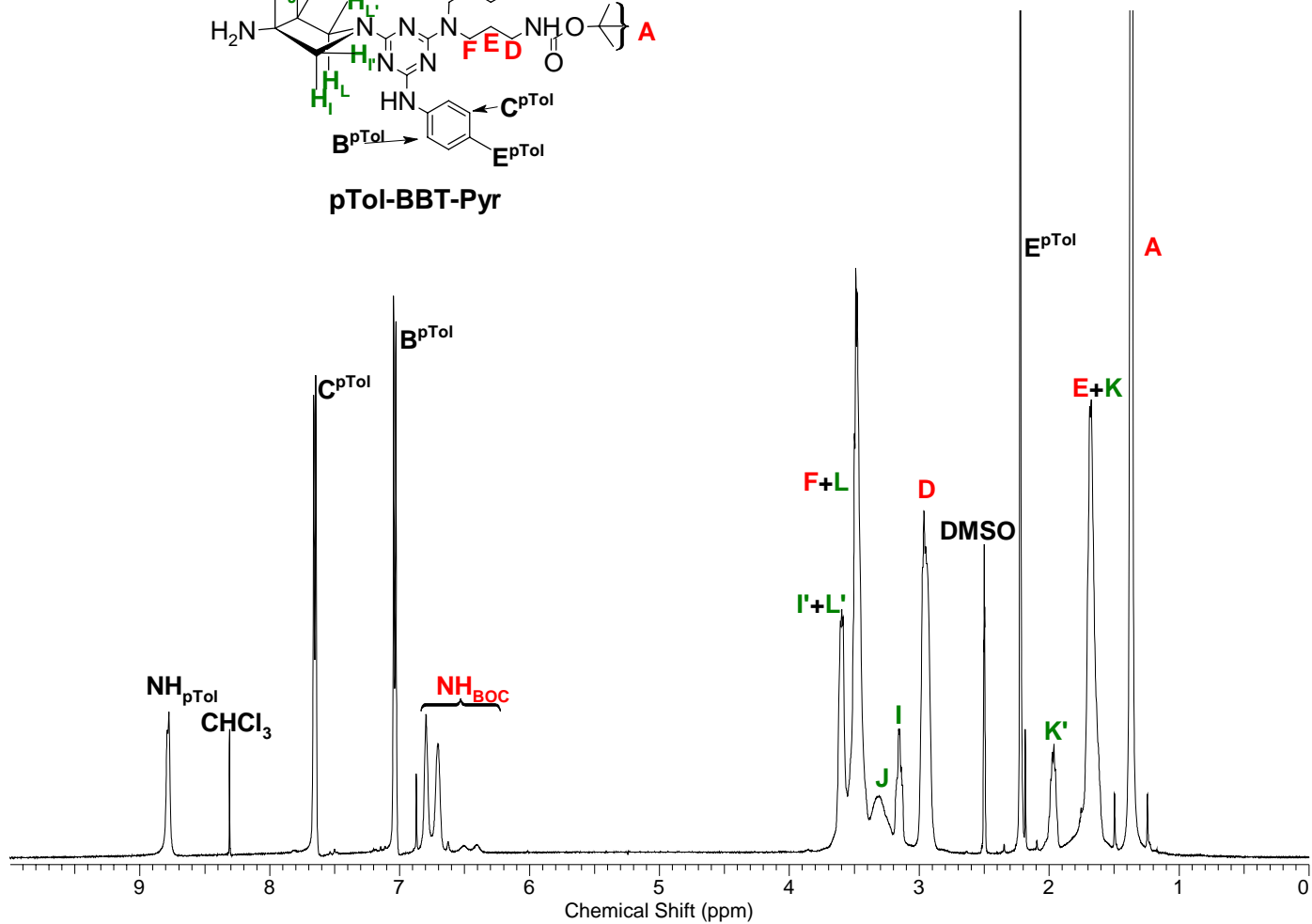
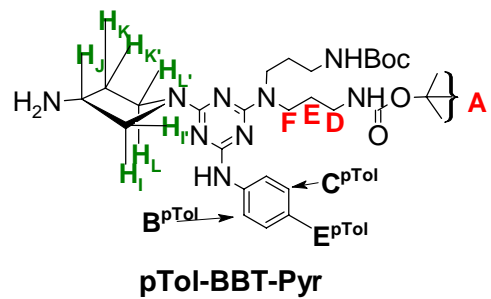
Mono(*p*-toluidine)-mono(Bis(3-Boc-3-aminopropyl)amine)-monochlorotriazine (pTol-BBT-Cl) – ^1H Spectrum (DMSO- d_6 , T = 25 °C)



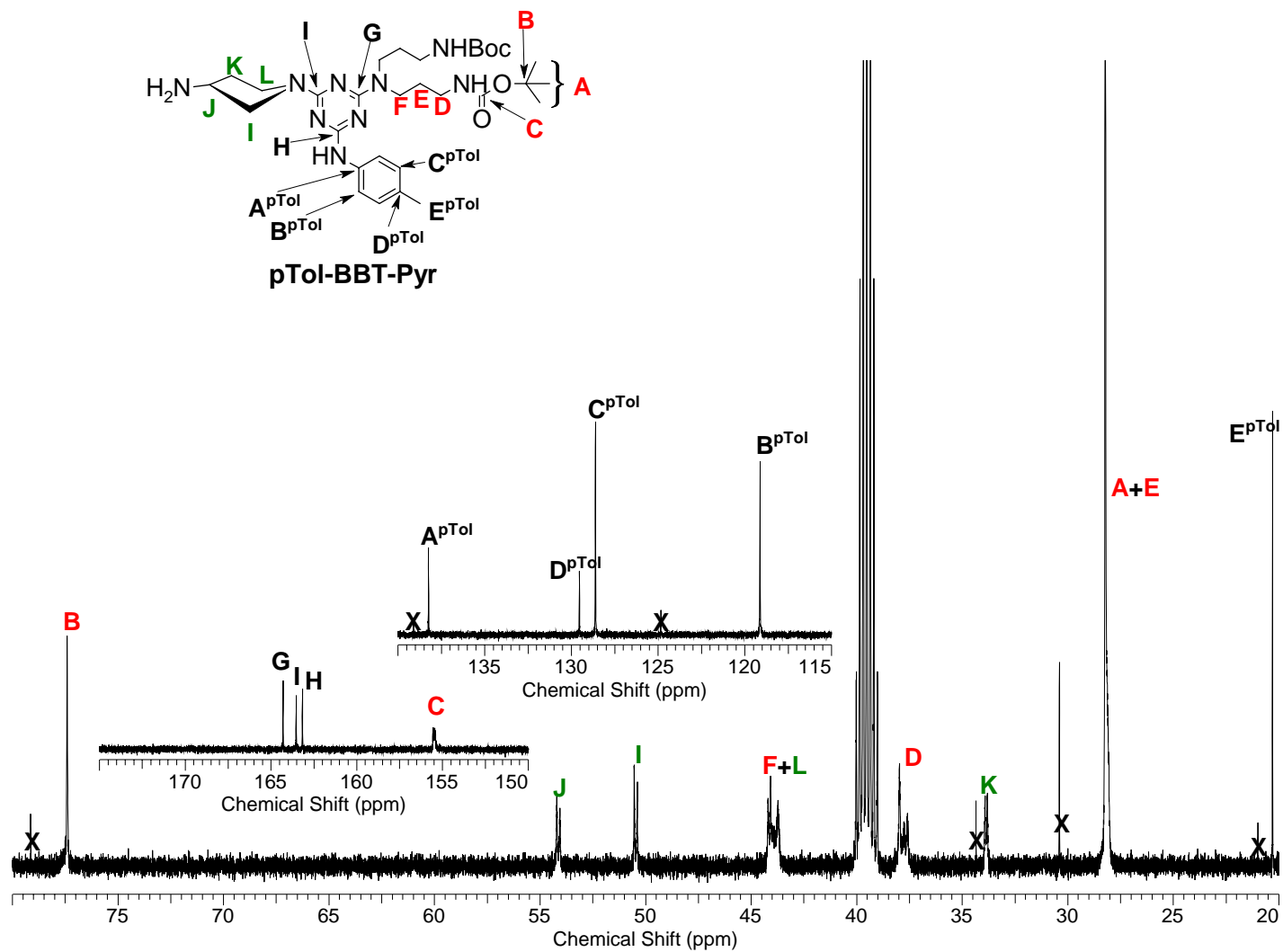
Mono(*p*-toluidine)-mono(Bis(3-Boc-3-aminopropyl)amine)-monochlorotriazine (pTol-BBT-Cl) – ^{13}C Spectrum (DMSO- d_6 , T = 25 °C)



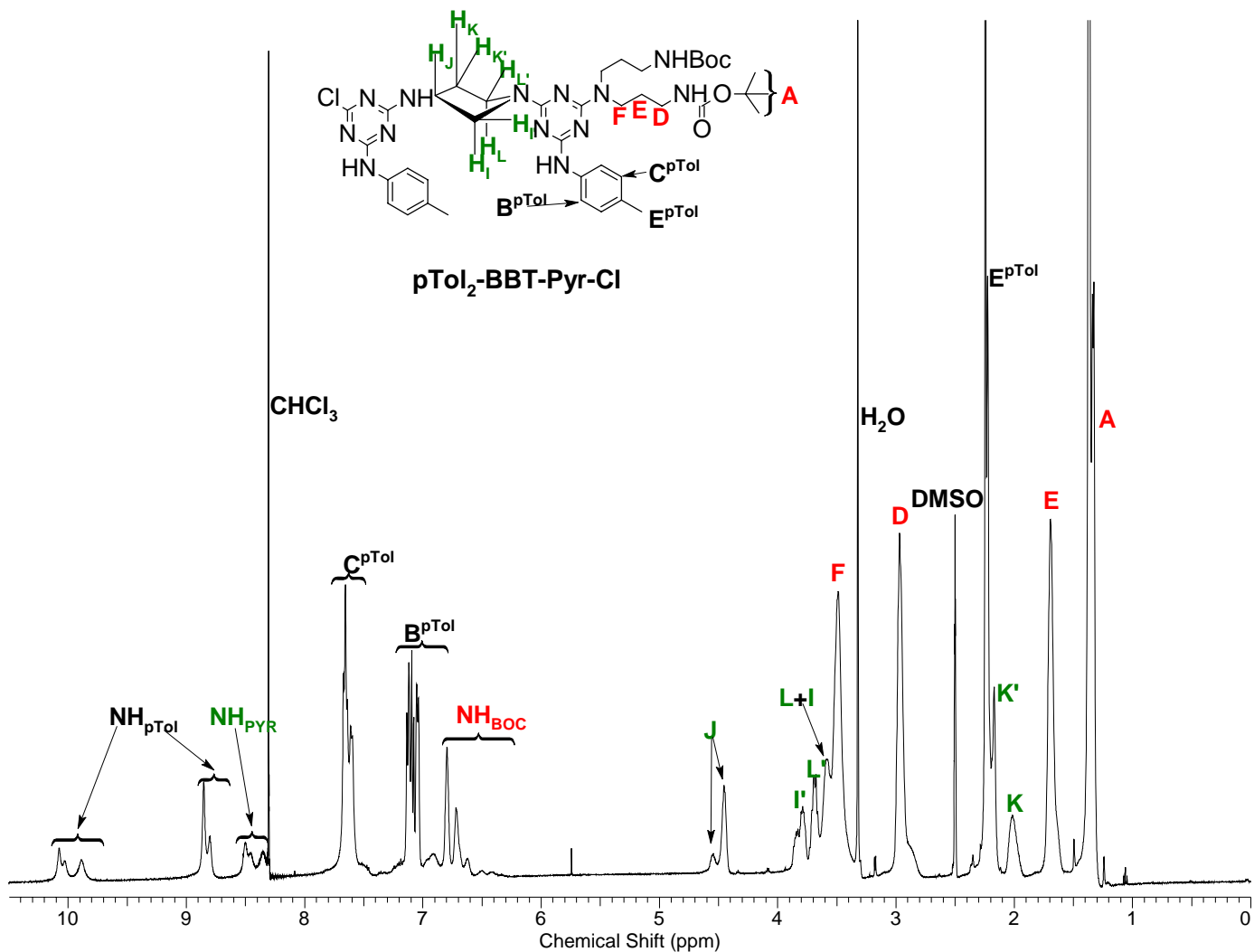
Mono(*p*-toluidine)-mono(Bis(3-BOC-3-aminopropyl)amine)-monopyrrolidinotriazine (pTol-BBT-Pyr) – ¹H Spectrum (DMSO-*d*₆, T = 25 °C)



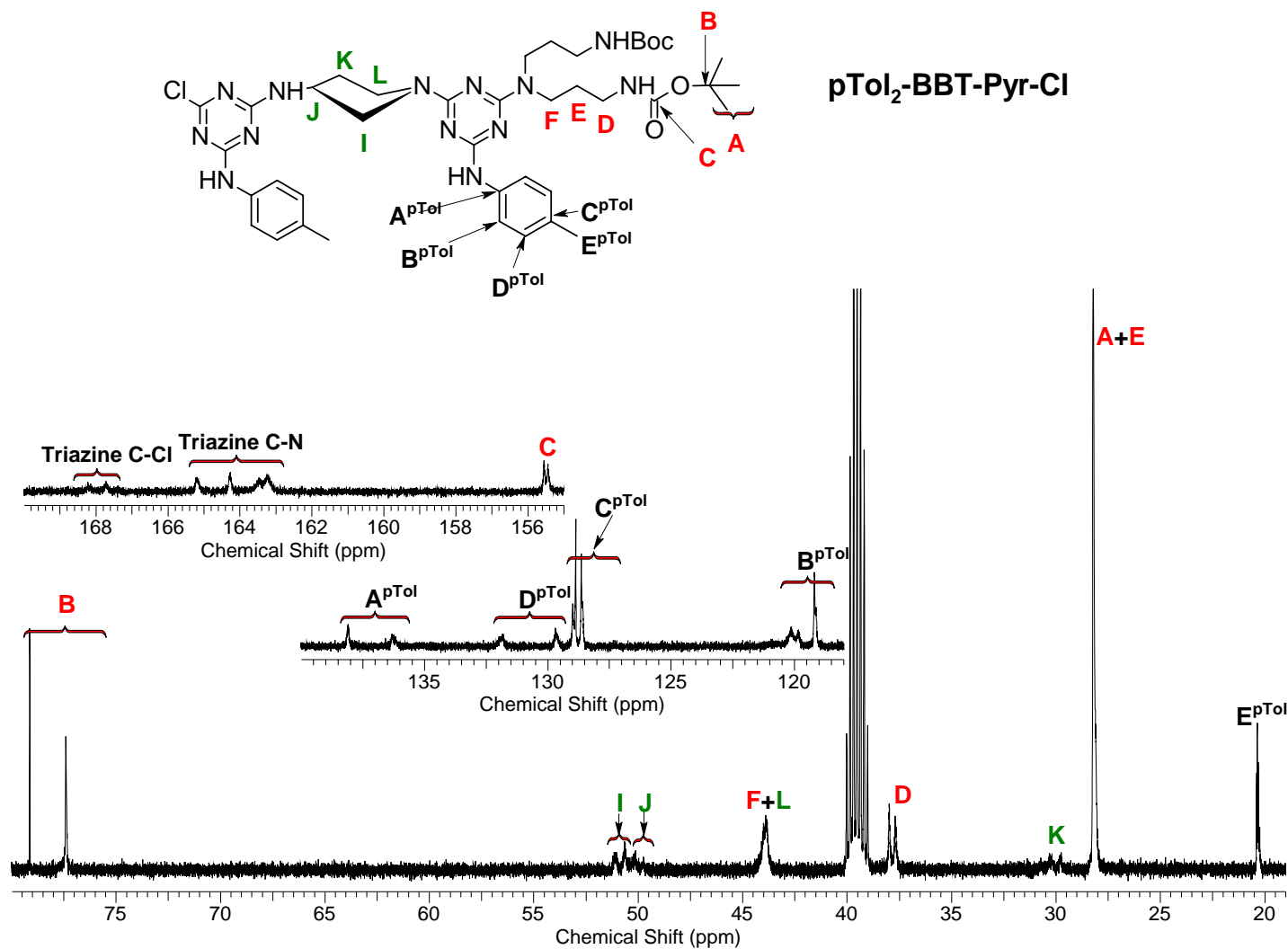
**Mono(*p*-toluidine)-mono(Bis(3-BOC-3-aminopropyl)amine)-monopyrrolidintriazine (pTol-BBT-Pyr) – ^{13}C Spectrum
(DMSO- d_6 , T = 25 °C)**



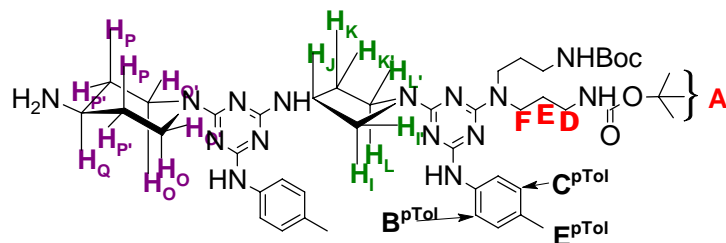
**Bis(*p*-toluidine)-mono(Bis(3-BOC-3-aminopropyl)amine)-monopyrrolidine-monochlorotriazine (pTol₂-BBT-Pyr-Cl) –
¹H Spectrum (DMSO-*d*₆, T = 25 °C)**



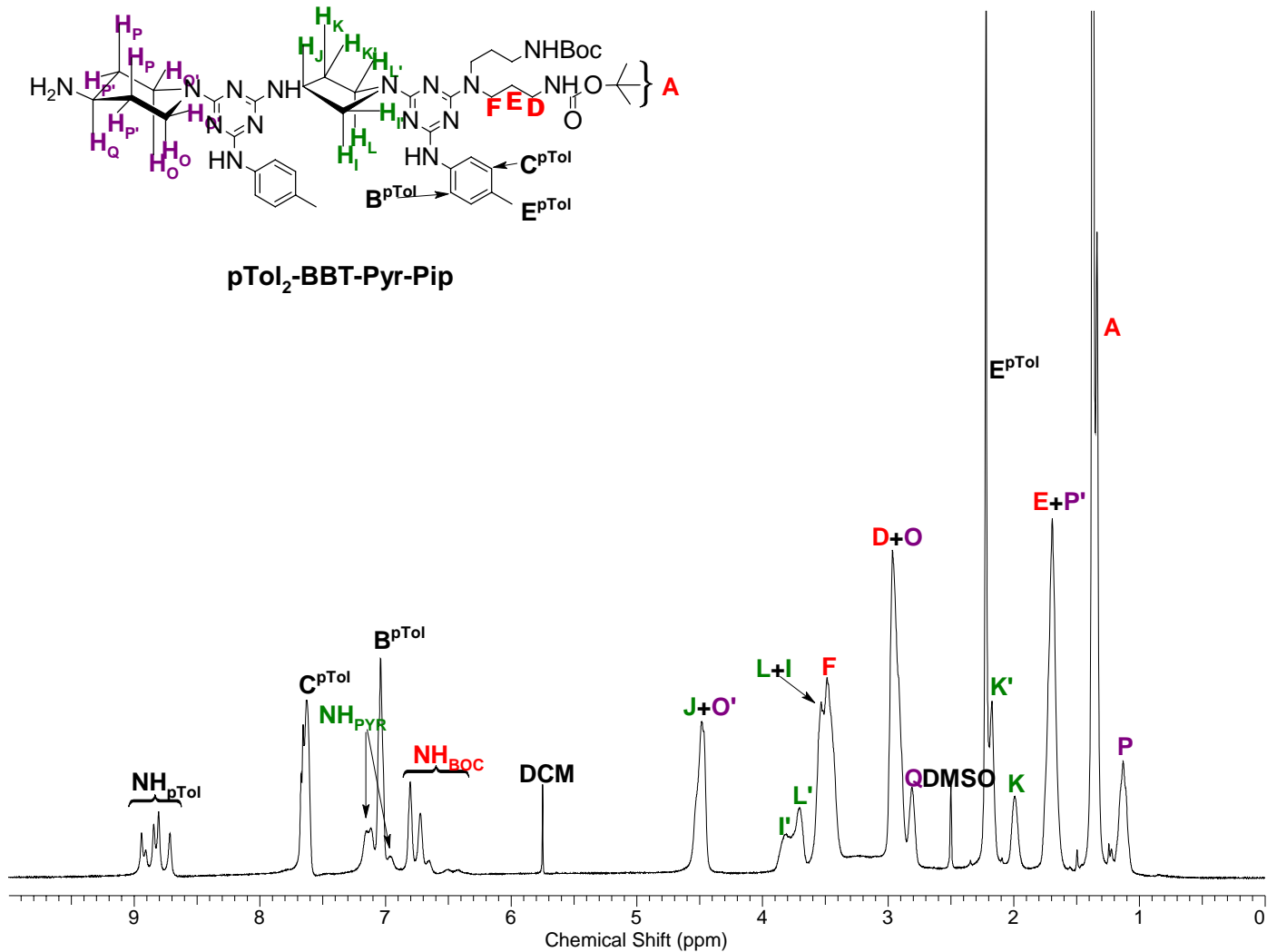
Bis(*p*-toluidine)-mono(Bis(3-BOC-3-aminopropyl)amine)-monopyrrolidine-monochlorotriazine (pTol₂-BBT-Pyr-Cl) – ¹³C Spectrum (DMSO-*d*₆, T = 25 °C)



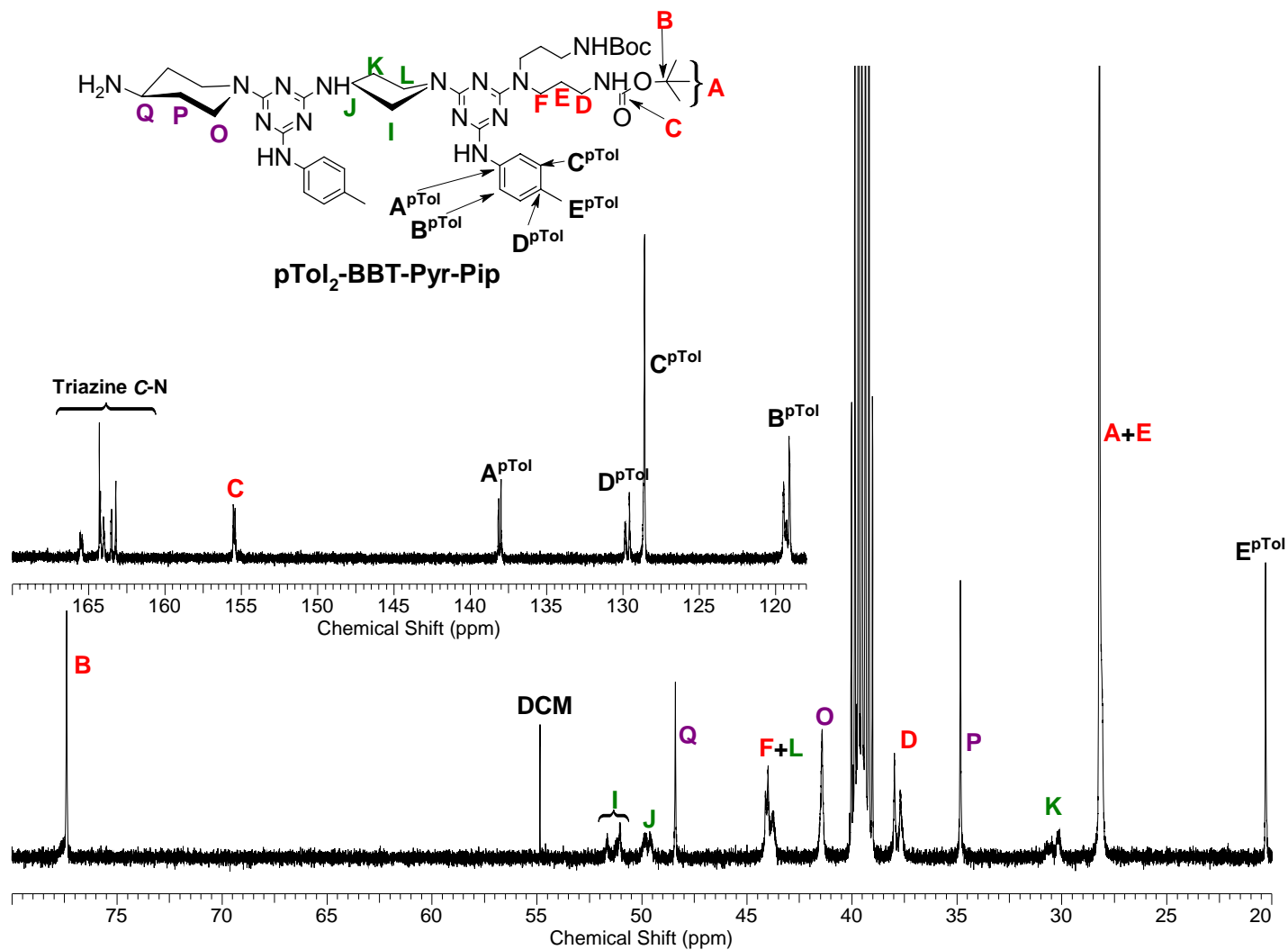
Bis(*p*-toluidine)-mono(Bis(3-BOC-3-aminopropyl)amine)-monopyrrolidine-monopiperidinotriazine (pTol₂-BBT-Pyr-Pip) – ¹H Spectrum (DMSO-*d*₆, T = 25 °C)



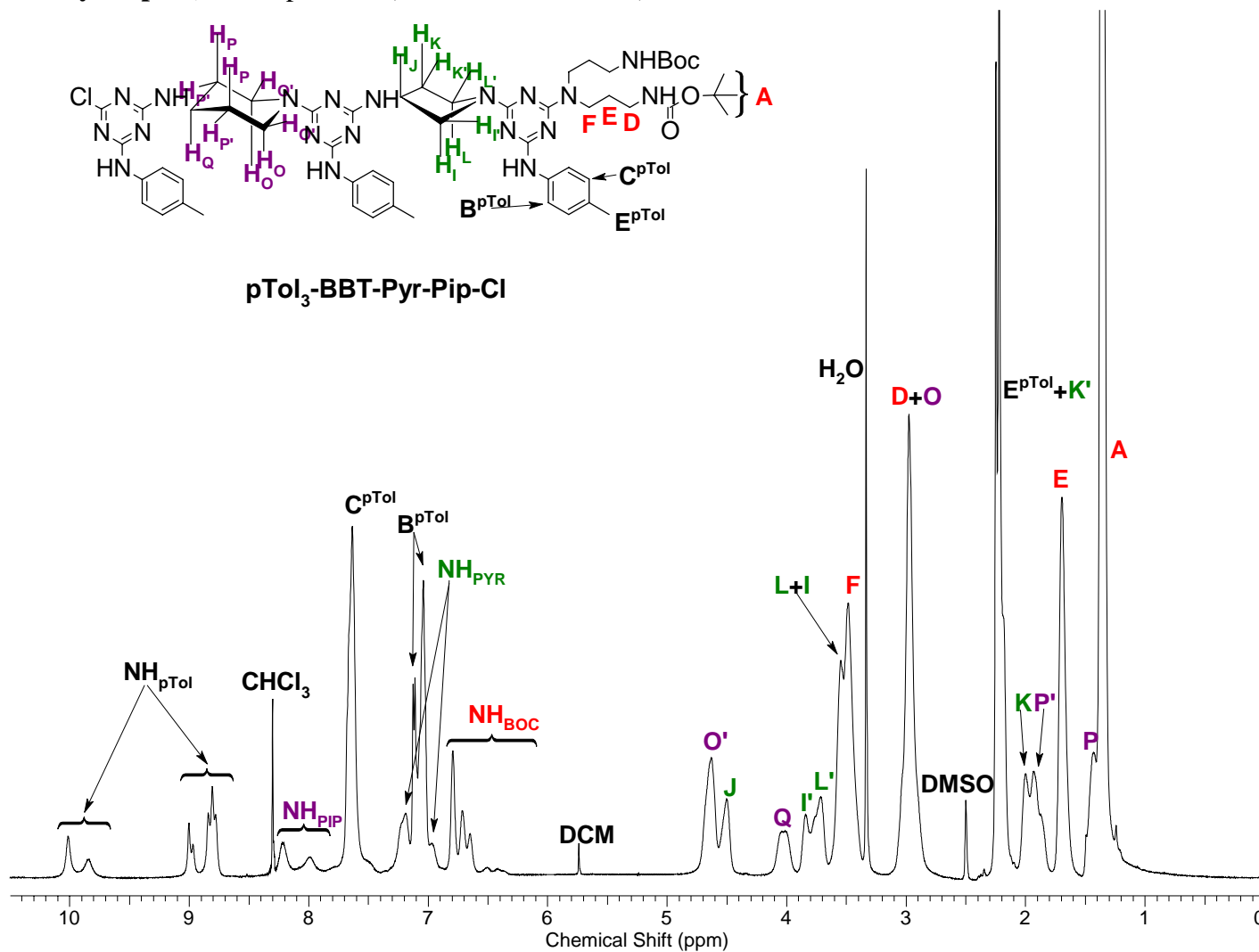
pTol₂-BBT-Pyr-Pip



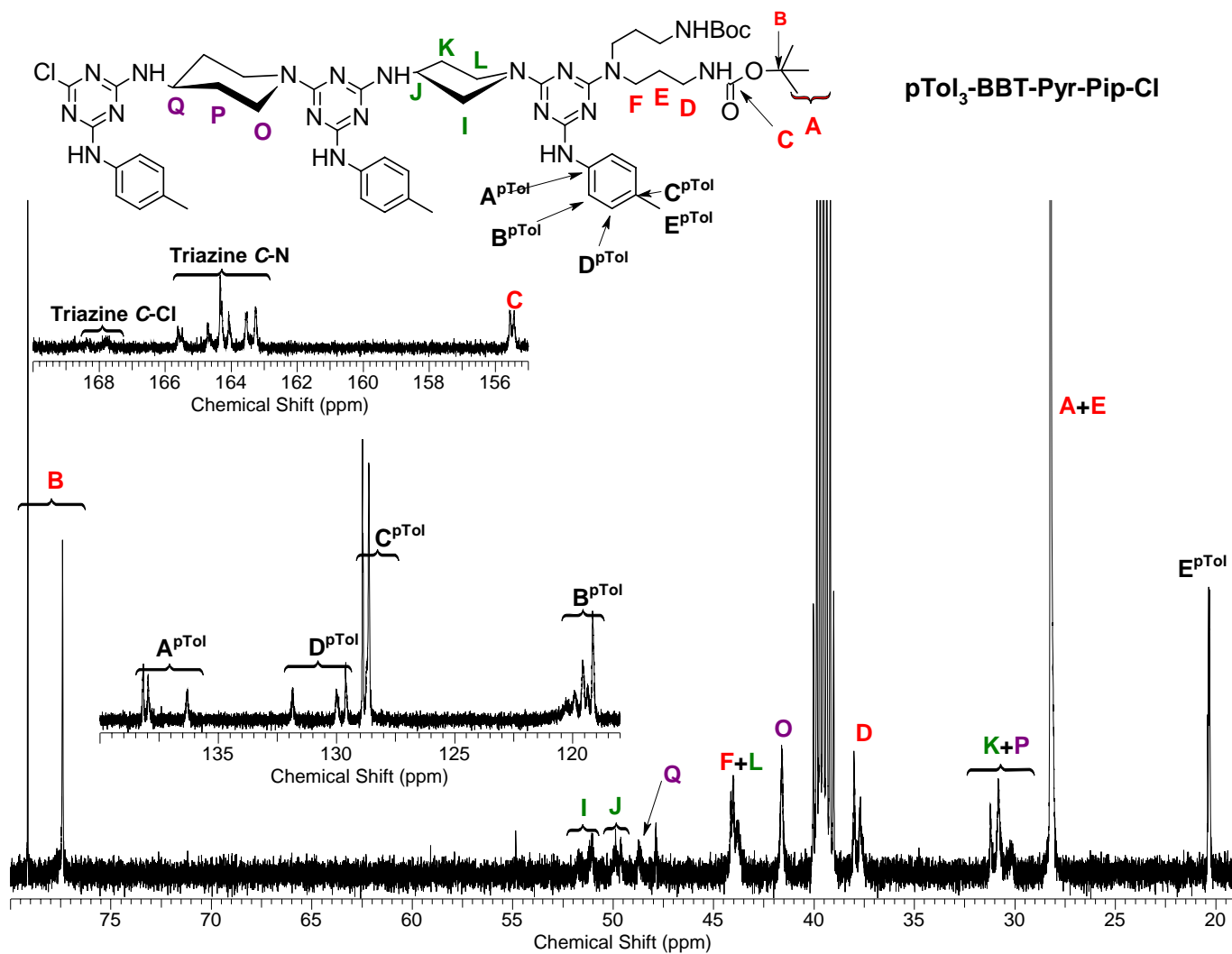
Bis(*p*-toluidine)-mono(Bis(3-BOC-3-aminopropyl)amine)-monopyrrolidine-monopiperidinotriazine (pTol₂-BBT-Pyr-Pip) – ¹³C Spectrum (DMSO-*d*₆, T = 25 °C)



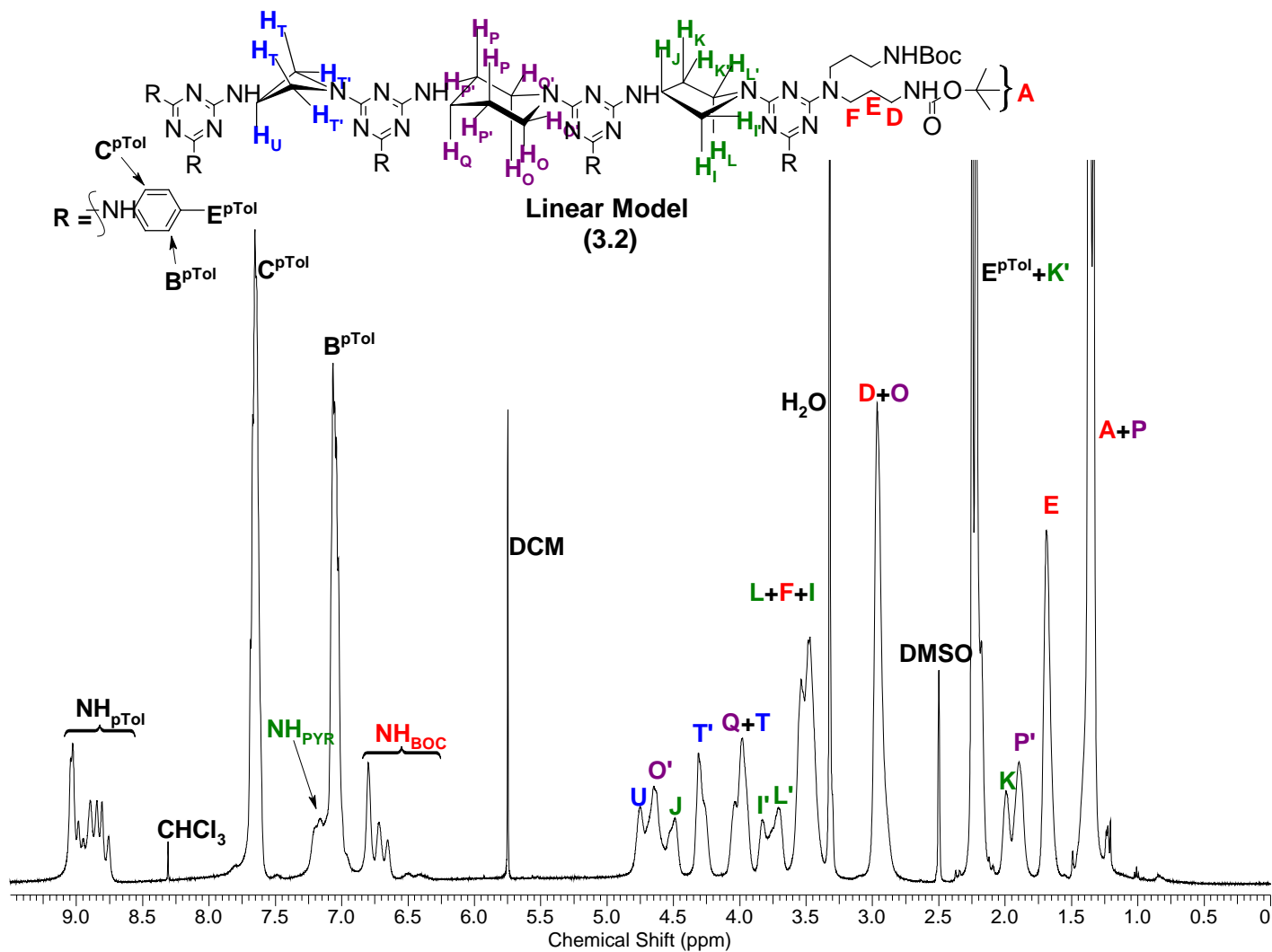
Tris(*p*-toluidine)-mono(Bis(3-BOC-3-aminopropyl)amine)-monopyrrolidine-monopiperidine-monochlorotriazine
(*p*Tol₃-BBT-Pyr-Pip-Cl) – ¹H Spectrum (DMSO-*d*₆, T = 25 °C)



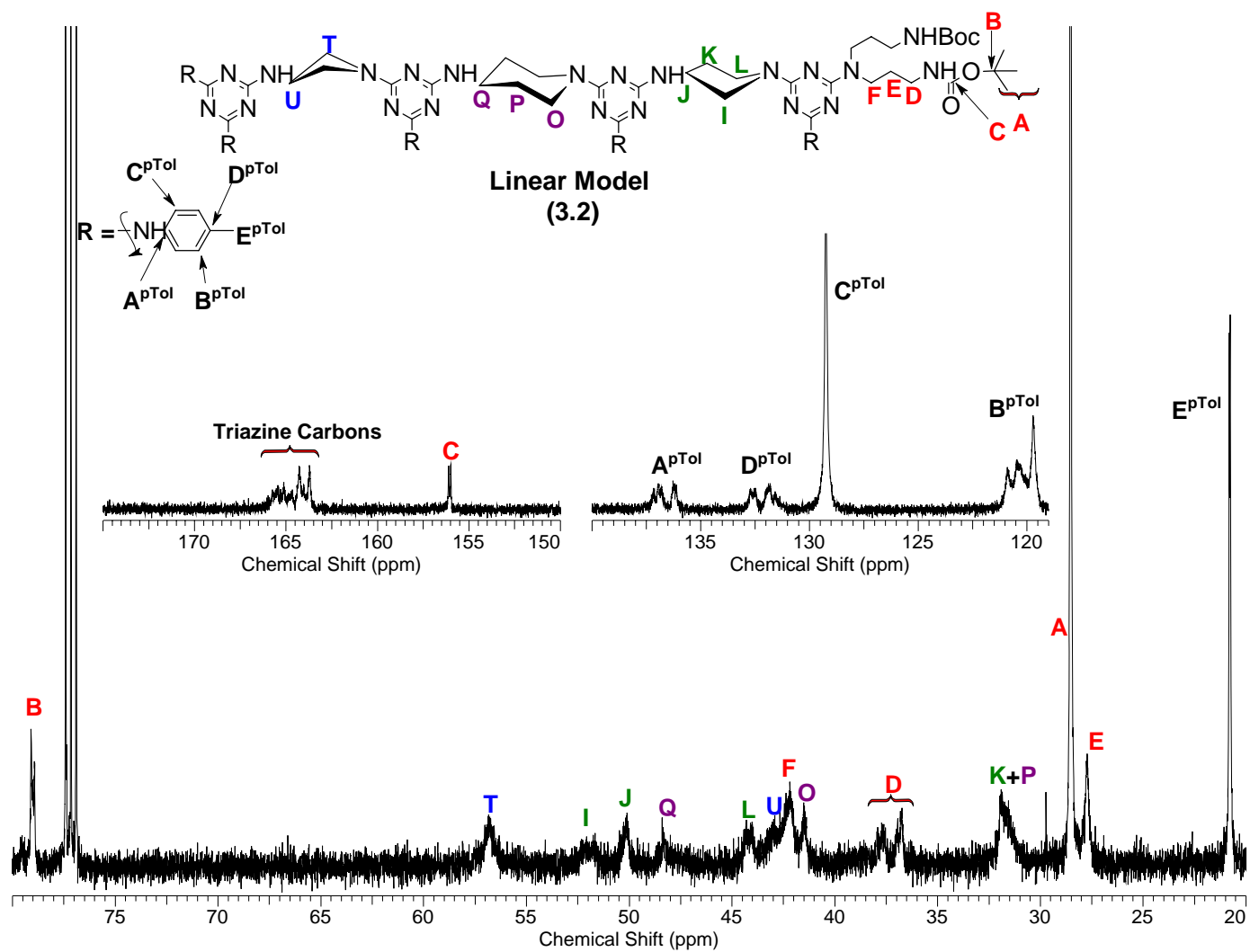
Tris(*p*-toluidine)-mono(Bis(3-BOC-3-aminopropyl)amine)-monopyrrolidine-monopiperidine-monochlorotriazine
 (pTol₃-BBT-Pyr-Pip-Cl) – ¹³C Spectrum (DMSO-*d*₆, T = 25 °C)



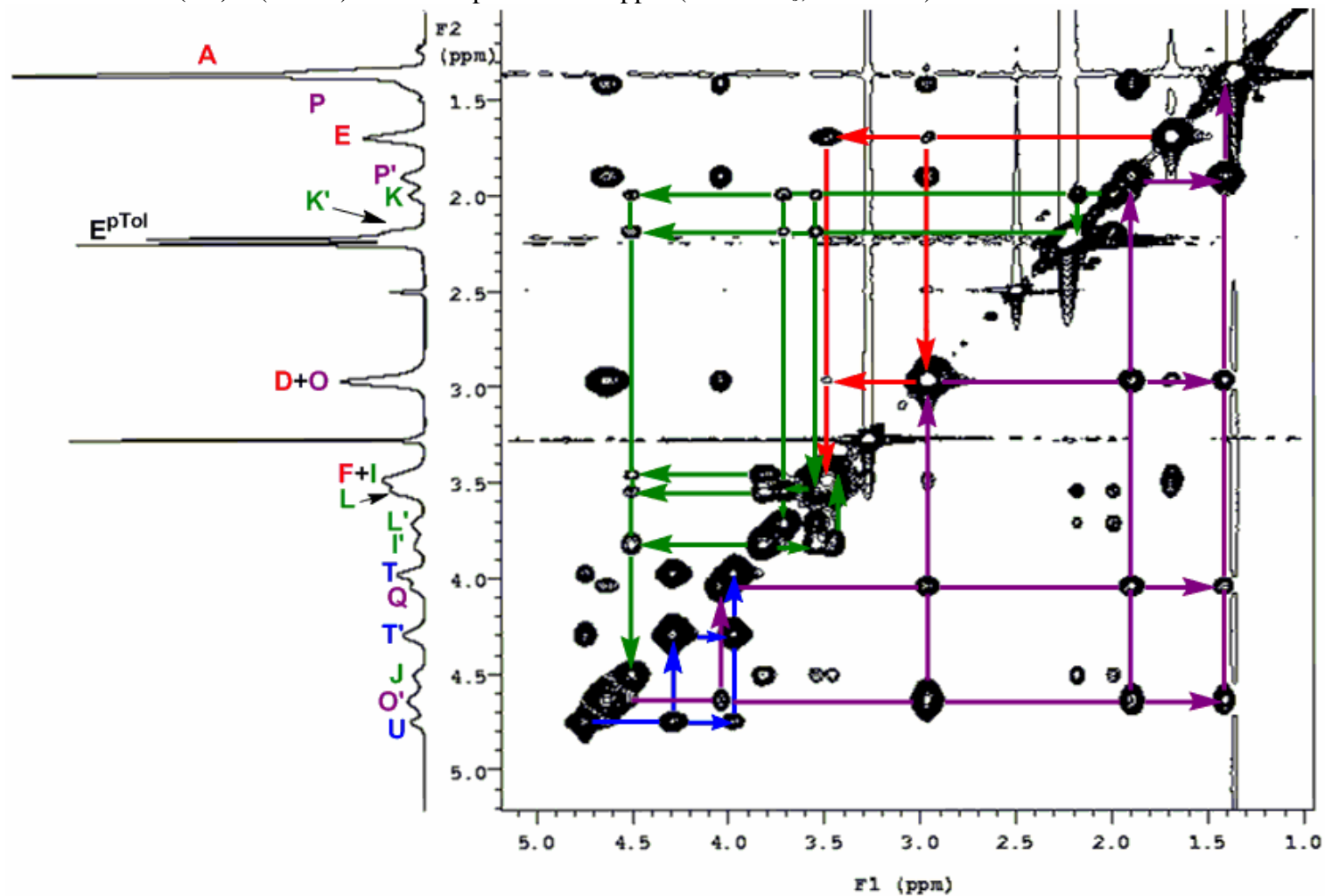
Linear Model (3.2) – ^1H Spectrum (DMSO- d_6 , T = 25 °C)



Linear Model (3.2) – ^{13}C Spectrum (DMSO- d_6 , T = 25 °C)



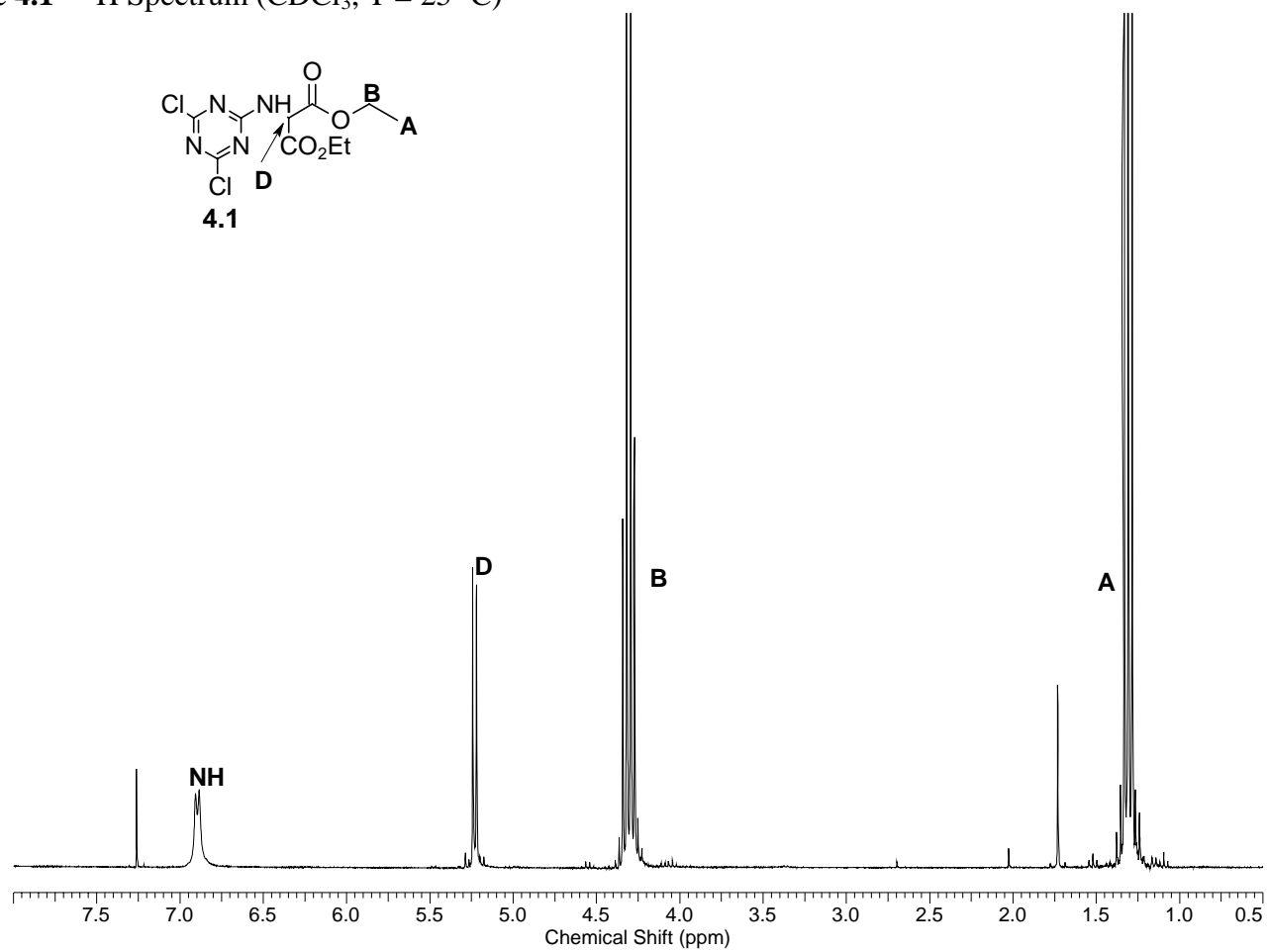
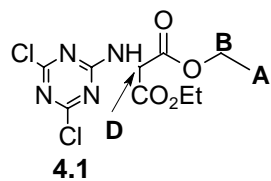
Linear Model (3.2) – (¹H–¹H) NOESY Spectrum 1–5 ppm (DMSO-*d*₆, T = 35 °C)



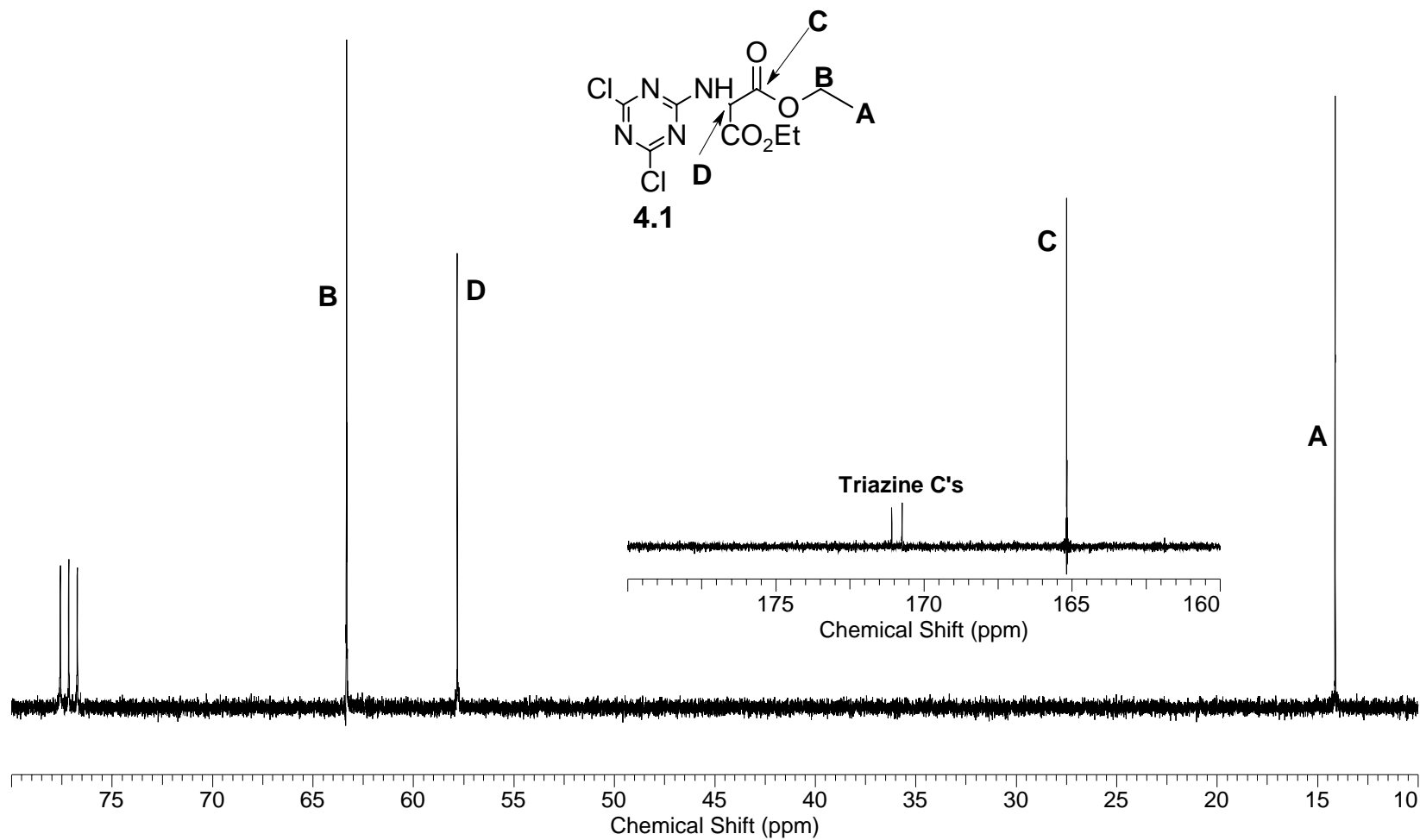
APPENDIX C

SELECTED NMR SPECTRA FOR COMPOUNDS DESCRIBED IN CHAPTER IV

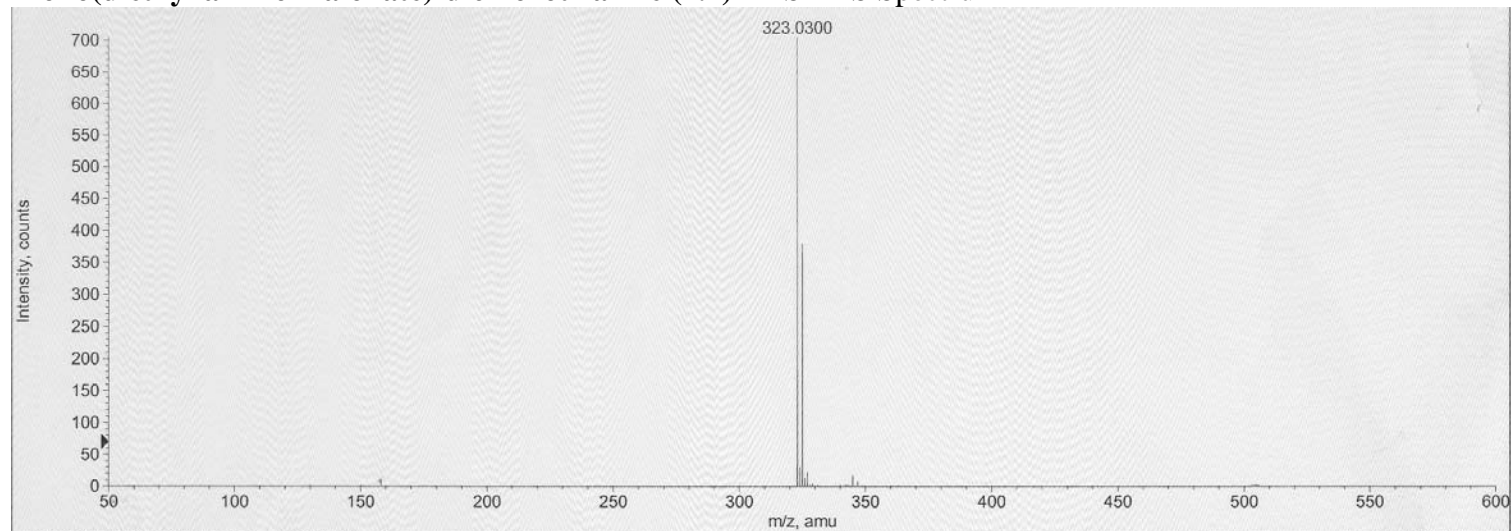
Intermediate 4.1 – ^1H Spectrum (CDCl_3 , $T = 25\text{ }^\circ\text{C}$)



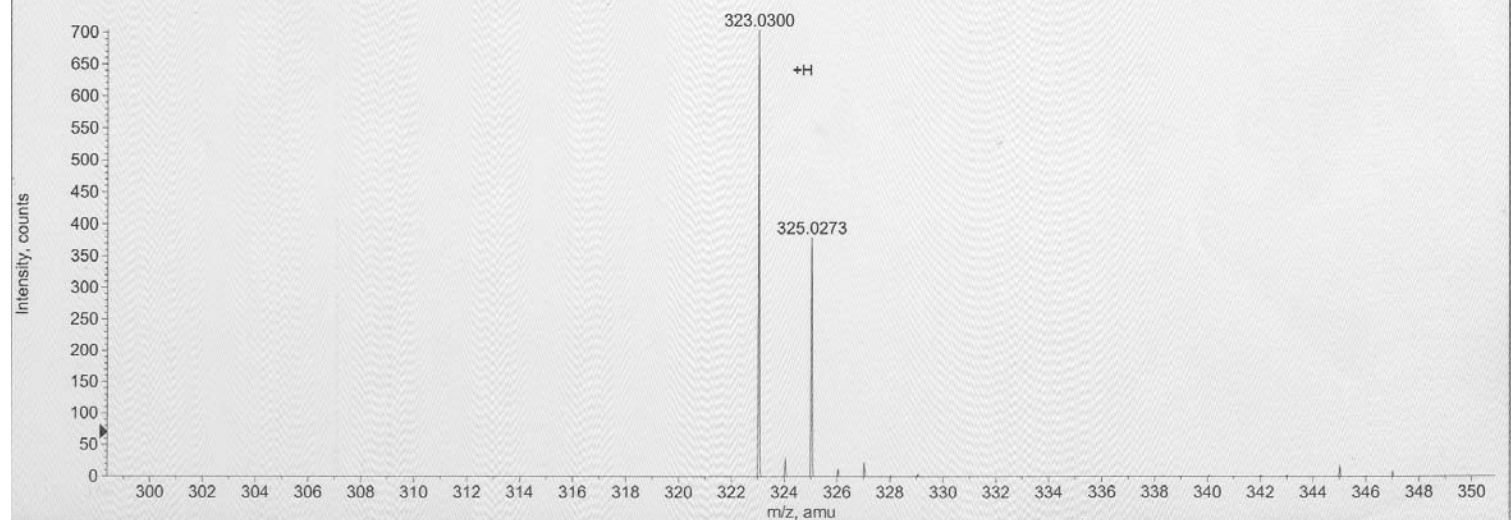
Intermediate 4.1 – ^{13}C Spectrum (CDCl_3 , $T = 25^\circ\text{C}$)



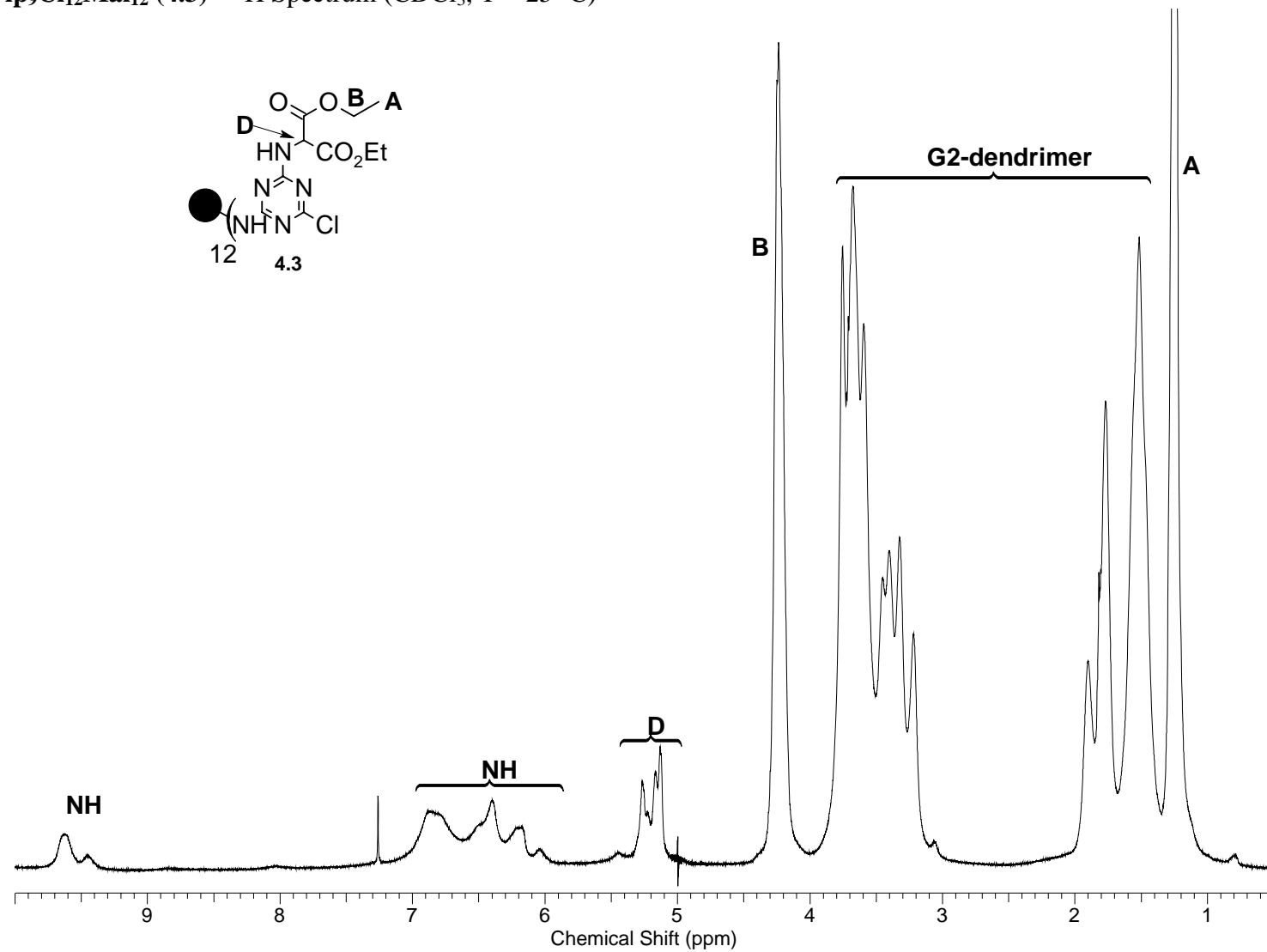
Mono(diethyl amino malonate)-dichlorotriazine (4.1) – ESI-MS Spectrum



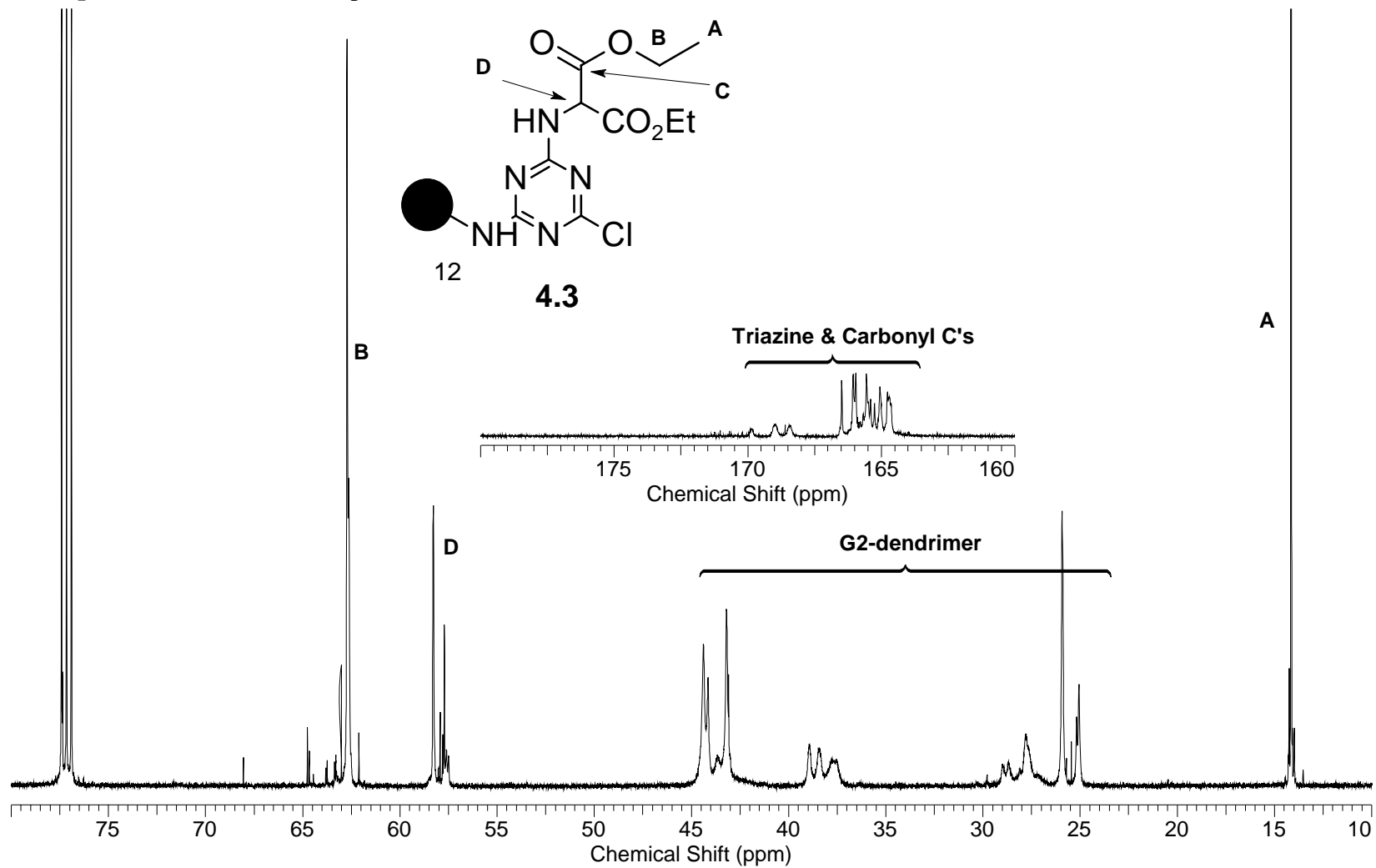
+TOF MS: 0.250 to 0.267 min from 07060719.wiff
a=3.55567823748856390e-004, t0=4.65093670219903290e+001 Max. 704.0 counts



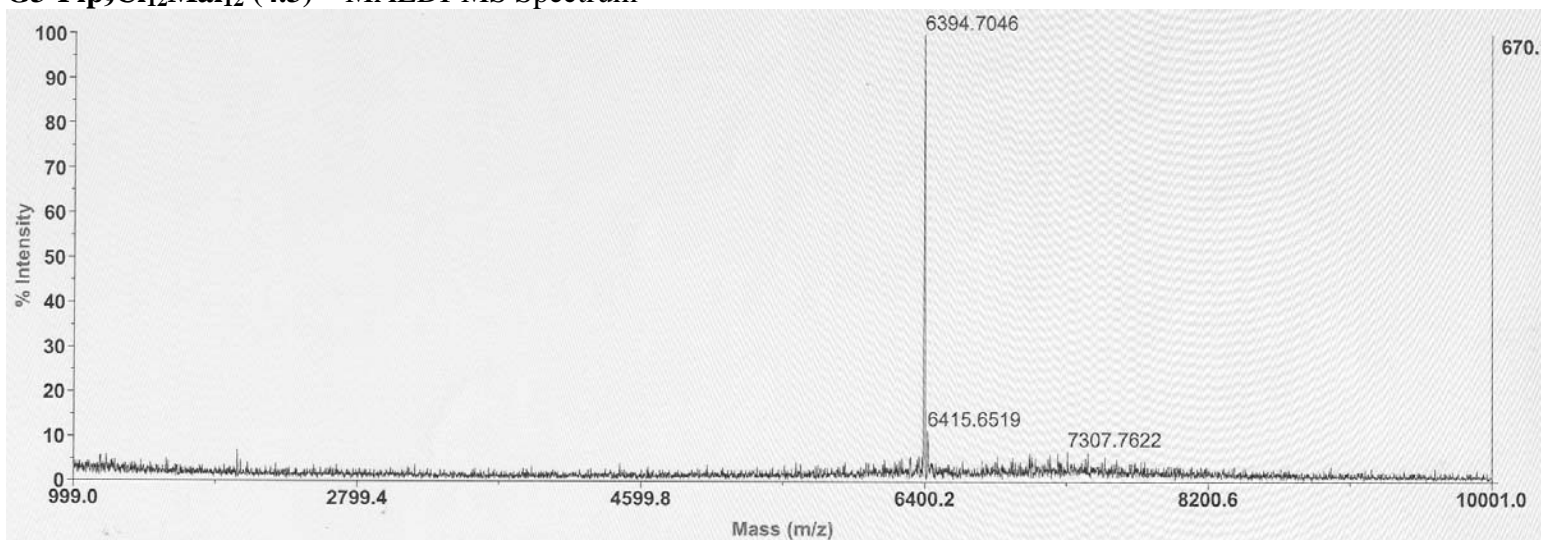
G3-Pip₉Cl₁₂Mal₁₂ (4.3) – ¹H Spectrum (CDCl₃, T = 25 °C)



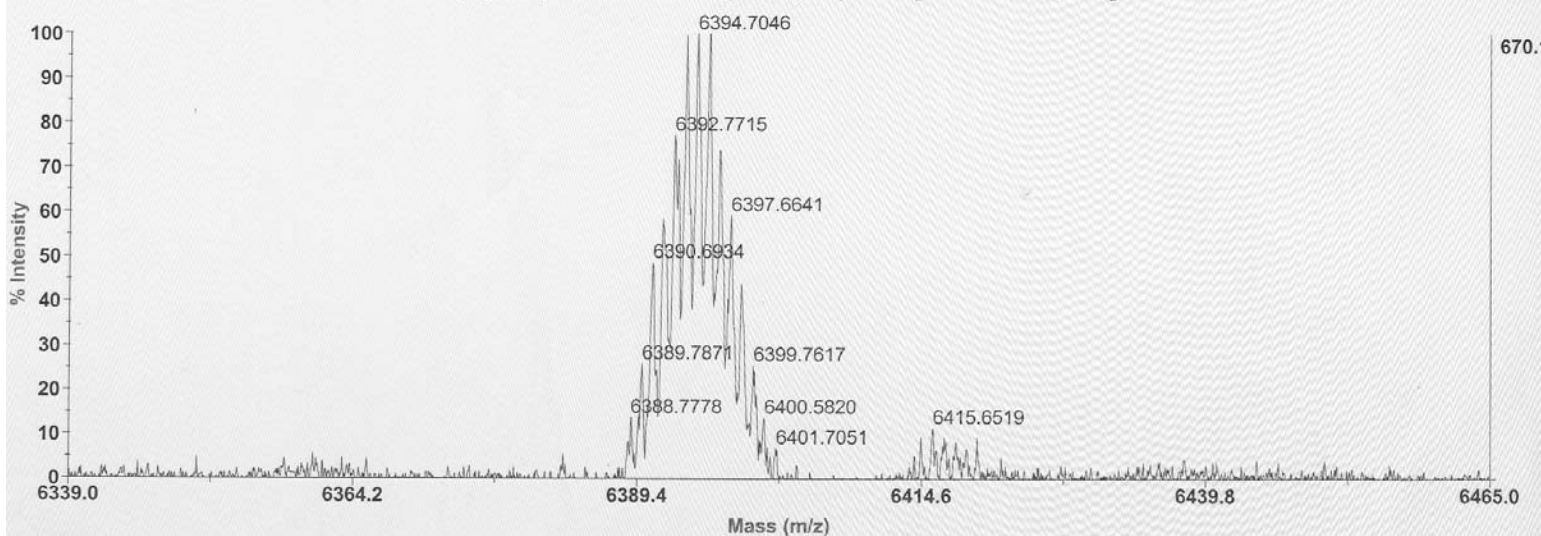
G3-Pip₉Cl₁₂Mal₁₂ (4.3) – ¹³C Spectrum (CDCl₃, T = 25 °C)



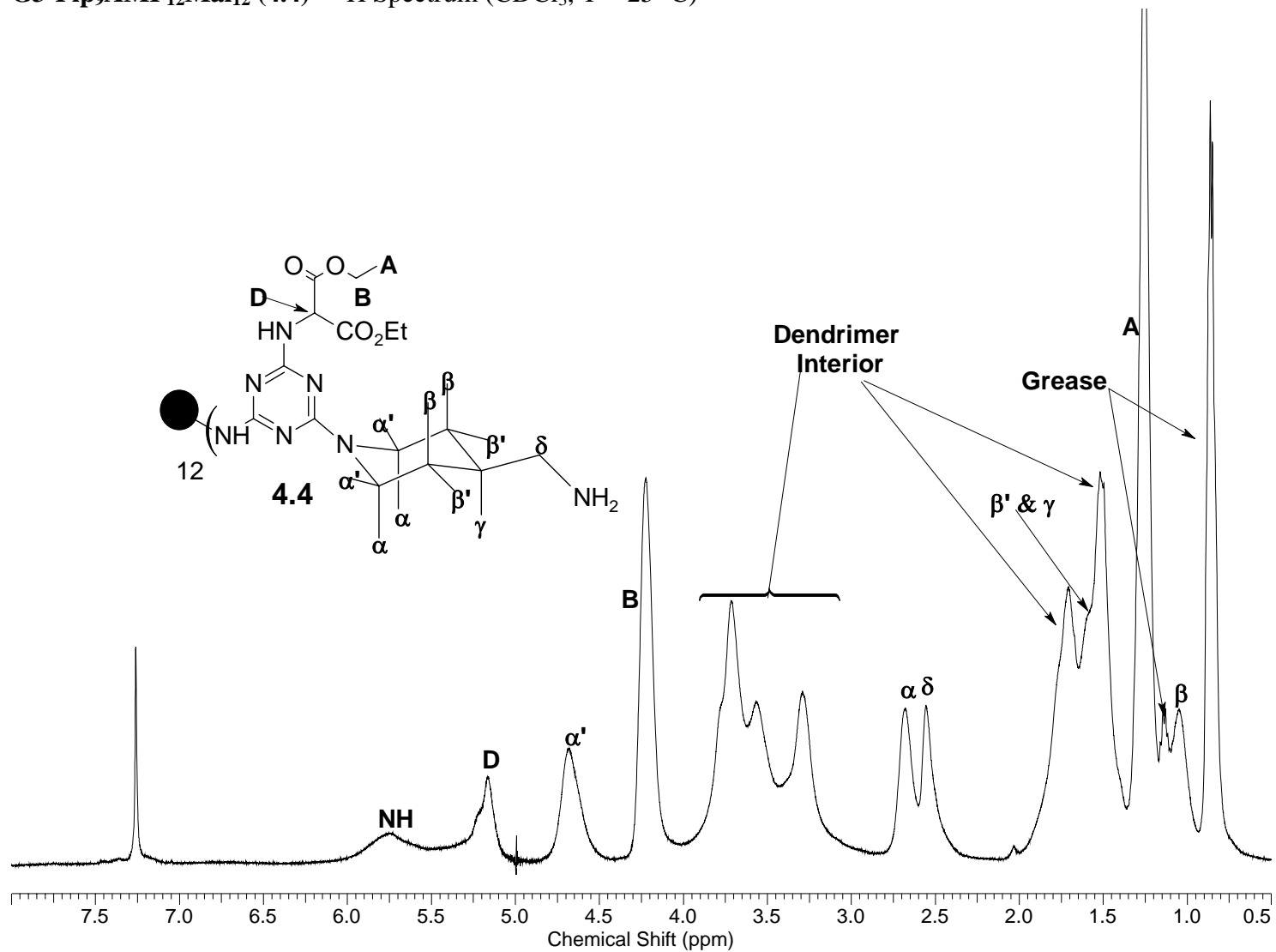
G3-Pip₉Cl₁₂Mal₁₂ (4.3) – MALDI-MS Spectrum



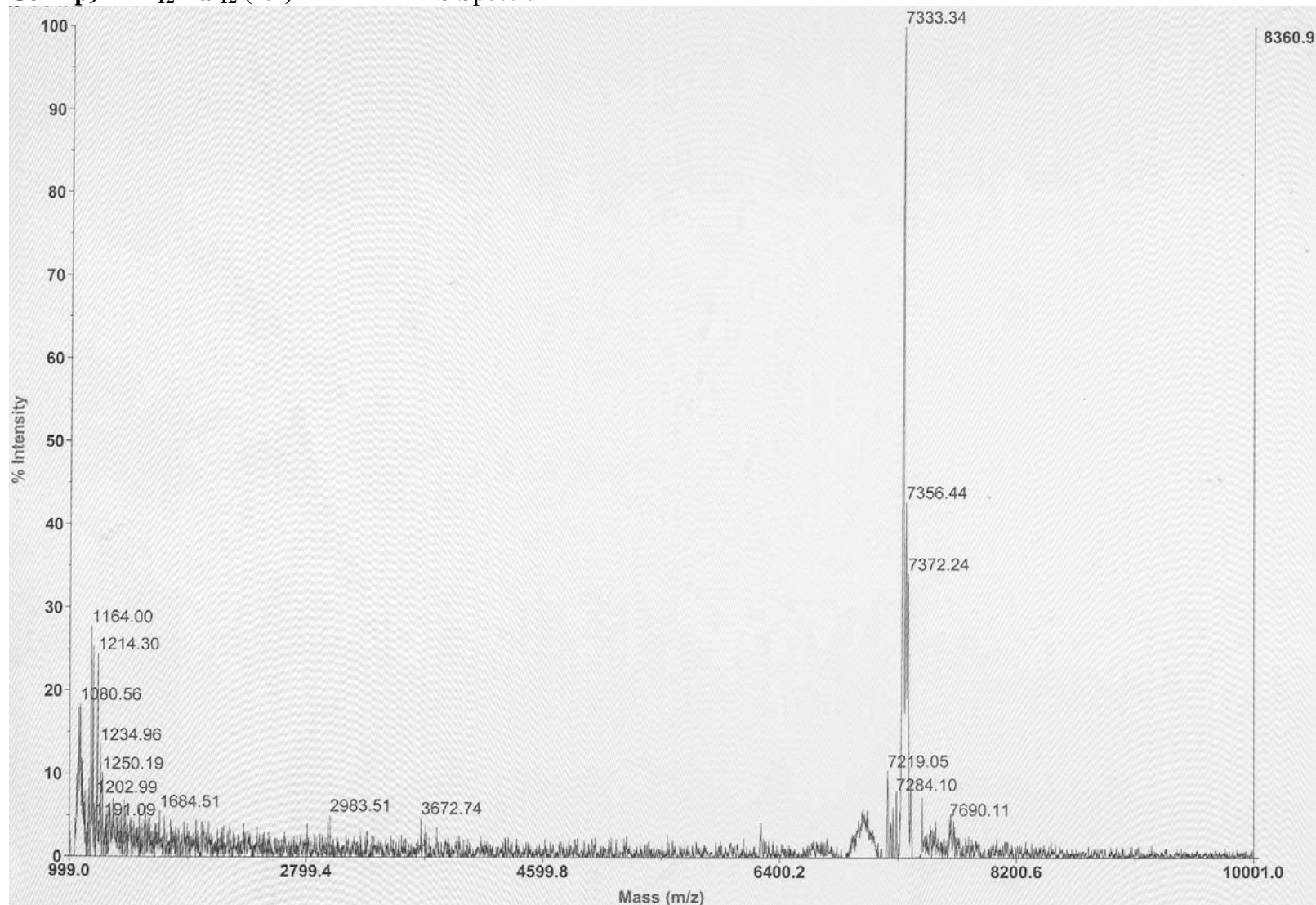
Voyager Spec #1=>AdvBC(32,0.5,0.1)=>MC[BP = 6394.7, 670]



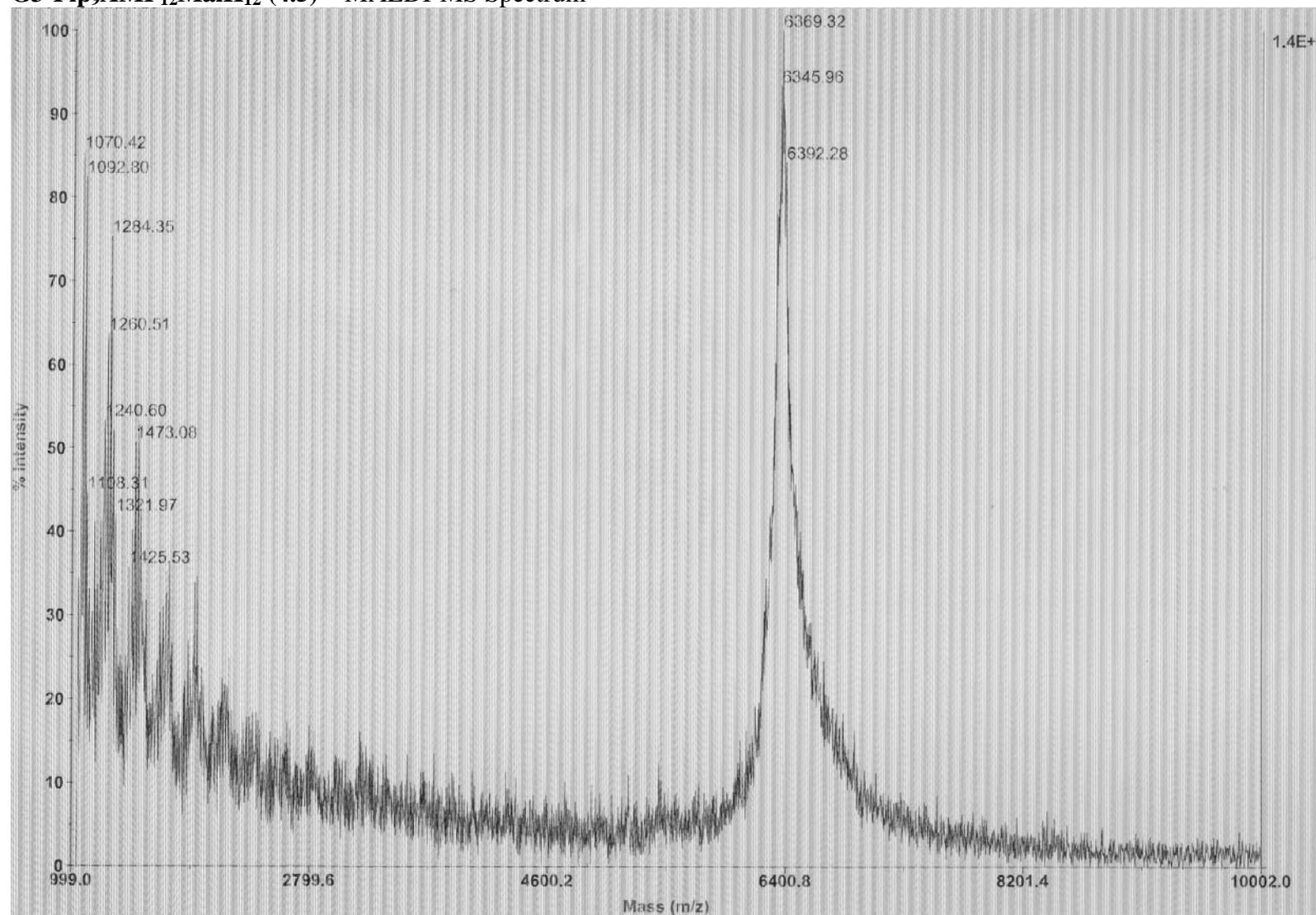
G3-Pip₉AMP₁₂Mal₁₂ (4.4) – ¹H Spectrum (CDCl₃, T = 25 °C)



G3-Pip₉AMP₁₂Mal₁₂ (4.4) – MALDI-MS Spectrum



G3-Pip₉AMP₁₂MalH₁₂ (4.5) – MALDI-MS Spectrum



VITA

Name: Karlos Xavier Moreno

Address: 702 E. 9th Street
Del Rio, TX 78840

Email Address: Karlos_moreno@hotmail.com

Education: B.S., Chemistry and Biology, The University of Texas at San
Antonio, 2003
Ph.D., Chemistry, Texas A&M University, 2007